

UNIVERSITÉ DE NICE SOPHIA-ANTIPOLIS

STATISTICAL COMPUTING ON MANIFOLDS
FOR COMPUTATIONAL ANATOMY

Mémoire présenté pour l'obtention de

L'HABILITATION À DIRIGER DES RECHERCHES

par

XAVIER PENNEC

le 18 décembre 2006,

Rapporteurs : Guido Gerig – Professor, UNC Chapel Hill, USA
Mads Nielsen – Professor, IT University of Copenhagen, DK
Paul Thompson – Associate Professor, UCLA, USA
Examineurs : Nicholas Ayache – Directeur de recherche INRIA
Sir Michael Brady – Professor, University of Oxford, UK.
Olivier Faugeras – Directeur de recherche INRIA
Line Garnero – Directrice de recherche CNRS
Jean-Marie Morvan – Professeur, Université de Lyon 1
Invité : Jean-Daniel Boissonnat, – Directeur de recherche INRIA

Contents

Forward	3
I Research Activities	7
1 Extended summary	9
2 Intrinsic statistics on Riemannian manifolds	15
2.1 Motivation	15
2.1.1 Invariance and consistency	15
2.1.2 Barycenters are not intrinsic	17
2.2 A Riemannian computing framework	17
2.2.1 Riemannian geometry	18
2.2.2 Exponential chart	18
2.2.3 A practical computing framework	19
2.3 Simple statistics on Riemannian manifolds	20
2.3.1 Measures and expectation of observables	21
2.3.2 Riemannian center of mass	22
2.3.3 An algorithm to compute the mean	22
2.3.4 Covariance and Mahalanobis distance	24
2.3.5 Gaussian and χ^2 law	24
2.4 Example manifolds	26
2.4.1 Invariant metrics on connected Lie groups	26
2.4.2 Practical averaging of 3D rotations	28
2.4.3 Limitations of invariant metrics	29
2.4.4 Homogeneous manifolds	30
2.4.5 Robust statistics using ϕ -connectors	31
2.5 Applications in matching and registration	33
3 Manifold-valued images and tensors computing	35
3.1 Metrics on tensors	37
3.1.1 Affine invariant Riemannian metrics	37
3.1.2 Log-Euclidean metrics	39

3.1.3	Which metric for which problem?	40
3.2	Computing on Riemannian manifolds	42
3.2.1	Interpolation as a weighted mean	42
3.2.2	Gaussian and kernel-based filtering	42
3.2.3	Gradient and Laplacian	43
3.2.4	Anisotropic diffusion	45
3.2.5	Diffusion-based interpolation and extrapolation	46
3.3	Application to diffusion tensor imaging (DTI)	46
3.3.1	Noise models for the estimation of the tensor field	47
3.3.2	Joint estimation and smoothing	48
3.4	Conclusion	50
4	Medical image registration	55
4.1	Rigid registration for image guided therapy	55
4.1.1	Endoscopic brain surgery	56
4.1.2	Dental implantology	58
4.1.3	Liver puncture guidance	58
4.1.4	Confocal microscopic imaging	61
4.2	Evaluation of the registration performances	63
4.2.1	Error prediction	64
4.2.2	Consistency loops	65
4.2.3	The bronze standard method	66
4.2.4	Grid-based registration evaluation	68
4.3	Non-linear registration	70
4.3.1	Demon's like algorithms	70
4.3.2	The Pasha algorithm	72
4.3.3	Hybrid iconic and geometric registration	74
4.3.4	High performance computing for "human-time" registration	76
4.3.5	Non stationary regularization with anatomical a priori	78
4.3.6	Polyrigid and Polyaffine Transformations	82
5	Computational models of the anatomy	85
5.1	A statistical model of the scoliotic spine	86
5.1.1	Towards an augmented reality system for laparoscopic spine surgery	86
5.1.2	Mean spine shape and local variability	87
5.1.3	Principal modes of variation	88
5.2	Modeling the anatomical variability of the brain	89
5.2.1	Measuring the variability of sulcal lines	91
5.2.2	A model of the full brain variability by extrapolation	93
5.2.3	Model evaluation	95
5.2.4	Neuroanatomical interpretations	96
5.2.5	Measuring the asymmetry	98
5.2.6	Conclusion	100
5.3	Learning the metric of anatomical deformations	100

5.3.1	Deformation statistics to improve inter-subject registration	101
5.3.2	Riemannian elasticity: an integrated framework	102
5.3.3	Optimizing the Riemannian elasticity	104
5.3.4	Left-Invariant Riemannian Elasticity	105
5.3.5	Conclusion	105
6	Perspectives	107
6.1	Computational anatomy	107
6.2	Statistical computing on manifolds	110
6.3	Applications in medical image analysis	113
	References	113
II	Synthesis of Activities	139
	Curriculum Vitae	141
	Education	141
	Positions	141
	Grants and Contracts	142
	Scientific responsibilities	143
	Software	144
	Patents	144
	Prizes and Awards	145
	Teaching	147
	Supervision of research activities	147
	Former PhD Students	149
	Current PhD Students	152
	DEA and Master Students	155
	Publications	156
	Books and Proceedings	157
	Thesis	157
	Articles in international peer-reviewed journals	157
	Submitted Journal Papers	160
	Book chapters, editorials and general purpose magazine articles	160
	Full-length articles in selective international peer-reviewed conferences	161
	Articles in international conferences and workshops	166
	National reviewed workshops	169
	Research Reports	169
	Technical Reports and Deliverables	172

To my wife Myriam.

Forward

During the last decade, my main research topic was on medical image analysis, and more particularly on image registration. However, I was also following in background a more theoretical research track on statistical computing on manifolds. With the recent emergence of computational anatomy, this topic gained a lot of importance in the medical image analysis community. During the writing of this habilitation manuscript, I felt that it was time to present a more simple and unified view of how it works and why it can be important. This is why the usual short synthesis of the habilitation became a hundred pages long text where I tried to synthesize the main notions of statistical computing on manifolds with application in registration and computational anatomy. Of course, this synthesis is centered on and illustrated by my personal research work.

Manuscript Organization

The manuscript is divided in two parts. The first part details the scientific work. After an executive summary of the contributions, Chapter 2 describes the theory of intrinsic statistics on Riemannian manifolds, and show how we can turn it into a practical computing framework. Chapter 3 extends this framework to manifold-valued images with the important example of diffusion tensors. With Chapter 4, we turn to more classical image analysis applications with rigid and non-rigid registration. The performance evaluation framework we proposed for rigid registration is a direct application of the statistical computing framework on manifolds, while inter-subject non-rigid registration problems drove our interest towards the emerging field of computational anatomy. We present in Chapter 5 our contributions in this area, based on the three previous chapters. Finally, Chapter 6 presents a few perspectives for future research.

The second part of the manuscript provides a summary of my activities in terms of education, responsibilities, supervision of students and publications. As the first part of this habilitation extensively covers my research work, I felt that it was not necessary to attach to this manuscript the main journal papers covering these topics. However, the principal publications on which the text is based are bold-faced in my publication list at the end of the document and an URL link is provided to retrieve them.

Acknowledgments

I would first like to warmly thank the reviewers of this habilitation manuscript: Guido Gerig, Taylor Grandy Professor of Computer Science and Psychiatry at the University of North Carolina at Chapel Hill, USA, Mads Nielsen, Professor and head of the Image Analysis Group at the Information Technology University of Copenhagen, Denmark, and Paul Thompson, Associate Professor of Neurology at the Laboratory of neuro-Imaging (LONI), University of California at Los-Angeles school of Medicine, USA. I would then like to thank the other members of the jury, Sir Michael Brady, BP Professor of Information Engineering at Oxford University, Line Garnero, Research director at CNRS / Hopital la Pitié Salpêtrère (LENA UPR 640), Jean-Marie Morvan, Professor at the University Claude Bernard (Lyon I), Olivier Faugeras research director at INRIA Sophia Antipolis, and Jean-Daniel Boissonnat, research director at INRIA Sophia Antipolis. I should finish by acknowledging the very important role of Nicholas Ayache, research director at INRIA Sophia Antipolis, founder and leader of the internationally renown Epidaure/Asclepios team in which I have done the research presented in this habilitation during the last 9 years.

I am indebted to all the present and past members of the Epidaure/Asclepios team for the very fruitful research environment. I really felt that we were doing a joint work and that all the members of the team are responsible for something in the work I present here. Among them, I should particularly mention the PhD students with whom I closely worked: Pascal Cathier, Sébastien Granger, Guillaume Flandin, Radu Stefanescu, Vincent Arsigny, Jonathan Boisvert, Pierre Fillard, Heike Hufnagel, Tom Vercauteren and Stanley Durrleman. Without them, this habilitation would have been much lighter.

Last but not least, I dedicate this manuscript to my wife who supported me with patience during the writing of this manuscript.

Part I

Research Activities

Chapter 1

Extended summary

The quality of biomedical images is ever increasing: better spatial and temporal resolution, better signal-to-noise ratio. New imaging protocols bring new information about the anatomy, the function or the physiology of living systems. The dimensionality of the data also increases: to the usual three spatial dimensions, one often adds a fourth temporal dimension which can be at the level of the second (heart beats) or years (growth or pathology follow-up). At yet another scale, one could conceive a fifth dimension by considering the variability of an organ in a population. Computational anatomy is an emerging discipline that aim at analyzing and modeling the biological variability of the human anatomy at the population scale. The goal is not only to model the normal variations among a population, but also to discover morphological differences between normal and pathological populations, and possibly to detect, model and classify the pathologies from structural abnormalities. Examples that we investigated are the shape of the scoliotic spine and the variability of the brain normal.

The method is to identify anatomically representative geometric features, to describe their statistical variability across populations, and test for statistical differences. However, it appeared over the last years that one should conceive a new way to perform the statistics because most of the geometric features (curves, surfaces, deformations) do not belong to Euclidean spaces but rather to curved manifolds. To that aim, we propose the Riemannian metric as the basic structure. Theoretical developments demonstrate that this is a very powerful tool and example applications on diffusion tensor images show the well-posedness and the efficiency of the method. A second fundamental tool of computational anatomy is registration in the broad sense, which consists in finding the geometric transformation that best superimposes the data (features or images) in a common reference frame. Several applications in image guided therapy led us to develop and enhance methods to rigidly and non-rigidly register medical images. One of the key problem is to evaluate the performances of the algorithm: this is once again a statistical estimation problem on geometric features (transformations). The second key problem is to introduce prior information about the anatomy and the pathology in the algorithm to robustify them while drastically reducing the computation times, in order to bring the algorithm closer to their use in real clinical applications. In this setting, finding the optimal regularization prior for a particular medical image registration problem is also a computational anatomy problem as it amounts to modeling the expected variability of the transformation.

Statistical computing on manifolds, image registration and computational models of the anatomy, these are the three inter-related problems that we tackle in this habilitation.

Intrinsic Statistics on Riemannian Manifolds

Measurements of geometric primitives are often noisy in real applications and we need to use statistics either to reduce the uncertainty (estimation), to compare measurements, or to test hypotheses. Unfortunately, geometric primitives often belong to manifolds that are not vector spaces, and we showed that using standard statistics sometimes leads to apparent paradoxes [Pennec and Ayache, 1998].

Based on a Riemannian manifold structure, we present in [Pennec, 2006a] a consistent development of statistical notions like the mean value and the covariance matrix of a random element, normal law, Mahalanobis distance and test. We provide a characterization theorem of the Fréchet mean which is more general than the previous ones and an efficient gradient descent algorithm to compute it. The notion of Normal law we propose is based on the the minimization of the information knowing the mean and covariance of the distribution. The resulting family of pdfs is different from the heat kernel induces by a Brownian motion on the manifold but also spans the whole range from uniform (on compact manifolds) to the point mass distribution. We were able to provide tractable approximations (with their limits) for small variances which allows to use these distributions very easily in practice.

One of my important contributions was to show that the Riemannian structure is not only good from a theoretical point of view but that is also provides an efficient practical computing framework. The key is to replace straight lines by the geodesics of the manifold, and vectors by bi-points, a 19th century concept ancestor of the vectors. It is then possible to cleanly unfold the manifold along its geodesics to obtain a locally flat representation that conserves radial distances (the Riemannian log map), or conversely to walk along a geodesic starting with a given tangent vector (the Riemannian exponential map). The implementation of these two maps at each point is the basis of programming on Riemannian manifolds [Pennec et al., 2006].

We were among the very first to introduce these notions of geometrical statistics in medical image analysis [Pennec, 1999], in particular to estimate the error on the rigid registration [Pennec et al., 2000]. Some tentative extensions of the theory to spatially extended features like surfaces of functions irregularly sampled in space are not described in this habilitation because only very partial solutions did emerge. The key ideas were the use of the EM algorithm for dealing jointly with the sampling and matching problem on surfaces [Granger and Pennec, 2002a, Granger, 2003] and for realizing a joint spatial and signal parcellation of fMRI sequences [Flandin et al., 2002, Flandin, 2004]. A similar idea, although non uniform, was also exploited with Generalized image models [González Ballester et al., 2004].

Manifold-Values Images: the Tensor Computing Example

We extended in [Pennec et al., 2006] the Riemannian computing framework to fields of features with the example of positive definite symmetric matrices (tensors). Tensors are nowadays common geometric data. They are used for instance to encode the directional diffusion of water molecules

in Diffusion Tensor Imaging, or as covariance matrices to describe the joint variability at different places (Green function) in shape variability analysis. As tensors constitute a convex half-cone in the vector space of matrices, many usual operations (like the mean) are stable in this space. However, problems arise when estimating tensors from data (in standard DTI, the estimated symmetric matrix could have negative eigenvalues), or when smoothing fields of tensors: the numerical schemes used to solve the Partial Differential Equation (PDE) often lead to negative eigenvalues if the time step is not small enough.

Our basic idea was to provide the tensor space with a Riemannian metric invariant under the action of affine transformations of the underlying space [Pennec et al., 2006]. We show in Chapter 3 that it leads to a two parameters family of metrics that share the same geodesics with very strong theoretical properties: the cone of positive definite symmetric matrices is replaced by a regular manifold of “constant” (homogeneous) non-scalar curvature without boundaries (null eigenvalues are at the infinity), the geodesic between two tensors and the mean of a set of tensors are uniquely defined, etc. We also introduced in [Arsigny et al., 2006d, Arsigny et al., 2006c] another family of metrics that share very similar properties: Log-Euclidean metrics. These new metrics give results very similar to the affine invariant ones, but lead to drastically simpler computations because they give a vector space structure to tensors.

The choice of a convenient Riemannian metric allows to generalize to tensor fields many important geometric data processing algorithms such as interpolation, filtering, diffusion and restoration of missing data [Pennec et al., 2006]. For instance, most interpolation schemes and Gaussian filtering can be tackled efficiently through a weighted mean computation. Linear and anisotropic diffusion schemes can be adapted to the Riemannian framework through partial differential evolution equations, provided that the metric of the tensor space is taken into account. For that purpose, we provide generic and intrinsic numerical schemes based on the logarithmic map to compute the gradient and Laplacian operators. Finally, to enforce the fidelity to the data (either sparsely distributed tensors or complete tensors fields) we propose least-squares criteria based on the Riemannian distance that are particularly simple and efficient to solve.

The excellent properties of the Riemannian computing framework were exemplified on the estimation and regularization of Diffusion Tensor MR Images (DTI), in view of the tracking of the white matter fibers within the brain [Fillard et al., 2006a, Fillard et al., 2006b]. The careful modeling of the noise on the data led us to propose new Rician ML and MAP estimation frameworks which can cope with a much lower SNR compatible with clinical applications.

Medical Image Registration

Before being a fundamental tool of computational anatomy, image registration was central problem in medical image analysis. This is still an open problem for large deformation between images of different subjects. Historically, rigid registration was one of my important research themes. The objective was not only to design neat theoretical methods, but also to reach clinically usable algorithms, in particular for image guided therapy.

In each application, the method was to revisit the registration criteria to better take into account the noise assumptions on the data. For instance, we designed in the European project ROBOSCOPE the prototype of an image-assisted robotic system for endoscopic brain surgery.

We were among the very first to register MRI to per-operative 3D ultrasound images. A careful modeling of the image intensity signals in both modalities led us to propose an innovative similarity measure depending on both the MR intensity and its gradient: the bivariate correlation ratio [Roche et al., 2001]. Then, brain deformations were followed in the 3D ultrasound sequence [Pennec et al., 2003, Pennecc et al., 2005a].

A transversal axis of my research was to develop performance evaluation methods for rigid registration algorithms in terms of robustness, precision and accuracy. In a probabilistic setting, this amounts to doing statistics on rigid-body transformations, which was one of my original motivation for deriving proper statistical methods on manifolds. To establish a reference (a Bronze Standard) in the absence of a Gold Standard, we proposed a multiple registration protocol involving multiple methods and a database of images representative of clinical conditions. That way, the (possible) bias of each method becomes a random variable and is taken into account in the final mean registration (see [Glatard et al., 2006f] for a recent review). Using this type of technique, we were able to certify the accuracy of the 2D/3D registration procedure in the augmented reality system we developed with S. Nicolau at IRCAD for guiding percutaneous radio-frequency ablations of the liver [Nicolau et al., 2004a]. This was an important security issue for its clinical use. Since then, the system was tested on more than 10 patients in the operating room and we showed that it could reach the accuracy of the practitioner with a much faster gesture and no intermediate CT scan [Nicolau et al., 2006].

To recover more complex deformations, we analyzed with P. Cathier the very efficient Demon's algorithm. The goal was to guaranty the convergence and to better adapt the algorithm to specific application constraints and assumptions. By introducing voxel matches as auxiliary variables in addition to the geometric transformation, we proposed a very efficient and well posed two-steps iterative minimization framework [Cachier et al., 2003]. Moreover, additional constrains such as sulcal line correspondences could be considered with almost no addition computational complexity [Cachier et al., 2001]. To further accelerate the algorithm, we proposed with R. Stefanescu a generic "pipeline" method to parallelize recursive image filtering algorithms on a cluster of personal computers [Stefanescu et al., 2004b]. This was also combined with a space-varying transformation regularization based on the underlying tissue type, and a non-stationary tradeoff between the image similarity and regularization to better match the reliable information (e.g. edges) while interpolating within homogeneous image areas. This allows to take into account very easily and efficiently pathologies like tumors in the atlas-based segmentation of brain images for radiotherapy planning [Stefanescu et al., 2004c].

In between rigid transformations and dense deformation fields, we designed with V. Arsigny a new class of parametric transformations that exhibit a locally rigid or affine behavior while staying diffeomorphic [Arsigny et al., 2005c]. This allows to better model the physical deformations that occur in articulated systems or in histological slices for instance. Revisiting the link between these transformations and general diffeomorphisms led us to propose in [Arsigny et al., 2006a] very efficient algorithms to compute the group logarithm of general diffeomorphisms (and the reverse map the exponential). Although there are still some theoretical concerns, this opens a new practical and very efficient way to perform statistics on diffeomorphisms which could become soon a central too for modeling the anatomical variability.

Computational Models of the anatomy

There are nowadays a growing number of geometrical and physically-based registration methods that can faithfully deal with intra-patient deformations. However, one need to rely on statistics to learn the relationship between the anatomy of different subjects. The method is to identify anatomically representative geometric features (points, tensors, curves, surfaces, volume transformations), and to model their statistical distribution. This can be done for instance via a mean shape and covariance structure after a group-wise matching. Therefore, computational anatomy is at the interface of geometry, statistics and image analysis. This is currently a very active research field, as exemplified by the quality of the submissions and the number of attendees (almost 70 people) to the first workshop on the Mathematical Foundations of Computational Anatomy (MFCA'06) organized in conjunction with MICCAI'06 [Pennec and Joshi, 2006].

In this context, our statistical computing framework on manifolds allows to decouple the anatomical modeling problem (representing the observations with maximally informative parameters) from the technical difficulties of computing with the model due to manifold nature of the parameter space. This is illustrated in Chapter 5 with the construction of a statistical model of the scoliotic spine. By using an articulated model based on the relative position and orientation of the vertebrae (i.e. rigid body transformations), we were able with J. Boisvert to analyze the variability of the spine shape over a database of more than 300 patients and to assess the evolution of the deformation during orthopedic treatments [Boisvert et al., 2006c]. Moreover, the four first modes of variation are very closely correlated to the clinical classification of scolioses [Boisvert et al., 2006e], which demonstrate the truthfulness of the approach.

In collaboration with P. Thompson at LONI, we proposed with P. Fillard to model the variability of the brain from a dataset of precisely delineated anatomical structures (sulcal lines) on the cerebral cortex. we model the first and second order moments of sulci by an average sulcal curve and a sparse field of covariance tensors along these curves. This information is then extrapolated to the whole brain using an harmonic diffusion PDEs on tensor fields. As a result, we obtain a dense 3D variability map which proves to be in accordance with previously published results on smaller samples subjects. We also propose statistical tests which demonstrate that our model is globally able to recover the missing information and innovative methods to analyze the asymmetry of brain variability [Fillard et al., 2006c]. Preliminary results on the correlation between local and distant displacements indicate that the displacement of the symmetric point is correlated. Other long distance correlations also appear, but their statistical significance still needs to be established.

Another way to gather statistics on inter-subject brain variability is to perform multiple deformable registration between a reference image and subject images. We proposed in [Pennec, 2006b] a consistent mathematical framework to learn the shape deformation metric from a set of registration results and to use it as a regularization penalization in non-rigid registration. First experiments indicate that the method is sound and effective. The next step will be to analyze the results with different registration algorithms and to compare and combine them to the sulcal variability. The ultimate goal is to include many additional sources of information: other cortical landmarks like sulcal ribbons and gyri, the surface of internal structures like the ventricles, the hippocampus or the corpus callosum, or fiber pathways mapped from DTI. These sources of information are individually providing a partial and biased view of the whole variability. Thus, we expect to observe a good

agreement in some areas, and complementary measures in other areas. This will most probably lead in a near future to new neuroanatomical findings and more robust medical image analysis applications.

Chapter 2

Intrinsic statistics on Riemannian manifolds

2.1 Motivation

Measurements are often noisy in real image analysis applications and we need to use statistics either to reduce the uncertainty (estimation), to compare measurements, or to test hypotheses. Examples of simple features that I historically considered in medical imaging applications are 3D rotations, 3D rigid transformations, frames (a 3D point and an orthonormal trihedron), semi-oriented frames (where some of the trihedron unit vectors are given up to their sign) [Pennec et al., 2000, Pennec et al., 1998], oriented or directed points [Granger et al., 2001, Granger and Pennec, 2002b], positive definite symmetric matrices (so-called tensors) coming from diffusion tensor imaging [Fletcher and Joshi, 2004, Lenglet et al., 2006, Batchelor et al., 2005, Pennec et al., 2006] or from variability measurements [Fillard et al., 2005c].

Unfortunately, these geometric primitives often belong to manifolds rather than to Euclidean spaces, which prevents using the standard statistical tools. Throughout this chapter, I will illustrate the construction of a statistical computing framework on manifolds with the above simple features. Besides their practical value in some applications, their interest is to illustrate quite clearly most of the problems that appear for computing on manifolds, and to guide the solutions towards generic methods. This is particularly important in view of dealing in the future with more complex manifolds like curves, surfaces, parametric or general diffeomorphic transformations [Commowick et al., 2005, Pennec et al., 2005b], etc.

2.1.1 Invariance and consistency

Processing geometric features is far more difficult than processing points, and a number of paradoxes can arise. For instance, we have shown in [Pennec and Thirion, 1997] that additive noise was not well suited for describing the uncertainty of frames and could be advantageously replaced by a “compositive” model of noise. We investigated in [Pennec and Ayache, 1998] three other basic problems that often arise when processing geometric features or in a statistical setting. The first one is the quantification of the probability of occurrence of an event when some geometric features

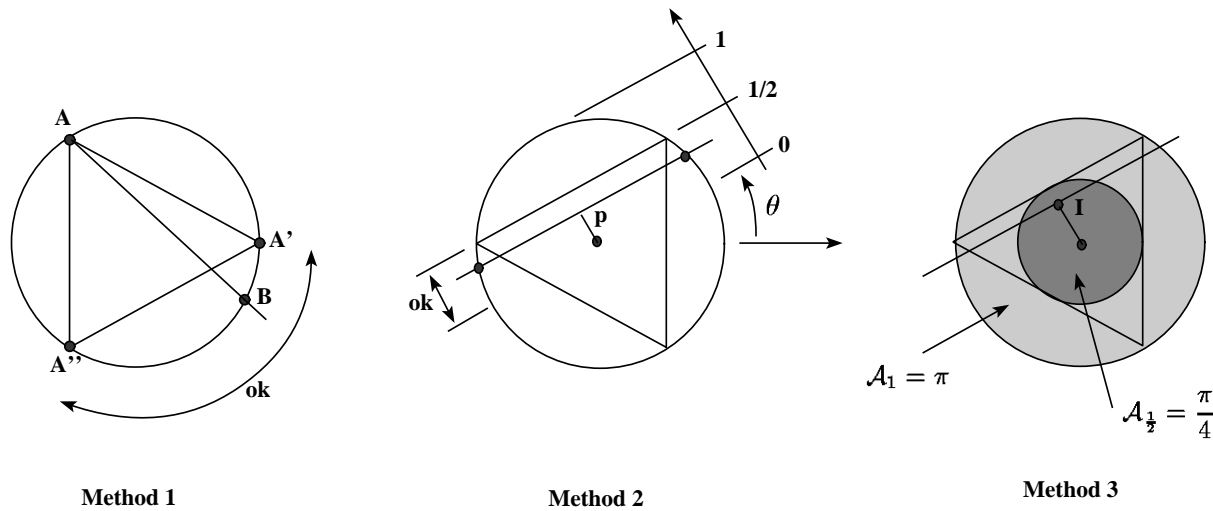


Figure 2.1: **Bertrand's Paradox (1907)**: three methods for computing the probability that a “random” chord of a circle has a length greater than the side of an inscribed equilateral triangle. From left to right, the methods give a probability of $1/3$, $1/2$ and $1/4$. The three solutions are correct but they do not refer to the same notion of uniformity in the way we choose the chord. **Method 1**: A chord intersects the circle in two points that we assume to be equally and independently distributed on the circle. If the first point is A , the second point has to lie between A' and A'' in the circle for the chord to be greater than the triangle side. This is just $1/3$ of the circumference and the searched probability is then $1/3$. **Method 2**: A chord is characterized by its distance p to the center (between 0 and 1) and its orientation θ w.r.t. a fixed line (between 0 and 2π). Drawing an inscribed equilateral triangle parallel to the chord, we can see that the distance d has to be less than $1/2$ in order to have a chord length greater than $\sqrt{3}$. By assuming a uniform orientation and distance to the origin, we find a normalized probability of $1/2$. **Method 3**: A chord is uniquely defined by the orthogonal projection I of the circle center onto it. It has to lie inside the disc of radius $1/2$ in order to have a sufficient length. Assuming that I is uniformly distributed over the interior of the circle, the normalized probability is $1/4$.

are randomly distributed. Bertrand's paradox [Poincaré, 1912, Kendall and Moran, 1963] illustrate the fact that different notions of uniformity lead to different statistical results. The solution is to require the invariance of the uniform distribution under the action of a given group of transformation. For instance, in Fig. 2.1, the three solutions are invariant by rotation, but only the second one is invariant by the full rigid body transformations group. A direct application is the quantification of the false positives alarm in matching algorithms (Section 2.5).

The same type of paradox can be established for “distances” between features, which is one of the mostly used operations in image processing algorithms. Measuring the Euclidean distance between parameters in different charts (or representations) obviously leads to different results. Considering a true distance on the manifold (a symmetric positive definite bivariate function with the triangular inequality) allows to be independent of the chart, but is not sufficient to ensure the stability of the results with respect to a change of the reference frame of the physical space (the action of a transfor-

mation on our features). Once again, the solution we suggested in [Pennec and Ayache, 1998] was to choose a distance which is invariant under the action of a given group of transformation. Under some specific conditions detailed in [Pennec and Ayache, 1998], such an invariant distance can be induced on the manifold by a left invariant distance on the transformation group.

2.1.2 Barycenters are not intrinsic

Last but not least, let us investigate the notion of a mean feature. For 3D rotations, we can for instance compute the mean rotation matrix $\underline{R} = \frac{1}{n} \sum_i R_i$, the mean quaternion $\underline{q} = \frac{1}{n} \sum_i q_i$ by using the unit quaternion representation, or the mean rotation vector $\underline{r} = \frac{1}{n} \sum_i r_i$. These three methods give different results: the two first are not even rotations and none of them is stable with respect to a change of reference frame. The definition of the mean should of course be independent of the chart used to represent the manifold. The main problem here is that the addition and multiplication by a scalar are operators that are only defined in a vector space (for instance in each chart). As they are not intrinsic to our manifold, their result will inevitably change with the chart used. Similarly, we cannot generalize the standard statistical expectation operator $\bar{x} = \int x dP(x)$ to manifolds since an integral is a linear operator, and there is no such things as linearity in manifolds. Thus, a new definition of mean is needed, which implies revisiting an important part of the theory of statistics. We were among the very first in 1996 [Pennec and Ayache, 1996, Pennec, 1996, Pennec and Ayache, 1998] to propose the use of the Fréchet expectation. This will be detail from a theoretical view point in Section 2.3. The basic idea is to change a closed form (the barycenter) into a minimization problem (the minimum of the variance, i.e. expected squared distance). Since the distance is intrinsic to the manifold, the result of the minimization is also intrinsic. This idea of redefining values through the minimization of intrinsic quantities turned out to be one of the most powerful for developing a computational framework on manifolds Section 3.1.3 will focus on how to choose the metric for the important classes of Lie groups and homogeneous manifolds, with a practical example on 3D rotations. Last but not least, Section 2.5 will present application examples in computer vision with the generalization of several matching algorithms to noisy geometric features.

2.2 A Riemannian computing framework

Based on group and invariance properties, we developed in [Pennec and Thirion, 1997] a statistical estimation and optimization framework for rotations and rigid body motions where composition and inversion replaced addition and subtraction. Using the idea of the Fréchet mean, we were able to reshape that framework in an intrinsic way and to extend it to more general Lie groups in [Pennec, 1996]. To work on features that do not belong a Lie groups, we investigated homogeneous manifolds (manifolds on which a transformation group act transitively, i.e. where there always exists a transformation that transforms any given point to any other given point of the manifold) [Pennec, 1996, Chapter 6].

In both cases, the geometric invariance properties were incidentally providing an (invariant) Riemannian metric, that was in turn used to define geodesics and other notions. In 1997, it became clear that both frameworks could be merged and reformulated only on the basis of a Riemannian

metric, the invariance properties being only used to determine a consistent (Riemannian) metric. Moreover, Riemannian manifolds include a much larger set of manifolds, and in particular quite general curves and surfaces. This gives to the computing framework a much larger range of applications. However, if all the ideas were in place at that time [Penec, 1999], the conditions under which the variance was differentiable were remaining obscure, and the gradient of the variance was needed in order to justify the gradient descent algorithm that we proposed to compute the Fréchet mean. The generalization (to the non compact case with arbitrary distributions) of a first proof of the differentiability of the variance (for the uniform distribution on compact manifolds) proposed by [Maillot, 1997] considerably delayed the proposal of the general Riemannian framework [Penec, 2006a].

We summarize below the basic elements of Riemannian geometry that are needed before turning in Section 2.3 on the statistical computing framework itself. The interested reader may refer to [do Carmo, 1992] for a more complete but still affordable presentation of Riemannian geometry and to [Spivak, 1979, chap. 9] and [Klingenberg, 1982, Gallot et al., 1993] for more details.

2.2.1 Riemannian geometry

A *Riemannian metric* on a manifold \mathcal{M} is a continuous collection of scalar products on the tangent space at each point of the manifold. Thus, if we consider a curve on the manifold, we can compute at each point the norm of the speed vector (the instantaneous speed). To compute the length of the curve, we then proceed as usual by integrating this value along the curve. The distance between two points of a connected Riemannian manifold is the minimum length among the curves joining these points. The curves realizing this minimum for any two points of the manifold are called geodesics. The calculus of variations shows that geodesics are the solutions of a system of second order differential equations depending on the Riemannian metric. In our framework, we assumed that the manifold is *geodesically complete*, i.e. that the definition domain of all geodesics can be extended to \mathbb{R} . This means that the manifold has no boundary nor any singular point that we can reach in a finite time. As an important consequence, the Hopf-Rinow-De Rham theorem states that there always exists at least one minimizing geodesic between any two points of the manifold (i.e. whose length is the distance between the two points). In our statistical computing framework, we will implicitly assume that the manifolds are geodesically complete. The impact of removing this assumption is not completely clear yet.

2.2.2 Exponential chart

Let x be a point of the manifold that we consider as a local reference and $\vec{x}y$ a vector of the tangent space $T_x\mathcal{M}$ at that point. From the theory of second order differential equations, we know that there exists one and only one geodesic starting from that point with this tangent vector. This allows to develop the manifold in the tangent space along the geodesics (think of rolling a sphere along its tangent plane at a given point). The geodesics going through the reference point are transformed into straight lines and the distance along these geodesics is conserved (at least in a neighborhood of x).

The function that maps to each vector $\vec{x}y \in T_x\mathcal{M}$ the point y of the manifold that is reached after a unit time by the geodesic starting at x with this tangent vector is called the *exponential*

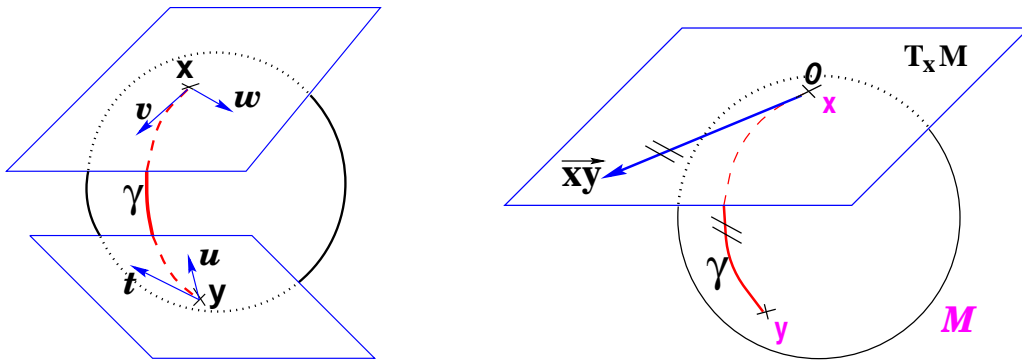


Figure 2.2: **Left:** The tangent planes at points x and y of the sphere \mathcal{S}_2 are different: the vectors v and w of $T_x\mathcal{M}$ cannot be compared to the vectors t and u of $T_y\mathcal{M}$. Thus, it is natural to define the scalar product on each tangent plane. **Right:** The geodesics starting at x are straight lines in the exponential map and the distance along them is conserved.

map. This map is defined in the whole tangent space $T_x\mathcal{M}$ (since the manifold is geodesically complete) but it is generally one-to-one only locally around 0 in the tangent space (i.e. around x in the manifold). In the sequel, we denote by $\overrightarrow{xy} = \log_x(y)$ the inverse of the exponential map: this is the smallest vector such that $y = \exp_x(\overrightarrow{xy})$. If we look for the maximal definition domain, we find out that it is a star-shaped domain delimited by a continuous curve C_x called the *tangential cut-locus*. The image of C_x by the exponential map is the cut locus \mathcal{C}_x of point x . This is the closure of the set of points where several minimizing geodesics starting from x meet. On the sphere $\mathcal{S}_2(1)$ for instance, the cut locus of a point x is its antipodal point and the tangential cut locus is the circle of radius π . It becomes much more complex on the ellipsoid.

The exponential map within this domain realizes a chart called *the exponential chart*. It covers all the manifold except the cut locus of the reference point x , which has a null measure. In this chart, geodesics starting from x are straight lines, and the distance from the reference point are conserved. This chart is somehow the “most linear” chart of the manifold with respect to the reference point x .

2.2.3 A practical computing framework

In fact, most of the usual operations using additions and subtractions may be reinterpreted in a Riemannian framework using the notion of *bipoint*, an antecedent of vector introduced during the 19th Century. Indeed, one defines vectors as equivalent classes of bipoints (oriented couples of points) in a Euclidean space. This is possible because we have a canonical way (the translation) to compare what happens at two different points. In a Riemannian manifold, we can still compare things locally (by parallel transportation), but not any more globally. This means that each “vector” has to remember at which point of the manifold it is attached, which comes back to a bipoint.

However, one can also see a vector \overrightarrow{xy} (attached at point x) as an element of the tangent space at that point. Such a vector may be identified to a point on the manifold using the geodesic starting at x with tangent vector \overrightarrow{xy} , i.e. using the exponential map: $y = \exp_x(\overrightarrow{xy})$. Conversely, the logarithmic map may be used to map almost any bipoint (x, y) into a vector $\overrightarrow{xy} = \log_x(y)$ of $T_x\mathcal{M}$. This reinterpretation of addition and subtraction using logarithmic and exponential maps

is very powerful to generalize algorithms working on vector spaces to algorithms on Riemannian manifolds, as illustrated by Table 2.1. It is also very powerful in terms of implementation since we can practically express all the geometric operations in these terms: the implementation of \log_x and \exp_x is the basis of any programming on Riemannian manifolds, as we will see in the following.

	Vector space	Riemannian manifold
Subtraction	$\vec{xy} = y - x$	$\vec{xy} = \log_x(y)$
Addition	$y = x + \vec{xy}$	$y = \exp_x(\vec{xy})$
Distance	$\text{dist}(x, y) = \ y - x\ $	$\text{dist}(x, y) = \ \vec{xy}\ _x$
Mean value (implicit)	$\sum_i \vec{xx}_i = 0$	$\sum_i \log_{\bar{x}}(x_i) = 0$
Gradient descent	$x_{t+\varepsilon} = x_t - \varepsilon \nabla C(x_t)$	$x_{t+\varepsilon} = \exp_{x_t}(-\varepsilon \nabla C(x_t))$
Linear (geodesic) interpolation	$x(t) = x_1 + t \vec{x_1x_2}$	$x(t) = \exp_{x_1}(t \vec{x_1x_2})$

Table 2.1: Re-interpretation of basic standard operations in a Riemannian manifold.

2.3 Simple statistics on Riemannian manifolds

Statistical analysis on manifolds is a relatively new domain at the confluence of several mathematical and application domains. Its goal is to study statistically geometric objects living in differential manifolds. Directional statistics [Bingham, 1974, Jupp and Mardia, 1989, Kent, 1992, Mardia, 1999] provide a first approach to statistics on manifold. As the manifolds considered here are spheres and projective spaces, the tools developed were mostly *extrinsic*, i.e. relying on the embedding of the manifold in the ambient Euclidean space. More complex objects are obtained when we consider the “shape” of a set of k points, i.e. what remains invariant under the action of a given group of transformation (usually rigid body ones or similarities). The statistics on these shape spaces [Kendall, 1989, Dryden and Mardia, 1991, Le and Kendall, 1993, Small, 1996] raised the need for intrinsic tools. In these works, the link between the tools developed, the metric used and the space structure is not always very clear.

Another mathematical approach was provided by the study of stochastic processes on Lie groups. For instance, [Grenander, 1963] derived central limit theorems on different families of groups and semi-groups with specific algebraic properties. Since then, several authors in the area of stochastic differential geometry and stochastic calculus on manifolds proposed results related to mean values [Karcher, 1977, Kendall, 1991, Emery and Mokobodzki, 1991, Arnaudon, 1995, Picard, 1994, Darling, 1996]. On the applied mathematics and computer science side, people get interested in computing and optimizing in specific manifolds, like rotations and rigid body transformations [Pennec et al., 1998, Grenander et al., 1998, Pennec, 1998a, Gramkow, 2001, Moakher, 2002], Stiefel and Grassmann manifolds [Edelman et al., 1998], etc.

Over the last years, several groups attempted to federate some of the above approaches in a general statistical framework, with different objectives in mind. For instance, the aim of the theory of statistical manifolds [Amari, 1990, Oller and Corcuera, 1995] is to provide a Riemannian structure to the space of parameters of statistical distribution. In this spirit, [Hendricks, 1991,

Oller and Corcuera, 1995] characterized the performances of some statistical parametric estimators in manifolds like the bias and the mean square error. [Hendricks, 1991] considered extrinsic statistics, based on the Euclidean distance of the embedding space, while [Oller and Corcuera, 1995] considered the intrinsic Riemannian distance, and refined the Cramer-Rao lower bound using bounds on the sectional curvature of the manifold. In [Bhattacharya and Patrangenaru, 2002, Bhattacharya and Patrangenaru, 2003], the authors focused on the asymptotic consistency properties of the extrinsic and intrinsic means and variances for large sample sizes, and were able to propose a central limit theorem for flat manifolds.

In view of computer vision and medical image analysis applications, our concern was quite different [Pennec, 1999, Pennec, 2006a]: we aimed at developing computational tools that can consistently deal with geometric features, or that provide at least good approximations. As we often have few measurements, we were interested in small sample sizes rather than large one, and we preferred to obtain approximations rather than bounds on the quality of the estimation. Thus, one of our special interest was to develop Taylor expansions with respect to the variance, in order to evaluate the quality of the computations with respect to the curvature of the manifold.

In [Bhattacharya and Patrangenaru, 2002, Bhattacharya and Patrangenaru, 2003, Oller and Corcuera, 1995] as well as in our work, the chosen framework is the one of geodesically complete Riemannian manifolds, which appears to be powerful enough to support an interesting theory. To ensure a maximal consistency of the theory, we chose to rely only on intrinsic properties of the Riemannian manifold, thus excluding methods based on the embedding of the manifold in an ambient Euclidean space.

2.3.1 Measures and expectation of observables

As any metric in a Euclidean space, the Riemannian metric $G(x)$ induces an infinitesimal volume element $d\mathcal{M}(x) = \sqrt{\det(G(x))} dx$ in any chart (the volume of the parallelepiped spanned by the vectors of an orthonormal basis of the tangent space). The difference is that the measure is now different at each point since the local expression of the metric G is changing. The measure $d\mathcal{M}$ on the manifold that can be used as a reference to measure random events on the manifold and to define their *probability density function* (if it exists), i.e. the function $p(x)$ on the manifold such that $dP(x) = p(x) d\mathcal{M}(x)$. This pdf is intrinsic because it does not depend on the chart used, contrarily to the expression in any chart with respect to the Lebesgue measure $dP(x) = p(x) \sqrt{\det(G(x))} dx$ which depends on the local expression of the metric.

It is worth noticing that the induced measure $d\mathcal{M}$ represents the notion of *uniformity* according to the chosen Riemannian metric. This automatic derivation of the uniform measure from the metric gives a rather elegant solution to the Bertrand paradox for geometric probabilities that we considered in introduction.

With the probability measure of a random element, we can integrate functions $\phi(x)$ from the manifold to any vector space, thus defining the expected value of this function:

$$\mathbf{E}[\phi(\mathbf{x})] = \int_{\mathcal{M}} \phi(x) dP(x) = \int_{\mathcal{M}} \phi(x) p(x) d\mathcal{M}(x)$$

This notion of expectation corresponds to the one we defined on real random variables and vectors. However, we cannot directly extend it to define the mean value of the distribution since we have no

way to generalize this integral in \mathbb{R} into an integral with value in the manifold.

2.3.2 Riemannian center of mass

As one cannot define the mean or expected “value” of a random manifold element using a weighted sum or an integral as usual, several alternative definitions based on properties on the usual mean were proposed (see [Picard, 1994] and [Penec, 2006a, Sec. 4.3] for a review). The most interesting ones for general geodesically complete Riemannian manifolds were proposed by Fréchet, Karcher and Emery.

[Fréchet, 1944, Fréchet, 1948] proposed to define the mean as the set of points realizing the global minimum of the variance $\sigma_{\mathbf{x}}^2(y) = \mathbf{E} [\text{dist}(\mathbf{x}, y)^2]$ in metric spaces. Following the same principle, one can define the *deviation at order α* as $\sigma_{\mathbf{x},\alpha}(y) = (\mathbf{E} [\text{dist}(y, \mathbf{x})^\alpha])^{1/\alpha}$ and call *central points at order α* its minimizers. For instance, the *modes*, i.e. the points where the intrinsic density is locally maximum on the manifold, are obtained for $\alpha = 0$. The *median point* is obtained for $\alpha = 1$. For $\alpha \rightarrow \infty$, we obtain the “barycenter” of the distribution support (which has to be compact).

As the Fréchet mean is the result of a minimization, existence and uniqueness are not ensured. This has to be compared with some central values in vector spaces, for instance the modes. However, one only keeps the global modes here. To get rid of this constraint, [Karcher, 1977] proposed to consider the *local* minima of the variance instead of the global ones. We call these new set of means *Riemannian centers of mass*. Using this extended definition, [Karcher, 1977] and [Kendall, 1990] were able to establish existence and uniqueness theorems for distributions with a compact and small enough support. These theorems were extended by [Darling, 1996] to distributions with non-compact support in a very specific class of manifolds that includes the Hadamard manifolds¹ whose curvature is bounded from below. This does not include rigid body transformations, but this includes the manifold of tensors (Chap. 3).

[Emery and Mokobodzki, 1991] proposed to use the *exponential barycenters*, i.e. the points at which the mean is null in the local exponential chart : $\int_M \overrightarrow{xy} dP(y) = 0$. If the support of the distribution is included in a *strongly convex open set*², he showed that the exponential barycenters were the critical points of the variance. They are thus a superset of the Riemannian centers of mass that include themselves the Fréchet means. However, the notions are generally different for distributions with a larger support.

[Picard, 1994] realized a good synthesis of most of these notions of mean value and show that the definition of a “barycenter” (i.e. a mean value) is linked to a connector, which determines itself a connection, and thus possibly a metric. An interesting property brought by this formulation is that the distance between two barycenters (with different definitions) is of the order of $O(\sigma_{\mathbf{x}})$. Thus, for sufficiently concentrated random points, all these values are close.

2.3.3 An algorithm to compute the mean

To compute the Riemannian center of mass, the idea is to use a gradient descent algorithm. Thus, we have to compute the derivative of the variance. However, one cannot use the Lebesgue theorem

¹Simply connected and complete manifolds with non-positive sectional curvature

²Here, strongly convex means that for every two points there is a unique minimizing geodesic joining them that depend in a C^∞ of the two points.

to differentiate under the sum because the integration domain depends on the derivation point through its cut locus, unless there is no cut locus or the distribution has a sufficiently small compact support that does not intersect it, which was one of the properties used for the previous existence, uniqueness and equivalence theorems. It took me several years to generalize in [Pennec, 2006a] a differentiability proof of Pr Maillot [Maillot, 1997] originally designed for the uniform distribution on compact manifolds.

The theorem we obtain is that the variance is differentiable (if it is finite) at the points where the cut locus has a null probability measure. At such a point, it has the following gradient: $(\text{grad } \sigma^2)(y) = -2 \int_{\mathcal{M}} \vec{y}\vec{z} dP(z)$. When we have a measurable mass on the cut-locus, the right hand side of this equation is obviously not defined: the variance is continuous but can have a sharp extremum (most probably a maximum).

Thus, the extrema of σ^2 are exponential barycenters or points with $P(C(y)) > 0$. Similar results have been derived independently in [Oller and Corcuera, 1995], where it is assumed that the probability is dominated by the Riemannian measure (which explicitly excludes point-mass distributions and the case $P(C(y)) > 0$), and in [Bhattacharya and Patrangenaru, 2002, Bhattacharya and Patrangenaru, 2003] for simply connected Riemannian manifolds with non-positive curvature. Our proof extends this result to any kind of manifold. Basically, the characterization of the Riemannian center of mass is the same as in Euclidean spaces if the curvature of manifold is non-positive (and bounded from below), in which case there is no cut-locus. If the sectional curvature becomes positive, a cut locus may appear, and a non-zero probability on this cut-locus induces some discontinuities in the first derivative of the variance. This corresponds to something like a Dirac measure on the second order derivative, which is an additional difficulty to compute the Hessian matrix of the variance on these manifolds.

To effectively compute the mean, we proposed in [Pennec, 1996, Pennec, 1998a] a Gauss-Newton gradient descent algorithm on rotations and rigid-body motions. This algorithm was readily extended to general Riemannian manifolds in [Pennec, 1999, Pennec, 2006a] by approximating the variance using the following Taylor expansion in a normal coordinate system for a vector $v \in T_y\mathcal{M}$:

$$\sigma^2(\exp_y(v)) = \sigma^2(y) + \text{grad } \sigma^2(v) + \frac{1}{2}\text{Hess } \sigma^2(v, v) + O(\|v\|_y^2)$$

The Hessian is in fact the differential of the gradient $(\text{grad } \sigma^2)(y) = -2 \int_{\mathcal{M}} \vec{y}\vec{z} dP(z)$. As we explain above, there is a problem due to the cut locus. However, one can split the integral into one part that does not take into account the cut locus, which gives us a perfect positive definite matrix (2 times the identity), and one part that account for the cut locus, which can be expressed using integrals of Jacobi fields [Karcher, 1977]. For a toy example on the circle, see also [Pennec, 2006a]. Deliberately neglecting this second term gives us a perfectly concave “second order approximation” with the following Gauss-Newton scheme

$$y_{t+1} = \exp_{y_t} (\mathbf{E} [\vec{y_t \mathbf{x}}])$$

This algorithm essentially alternates the computation of the barycenter in the exponential chart centered at the current estimation of the mean value, and a re-centering step of the chart at the point of the manifold that corresponds to the computed barycenter (geodesic marching step). We found that this algorithm was very efficient and typically converging in 5 to 10 iterations. Notice that it converges towards the real mean in a single step in a vector space.

2.3.4 Covariance and Mahalanobis distance

Once we have determined the mean value, the random feature may be represented in the exponential chart at that point as a random vector with null mean in a star-shaped domain. With this representation, there is no difficulty to define the covariance matrix and potentially higher order moments as multilinear forms in the tangent space:

$$\text{Cov}_{\mathbf{x}} = \mathbf{E} \left[\overrightarrow{\bar{x}} \overrightarrow{\bar{x}}^{\text{T}} \right] = \int_{\mathcal{M}} (\overrightarrow{\bar{x}}) (\overrightarrow{\bar{x}})^{\text{T}} dP(x)$$

As in a Euclidean space, the trace of this matrix (expressed in an orthogonal coordinate system for the local metric) is equal to the variance.

Based on this covariance matrix, we defined in [Pennec, 1996] the Mahalanobis distance between a random manifold element $\mathbf{x} \sim (\bar{x}, \text{Cov}_{\mathbf{x}})$ and a (deterministic) point \mathbf{y} as the anisotropic weighting of the distance between the deterministic feature to the mean using the inverse of the covariance matrix: $\mu_{\mathbf{x}}^2(\mathbf{y}) = \overrightarrow{\bar{x}} \mathbf{y}^{\text{T}} \text{Cov}_{\mathbf{x}}^{-1} \overrightarrow{\bar{x}} \mathbf{y}$. This statistical distance is very useful to normalize different measurements according to their expected uncertainty, especially in “anisotropic” cases, which often occur with geometric features (e.g. translation in millimeters and rotations in radians or degrees for rigid transformations).

Interestingly, the expected Mahalanobis distance of a random element with itself is independent of the distribution and is equal to the dimension of the manifold, as in the vectorial case [Pennec, 2006a]: $\mathbf{E} \left[\mu_{\mathbf{x}}^2(\mathbf{x}) \right] = n$.

2.3.5 Gaussian and χ^2 law

Several generalizations of the Gaussian distribution to Riemannian manifolds have already been proposed so far. In the stochastic calculus community, one usually consider the heat kernel $p(x, y, t)$, which is the transition density of the Brownian motion [Grenander, 1963, Emery, 1989, Grigor’yan, 2006]. This is the smallest positive fundamental solution to the heat equation $\frac{\partial f}{\partial t} - \Delta f = 0$, where Δ is the Laplace-Beltrami operator (i.e. the standard Laplacian with corrections for the Riemannian metric). On compact manifolds, an explicit basis of the heat kernel is given by the spectrum of the manifold-Laplacian (eigenvalues λ_i with associated eigenfunctions f_i solutions of $\Delta f = \lambda f$). However, the explicit computation of this spectrum is impossible but in very few cases [Gallot et al., 1993].

To obtain tractable formulas, several alternative distributions have been proposed in directional statistics [Bingham, 1974, Jupp and Mardia, 1989, Kent, 1992, Mardia, 1999, Mardia and Jupp, 2000], in particular the wrapped Gaussian distributions. The basic idea is to take the image by the exponential of a Gaussian distribution on the tangent space centered at the mean value (see e.g. [Mardia and Jupp, 2000] for the circular and spherical case). It is easy to see that the wrapped Gaussian distribution tends towards the mass distribution if the variance goes to zero. In the circular case, one can also show that it tends toward the uniform distribution for a large variance. [Oller and Corcuera, 1995] extended this definition by considering non-centered Gaussian distributions on the tangent spaces of the manifold in order to tackle the asymptotic properties of estimators. In this case, the mean value is generally not any more simply linked to the Gaussian parameters. In view of a computational theory, the main problem is that the pdf of the wrapped

distributions can only be expressed if there is a particularly simple geometrical shape of the cut-locus. For instance, considering an anisotropic covariance on the n -dimensional sphere leads to very complex calculations.

Instead of keeping a Gaussian pdf in some tangent space, we propose in [Penec, 2006a, Penec, 1999, Penec, 1996] a new variational approach which is consistent with the previous definitions of the mean and covariance. The property that we take for granted is that the Gaussian distribution maximizes the entropy among all distributions when we know the mean and the covariance matrix. In the Riemannian setting, we defined the intrinsic entropy as the expectation of the logarithm of the intrinsic pdf:

$$\mathbf{H}[\mathbf{x}] = - \int_{\mathcal{M}} \log(p(x)) p(x) d\mathcal{M}(x) = - \int_{\mathcal{M}} \log(p(x)) dP(x)$$

Our definition is consistent with the measure inherited from the Riemannian metric since the pdf that maximizes the entropy when we only know that the result is in a compact set \mathcal{U} is the uniform density in this set:

$$p_{\mathcal{U}}(x) = \mathbb{I}_{\mathcal{U}}(x) / \int_{\mathcal{U}} d\mathcal{M}(y)$$

We were able to show in [Penec, 2006a, Penec, 1999, Penec, 1996] that the intrinsic pdf maximizing this entropy knowing the mean \bar{x} and the covariance matrix Σ was a Gaussian distribution on the exponential chart centered at the mean point and truncated at the cut locus (if there is one)³ $N_{(\bar{x}, \Gamma)}(y) = k \exp\left(-\frac{1}{2} \bar{x} \vec{y}^T \Gamma \vec{x} \vec{y}\right)$. However, the relation between the concentration matrix (the “metric” Γ used in the exponential of the probability density function) and the covariance matrix Σ is slightly more complex than the simple inversion of the vectorial case, as it has to be corrected for the curvature of the manifold. Using a Taylor expansion of the Riemannian measure, we were able to provide computationally tractable approximations for any manifold in case of small variances: Let $r = i(\mathcal{M}, \bar{x})$ be the injectivity radius at the mean point, i.e. the shortest distance to the cut-locus (by convention $r = +\infty$ if there is no cut-locus). Assuming a finite variance for any concentration matrix Γ , we have the following Taylor expansions:

$$k = \frac{1 + O(\sigma^3) + \epsilon\left(\frac{\sigma}{r}\right)}{\sqrt{(2\pi)^n \det(\Sigma)}} \quad \text{and} \quad \Gamma = \Sigma^{(-1)} - \frac{1}{3} \text{Ric} + O(\sigma) + \epsilon\left(\frac{\sigma}{r}\right)$$

Here, $\epsilon(x)$ is a function that is a $O(x^k)$ for any positive k , with the convention that $\epsilon\left(\frac{\sigma}{+\infty}\right) = \epsilon(0) = 0^4$.

This family of distributions ranges from the point-mass distribution (for $\Gamma = \infty$) to the uniform measure (i.e. uniform density for compact manifolds) for a null concentration matrix. For some theoretical reasons (including the non-differentiability at the cut locus), this is probably not be the best generalization of the Gaussian. However, from a practical point of view, it provides effective and computationally tractable approximations for any manifold in case of small variances that we were not able to obtain from the other definitions.

³The definition domain of the exponential at the mean point has to be symmetric to obtain this result. This is the case in particular for symmetric spaces, i.e. a Riemannian spaces which metric is invariant under some symmetry.

⁴More precisely, this is a function such that $\forall k \in \mathbb{R}^+$, $\lim_{0^+} x^{-k} \epsilon(x) = 0$

Last but not least, we proposed a generalization of the χ^2 law to manifolds by considering the Mahalanobis distance of a normally distributed random feature. In the same conditions as for the Gaussian, we were able to show that it has the same density as in the vectorial case up to an order 3 in σ . This opens the way to the generalization of many other statistical tests, as we may expect similarly simple approximations for sufficiently centered distributions.

2.4 Example manifolds

In the Riemannian setting presented up to here, all definitions are derived from the Riemannian metric of the manifold. A natural question arising at that point is how to choose this metric? As suggested in Section 2.1, invariance properties provide a partial answer for connected Lie groups and homogeneous manifolds [Penec, 1996, Penec, 2004].

2.4.1 Invariant metrics on connected Lie groups

A Lie group is a differentiable manifold which has smooth compatible group operations. Thanks to this structure, there are two canonical ways to define a Riemannian metric in order to apply our statistical framework: we can go from the identity Id to any point g of the group by left or right composition: $g = g \circ Id = Id \circ g$. The differentials of these translations transport vectors from the tangent space at the identity to the tangent space at g , and can thus be used to transport any dot product $\langle \cdot | \cdot \rangle_{Id}$ given on the tangent at the identity to any point of the group, giving rise to left or right invariant metrics:

$$\langle v | w \rangle_g^L = \langle D_L(g)^{(-1)}.v | D_L(g)^{(-1)}.w \rangle_{Id} \quad \text{or} \quad \langle v | w \rangle_g^R = \langle D_R(g)^{(-1)}.v | D_R(g)^{(-1)}.w \rangle_{Id}$$

When the group is compact (for instance rotations), there exists a metric which is left and right invariant [Spivak, 1979, do Carmo, 1992] and the geodesics for this metric (starting from the identity) are also the one parameter sub-groups. This is not true any more for more general non compact groups (such as rigid transformations for instance): left and right invariant metrics are generally different, and lead to different geodesics. We will see later on that this is one of the main problems: they are only partially consistent with the group operations.

The uniform measures associated to these invariant metrics are the Haar measures of the group [Penec and Ayache, 1998], well known in geometric probabilities [Kendall and Moran, 1963, Matheron, 1975, Santalo, 1976]. Since the metric is left (resp. right) invariant, the geodesics are globally conserved by left (resp. right) translation and one can determine only the geodesics starting from the identity. Thus, the left (resp. right) translations and their differentials realize a mapping of exponential charts and allows us to identify the exponential chart at any point to the one at the identity.

From a computer science point of view, this means that we have only one chart to deal, instead of one at each point. This provides us with a particularly simple computational framework (which was in fact the first one I developed, see e.g. [Penec, 1996, Chapter 6]) where we only need to implement the exponential and logarithmic maps at the identity (called the principal chart), and the differential of the left (resp. right) translation. Whenever we need to compute at one point, the basic idea is to go back to the identity using left (resp. right) translation (or its differential for

tangent vectors), compute in the principal chart, and come back to the original point, still using left (resp. right) translation.

This scheme only need to be slightly modified to fit our general Riemannian computing framework: rather than translating back and forth before and after each operation, we may integrate this translation in the definition the exponential chart at each point. For instance, we obtain the left-invariant geodesic starting at x with tangent vector \overrightarrow{xy} as the left translation by x of the geodesic starting at the identity with the left translation by $x^{(-1)}$ of the tangent vector \overrightarrow{xy} :

$$\begin{aligned}\exp_x(\overrightarrow{xy}) &= x \circ \exp_{Id}(D_L(x^{-1}).\overrightarrow{xy}) \\ \overrightarrow{xy} = \log_x(y) &= D_L(x).\log_{Id}(x^{-1} \circ y) = D_L(x).\overrightarrow{(x^{-1} \circ y)}\end{aligned}$$

From a practical point of view, this means that we only need to determine the equations of the left- (or right-) invariant geodesics starting from the identity and to implement the mappings \exp_{Id} and \log_{Id} . Then, we automatically have the \exp_x and \log_x mappings at any point, and the power of our computational framework on manifolds. Of course, many algorithms can be implemented much more efficiently by expanding the formulas and simplifying the differentials. For instance, the Gauss-Newton algorithm for the left-invariant mean is simplified into $\bar{x}_{t+1} = \bar{x}_t \circ \exp_{Id}(\frac{1}{n} \sum \log_{Id}(\bar{x}_t^{-1} \circ x_i))$. This brings back to the invariant computational framework that we originally designed in [Pennec, 1996].

Actually, it has to be noticed that the equation of the geodesics are only needed for the sake of computational efficiency: geodesics are curves minimizing the distance but also the Riemannian energy (the integral of the squared speed) between two points. Thus computing $\overrightarrow{xy} = \log_x(y)$ may be posed as an optimal control problem [Kaya and Noakes, 1997, Allasonnière et al., 2005], and computing $\exp_x(v)$ as a numerical integration problem (see e.g. [Helmke and Moore, 1994, Hairer et al., 2002]). This opens the way to statistics interpolation, extrapolation and PDEs in more complex spaces than the one we considered up to now, like curves [Michor and Mumford, 2006, Klassen et al., 2004, Younes, 1998], surfaces, and diffeomorphic transformations.

For instance, the large deformation diffeomorphic metric mapping (LDDMM) method proposed for inter-subject image registration in computational anatomy [Beg et al., 2005, Miller et al., 2003, Miller and Younes, 2001, Joshi and Miller, 2000] finds the geodesic in the joint intensity and deformation space by minimizing the Riemannian length of the deformation for a given right-invariant metric. Through the so called EPDiff equation (Euler-Poincaré equation for diffeomorphisms), this optimization framework has been recently rephrased in an exponential/logarithm framework similar to the one developed here [Miller et al., 2006]. One additional complexity is that the space has an infinite number of dimensions, which forbids the use of some of the tools (for instance the generalized Gaussian distribution). However, simple statistics like the mean and the principal component analysis of a (finite) set of samples may still be computed [Vaillant et al., 2004]. There are also infinitely many left- or right-invariant metrics on diffeomorphisms, and I believe that choosing the ones that are adapted to the problem that we are investigating is also one of the key problem from the application point of view (see also 3.1.3).

2.4.2 Practical averaging of 3D rotations

Let us come back to a much more simple group: 3D rotations. This is the submanifold of 3x3 matrices that are orthogonal with a positive determinant and constitute a compact and connected Lie group with the matrix multiplication and inversion. Differentiating the orthogonality constraint $R.R^t = Id$, we can see that a tangent vector dR at R is characterized by $R.dR^t = -dR.R^t$, i.e. it is the left (or right) translation by R of a skew symmetric matrix. The tangent space at the identity is the space of skew-symmetric matrix. To define a metric on the rotation group, we can either consider the metric induced by the embedding in the vector space of matrices or chose a metric on the tangent space at the identity and propagate it to all other points by left or right translation.

In fact, as the 3D rotation group is compact, there exists a bi-invariant metric (which is moreover unique up to a scalar), and one easily verifies that it also corresponds to the metric induced by the standard Froebenius metric on matrices: Let dR_1 and dR_2 be tangent vectors at R . then $R^t.dR_1$ and $R^t.dR_2$ are tangent vectors at the identity. Taking the (half) Froebenius dot product at the identity $\langle A | B \rangle_{Id} = \frac{1}{2}\text{Tr}(A.B^t)$, one obtain a left-invariant dot product at R which is still the (half) Froebenius one:

$$\langle dR_1 | dR_2 \rangle_R = \langle R^t.dR_1 | R^t.dR_2 \rangle_{Id} = \frac{1}{2}\text{Tr}(dR_1.dR_2^t)$$

To determine the geodesics starting from the identity, one may rely on one-parameter subgroups (since the group is compact). These are rotation subgroups such that $R(s+t) = R(s).R(t) = R(t).R(s)$. It is well known that a 3D rotation can be characterized by an angle θ around a unit axis n , and that two rotation in general conditions commute if they have the same axis. This means that one parameter subgroups are the curves $R(t) = R(t.\theta, n)$, parameterized by the time t . The initial velocity is the skew-symmetric matrix dR such that for any vector v , $dR.v = \theta n \times v$. The projection of this tangent vector at identity in a minimal orthonormal basis gives the rotation vector $r = \theta.n$. For bi-invariant metrics, the Riemannian exponential map also corresponds to the Lie-group (here the matrix) exponential. In the case of 3D rotations, the power series defining the matrix exponential can be drastically simplified, leading to a very efficient computation thanks to Rodrigues' formula. Details about the numerical aspects can be found in [Pennec and Thirion, 1997, Pennec, 1996]. For higher dimensions, similar simplifications also exist but are harder to obtain [Gallier and Xu, 2002]. Finally, the length of the geodesics starting at identity is given by the angle of the rotation reached in a unit time. By invariance, the distance between any two rotations is thus given by the angle of the residual rotation $\text{dist}(R_1, R_2) = \theta(R_2^t.R_1)$.

As we will see in Section 3.2.3, averaging is the key for generalizing many algorithms to manifolds (interpolation, filtering, etc). In [Pennec, 1998a], we evaluated the computational and accuracy performances of three criteria to average elements on a Riemannian manifold: Least-squares corresponds to the Riemannian center of mass; weighted least-squares and least Mahalanobis distanced are the immediate generalization for heteroscedastic and anisotropic errors. The optimization was solved as before using a Gauss-Newton gradient descent and geodesic walking. We also proposed an estimation of the uncertainty of the resulting average using first order error propagation techniques. The method was exemplified on 3D rotations and other features like frames. Results showed that the accuracy prediction was statistically correct if there are enough features to estimate the noise level, and computations times where within 3 to 20 times the one for points. This showed the

efficiency of the computational framework.

Although this research report was not published as a journal paper, it is referred to by several authors as this was one of the first descriptions of a practical algorithm to obtain the Riemannian mean of 3D rotations. For instance [Gramkow, 2001], performed a comparative study of the accuracy and time performances of our intrinsic mean algorithm and the closed form solution obtained by minimizing more standard extrinsic least-squares criteria (e.g. minimizing the Euclidean norm between rotation matrices or unit quaternions). The intrinsic rotation averaging was rediscovered recently in applied mathematics [Moakher, 2002].

2.4.3 Limitations of invariant metrics

In [Pennec, 2004], we investigated how the statistical properties of random transformations were affected by the group operations. It turns out that if all operations are perfectly compatible with the left translation when we choose the left-invariant metric, things are getting more complex with respect to the right translation.

For instance, the (left-invariant) intrinsic pdf of the left translation of a random transformation \mathbf{f} is simply $p_{(h \circ \mathbf{f})}(g) = p_{\mathbf{f}}(h^{(-1)} \circ g)$ while we have to use the modulus⁵ $\Delta\mathcal{G}(g)$ of the group for the right translation: $p_{(\mathbf{f} \circ h)}(g) = \Delta\mathcal{G}(g \circ f_o^{(-1)}) / \Delta\mathcal{G}(g) \cdot p_{\mathbf{f}}(g \circ h^{(-1)})$. As the inversion permutes left and right⁶, the modulus also appear for the inversion of a random transformation $p_{\mathbf{f}^{(-1)}}(g) = \Delta\mathcal{G}(g^{(-1)}) \cdot p_{\mathbf{f}}(g^{(-1)})$. Interestingly, there is a simple expression for the pdf of the composition of two random transformations (thanks to the integration with the left Haar measure) that generalizes convolution product used for the addition of two random vectors: $p_{(\mathbf{f} \circ \mathbf{g})}(h) = \int_{\mathcal{G}} p_{\mathbf{f}}(k) \cdot p_{\mathbf{g}}(k^{(-1)} \circ h) \cdot d_L\mathcal{G}(k)$.

As far as the moments of the distribution are concerned, one easily show that the Riemannian mean for a left invariant metric is stable under left translation but *not* under the right translation and the inversion, unless the metric is also right invariant. We give in Fig. 2.3 a counter-example on 2D rigid transformations which shows that the empirical mean value of the inverse is generally not the inverse of the mean value. As we know that there is generally no left and right invariant metrics on a Lie group as soon as it is not compact [Arsigny et al., 2006e], this means that we cannot reach a fully consistent statistical computing framework on Lie groups with left- or right-invariant metrics. Even worse, one can show on the example of rigid body transformations that there is no Riemannian metric that could be completely compatible with all group operations [Zefran et al., 1999].

Thus, there is a need for new research to find the alternative to the Riemannian structure for Lie groups. Based on the results of [Swann and Olsen, 2003] for shapes, we began to investigate with V. Arsigny the idea on relying on one-parameter subgroups instead of geodesics. Preliminary results indicate that this may provide an interesting structure (see [Arsigny et al., 2006b, Arsigny et al., 2006a] and Section 4.3.6).

⁵The modulus quantifies the ratio between left and right Haar measures: $d_L\mathcal{G}(g) = \Delta\mathcal{G}(g) \cdot d_R\mathcal{G}(g)$.

⁶This remark is much more powerful than it appears at first sight. For instance, one may compute right invariant geodesics simply by taking the inverse of left-invariant ones.

A 2D rigid transformation f is characterized by an angle of rotation $\theta \in [-\pi; \pi[$ and a translation vector $t \in \mathbb{R}^2$. The composition of two transformations is given by:

$$f_1 \circ f_2 = \begin{cases} (\theta_1 + \theta_2) [2\pi] \\ R(\theta_1).t_2 + t_1 \end{cases} \quad \text{with} \quad R(\theta) = \begin{bmatrix} \cos \theta & \sin \theta \\ -\sin \theta & \cos \theta \end{bmatrix}$$

With an isotropic metric at identity, we obtain a flat left-invariant metric since the translation and rotation parts are not correlated in the differential of the left translation: $D_L(f) = \begin{bmatrix} 1 & 0 \\ 0 & R(\theta) \end{bmatrix}$. Thus, the Christoffel symbols vanish and the geodesics starting from 0 (the identity) are straight lines: our representation is the exponential chart at identity.

Now, let $f_1 = (\pi/4; -\sqrt{2}/2; \sqrt{2}/2)$, $f_2 = (0; \sqrt{2}; 0)$ and $f_3 = (-\pi/4; -\sqrt{2}/2; -\sqrt{2}/2)$ be three transformations. One easily verify that their barycenter is zero. Thus, $\bar{f} = (0; 0; 0) = \text{Id}$ is a Riemannian center of mass. In this case, this is the only one: $\mathbf{E}[\{f_1, f_2, f_3\}] = \{(0; 0; 0)\}$.

The inverse of these transformations is easy to compute: $f_1^{(-1)} = (-\pi/4; 0; -1)$, $f_2^{(-1)} = (0; -\sqrt{2}; 0)$ and $f_3^{(-1)} = (+\pi/4; 0; 1)$. This time, the barycenter $\bar{f}^{(-1)} = (0; -\sqrt{2}/3; 0)$ is null for the rotation part, but not for the translation: the mean value of the inverse transformations is not the identity: $\mathbf{E}[\{f_1^{(-1)}, f_2^{(-1)}, f_3^{(-1)}\}] \neq \mathbf{E}[\{f_1, f_2, f_3\}]^{(-1)}$.

Figure 2.3: Inconsistency of the left-invariant Riemannian mean and inversion in the 2D rigid transformation group.

2.4.4 Homogeneous manifolds

Another example of interesting spaces is given by manifolds on which acts a transformation group in a *transitive* way, i.e. such that there exists a transformation that can map any point to the any other point. In that case, one can identify the elements of the manifolds with subsets of the group. Let o be a particular point of the manifold that we call *the origin*. The set of transformations \mathcal{H} that leave the origin unchanged is called the *isotropy subgroup* or *stabilizer* of the origin. A left translation of the isotropy group is a set of transformations (which is generally not a subgroup) that map the origin to the same point, say x . These *cosets* and are in facts the elements of the quotient space \mathcal{G}/\mathcal{H} . As the action of the group is assumed to be transitive, all the points of the manifolds can be reached from the origin, which means that there is one (and only one) coset for each point: the manifold can identified to the quotient space $\mathcal{M} = \mathcal{G}/\mathcal{H}$.

This isomorphism is the basis of the properties of the homogeneous manifolds. For instance, an invariant distance can be induced on the manifold by the group distance under some specific conditions [Pennec and Ayache, 1998]. However, it is easier to define an invariant Riemannian metric by choosing a metric on the tangent space of the identity, and propagating it to the tangent space at the other points of the manifold using the group action. Obviously, the metric should be the same whatever transformation of each coset we take: this boils down to the invariance of the metric on the tangent space at the origin with respect to the isotropy group. This condition is actually necessary and sufficient (see [Pennec, 2004] for more details).

Notice that there does not always exists an invariant metric if the group is too large: take for instance points under the affine group. When the invariant metric exists, the induced measure is our invariant measure of [Pennec and Ayache, 1998]. However, the converse is false: there can be

an invariant measure with no invariant metric (e.g. the Lebesgue measure on points under the unimodular group).

Examples of homogeneous manifolds used in real applications of our framework are oriented or directed points [Granger et al., 2001, Granger and Pennec, 2002b] for representing surface elements (see below), or for the analysis of fracture geometry in rock mechanics [Rasouli, 2002]; quotient spaces of rigid body transformations (i.e. semi- or non-oriented frames where 2 (resp. 3) of the trihedron unit vectors are given up to their sign) to obtain the manifold of extremal points on smooth surfaces in 3D images [Pennec et al., 2000, Pennec et al., 1998]. More recently, the manifold of positive definite symmetric matrices (so-called tensors) took a particular importance for processing and analyzing diffusion tensor images [Batchelor et al., 2005, Fletcher and Joshi, 2004, Lenglet et al., 2006, Pennec et al., 2006], or to model the brain variability [Fillard et al., 2005c]. Tensor computing and its applications will be presented in more detail in the next chapter to illustrate further developments of the theory of statistical computing on manifolds.

2.4.5 Robust statistics using ϕ -connectors

In view of developing a statistical representation of surfaces based on unstructured sets of oriented points that could potentially explain the efficiency of tensor-voting techniques [Medioni et al., 2000], we investigated in [Granger and Pennec, 2002b] some robust statistics on directions and orientations. We considered more specifically M-estimators [Rousseeuw and Leroy, 1987] of the distance $d_\phi(x, y) = \phi(\text{dist}(x, y))$ with $\phi(0) = 0$ and $\dot{\phi}$ decreasing from 1 at zero while remaining non negatives. These conditions ensure that d_ϕ remains a distance which is equivalent to the Riemannian one for small distances, while giving less weight to points that are far away by tempering their distance.

When the original Riemannian distance is invariant, the robust metric is also invariant, but is not any more Riemannian. For instance, it can model extrinsic distances (like the Euclidean distance on unit vectors), as we will exemplify below. This lead in some cases to very efficient approximations of the Riemannian mean for sufficiently peaked distributions.

We showed in [Granger and Pennec, 2002b] that using such a ϕ -function amounts to replace the tangent vector \overrightarrow{xy} by the vector:

$$\psi(\overrightarrow{xy}) = \frac{\phi(\|\overrightarrow{xy}\|_x)}{\|\overrightarrow{xy}\|_x} \overrightarrow{xy} = \frac{\phi(\text{dist}(x, y))}{\text{dist}(x, y)} \overrightarrow{xy} = \overrightarrow{xy} + O(\|\overrightarrow{xy}\|^2)$$

This mappings constitute a (convex) connector in the sense of [Picard, 1994]: it formalizes a relationship between the manifold and its tangent space at point x , exactly in the way we used the exponential map of the Riemannian metric. Thus, we could think of defining mean values, higher order moments and other statistical operations by replacing everywhere the Riemannian logarithmic and exponential map with their ϕ -equivalent.

For instance, one can verify that $\|\psi(\overrightarrow{xy})\|_x = d_\phi(x, y)$. This show that the ϕ -variance of a random point $\sigma_\phi^2(x) = \mathbf{E} \left[d_\phi^2(\mathbf{y}, x) \right] = \int_{\mathcal{M}} \|\psi(\overrightarrow{xy})\|_x^2 dP(\mathbf{y})$ is properly defined. Likewise, one can define the ϕ -covariance $\Sigma_\phi(x) = \mathbf{E} \left[\psi(\overrightarrow{xy}) \cdot \psi(\overrightarrow{xy})^t \right]$, which trace is still equal to the ϕ -variance. Like in the Riemannian case, one can differentiate this ϕ -variance at the points where the cut-locus has a null probability measure (the same proof applies because the ϕ -distance is dominated by the Riemannian distance), and we obtain: $\text{grad } \sigma_\phi^2(x) = -2 \int_{\mathcal{M}} \dot{\phi}(\|\overrightarrow{xy}\|_x) \psi(\overrightarrow{xy}) dP(\mathbf{y})$.

This formula is interesting as it shows the limits of the equivalence of the results between the Riemannian and convex connectors: the ϕ -center of mass is a weighted barycenter both in the Riemannian and in the ϕ exponential charts, but it is generally different from the (unweighted) ϕ -exponential barycenter. With convex connectors, the different notions of means are not any more subsets of each others. However, there are interesting applications from a computational points of view.

Let us consider first the unit vectors (orientations) of \mathbb{R}^n . The Euclidean metric induces on the sphere \mathcal{S}_{n-1} a rotationally invariant Riemannian metric for which geodesics are great circles, and the distance between two unit vectors u and v is the angle $\theta = d(u, v) = \arccos(u^t \cdot v)$. The Euclidean metric $d_E(u, v) = \|u - v\|$ can be considered as a ϕ estimator with $\phi(\theta) = 2 \sin(\theta/2)$. With the help of a Lagrange multiplier, one easily compute that the extrinsic Euclidean mean is the renormalized Euclidean mean $\bar{u} = \int u dP(u) / \|\int u dP(u)\|$, which is thus a robust estimator or the Riemannian mean!

Another quite used encoding of the directions is the tensor $u \cdot u^t$, which may be seen as an immersion of the projective space \mathcal{P}_{n-1} into the vector space of $n \times n$ matrices (\mathbb{R}^{n^2}). With this embedding, the squared extrinsic Euclidean distance (renormalized to be consistent with the previous ones) is $d^2(u, v) = \frac{1}{2} \|u \cdot u^t - v \cdot v^t\|^2 = 1 - (u^t v)^2 = \sin^2(\theta)$. This is also a robust distance with $\phi(\theta) = \sin(\theta)$ (for $\theta \leq \pi$). In the tensor space, the encoding of a random direction is the random tensor $T_u = \mathbf{E} [u \cdot u^t]$. One should notice that the tensor has unit trace (by linearity since u has unit length), which gives in practice one degree of freedom that can be used for instance to encode for the probability of the position in fields of directions (e.g. in tensor voting). The mean direction is represented by the tensor $\bar{u} \cdot \bar{u}^t$ which is closest to T_u in the Euclidean sense: this is the eigenvector(s) of T_u corresponding to the largest eigenvalue. Even more, we were also able to show that the ϕ -covariance of the direction was given directly by the restriction of the tensor to the hyperplane orthogonal to the first eigenvector. Thus, the random tensor encodes not only for a robust estimation of the Riemannian mean but also for (an approximation) of the second order moments.

Simulations were run on a large number of cases to measure the relative accuracy of the vector and tensor estimations with respect to the Riemannian mean. Up to a variance of 20 degrees, the three methods have a similar accuracy and results are almost not distinguishable. Between 20 and 40 degrees of variance, the tensor estimation becomes different from the two others while keeping a comparable global accuracy. After 40 degrees, the accuracy of the tensor mean highly degrades and becomes useless (maximal errors are too large); the vector mean becomes different from the Riemannian means while keeping for a while a similar accuracy. These experiments showed a first example of extrinsic approximations that prove to be computationally more efficient than the Riemannian mean. However, the intrinsic theory is central to compare and to control the limits of these approximations.

Interestingly, a very similar analysis can be done with 3D rotations: one can also model two well known extrinsic methods to compute the mean as ϕ -connectors. The first method is to represent rotations using unit quaternions, and to compute the renormalized Euclidean mean on the sphere of unit quaternions. As rotation quaternions are defined up to their signs, one theoretically need to iterate this process and to re-orient the unit quaternions at each step in the hemisphere chosen to represent the mean in order to converge. This method amounts to consider the ϕ -distance

$d_{quat}(\theta) = 4 \sin(\theta/4)$. The second method is to average the rotation matrices directly in the 3×3 matrix space. Then, the mean is “renormalized” by looking for the rotation matrix which is closest to this result in the Euclidean matrix distance (Froebenius) sense. This can be easily realized using a SVD decomposition on the mean matrix. This method amounts to consider the ϕ -distance $d_{mat}(\theta) = 2 \sin(\theta/2)$.

Simulation experiments were performed for the two extrinsic methods by [D.W. Eggert, 1997] in a registration context, and later on for the mean with the three methods by [Gramkow, 2001]. Like for unit directions/orientations, they showed that estimation results were similar up to 40 degrees of variance in the input rotations. Once again, this shows that efficient approximations could be designed and used in practice, provided that we have a way to estimate their limits, which is one of the results of the theory of statistical computing on manifolds.

2.5 Applications in matching and registration

The first applications of the statistical framework that I considered were for recognition and registration. In computer vision, one often model the image information by a set of low level geometric features (e.g. corners or edge elements in 2D, crest lines and points in 3D [Pennec et al., 2000]). Due to occlusion and the appearance of multiple objects in a single image, one need to find the subset of features of a prototype object that are present in the image (up to a given transformation) in order to recognize it: one calls *recognition* the problem of finding subsets of corresponding features in two (or more) images. In this framework, *matching* corresponds to finding the individual correspondences between features while *registration* deals more with the computation of the transformation from matched features.

In the mid-nineties, most generic recognition algorithms developed in computer vision (Interpretation trees, Hough transform, Alignment, Geometric Hashing, ICP) were considering point features, and were not always properly taking into account measurement errors. In [Pennec, 1998b], we tackle the problem of generalizing these algorithms to more complex geometric features in a consistent statistical framework. The basic idea was to use a Riemannian distance (or a Riemannian Mahalanobis distance) and to find the matching between features and the transformation that minimizes the (squared) distance after transformation. Rewriting the algorithms based only on these notions was easy except for Geometric hashing that had to be converted into a geometric invariant indexing technique. In fact, it turned out that all these methods could be consistently described as algorithmic variants (with different search and pruning strategies) of the interpretation trees, which is basically an exhaustive search over the matches.

We also carefully investigated the effect of errors in measurements in the algorithms and the way to modify them in order to guaranty their correctness (controlled probability of false negative). The drawback is of course the presence of false positives. Thanks to our consistent statistical framework on geometric features, we were able to developed a new method to analyze the probability of false positives in two particular algorithms. More interestingly, we were able to generalize this analysis to evaluate the intrinsic complexity of the matching problem (i.e. the expected number of false positives, independently of the method used). Doing so, we showed that using more informative features (such as frames instead of points) can drastically reduce this probability. For instance, allowing a rotational error as large as 90 degrees on the trihedron allows to reject 80% of the false

matches between individual features (under a uniform assumption). Using a more realistic bound of 18 degrees (which corresponds to the $3\text{-}\sigma$ threshold for the crest points extracted in typical medical images [Pennec et al., 2000]) increases the rejection rate to 99.85%. We would have to divide the standard deviation of the point position by 10 to obtain an equivalent feature selectivity! Such a reduction of the intrinsic complexity of the problem allows to use lower-complexity matching methods. Typically, we reduced the complexity of the 3D rigid substructure matching problem from $O(n^4)$ to $O(n^2)$ by using frames instead of points [Pennec et al., 2000, Guéziec et al., 1997].

For a computational point of view, we identified two main problems in implementing these generic matching algorithms. The first one is theoretical and concerns the structure of the space invariants of n features (under the considered transformation group action). It can be formalized with the shape-space theory, but it would be interesting to go one step further and to characterize not only the manifold of invariants but also a suitable and consistent metric structure on it. The second problem is linked to the efficiency of the clustering of features on a manifold in the presence of heteroscedastic noises. This can also be related to the efficiency of searching for the nearest neighbor with respect to the Riemannian metric or the Mahalanobis distance. We have observed that hashing techniques raise some important problems because of the non-Euclidean underlying metric. These problems turn crucial with invariants of features with high dimension. There is perhaps a trade-off to find between adaptive space sampling and hashing methods.

When the matches between features are found, the registration problem consist in computing the geometric transformation that best superimpose them. In our Riemannian framework, considering a random Gaussian noise naturally lead to optimize a least squares or a least Mahalanobis criterion. We showed in [Pennec et al., 1998] that the first order error propagation tools could be easily generalized to manifolds in order to estimate the uncertainty of the transformation estimation at the optimum. The principle is simple: the transformation f realizing the optimum of the criterion is defined through the implicit function of the data $\Phi(T, \chi) = \partial C(T, \chi) \partial T = 0$. This minimum is well defined if the Hessian matrix $H = \partial \Phi(T, \chi) / \partial T$ has full rank. At the first order, errors on the data $\vec{\delta\chi}$ are tangent vectors to the data manifold at the observed data point. Likewise, the induced error on the transformation $\vec{\delta T}$ is a tangent vector to the transformation space. Thanks to the implicit function theorem we can relate both first order errors using: $\vec{\delta T} = (\partial \Phi(T, \chi) / \partial T)^{(-1)} \cdot \partial \Phi(T, \chi) / \partial \chi \cdot \vec{\delta\chi}$. In a Euclidean space this amounts to perform a Taylor expansion of $\Phi(T + \vec{\delta T}, \chi + \vec{\delta\chi})$. As we assumed a Gaussian noise on the data, the expectation of the transformation error is null and its covariance is

$$\text{Cov}_{TT} = \mathbf{E} \left[\vec{\delta T} \cdot \vec{\delta T}^T \right] = H^{(-1)} \cdot \frac{\partial \Phi(f, \chi)}{\partial \chi} \cdot \text{Cov}_{\chi\chi} \cdot \left(\frac{\partial \Phi(f, \chi)}{\partial \chi} \right)^T \cdot H^{(-1)}$$

In medical image analysis, selected applications cover the validation of the rigid registration accuracy for time series [Pennec et al., 1998] and multimodal MR-Ultrasound images [Roche et al., 2001]. We also applied this error propagation scheme to the certification of the 2D-3D rigid registration for the guidance of the therapeutic gesture using augmented reality [Nicolau et al., 2003b]. This will be detailed in Section 4.2.3.

Chapter 3

Manifold-valued images and tensors computing

The previous chapter showed that the Riemannian structure was powerful enough to support a consistent generalization of basic statistical notions. In this chapter, we show with the example of tensors that one can go one step further and generalize on the same Riemannian basis many important image processing algorithms like interpolation, diffusion and restoration of missing data (extrapolation). For instance, most interpolation and filtering methods can be reformulated using weighted means. The linear and non-linear diffusion schemes can be adapted to Manifolds through PDEs, provided that we take into account the variations of the metric.

Positive definite symmetric matrices (so-called tensors in the medical image analysis community) are nowadays common geometric data. They are used for instance to encode the covariance matrix of the Brownian motion (diffusion) [Basser et al., 1994, Le Bihan et al., 2001] (see also Sect. 3.3 below) or of the joint variability at different places (Green function) in shape variability analysis to characterize statistics on deformations (see Chap. 5). More generally, they are widely used in image analysis to guide the segmentation, grouping and motion analysis [Medioni et al., 2000, Weickert and Brox, 2002, Brox et al., 2004, Weickert and Hagen, 2006]. They are also appearing in many other application domains, for instance in numerical analysis where they are used to locally drive the size of the adaptive meshes for solving PDEs in 3D [Mohammadi et al., 1997]. Another example is found in the formation of echographic Doppler or radar images where Teoplitz Hermitian positive definite matrices uniquely characterized circular complex random processes with a null mean [Moran et al., 2005].

The measurements of these tensors is often noisy in real applications and we would like to perform estimation, smoothing and interpolation of fields of this type of features. The main problem is that the tensor space is a manifold that is not a vector space with the usual additive structure. As symmetric positive definite matrices constitute a convex half-cone in the vector space of matrices, convex operations (like the mean) are stable in this space. However, problems arise when estimating tensors from data (the standard linear estimation of DTI from diffusion weighted images leads to negative eigenvalues), or when smoothing fields of tensors with gradient descents: there is inevitably one point in the image where the time is not small enough and the results is out of the space (i.e. with a negative eigenvalue). Even when a spectral decomposition is performed to smooth independently the

rotation (eigenvectors basis trihedron) and eigenvalues [Tschumperlé, 2002, Chéfd’hotel et al., 2002], there is a continuity problem around equal eigenvalues. For instance one cannot find a locally consistent orientation rule for the principal eigenvectors of three tensors similarly elongated along the edges of an equilateral triangle.

To answer that problem, we proposed in [Pennec et al., 2006] to provide the space of tensors with a geodesically complete Riemannian metric, and to further develop the intrinsic computational framework on manifolds on that basis. The affine-invariant metric we proposed is detailed in Section 3.1.1. We demonstrate that it leads to a very regular manifold structure where tensors with null and infinite eigenvalues are both at an infinite distance of any positive definite symmetric matrix: the cone of positive definite symmetric matrices is replaced by a space of “constant” (homogeneous) non-scalar curvature without boundaries (null eigenvalues are at the infinity). Moreover, there is one and only one geodesic joining any two tensors, the mean of a set of tensors are uniquely defined, and we can even define globally consistent orthonormal coordinate systems of tangent spaces. Thus, the structure we obtain is very close to a vector space, except that the space is curved.

By trying to put a Lie group structure on the tensor manifold, Vincent Arsigny came out one year later with Log-Euclidean metrics [Arsigny et al., 2006d, Arsigny et al., 2006c, Arsigny et al., 2005a]. These metrics give a vector space structure to this manifold while keeping most of its interesting properties (Section 3.1.2), thus simplifying drastically the algorithms and speeding computations. Other non Riemannian metrics or parameterizations were also proposed. We briefly present them for completeness and we turn in Section 3.1.3 to an important question raised by all these possible choices: how to choose the metric depending on the nature and natural properties of the data that we need to process? A tentative application of our Riemannian metrics to structure tensors [Fillard et al., 2005a] showed for instance that there is no universal metric for a given manifold: there are different families of metrics different characteristics, and one may rely on one or the other depending on the specificities of the application.

The affine-invariant Riemannian metric was independently proposed by at least three other groups (see bibliography below) but was only used for computing means, covariance matrices and geodesic interpolation. We extended in [Pennec et al., 2006] our previous statistical tools into a complete computational framework on manifold-valued images by generalizing many important geometric data processing algorithms such as interpolation, filtering, diffusion and restoration of missing data. For instance, most interpolation schemes and Gaussian filtering can be tackled efficiently through a weighted mean computation. Linear and anisotropic diffusion schemes can be adapted to our Riemannian framework, through partial differential evolution equations, provided that the metric of the tensor space is taken into account. For that purpose, we provide intrinsic numerical schemes to compute the gradient and Laplacian operators. We detail these contributions in Section 3.2.

Section 3.3 finally presents an important application example of the Riemannian computing framework: the estimation and regularization of Diffusion Tensor MR Images (DTI), in view of the tracking of the white matter fibers within the brain [Fillard et al., 2006a, Fillard et al., 2005b]. Two other important application of tensor computing will be developed in Chapter 5 with the statistical modeling of the variability of the brain from a dataset of precisely delineated anatomical structures (sulcal lines) in the cerebral cortex [Fillard et al., 2005c], and from the deformation fields resulting from non-rigid registration algorithms (Riemannian Elasticity [Pennec et al., 2005b]).

3.1 Metrics on tensors

3.1.1 Affine invariant Riemannian metrics

From the theory presented in the previous chapter, we know how to work on homogeneous manifolds: the basic idea is to define a group action and to provide the space \mathcal{Sym}_n^+ of positive definite symmetric matrices (tensors) with an invariant Riemannian metric. In [Penne⁺ et al., 2006]¹, we considered the action $A \Sigma A^T$ of a matrix A of the linear group GL_n on a tensor Σ . This group action corresponds to the standard action of the affine group on the covariance matrix of a random variables in \mathbb{R}^n , hence the name of the metric.

Tangent vectors to tensors are simply symmetric matrices with no constraint on the eigenvalues. The group action naturally extends to them: if W is a tangent vector at Σ , then $A W A^T$ is a tangent vector at $A \Sigma A^T$. An affine-invariant dot product obviously verifies $\langle V | W \rangle_\Sigma = \langle A V A^T | A W A^T \rangle_{A \Sigma A^T}$. In particular, this should be true for the isotropy group of the identity (the linear transformations that leave the identity matrix unchanged: the rotation matrices). All the rotationally invariant dot products on symmetric matrices are given (up to a constant global multiplicative factor) by:

$$\langle V | W \rangle_{\text{Id}} = \text{Tr}(V W) + \beta \text{Tr}(V) \text{Tr}(W) \quad \text{with} \quad \beta > -\frac{1}{n}$$

where n is the dimension of the space. These metrics are derived from rotationally invariant norms $\|W\|^2$, which are quadratic forms on (symmetric) matrices. By isotropy, they can only depend on the matrix invariants $\text{Tr}(W)$, $\text{Tr}(W^2)$ and $\text{Tr}(W^3)$. However, as the form is quadratic in W , we are left only with $\text{Tr}(W)^2$ and $\text{Tr}(W^2)$ that can be weighted by α and β . One easily verifies that $\beta > -\alpha/n$ is a necessary and sufficient condition to ensure positive definiteness.

The metric at the identity can be transported at any point by the group action using the fact that the (symmetric) square root $\Sigma^{-1/2}$ is a transformation that brings Σ to the identity:

$$\langle V | W \rangle_\Sigma = \left\langle \Sigma^{-\frac{1}{2}} V \Sigma^{-\frac{1}{2}} \mid \Sigma^{-\frac{1}{2}} W \Sigma^{-\frac{1}{2}} \right\rangle_{\text{Id}} = \text{Tr}(V \Sigma^{-1} W \Sigma^{-1}) + \beta \text{Tr}(V \Sigma^{-1}) \text{Tr}(W \Sigma^{-1})$$

For $\beta = 0$, we retrieve the affine-invariant metric that was proposed in [Skovgaard, 1984, Förstner and Moonen, 1999, Bhatia, 2003, Fletcher and Joshi, 2004, Lenglet et al., 2006, Penne⁺ et al., 2006]. For $\beta = -1/(n+1)$, we find the metric that [Lovrić and Min-Oo, 2000] proposed by embedding the space of tensors of dimension n into the space of $n+1$ square matrices using homogeneous coordinates (this allows them to seamlessly take into account an additional point position for the mean of the Gaussian distribution), and by quotienting out $n+1$ dimensional rotations. The same trick could be used to embed tensors in the higher dimensional spaces of square matrices of dimension $n+p+1$, in which case one would obtain the invariant metric with $\beta = -1/(n+p+1)$. Interestingly, $-1/\beta = n+1$ is the first authorized integer to obtain a proper metric! In fact, one can show that all these metrics have the same connection, which means that they share the same geodesics, but distances along them are different: each exponential chart is globally the same but the orthonormal basis is different. From the connection, one can compute the curvature tensor of the manifold [Skovgaard, 1984]. It is the

¹We refer the reader to this paper for all the mathematical and technical details.

same for all affine-invariant metrics and one can show that the manifold has a non positive and bounded sectional curvature. Thus, it is Hadamard manifold, i.e. a kind of hyperbolic space in which we have for instance the existence and uniqueness of the mean. There is also no cut-locus, which simplifies the computations.

To find the geodesic without going through the computation of Christoffel symbols, we may rely on a result from differential geometry [Gamkrelidze, 1991, Helgason, 1978, Kobayashi and Nomizu, 1969] which says that the geodesics for the invariant metrics on affine symmetric spaces are generated by the action of the one-parameter subgroups of the acting Lie group. As the one parameter subgroups of the linear group are given by the matrix exponential, the geodesics starting from the identity are $\Gamma_{(\text{Id}, W)}(t) = \exp(t W)$. Other geodesics are obtained by translation using group elements. From the equations of the geodesics, one finally obtains the Riemannian exponential map at each point, which can be inverted to obtain the logarithmic map:

$$\exp_{\Sigma}(W) = \Sigma^{\frac{1}{2}} \exp\left(\Sigma^{-\frac{1}{2}} W \Sigma^{-\frac{1}{2}}\right) \Sigma^{\frac{1}{2}} \quad \text{and} \quad \log_{\Sigma}(\Lambda) = \Sigma^{\frac{1}{2}} \log\left(\Sigma^{-\frac{1}{2}} \Lambda \Sigma^{-\frac{1}{2}}\right) \Sigma^{\frac{1}{2}}.$$

The Riemannian distance is obtained by integration, or more easily by the norm of the initial tangent vector of the geodesic joining the two points:

$$\text{dist}^2(\Sigma, \Lambda) = \|\log_{\Sigma}(\Lambda)\|_{\Sigma}^2 = \text{Tr}\left(\log(\Sigma^{-\frac{1}{2}} \Lambda \Sigma^{-\frac{1}{2}})^2\right) + \beta \text{Tr}\left(\log(\Sigma^{-\frac{1}{2}} \Lambda \Sigma^{-\frac{1}{2}})\right)^2$$

It is worth noticing that tensors with null eigenvalues are at an infinite distance of any regular tensor, as are tensors with infinite eigenvalues: the original cone of positive definite symmetric matrices, a linear manifold with a flat but incomplete metric (there is a boundary at a finite distance) has been changed into a regular and complete (but curved) manifold with an infinite development in each of its $n(n+1)/2$ directions.

The idea of the invariant metric came to my mind during the IPMI conference in 2001 as an application to diffusion tensor imaging (DTI) of the statistics on Riemannian manifolds. However, this idea was not exploited until the end of 2003, when the visit of P. Thompson (UCLA, USA) raised the need to interpolate tensors that represent the variability from specific locations on sulci to the whole volume (see section 5.2). The expertise of Pierre Fillard on DTI [Fillard et al., 2003b] provided an ideal alternative application field.

From an historical point of view, the affine-invariant Riemannian metrics may be traced back to the work of [Nomizu, 1954] on affine invariant connections on homogeneous spaces. It is implicitly hidden under very general theorems on symmetric spaces in many differential geometry textbooks [Kobayashi and Nomizu, 1969, Helgason, 1978, Gamkrelidze, 1991].

The simplest affine-invariant metric (with $\beta = 0$) is considered as a well known result in mathematics [Bhatia, 2003]. An implicit form was introduced in [Helmke and Moore, 1994] for developing flows and dynamic systems on the space of symmetric matrices. The corresponding integrator (which corresponds to a geodesic walking with this Riemannian metric) was used for the anisotropic regularization of diffusion tensor images in [Chefd'hotel et al., 2004] and [Bierkens, 2004]. In this last work, the closed form expression of the metric was known but was only used to derive the flow as in [Chefd'hotel et al., 2004] without consistency on the norm of the gradient of the tensor field. In statistics, it has been introduced as the Fisher information metric to model the geometry of the multivariate normal family [Burbea and Rao, 1982, Skovgaard, 1984, Calvo and Oller, 1991].

Closer to our domain, the same invariant metric has been independently proposed by [Förstner and Moonen, 1999] to deal with covariance matrices, by [Fletcher and Joshi, 2004] for the analysis of principal modes of sets of diffusion tensors and by [Moakher, 2005] for its mathematical properties which were exploited in [Batchelor et al., 2005] for a new anisotropic DTI index. By looking for a suitable metric on the space of Gaussian distributions for the segmentation of diffusion tensor images, [Lenglet et al., 2004, Lenglet et al., 2006] also end-up with the same metric. It is interesting to see that completely different approaches, relying on an affine-invariant requirement on the one hand, and relying on an information measure to evaluate the distance between distributions on the other hand, lead to the same metric on the tensor space.

3.1.2 Log-Euclidean metrics

By trying to put a Lie group structure on the space of Tensors, Vincent Arsigny observed that the matrix exponential was a diffeomorphism from the space of symmetric matrices to the tensor space [Arsigny et al., 2006c, Arsigny et al., 2005b]. Thus, one can seamlessly transport all the operations defined in the vector space of symmetric matrices to the tensor space!

For instance, one defines a commutative product (the log-product) by $\Sigma_1 \diamond \Sigma_2 = \exp(\log(\Sigma_1) + \log(\Sigma_2))$. This gives a commutative group structure to the tensors, for which any metric at the tangent space at the identity is extended into a bi-invariant Riemannian metric on the manifold (left and right translation are identical since the group is commutative):

$$\langle V | W \rangle_{\Sigma} = \langle D \log(\Sigma)(V) | D \log(\Sigma)(W) \rangle_{\text{Id}} = \langle \partial_V \log(\Sigma) | \partial_W \log(\Sigma) \rangle_{\text{Id}}.$$

For such a metric, geodesics are translations of one-parameter subgroups (which are given by the matrix exponential): $\Gamma_{(\Sigma, W)}(t) = \exp(\log(\Sigma) + tW)$. One can see that geodesics going through the identity are the same as for the affine-invariant metrics, but this is not true any more in general at other points of the manifold. From the geodesics one can easily get the Riemannian exponential and logarithmic maps at any point:

$$\exp_{\Sigma}(W) = \exp(\log(\Sigma) + \partial_W \log(\Sigma)) \quad \text{and} \quad \log_{\Sigma}(\Lambda) = D \exp(\log(\Sigma)) (\log(\Lambda) - \log(\Sigma))$$

These formula look complex. However, they are in fact nothing but the transport of the addition and subtraction through the exponential of symmetric matrices. The only difficulty here is to compute the differential of the matrix exponential and logarithm in order to transport tangent vectors from one space to another. It turns out that these differentials can be computed in closed form [Pennec et al., 2005b].

Log-Euclidean metrics are intrinsically invariant by a change of scale and by inversion. Moreover, by choosing the scalar product invariant by rotation at the identity (i.e. $\|W\|_{\text{Id}}^2 = \text{Tr}(W^2) + \beta \text{Tr}(W)^2$ with $\beta > -1/n$ as above), we get all the similarity invariant log-Euclidean metrics:

$$\text{dist}_{LE}^2(\Sigma_1, \Sigma_2) = \|\log(\Sigma_1) - \log(\Sigma_2)\|_{\text{Id}}^2 = \text{Tr}((\log(\Sigma_1) - \log(\Sigma_2))^2) + \beta \text{Tr}(\log(\Sigma_1) - \log(\Sigma_2))^2$$

By adding the logarithmic scalar multiplication $\lambda \star \Sigma = \exp(\lambda \log(\Sigma)) = \Sigma^{\lambda}$, we get a complete structure of vector space on tensors. This means that most of the operations that were generalized

using minimizations for the affine-invariant metric do have a closed-form with a log-Euclidean metric. For instance, the log-Euclidean mean is simply:

$$\bar{\Sigma}_{LE} = \exp \left(\frac{1}{n} \sum_i^n \log(\Sigma_i) \right)$$

while the affine-invariant mean is obtain through the iterative algorithm:

$$\bar{\Sigma}_{t+1} = \bar{\Sigma}_t^{\frac{1}{2}} \exp \left(\frac{1}{n} \sum_{i=1}^n \log \left(\bar{\Sigma}_t^{-\frac{1}{2}} \Sigma_i \bar{\Sigma}_t^{-\frac{1}{2}} \right) \right) \bar{\Sigma}_t^{\frac{1}{2}}.$$

This last expression can only be simplified if all the Σ_i 's commute with the mean value $\bar{\Sigma}_t$, in which case the affine-invariant and log-Euclidean means are identical. When they are not equal, one can show that (close enough to the identity) the log-Euclidean mean is slightly more anisotropic [Arsigny et al., 2006c].

Even if the gradient descent algorithm usually converges in about 10 iterations for the affine-invariant mean, log-Euclidean computations are obviously more efficient. In practice, the log-Euclidean framework consist in taking the logarithm of the tensor data, computing like usual in the Euclidean space of symmetric matrices, and coming back at the end to the tensor space using the exponential [Arsigny et al., 2006d, Arsigny et al., 2005a]. This simple framework only needs to be complemented by the differential of the exponential and the logarithm for relating the tangent vectors in gradient descent algorithms. This is in essence the mechanism that we patented for dealing with tensor images [Arsigny et al., 2005d].

A careful comparison of the log-Euclidean and affine-invariant metrics on the algorithms described in the following sections [Arsigny et al., 2005a, Arsigny et al., 2006d] showed that there was very few differences on the results (of the order of 1%) on real DTI images, but that the log-Euclidean computations where 4 to 10 times faster. Thus, for this type of application, the log-Euclidean framework seems to be perfectly suited. For other types of applications, like adaptive re-meshing [Mohammadi et al., 1997], the anisotropy of the tensors can be much larger, which may lead to larger differences. In any case, if one wants to work with the affine-invariant, one should initialize the iterative optimizations close to the correct solution using the log-Euclidean result in order to speed-up the convergence of iterative Riemannian algorithms.

3.1.3 Which metric for which problem?

Affine-invariant and Log-Euclidean metrics seem to be well adapted for DTIs and covariance matrices: they provide a geometric interpolation for which the fractional anisotropy (FA) is quasi linear; Null eigenvalues are at an infinite distance of any tensor, so that there is no risk to reach them in a finite time and gradient descents are well posed; The affine-invariant metrics gives to the tensor manifolds a Hadamard structure (a hyperbolic space with non-positive curvature which is diffeomorphic to R^n) while the Log-Euclidean ones give it a complete euclidean structure; With both metrics, the mean always exists and is unique; etc.

Thus, it seems that these metrics could fit many problems. In [Fillard et al., 2005a], we tried to apply them to the smoothing of structure tensors. These tensors are classically obtained by

convolving the tensor product of the gradient of an image by a Gaussian: $S_\sigma = G_\sigma \star (\nabla I \cdot \nabla I^t)$. They reveal structural information about the image and are used to detect edges and corner points or to drive some anisotropic filtering methods. The noisier the image is, the higher σ must be to obtain a smooth field, but small structures may be wiped out. By contrast, smaller values of σ can help to extract low level features in images, but the resulting structure tensor field may be noisy. Thus, the idea is to smooth anisotropically this tensor field to regularize homogeneous regions while preserving edges. An anisotropic filtering of the coefficients (Euclidean structure) fails because we end up with negative eigenvalues.

Thus, we proposed to minimize a ϕ -function of the affine-invariant norm of the gradient of the tensor field (see 3.2.4). However, the results clearly showed that this method also fails: Since the Riemannian metric is scale invariant, small differences in small tensors have the same importance as large differences in large ones. This is catastrophic here because the anisotropic diffusion enhance these small details as much as the large scale ones. Moreover, the anisotropic smoothing does not allows to reach tensors with only one non-null eigenvalue which would represent perfect infinite edges! For this type of tensors, it seems that we need to find another metric for which the null eigenvalues should be reachable, but not the negative ones.

The Cholesky decomposition proposed by [Wang et al., 2004] may provide the right structure for that and it would be interesting to see if it corresponds to a Riemannian metric. As an example, we illustrate in Fig. 3.1 the value of the tensors along a geodesic starting with the same tangent vector for the Euclidean metric, the log-Euclidean metric (the affine-invariant is very close), and a straight line in the Cholesky parameterization proposed by [Wang et al., 2004]. This last curve in the tensor space is given by $\Sigma(t) = L(t) \cdot L(t)^t$ where $L(t) = t \cdot \dot{L}_0$ and \dot{L}_0 is a lower triangular matrix (with positive elements on the diagonal) solution of $\dot{\Sigma}_0 = L_0 \cdot \dot{L}_0^t + \dot{L}_0^t \cdot L_0$. In the Euclidean case, one quickly reach the boundary of the space (tensors with non-positive eigenvalues are not displayed). In the log-Euclidean case, the size of the tensors exponentially decreases but actually reach a null eigenvalue only asymptotically. The Cholesky parameterization behaves like the square function: it reaches a null eigenvalue in a finite time but then bounce back into the space of tensors.



Figure 3.1: **Geodesic shooting from the tensor $\Sigma = \text{diag}(4, 1)$ with the tangent vector $\dot{\Sigma} = \text{diag}(-8)$.** **Left:** The Euclidean case. $2/3$ of tensors are not positive definite and thus are not displayed. **Middle:** The Cholesky case: the null matrix is reached (exact middle value) and values beyond are the mirrored versions of the previous ones. **Right:** The Log-Euclidean case: all tensors are positive definite, and the null tensor is never reached.

This experiment shows that there is not universal metric for one type of features: there are different families of metrics with similar or different characteristics, and one may rely on one or the other depending on the specificities of the application.

3.2 Computing on Riemannian manifolds

3.2.1 Interpolation as a weighted mean

An important operations in geometric data processing is to interpolate values between known measurements. In 3D image processing, (tri-) linear interpolation is often used thanks to its very low computational load and comparatively much better results than nearest neighbor interpolation. Other popular methods include the cubic and, more generally, spline interpolations [Thévenaz et al., 2000, Meijering, 2002].

The standard way to define an interpolation on a regular lattice of dimension d is to consider that the interpolated function $f(x)$ is a linear combination of samples f_k at integer (lattice) coordinates $k \in \mathbb{Z}^d$: $f(x) = \sum_k w(x - k) f_k$. A typical example where the convolution kernel has an infinite support is the sinus cardinal interpolation. With the nearest-neighbor, linear (or trilinear in 3D), and higher order spline interpolations, the kernel is piecewise polynomial, and its support is limited to a few neighboring points in the lattice. Assuming normalized weights, this interpolation is a weighted mean, and can thus be generalized in our manifold framework as an optimization problem: the interpolated value $\Sigma(x)$ on our tensor manifold is the tensor that minimizes $C(\Sigma(x)) = \sum_{i=1}^n w_i(x) \text{dist}^2(\Sigma_i, \Sigma(x))$. To reach this solution, it is easy to adapt the Gauss-Newton scheme proposed for the Karcher mean.

The linear interpolation is interesting as it can be written explicitly as a simple geodesic walking scheme: the generic interpolation equation between points x_1 and x_2 is $x(t) = \exp_{x_1}(t \overrightarrow{x_1 x_2}) = \exp_{x_2}((1-t) \overrightarrow{x_2 x_1})$. For our tensor example, this gives the following interpolation with the standard Euclidean, Log-Euclidean and Affine-invariant metrics give:

$$\begin{aligned} \Sigma_{Eucl}(t) &= (1-t) \Sigma_1 + t \Sigma_2 \\ \Sigma_{LE}(t) &= \exp((1-t) \log(\Sigma_1) + t \log(\Sigma_2)) \\ \Sigma_{Aff}(t) &= \Sigma_1^{1/2} \exp\left(t \log\left(\Sigma_1^{-1/2} \Sigma_2 \Sigma_1^{-1/2}\right)\right) \Sigma_1^{1/2} \end{aligned}$$

One can show that the volume of the tensors (the determinant) is geometrically interpolated with the Log-Euclidean and Affine invariant metrics (their logarithm is linearly interpolated) [Arsigny et al., 2006c] while the trace of the tensor is linearly interpolated for Euclidean metric.

3.2.2 Gaussian and kernel-based filtering

Many other operators can be rephrased as weighted means. For instance approximations and convolutions like Gaussian filtering can be viewed as the average of the neighboring values weighted by a (Gaussian) function of their spatial distances. Assuming a normalized kernel K , a filtered vector field $\hat{F}(x) = \int_{\mathbb{R}^n} K(u) F(x+u) du$ is the result of the minimization of $C(\hat{F}) = \int_{\mathbb{R}^n} K(u) \text{dist}^2(F(x+u), \hat{F}(x)) du$. In this formulation the kernel can be a discrete measure, for instance if samples are defined on the points of a grid. In a Riemannian manifold, this minimization problem is still valid, but instead of a closed-form solution, we have once again a Gauss-Newton iterative gradient descent algorithm to reach the filtered value. With tensor notations, this gives:

$$\hat{\Sigma}_{t+1}(x) = \int_{\mathbb{R}^n} K(u) \overrightarrow{\hat{\Sigma}_t(x) \Sigma(x+u)} du$$

An example of a comparative Gaussian filtering of a diffusion tensor image with the flat Euclidean metric and the affine-invariant one is provided in Fig. 3.2. The log-Euclidean result is very similar to the affine-invariant result (the difference has to be multiplied by 100 to be visible). One can see a more important blurring of the corpus callosum fiber tracts using the flat metric.

In this generalization, we can also use an anisotropic and non-stationary kernel $K(x, u)$. For instance, it can be modulated by the norm of the derivative of the field in the direction u (here $\partial_u \Sigma$). This is one way to perform an anisotropic regularization that we used in [Pennec, 2002] to perform a discontinuity preserving regularization of rigid-body transformation in a time sequence of functional MR images (fMRI). Inspired by our Gaussian filtering of tensors, a similar technique has been recently proposed for the anisotropic diffusion of DTI [Castano-Moraga et al., 2006].

3.2.3 Gradient and Laplacian

An alternative to kernel filtering is to consider a regularization criterion that aims at reducing the amount of the spatial variations of the field. The simplest criterion is the squared norm of the spatial gradient. By definition, the gradient encodes the directional spatial derivatives through $\nabla \Sigma(x)^T u = \partial_u \Sigma(x)$. It may be computed as the matrix that best approximates (in the least-square sense) the directional derivatives in the neighborhood (e.g. 6, 18 or 26 connectivity in 3D). We experimentally found in other applications (e.g. to compute the Jacobian of a deformation field in non-rigid registration [Rey et al., 2002, p. 169]) that this approximation scheme was more stable and much faster than computing all derivatives using convolutions, for instance by the derivative of the Gaussian. In a Riemannian manifold, the directional derivatives $\partial_u \Sigma(x)$ are tangent vectors of $T_{\Sigma(x)} \mathcal{M}$ that can be approximated using finite “differences” in our exponential chart [Pennec et al., 2006]:

$$\partial_u \Sigma(x) \simeq \log_{\Sigma(x)}(\Sigma(x+u)) = \overrightarrow{\Sigma(x) \Sigma(x+u)}$$

For tensors, this tangent vector is a simple symmetric matrix which is expressed in the standard matrix coordinate system (coefficients), i.e. in a non orthonormal coordinate system for our Riemannian metric. Thus, to quantify the local amount of variation, we have to take the metric at the current point into account, and to measure the variations in all spatial directions. Once again, this estimation can be robustified by averaging over more directions:

$$\|\nabla \Sigma(x)\|_{\Sigma(x)}^2 = \sum_{i=1}^d \|\partial_{x_i} \Sigma(x)\|_{\Sigma(x)}^2 \simeq \frac{d}{\text{Card}(\mathcal{V})} \sum_{u \in \mathcal{V}} \frac{1}{\|u\|^2} \left\| \overrightarrow{\Sigma(x) \Sigma(x+u)} \right\|_{\Sigma(x)}^2.$$

After integration over a spatial domain Ω , the Euler-Lagrange equations of the criterion $\text{Reg}(\Sigma) = \int_{\Omega} \|\nabla \Sigma(x)\|_{\Sigma(x)}^2 dx$ with Neumann boundary conditions for the affine-invariant metric are finally [Pennec et al., 2006]:

$$\nabla \text{Reg}(\Sigma) = -2 \Delta \Sigma \quad \text{where} \quad \Delta \Sigma = \sum_{i=1}^d \partial_{x_i}^2 \Sigma - (\partial_{x_i} \Sigma) \Sigma^{(-1)} (\partial_{x_i} \Sigma)$$

is the Laplacian operator on our manifold for our metric. As we can see, the flat Euclidean second order directional derivatives $\partial_i^2 \Sigma$ are corrected by an additional term due to the curvature of our manifold.

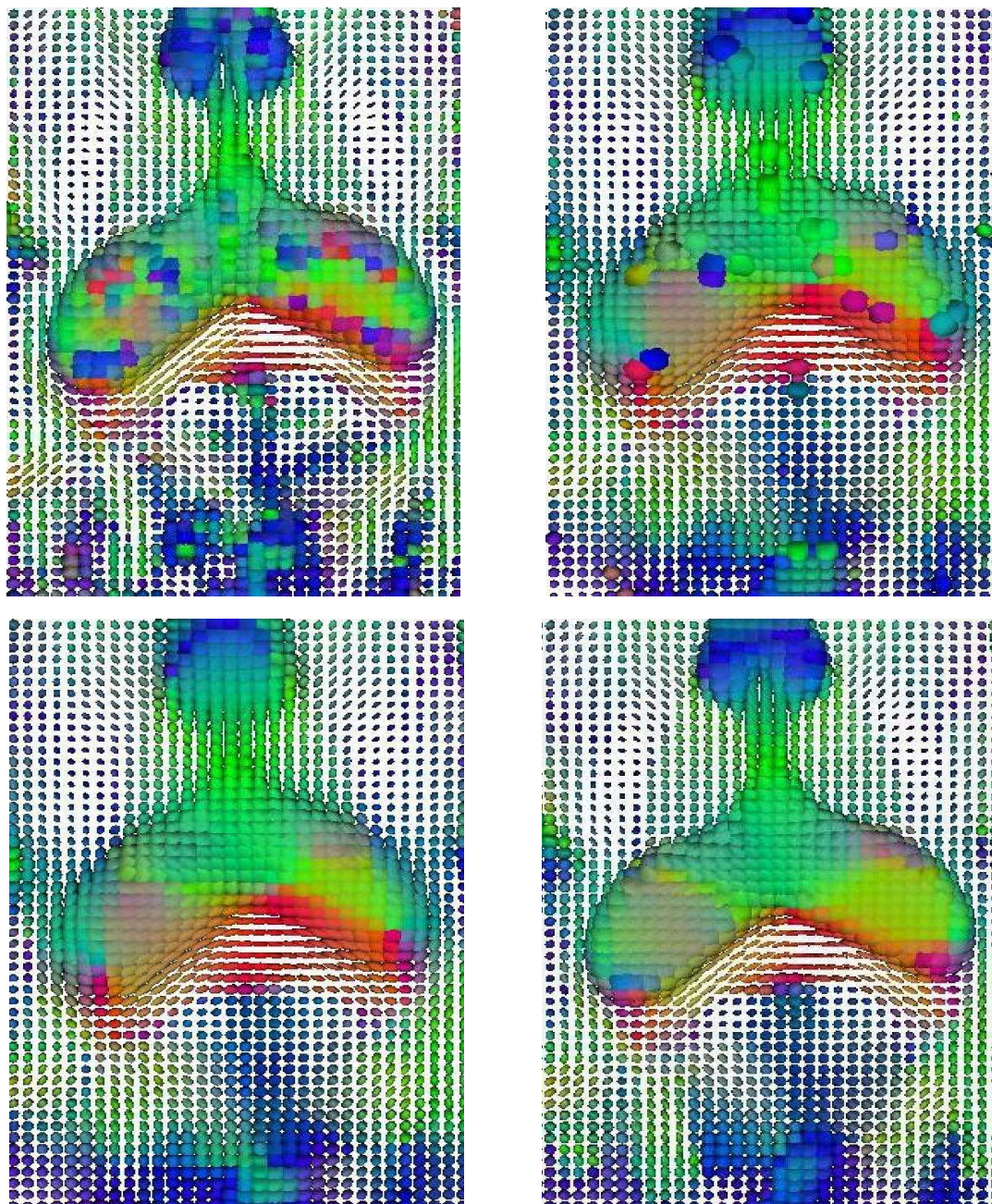


Figure 3.2: Results of the different filtering methods on a 3D DTI of the brain (Closeup around the splenium of the corpus callosum) The color codes for the direction of the principal eigenvector (red: left-right, green: posterior-anterior, blue: inferior-superior). **Top left:** Original image. **Top right:** Gaussian filtering using the flat metric (5×5 window, $\sigma = 2.0$). This metric gives too much weight to tensors with large eigenvalues, thus leading to clear outliers in the ventricles or in the middle of the splenium tract. **Bottom left:** Gaussian filtering using the Riemannian metric (5×5 window, $\sigma = 2.0$). Outliers disappeared, but the discontinuities are not well preserved, for instance in the ventricles at the level of the cortico-spinal tracts (upper-middle part of the images). **Bottom right:** Anisotropic filtering in the Riemannian framework (time step 0.01, 50 iterations). The ventricles boundary is very well conserved with an anisotropic filter and both isotropic (ventricles) and anisotropic (splenium) regions are regularized. Note that the U-shaped tracts at the boundary of the grey/white matter (lower left and right corners of each image) are preserved with an anisotropic filter and not with a Gaussian filter.

From a practical point of view, the Laplacian operator may be computed from finite differences approximations of the Euclidean derivatives, but we proposed in [Pennec et al., 2006] a more efficient and general scheme: as the Christoffel symbols and their derivatives *along the geodesics* vanish at the origin of the exponential chart (the geodesics are parameterized by arc-length), the correction for the curvature is in fact already included in the exponential chart: by computing the standard Laplacian in that map, one gets the manifold-valued Laplacian operator for free. For tensors with the affine-invariant metric, we detailed in [Pennec et al., 2006] the computations to prove that the symmetric average $\overrightarrow{\Sigma(x)\Sigma(x+u)} + \overrightarrow{\Sigma(x)\Sigma(x-u)} = \Delta_u \Sigma + O(\|u\|^4)$ is a fourth order approximation of the directional manifold Laplacian. By averaging once again over all the directions in a (symmetric) local neighborhood, the numerical scheme we proposed was:

$$\Delta \Sigma(x) = \frac{2d}{\text{Card}(\mathcal{V})} \sum_{u \in \mathcal{V}} \frac{1}{\|u\|^2} \overrightarrow{\Sigma(x)\Sigma(x+u)}$$

3.2.4 Anisotropic diffusion

Harmonic diffusion is the minimization of the square norm of the gradient of the field. Its practical implementation is very easy using a geodesic gradient descent technique. At each time t one compute the current derivative of the regularization criterion using the above numerical scheme for the manifold Laplacian, and one walk at each point along the geodesic with the opposite tangent vector:

$$\Sigma_{t+\varepsilon}(x) = \exp_{\Sigma_t(x)}(-\varepsilon \Delta \Sigma_t(x))$$

This geodesic gradient descent technique will be used to optimize all the PDEs appearing in the following of this section.

In order to filter in homogeneous regions but not across their boundaries, the basic idea is to penalize the smoothing in the directions where the derivative is important [Perona and Malik, 1990, Gerig et al., 1992]. This can be realized directly in the discrete implementation of the Laplacian by weighting the contribution $\Delta_u \Sigma$ of the spatial direction u to the Laplacian by a decreasing function of the norm $\|\partial_u \Sigma\|_\Sigma$ of the gradient in that direction. In [Pennec et al., 2006], we took, $c(x) = \exp(-x^2/\kappa^2)$, where the threshold κ controls the amount of local regularization: for a gradient magnitude greater than 2 to 3 κ , there is virtually no regularization, while the field is almost linearly smoothed for gradient magnitudes below a fraction (say 0.1) of κ .

Figure 3.2 shows an example result with the affine invariant metric on the same data as for the Gaussian filtering. The anisotropic filtering further improves the results by preserving the discontinuities of the tensor scale (e.g. at the boundary of the ventricles), but also the discontinuities of the tensor orientation, which is exactly what is need for fiber tracking in DTI.

As there is no convergence guarantee in this scheme (anisotropic regularization “forces” may not derive from a well-posed energy), we reformulated in [Fillard et al., 2005a] the problem as the optimization of a (decreasing) ϕ -function of the Riemannian norm of the spatial gradient: $Reg_\phi(\Sigma) = \frac{1}{2} \int_\Omega \phi(\|\nabla \Sigma(x)\|_{\Sigma(x)}) dx$. By choosing an adequate ϕ -function, one can give to the regularization an isotropic or anisotropic behavior [Aubert and Kornprobst, 2001]. In our experiments, we use $\phi(s) = 2\sqrt{1 + s^2/\kappa^2} - 2$. Using $\Psi(x) = \Phi'(x)/x$, we have:

$$\partial_W Reg_\phi(\Sigma) = \frac{1}{2} \int_\Omega \Psi(\|\nabla \Sigma\|_\Sigma) \cdot \partial_W(\|\nabla \Sigma\|_\Sigma^2) = \int_\Omega \Psi(\|\nabla \Sigma\|_\Sigma) \cdot \langle \text{grad} \Sigma \mid \text{grad} W \rangle_\Sigma$$

Using an integration by part with proper Neumann boundary conditions, we obtain:

$$\partial_W \text{Reg}_\phi(\Sigma) = - \int_{\Omega} \langle \text{div}(\Psi(\|\nabla\Sigma\|_{\Sigma}).\text{grad}\Sigma) \mid W \rangle_{\Sigma}$$

Finally, by definition of the gradient and by distributing the divergence, we get the usual formula:

$$\nabla \text{Reg}_\phi(\Sigma) = \text{div}(\Psi(\|\nabla\Sigma\|_{\Sigma}).\text{grad}\Sigma) = \Psi(\|\nabla\Sigma\|_{\Sigma}).\Delta\Sigma + \sum_i (\partial_i \Psi(\|\nabla\Sigma\|_{\Sigma})).\partial_i \Sigma$$

The main difference with a classical Euclidean calculation is that we have to use the manifold Laplacian to take the curvature of the tensor manifold into account.

3.2.5 Diffusion-based interpolation and extrapolation

The pure diffusion is efficient to reduce the noise in the data, but it also reduces the amount of information. Moreover, the diffusion time (time step ε times the number of iterations) that controls the amount of smoothing is difficult to estimate. At an infinite diffusion time, the field will be completely homogeneous (possibly by part).

It is much more interesting to consider the data as noisy observations and the regularization as a prior on the spatial regularity of the field. Usually, one assumes a Gaussian noise independent at each position, which leads to a least-squares criterion through a maximum likelihood approach. The only difference here is that it uses our Riemannian distance. For a dense data field (i.e. if the data are already provided on the grid on which we are solving the PDE), the similarity criterion that is added to the regularization criterion is simply $\text{Sim}(\Sigma) = \int_{\Omega} \text{dist}^2(\Sigma(x), \Sigma_0(x)) dx$. It simply adds a linear (geodesic) spring $\nabla_{\Sigma} \text{dist}^2(\Sigma, \Sigma_0) = -2 \overrightarrow{\Sigma \Sigma_0}$ to the global gradient to prevent the regularization from pulling to far away from the original data.

For sparse measures, using directly the maximum likelihood on the observed data $\text{Sim}(\Sigma) = \sum_{i=1}^n \text{dist}^2(\Sigma(x_i), \Sigma_i)$ leads to deal with Dirac (mass) distributions in the derivatives, which is a problem for the numerical implementation. In [Pennec et al., 2006], we considered the Dirac distribution as the limit of the Gaussian function G_{σ} when σ goes to zero.

$$\text{Sim}_{\sigma}(\Sigma) = \int_{\Omega} \sum_{i=1}^n G_{\sigma}(x - x_i) \text{dist}^2(\Sigma(x), \Sigma_i) dx \quad \text{and} \quad \nabla \text{Sim}_{\sigma}(x) = -2 \sum_{i=1}^n G_{\sigma}(x - x_i) \overrightarrow{\Sigma(x) \Sigma_i}.$$

From a practical point of view, one needs to use a σ of the order of the spatial resolution of the grid so that all measures can at least influence the neighboring nodes. After convergence, the value can be slowly decreased if one wants to be more accurate. Figure 3.3 presents an example of the extrapolation that can be obtained from four tensors with the affine-invariant metric. Interestingly, there is an identity tensor at the center of the grid around which there does not exist a consistent orientation of the first eigenvector. This is not a problem for the Riemannian methods.

3.3 Application to diffusion tensor imaging (DTI)

Diffusion tensor Imaging (DTI) is a unique tool to assess in vivo oriented structures within tissues via the directional measure of water diffusion. However, most of the current applications are in neuroscience, with high signal-to-noise ratios (SNR) images on subjects rather than patients. Even if there

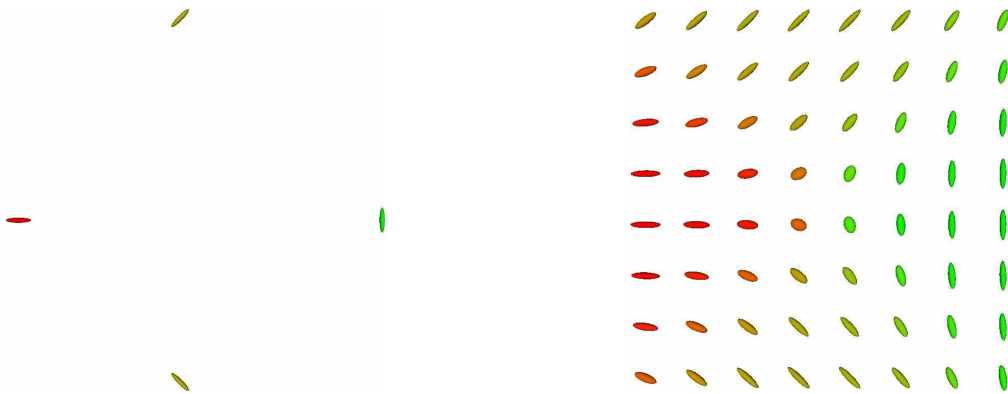


Figure 3.3: **Interpolation and extrapolation using diffusion.** **Left:** The four initial tensor measurements. **Right:** result of the extrapolation by diffusion (time-step $\varepsilon = 1$, $\lambda = 0.01$, $\sigma = 1$ pixel of the reconstruction grid). The algorithm converged in about 100 iterations.

there begin to be a few clinical indications for DTI [Provenzale et al., 2006, Rovaris et al., 2005], using such a modality in a clinical environment is difficult: data often have to be acquired quickly because the patient cannot stay in a static position for too long due to pathologies. This results in acquisitions with a limited number of encoding gradients and low SNR. Moreover, the estimation of the diffusion tensor field from diffusion weighted images (DWI) being noise-sensitive, clinical DTI is often not suitable for fiber tracking, which prevent the development of new clinical indications.

In order to bridge this gap, we proposed in [Fillard et al., 2006a, Fillard et al., 2005b] a new method for the joint estimation and regularization of diffusion tensors from DWIs. The first idea is model the noise in the images very precisely in order to keep the maximum amount of information from the original data. We designed for that a new maximum likelihood (ML) criterion for the Rician noise. The second idea is to perform jointly the estimation and the regularization of the tensor field (rather than sequentially as usually done), so that we keep once again all the relevant information. This amounts to transform our ML into a maximum a posteriori (MAP) criterion by considering the regularization criterion as a kind of spatial prior on the tensor field regularity.

3.3.1 Noise models for the estimation of the tensor field

The Stejskal-Tanner diffusion equation [Basser et al., 1994] relates the diffusion tensor D to each noise-free DWI:

$$S_i = S_0 \exp(-b g_i^T D g_i)$$

where S_i is the original DWI corresponding to the encoding gradient g_i , S_0 the base image with a null gradient, and b the diffusion factor. By taking the logarithm of this equation, one obtain a linear system. Solving that system in a least square (LS) sense leads to the minimization of a quadratic criterion, which is easily performed using algebraic methods (see e.g. [Westin et al., 2002]). Doing this implicitly assumes a log-Gaussian noise on the images, which is justify for high SNRs. In that case, the noise is also well approximated by a Gaussian noise within the brain, but very few works were done on non log-Gaussian noise for the estimation of the tensor field because it was requiring

optimization techniques on tensors, which turned out to be very difficult to control with the standard Euclidean framework. One may cite however [Wang et al., 2004] (see Section 3.1.3), who proposed a computationally grounded optimization framework based on the Cholesky decomposition. With the log-Euclidean framework, such an optimization is not difficult (one also can restate everything within the affine-invariant framework but calculations are slightly more complex). For instance, in the case of a Gaussian noise on the DWIs, the tensor $D = \exp(L)$ is parameterized by its logarithm L , an unconstrained symmetric matrix. The criterion to optimize is $Sim_G(L) = \sum (\hat{S}_i - S_i(\exp(L)))^2$, and the gradient is

$$\nabla Sim_G(L) = 2b \sum (\hat{S}_i - S_i) \cdot \partial_L S_i \quad \text{with} \quad \partial_L S_i = S_i \partial_{g_i \cdot g_i^t} \exp(L)$$

For low SNRs, the real nature of the noise is Gaussian in the complex image. [Wang et al., 2004] proposed an estimation criterion on the complex DWI signal that is adapted to that noise. However, one usually only have access to the amplitude of the signal complex signal in clinical images: in that case, the noise is thus Rician. One can show that such a noise induces a signal-dependent bias of the order of $\sigma^2/2S$ on the DWI signal [Sijbers et al., 1998]. The signal being systematically larger than what it ought to be, the tensors will be under-estimated. To take explicitly the nature of this noise into account, we proposed to optimizing the log-likelihood of the signal corrupted by a Rician noise. This leads to a more complex criterion than above, but its gradient is very similar to the Gaussian case above: $\nabla Sim_R(L) = -1/\sigma^2 \sum (S_i - \alpha \hat{S}_i) \partial_L S$, except that we have a correcting factor $\alpha = I'_0/I_0(\hat{S}_i S_i/\sigma^2)$ depending on the signal and the noise variance (I_0 and I'_0 are computable Bessel functions). The noise variance can easily be estimated on the background of the image (outside the head) where there is no signal.

3.3.2 Joint estimation and smoothing

Fiber tracking is the ultimate application targeted by most of the researchers today in neuroscience, in order to investigate non invasively the anatomical-functional architecture of the brain. This might also prove to be an interesting quantification tool for medical diagnoses. However, the DTI data are usually too noisy to be used directly. When possible, multiple acquisitions are averaged to enhance the SNR. For medical applications, this is not a solution because patients tend to move during these very lengthy acquisitions. Thus, one need to regularize the tensor field without blurring the transitions between distinct fiber tracts, which delimit anatomical and functional brain regions. Smoothing independently each DWI before estimating the tensor results in a smoother tensor field but it also blurs the transitions between homogeneous regions, as this information is not accessible by taking each DWI individually. For instance, in brain DTI, only the combination of all the images reveals the complex neural structure of the white matter.

Consequently, one would like to perform an anisotropic regularization of the tensor field itself. Most of the methods developed so far spatially regularize some of the geometric features of the tensor field. For instance, [Coulon et al., 2004] anisotropically restores the principal direction of the tensor, and uses this regularized directions map as an input for the anisotropic regularization of the eigenvalues. A quite similar idea is adopted in [Tschumperlé, 2002], where a spectral decomposition of the tensor field is performed at each points to independently regularize the eigenvalues and eigenvectors (orientations). This approach requires an additional reorientation step of the rotation

matrices due to the non-uniqueness of the decomposition. An intrinsic integration scheme for PDEs that uses the exponential map has been added in [Chefd'hotel et al., 2002], and allows to perform PDEs evolution on the considered manifold without re-projections.

However, all these regularizations rely on the estimated tensor field and are not linked any more to the original DWI data. We believe that a better idea is to add a prior on the spatial regularity to a data attachment criterion which is statistically optimal with respect to the noise model. This performs a MAP estimation instead of regularizing an ML estimation. [Wang et al., 2004] made an important step in that direction by considering a Gaussian noise model on the (complex) DWIs and a joint anisotropic smoothing of the Cholesky decomposition of the tensors (see Section 3.1.3). Like the affine-invariant or the log-Euclidean metrics, this parameterization takes into account the complete tensor information for smoothing, and to keep the results of the computations positive (definite). However, they chose to rely on the Euclidean norm of the gradient of the tensor field (the Cholesky being only a parameterization and not a full metric) to drive the anisotropic diffusion, and the Euclidean metric is much more sensitive to changes in scales than to changes of orientations.

In [Fillard et al., 2006a, Fillard et al., 2005b, Fillard et al., 2006b], we proposed to model the prior of the spatial regularity in the log-Euclidean framework (i.e. the tensor field $\Sigma(x)$ is parameterized by its logarithm $L(x)$), and to account for discontinuities using through a ϕ -functional: $\text{Reg}(L) = \int_{\Omega} \phi(\|\nabla L\|)$. In our experiments, we use $\phi(s) = 2\sqrt{1 + s^2/\kappa^2} - 2$. The ϕ -function preserves the edges of the tensor field while smoothing homogeneous regions. To include this regularization as an a-priori into the ML optimization process of the previous section, we simply need to compute its gradient, which is simply $\nabla \text{Reg}(L) = -\psi(\|\nabla L\|) \Delta L - \sum_i \partial_i (\psi(\|\nabla L\|)) \cdot \partial_i L$ with $\psi(s) = \phi'(s)/s$. Directional derivatives, gradient and Laplacian were estimated with a finite differences scheme like with scalar images (see [Fillard et al., 2005b, Fillard et al., 2006b] for details).

Experiments on synthetic data with contours and a Rician noise showed that the gradient descent techniques were removing the negative eigenvalues that did appear in the standard estimation technique. However, ML and MAP (with regularization) methods with a Gaussian noise model were underestimating the volume of tensors even more than the standard log-Gaussian method (30% instead of 20%), while Rician ML and MAP methods were estimating it within 5%. The effect of the regularization was also spectacular, but it is difficult to generalize to real data where ‘‘edges’’ may be much more loosely defined.

More interestingly, the methods were tested on two clinical datasets of low and medium quality: a brain image with a very low SNR, and an experimental acquisition of the spinal chord, both with 7 gradient directions. This last type of acquisition is currently actively investigated in clinical research (e.g. [Facon et al., 2005]) and is difficult to perform: because the position is uncomfortable due to the pathology, the patient often cannot stay too long in the scanner. Moreover, the coil cannot be perfectly adapted to the body as it is for the head. The images are consequently much noisier than for the brain MRI. We performed the estimation of the tensor field with the three noise models on the data (Gaussian, log-Gaussian and Rician) and with or without an anisotropic log-Euclidean prior on the spatial regularity. The Gaussian ML and Rician MAP are displayed on top rows of Figs. 3.4 and 3.5. Then, we tracked the fibers using a simple method [Fillard et al., 2003a] (bottom row of Figs 3.4 and 3.5).

Like for synthetic data, using gradient descent techniques removed the negative eigenvalues of the standard method. To evaluate the impact of the noise model on the tensor reconstruction

in the brain, we computed the mean apparent diffusion coefficient (ADC), fractional anisotropy (FA) and volume of the diffusion tensors in the ventricles (high but anisotropic diffusion), and in the corpus callosum (lower diffusion with high anisotropy) [Fillard et al., 2006b]. Using the Rician noise model increase the tensor volume and the ADC by about 10% in isotropic regions and by 1 to 2% in anisotropic regions without modifying the FA. In the spinal chord, using the Rician noise model also lead to an increase of the tensors of about 30% in volume. This corresponds to the correction of the shrinking effect with Gaussian and Log-Gaussian noises that we demonstrated on synthetic data. Adding some spatial regularization (MAP methods) systematically decreases the FA. However, this effect is much lower for anisotropic regions and minimized with the Rician noise model: 3% only in the corpus callosum (versus 11% with log-Gaussian), and 15% in the ventricles (versus 30% with log-Gaussian). Thus, it seems that these measurements are more reproducible with the MAP Rician reconstruction.

The tractography results in a much smoother and longer fibers with less dispersion for the MAP Rician model. The overall number of reconstructed fibers is also much larger. The smoothness of the tensor field indeed leads to more regular and longer fibers: tracts that were stopped due to the noise are now fully reconstructed. A careful quantitative evaluation and validation of the whole framework however remains to be done. In particular, it would be necessary to evaluate the reproducibility across acquisitions and scanners, for instance using repeated scans of the same subject, as well as evaluations of physical phantoms.

3.4 Conclusion

In this chapter, we presented on the example of positive definite symmetric matrices an extension of the statistical computing framework developed in the previous chapter. Firstly, we showed that interpolation and kernel-based filtering methods can be generalized to Riemannian manifolds using weighted means. Secondly, many PDEs (including anisotropic diffusion) are easily implemented by first taking into account the Riemannian metric in the gradient computation, and second by using a geodesic marching scheme to integrate the path to the solution [Pennec et al., 2006]. We exemplified this framework with the important example of Diffusion Tensor Images (DTI). The careful modeling of the noise on the data led us to propose new Rician ML and MAP estimation frameworks which can cope with a much lower SNR compatible with clinical applications [Fillard et al., 2006a, Fillard et al., 2006b]. One of the interest of our methodology is that is provide a globally consistent computation framework for diffusion tensor estimation and interpretation. Tensors constitute an interesting manifold as it can support several simple families of metrics with very different properties. Some of them may perform very well for some problems (e.g. log-Euclidean or affine-invariant metrics for DTI), but fail for others (e.g smoothing structure tensors). This shows that there is not one Riemannian metric for all problems and raises the question of how to chose the optimal metric for each application.

From the methodological point of view, this chapter confirmed that the Riemannian metric can be considered as the basis of a complete computational framework on manifolds. The main method is to replace Euclidean integrals or sums of points by minimizations of intrinsic functionals (real functions on the manifold). We already had in the last chapter the examples of the Fréchet / Karcher means, where the barycenter is replaced by the minimization of the intrinsic variance, and

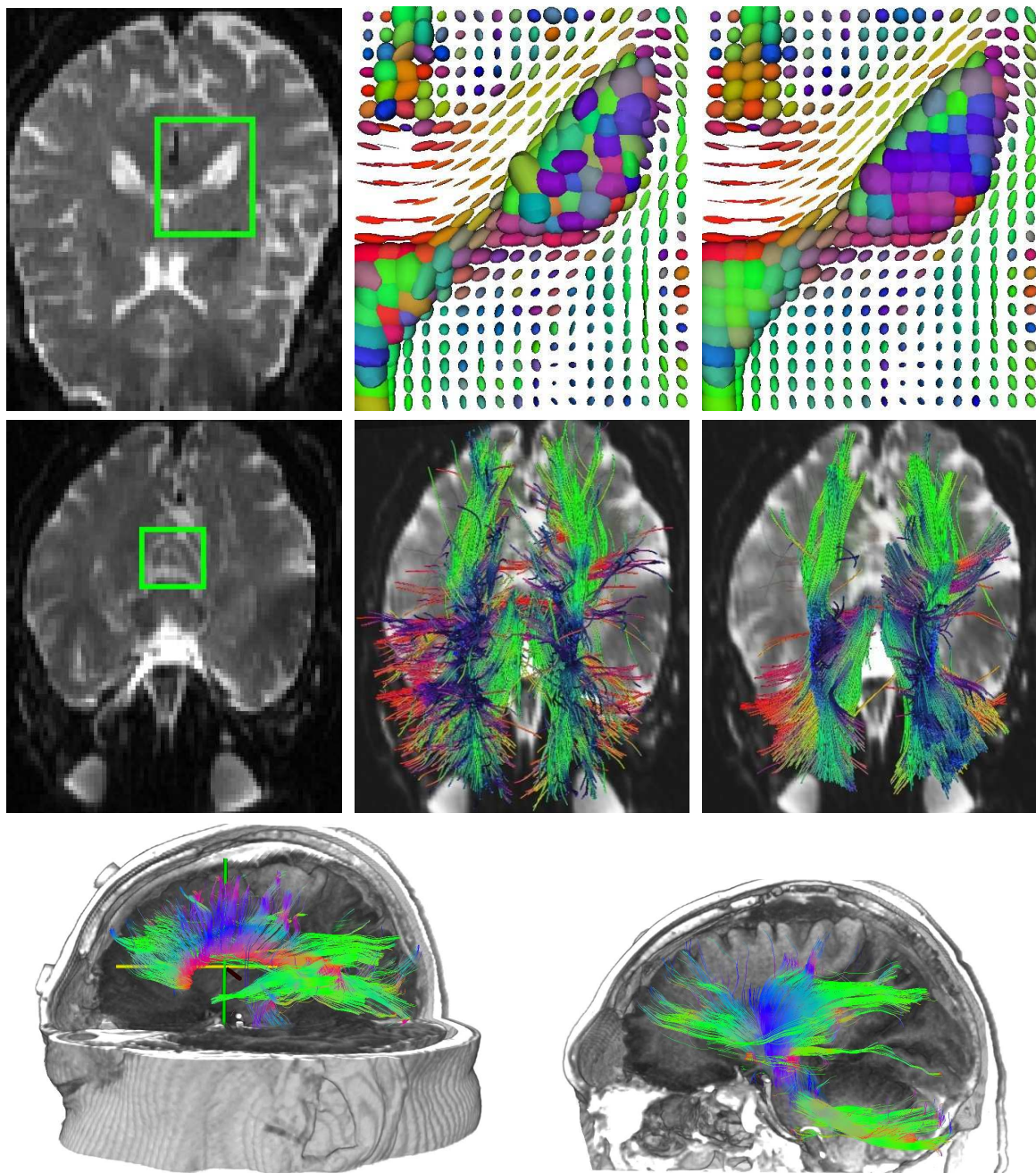


Figure 3.4: **Tensor field estimation of a brain (top row) and improvement of the fiber tracking (bottom row).** **Top Left:** A slice of the b_0 image. **Top Middle:** The classic log-Gaussian estimation on the ROI. The color codes for the principal direction of **blue:** inferior-superior. Missing tensors in the splenium region are non-positive. **Top Right:** The MAP estimation of the same region. **Middle row, Left:** ROI where the tracking is initiated. **Middle row, middle:** The cortico-spinal tract reconstructed after a classic estimation. **Middle row, Right:** Same tract reconstructed after our MAP estimation. **Bottom row:** Other examples of fiber tracking after our Rician MAP estimation, superimposed on a volume rendering of the T1 image. Images are obtained using the MedINRIA software developed by P. Fillard and N. Toussaint.

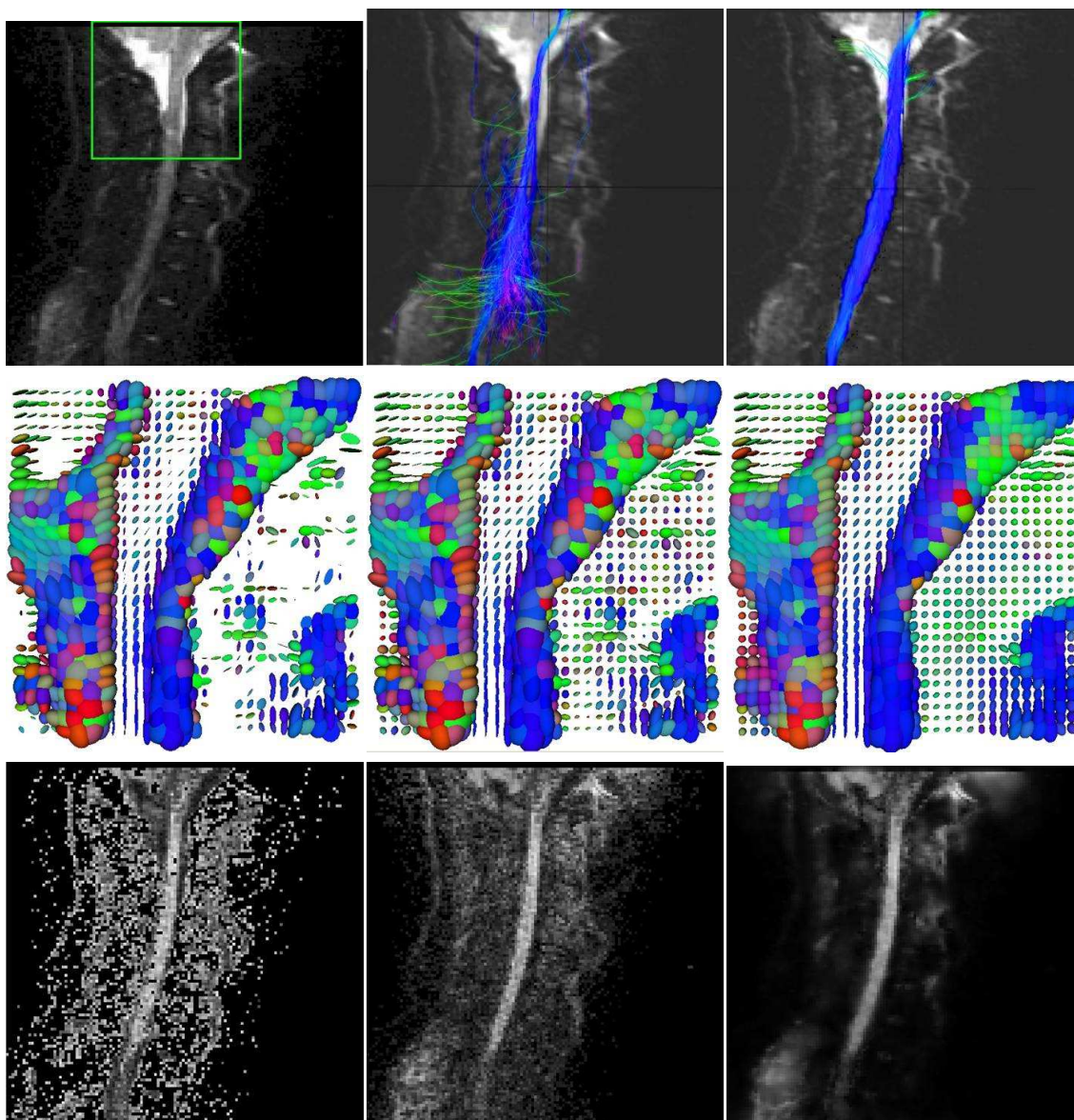


Figure 3.5: **Tensor field estimation of the spinal chord (middle and bottom row) and improvement of the fiber tracking (top row)**. Images are courtesy of D. Ducreux, MD. The color codes for the principal direction of tensors: **red:** left-right, **green:** anterior-posterior, **blue:** inferior-superior. **Top row:** A slice of the b_0 image with the ROI squared in green (**left**), spinal cord tract reconstruction with the classic **log-Gaussian ML** (**middle**) and **Rician MAP** (**right**) tensor estimation. **Middle row:** There are many missing (i.e. non-positive) tensors around and in the spinal cord with the classic **log-Gaussian ML** tensor estimation (**left**). Tensors are all positives for the **Rician ML** noise model (*middle*), and the field is much more regular while preserving discontinuities with the **Rician MAP** noise model (**right**). **Bottom row:** Fractional anisotropy of the classic **log-Gaussian ML** (**left**), **Rician ML** (**middle**) and **Rician MAP** (**right**) noise models.

the Gaussian distribution, defined through the maximization of the intrinsic conditional entropy of the distribution knowing the mean and the covariance. Here we showed that important image analysis tools such as filtering and convolutions can be also rephrased as weighted means, i.e. as intrinsic minimization problems.

The second most important tools are the Riemannian exponential and logarithmic maps. Typical examples were previously given by gradient descent algorithms through geodesic walking (a straight line from the reference point in the exponential map in the direction of the gradient is transformed into a geodesic path in the manifold), the definition of the covariance matrix and higher order moments... In this chapter, we show that the exponential map also provides the manifold-Laplacian for free. This particularly simplifies the implementation of many algorithms like diffusion and anisotropic regularization by providing efficient generic programming methods for all manifolds. All the complexity is deferred to the implementation of the Riemannian exponential and logarithmic maps. In the simple cases that we considered in these two chapters (rigid motions and tensors with invariant metrics), we were able to determine closed forms for these two maps. For more complex Riemannian manifolds, one has to rely on the numerical optimization of the Riemannian energy (the integral of the squared distance) to compute the geodesics. Of course, the efficiency is much lower, but the genericity is very high. One should notice that by a complex Riemannian manifold, we mean not only complex geometrical features (e.g. curves, surfaces, deformations), but also simple features with general Riemannian metrics. Indeed, we believe that choosing the right metric is the most important open problem from the application point of view: having a generic computing framework allows to design models where the metric could be learned to optimally represent observations. This idea will be exemplified in Chapter 5 with computational anatomy.

Chapter 4

Medical image registration

In the last two chapters, the focus was mainly on the methodological aspect of statistical computing on manifolds, with example applications in diffusion tensor image estimation and regularization. In this chapter, we turn to more standard medical image analysis. My interest was mainly on image registration, which consist in superimposing images acquires at different times, with different modalities, or between different subjects, in a common reference frame such that image points correspond to the same anatomical position. This is a central problem in medical image analysis for pathology follow-up in longitudinal studies, to compare the anatomy of different subjects or guide a therapeutic gesture with augmented reality. One can distinguish a hierarchy of problems going from rigid monomodal mono-subject, now well solved, to the still open multi-subject multi-modal highly deformable registration problem.

Section 4.1 provides an overview of the main projects in which I was involved in image guided therapy. In most of them, rigid registration is used to enhance the information available during the therapy using previously acquired images. In such a system, it is not only necessary to provide the geometric transformation, which is used to guide the therapeutic gesture, but also to quantify the accuracy and the robustness of the information provided in order to avoid potentially dangerous errors. To this aim, I became involved in the evaluation of the performances of rigid registration algorithms. My contributions on this topic are detailed in Section 4.2. Doing statistics properly on geometric transformations was actually one of the main motivations to develop the statistical computing framework on manifold presented in the first chapter. Last but not least, Section 4.3 presents our contributions on non-rigid registration. My research interest gradually moved from intra-subject registration to inter-subject registration, with an ever increasing need for robust and fast algorithms. The method was to include in an efficient way informative priors about the observation process (bias, confidence on the similarity criterion) and about the transformation. This last topic will be much more developed in the next Chapter with computational models of the anatomy.

4.1 Rigid registration for image guided therapy

Rigid registration for image guided therapy is one of the major application theme of my past research. Historically, I was involved in three main projects in image guided therapy that I detailed below. An additional project on biomedical images (confocal microscopy) is ongoing. In each project, my

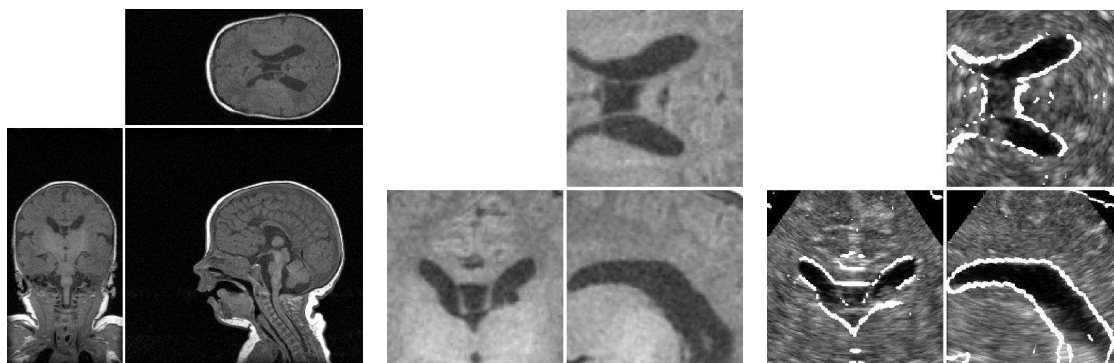
goal was to bring registration algorithms closer to their clinical use. The method was to revisit the criterion usually used in order to better model the acquisition process, and to design performance evaluation methods to validate the algorithms (see Section 4.2). This allows to better take into account the statistical nature of the information and of the noise on the data. An overview of the methods we developed for registration was published in the general purpose magazine *Pour la Science* [Pennec, 2005] in December 2005.

4.1.1 Endoscopic brain surgery

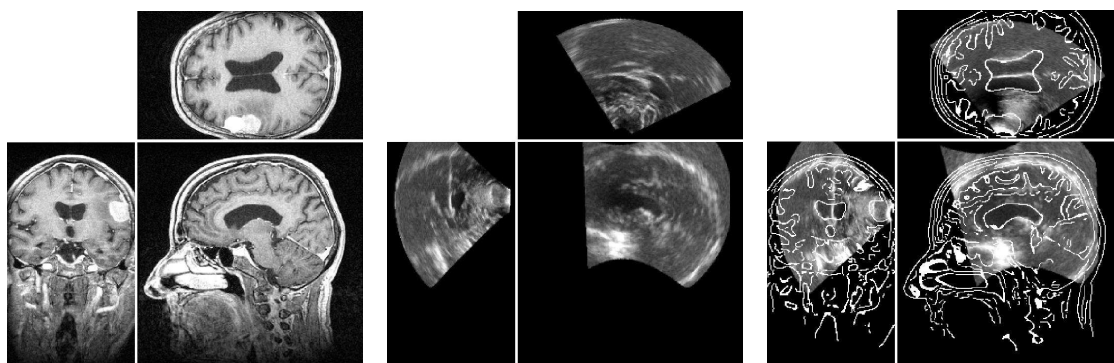
The goal of the European project ROBOSCOPE (1998-2000), a collaboration between The Fraunhofer Institute (Germany), Fokker Control System (Netherlands), Imperial College (UK), INRIA (France), ISM-Salzburg and Kretz Technik (Austria), was to assist neurosurgical operations using real-time 3D ultrasound images and a robotic manipulator arm. During an intervention, the brain tissues shift and warp. In order to keep an accurate positioning of the surgical instruments, one has to estimate this deformation from intra-operative images. 3D ultrasound (US) imaging is an innovative and low-cost modality which appears to be suited for such computer-assisted surgery tools. The idea is to track in real time the deformation of anatomical structures using 3D US images acquired during surgery. To calibrate the system (i.e. to relate the MR and the US coordinate systems) a first US image is acquired with dura mater still closed. As there is not motion of the brain yet, we just have to in perform a rigid registration with the preoperative MR. Then, per-operative 3D US images are continuously acquired during surgery to track the brain deformations. From these deformations, one can update the preoperative plan and synthesize a virtual MR image that matches the current brain anatomy.

In [Roche et al., 2001, Roche et al., 2000], we proposed one of the very first image-based technique to register rigidly intra-operative 3D US with a pre-operative MRI. A model of the signals and their acquisition led us to propose an original similarity measure between the images, the bivariate correlation ratio, that generalized the correlation ratio we previously proposed in [Roche et al., 1998a, Roche et al., 1998b]. In our model, the US intensity is assumed to be a unknown bivariate function of the intensity of the MRI and of its gradient. Optimizing alternatively for the geometric transformation and for this intensity transfer function led to a very efficient algorithm (see Figure 4.1. A careful evaluation of the algorithm performances using registration loops showed that we were able to reach an accuracy of the order of the voxel size of the MRI.

Once the US coordinate system is related to the pre-operative MR one, brain deformations are tracked tracked in the 3D US time-sequence using a “demon’s” like algorithm [Pennec et al., 2003, Pennec et al., 2001b]. To take into account intensity changes along time, we developed an original version of the local correlation coefficient [Cachier and Pennec, 2000]. Experiments show that a registration accuracy of the MR voxel size is achieved for the rigid part, and a qualitative accuracy of a few millimeters could be obtained for the complete tracking system. An overview of the whole rigid registration and non-rigid tracking system was published in [Pennec et al., 2001a, Pennec et al., 2005a].



Images of a baby (US images are acquired through the fontanelle and are not per-operative). From left to right: original MR T1 image, closeup on the ventricle area, and registered US image with MR contours superimposed.



Images of a patient with a brain tumor. The 3D US is a per-operative image. From left to right: MR T1 image with a contrast agent, manual initialization of the US image registration, and result of the automatic registration of the US image with the MR contours superimposed.

Figure 4.1: Example registration of MR and US images using the bivariate correlation ratio in the ROBOSCOPE project. Images courtesy of M. Rudolph and Dr Auer, Max-Planck-Institute for Psychiatry, Munich, Germany and ISM Austria, in the framework of the EC-funded ROBOSCOPE project HC 4018, a collaboration between The Fraunhofer Institute (Germany), Fokker Control System (Netherlands), Imperial College (UK), INRIA (France), ISM-Salzburg and Kretz Technik (Austria).

4.1.2 Dental implantology

The Cifre PhD of S. Granger took place in the framework of a research collaboration with the company AREALL for the development of DentalNavigator, a computer-guided surgery system dedicated to oral implantology surgery [Etienne et al., 2000b, Etienne et al., 2000a, Granger, 2003]. In this system, the operation was planned on a pre-operative CT-Scan and the purpose was to help the dentist surgeon to drill the implant in the predefined position and orientation in the mouth of the patient, with a minimally invasive apparatus. In the CT-Scan image, the teeth and jaw bone surfaces were easily segmented, resulting in about 100000 triangulated points. About 10000 unstructured points were measured on the patient teeth and jaw in the operating room using a 1D ultrasound probe whose position and orientation was tracked in 3D. The registration of the surfaces underlying these two unstructured point sets was then allowing to visually guides the surgeon to the planned position and orientation for drilling.

We investigated with Sebastien Granger the rigid registration of large sets of points, generally sampled from surfaces. We formulate this problem as a Maximum-Likelihood (ML) estimation. Under the Gaussian assumption, and when the matches are sought, this corresponds to the well known Iterative Closest Point algorithm (ICP) algorithm with the Mahalanobis distance [Granger et al., 2001].

Then, considering matches between the points of the two sets as a hidden variable, we obtain a slightly more complex non quadratic criterion that can be efficiently solved using Expectation-Maximization (EM) principles. This leads to an alternate optimization of the probability of the matches (E-step) knowing the transformation, and the optimization of the transformation knowing the probability of the matches (M-step). Still with Gaussian noise, this new methods corresponds to an ICP with multiple matches weighted by normalized Gaussian weights, giving birth to the EM-ICP acronym of the method. The variance of the Gaussian noise is a new parameter that can be viewed as a “scale or blurring factor” on the point clouds. From a theoretical point of view, we showed that EM-ICP robustly aligns the barycenters and inertia moments with a high variance, while its limit is the ICP for a variance smaller than the distance between neighboring points in each sets (i.e. points may be distinguished and there is no ambiguity in the matches). Practically, we used a coarse-to-fine approach which resolved robustness problems while improving the algorithm accuracy. Moreover, we were able to drastically increased the algorithm speed to almost real-time while preserving its very good performances using a simple down-sampling technique on the point-sets. Experiments on real data demonstrate a spectacular improvement of the performances of EM-ICP w.r.t. the standard ICP algorithm in terms of robustness (a factor of 3 to 4) and speed (a factor 10 to 20), with similar performances in precision [Granger and Pennec, 2002a, Granger, 2003].

These good results led us to reuse part of this formalism in a statistical framework for modeling noisy curves and surface using unstructured point sets for surface reconstruction, registration and fusion [Granger, 2003]. In particular, we were able to relate some of our results to the tensor voting techniques developed in [Medioni et al., 2000].

4.1.3 Liver puncture guidance

In collaboration with Luc Soler at IRCAD on computer aiding tools for digestive surgery [Delingette et al., 2006, Soler et al., 2004a, Soler et al., 2004b, Soler et al., 2004c], the goal of the

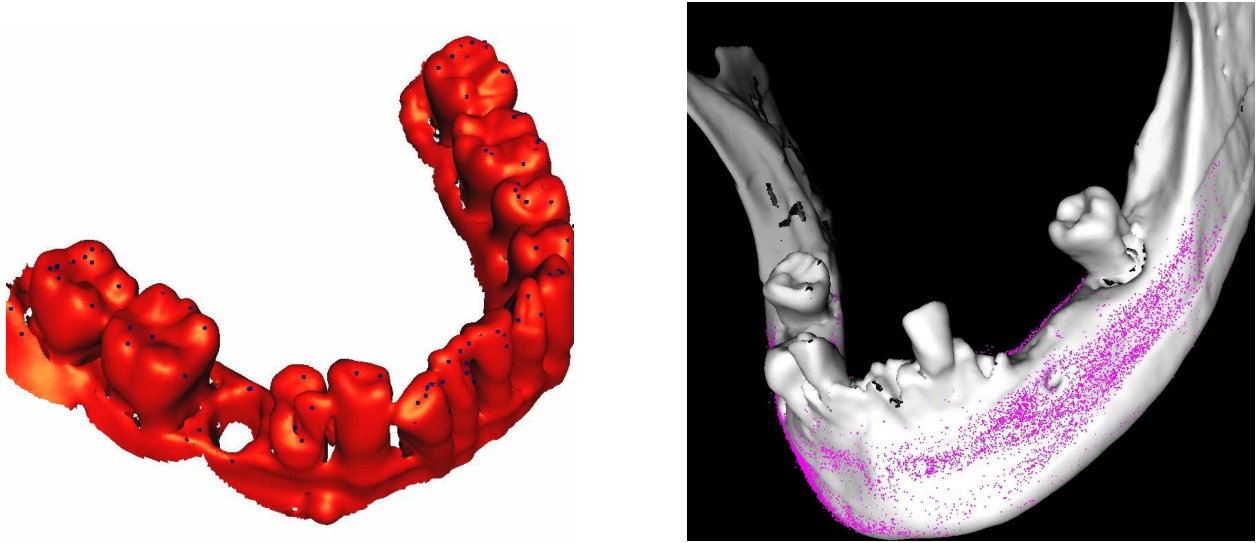


Figure 4.2: Registration of surfaces viewed as point sets for dental implantology guidance. **Left:** Registration of two sets of points measured on the surface of a dry (ex-vivo) jaw. The red surface is a regularly sampled surface of more than 130000 triangulated points segmented from a CT-Scan of resolution $0.25 \times 0.25 \times 0.5$ mm. 50 points (black dots) were measured on the surface of the teeth using a passive robotic arm. Experiments showed that ICP has a very small attraction basin (a few millimeters in translation) and an accuracy of 0.31 mm in the jaw area. The EM algorithm exhibits a much wider attraction basin (around 1 cm) with a better accuracy of 0.22 mm. This gain in robustness and accuracy is counterbalanced by a larger computation time (a factor 4), which remained however under 30 seconds without the multi-scale speedup [Granger et al., 2001]. **Right:** Registration of two sets of points measured on the surface of a dry (ex-vivo) jaw. The white surface is extracted from a CT scan as above. The purple points are obtained via a 1D ultrasound sensor mounted on a passive robotic arm with an accuracy of about 0.05 mm. This set of 25000 points is very heterogeneous, and presents many packets of highly correlated points. Using the multi-scale EM algorithm allows to reach a robustness of 90% in 1 minute while the ICP algorithm convergence to the right solution only 25% to 50% of the time in 5 to 10 minutes.[Granger and Pennec, 2002a]

PhD thesis of Stéphane Nicolau was to build a clinical prototype of an augmented reality guiding system that could be tested in the operating room. Hepatic tumor ablation by radio-frequencies is frequently performed at Strasbourg Hospital under radiologic assistance. However, inserting the needle within 5mm of the target point can require several CT-scan acquisitions to verify and correct the trajectory. This increases the radiation dose for the patient and lengthens the gesture. The needle even have sometimes to be removed and reinserted several times. Thus this radiologic intervention appeared to be a good candidate where augmented reality (AR) could provide an important help to shortening the intervention time.

The general principle of the AR system is to acquire a CT-scan of the abdomen at the beginning of the intervention. Then, a 3D reconstruction of the anatomical structures of interest (skin, liver,

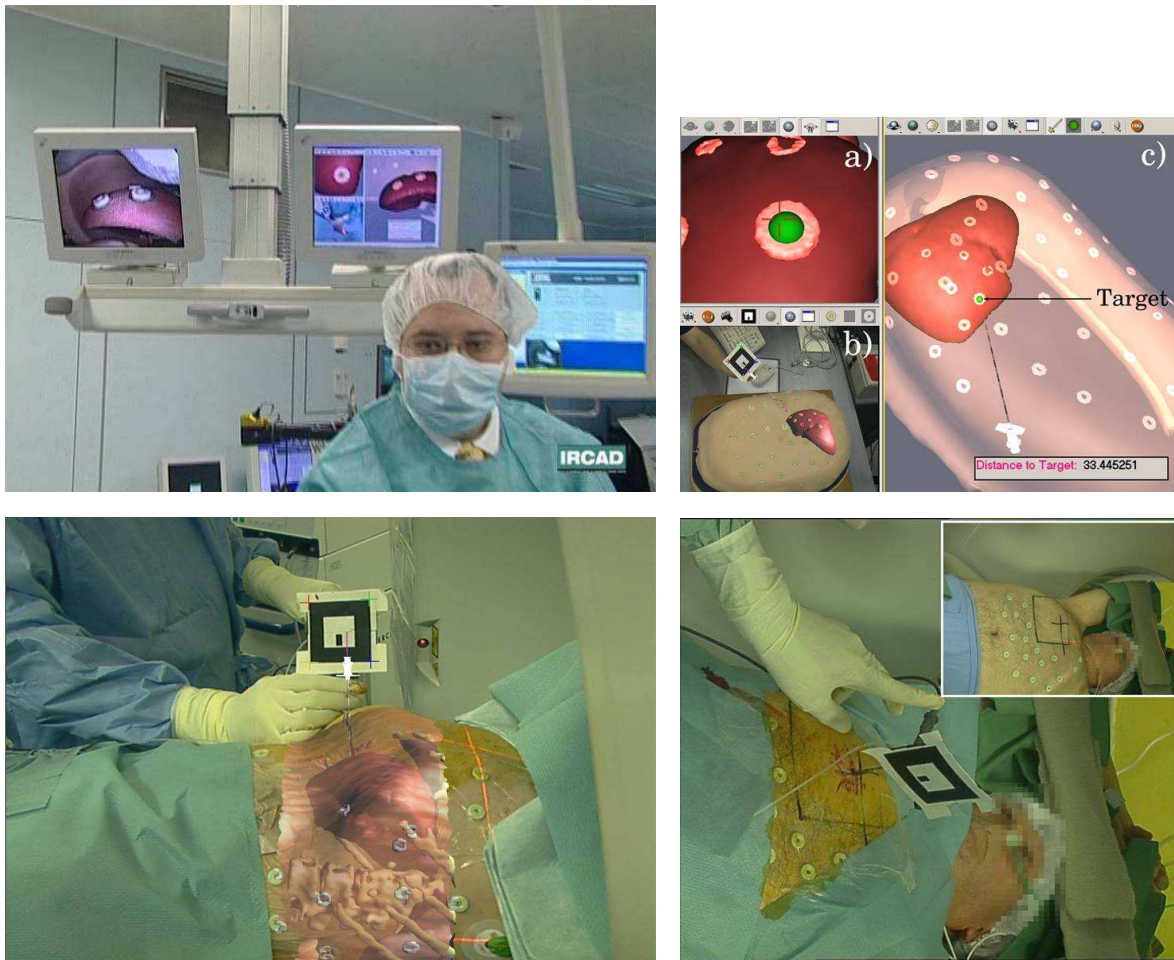


Figure 4.3: Augmented reality system for Liver puncture guidance. **Top:** experimental setup for the validation on the abdomen phantom in the operation room. On the right image, one can see the guidance interface (a close-up is displayed in the left image) and the endoscopic control image on the right. **Bottom:** passive validation experiments on real patients.

tumor...) is performed, in which the radiologist specifies the entry and target points. Two jointly calibrated cameras observe the patient's skin when the table of the scanner is out of the gantry. The hard clinical requirements about the robustness of the system led us to stick radio-opaque markers on the to perform the 3D CT-scan to 2D video images registration [Nicolau et al., 2005]. As 70% of the patients are under general anesthesia at Strasbourg hospital, the CT and gesture guidance is also performed only during the the expiratory phases of the patient in order to guaranty the accuracy. The needle is tracked by the cameras during its insertion so that its orientation and the position of its end point can be related to the entry and target points in order to guide the radiologist. The CT and needle model registration to the camera coordinate system is performed is

real-time so that the patient can be moved.

In this augmented reality system, our main contributions were three-folded. Firstly, we extended the usual 3D/2D point registration algorithms by explicitly considering noise on the the 3D point positions. This extended projective points criterion (EPPC) turns out to have a better robustness and accuracy than te usual 3D/2D registration criteria [Nicolau et al., 2003b]. We also provided a method to statistically estimate the accuracy of the resulting transformation, which was validated on controlled experiments with a phantom of the abdomen [Nicolau et al., 2004a]. This accuracy prediction scheme is an important security feature of the AR system as it allows to certify in real time that the registration is not potentially misled for instance by the occlusion of some markers or by a bad positioning of the cameras with respect to the field of view.

Secondly, the ergonomy of the augmented reality interface was carefully studied and optimized with the practitioners [Nicolau et al., 2004c] (see Fig. 4.3). Experiments on an abdominal phantom (with endoscopic control) in the operating room showed that a mean accuracy of 2mm could be reached with a targeting time of less than 30 seconds!

Last but not least, we set up a passive evaluation protocol on real patients in clinical conditions: the augmented reality system is installed and initialized, but the radiologist performs his gesture normally without any indication from the system. For the subset of patient chosen, the radiologist performs a CT-scan with contrast agent after the insertion of the needle to check if it is really well positioned. From this image, we can determine the actual point that was targeted using a 3D-3D registration to the pre-operative scan. By comparing this position to the one planned by the system, we can determine the accuracy of the guidance the system would have provided. The potential impact of the AR system presence in the OR was considered negligible by the practitioner and the anesthetist. A first evaluation on 5 patients showed that it was necessary to have a breath control not only during the needle insertion, but also during the CT scan acquisition to avoid important image distortions [Nicolau et al., 2004b, Soler et al., 2004d]. In a second round of evaluation on 5 other patients with breath control, the system accuracy increased from 10mm to 5mm, thus validating the system principle in pseudo-static conditions. We hope to show in future experiments that the active use of the system drastically reduces the time of the needle insertion and allows to decrease the number of intermediate scans during the gesture.

4.1.4 Confocal microscopic imaging

Fibered confocal microscopy (FCM) is a potential tool for *in vivo* and *in situ* optical biopsy. The principle of confocal microscopy is to perform an optical sectioning of a biological sample by selecting a clear in-focus image of a thin section within the sample and rejecting the light from out-of-focus planes. To adapt confocal microscope for *in vivo* and *in situ* imaging, the company Mauna-Kea Technology (MKT) proposed to replace the microscope objective by a probe of adequate length and diameter, linked to the scanning device by a fiber bundle [Le Goualher et al., 2004]. This imaging modality unveils the cellular structure of the observed tissue.

In close collaboration with MKT, the goal of the Cifre PhD of Tom Vercauteren is to enhance the possibilities offered by FCM by providing efficient image sequence mosaicing techniques to widen the field of view (FOV). This is a way to fill the gap between scales and to allow multi-scale information fusion for probe positioning and multi-modality fusion. Mosaicing also allows for quantitative and

statistical analysis on a wide field of view, especially when the element of interest is of the order of the size of a single image.

To explore a region of interest, the optical microprobe is glided along the soft tissues. This displacement may be described by a smooth rigid motion over time (with some jumps when the probe encounters some obstacles), with small non-rigid deformation of the tissues due to the probe pressure. FCM outputs a video sequence irregularly sampled in the space domain, each sampling point corresponding to a fiber center. An additional problem is that FCM is a laser scanning device: each sample point in the image is acquired at a different instant. This induces motion artifacts correlated with the probe motion. Thus, each image frame may be viewed as a partial, deformed and irregular sample of the unknown ground truth 2D scene.

The mosaicing approach chosen in [Vercauteren et al., 2006, Vercauteren et al., 2005] is basically an iterated optimization of the “likelihood” of the above generative model over the different unknowns (global 2D scene, probe motion, non-rigid deformations), embedded in a hierarchical framework to efficiently determine good initial values. The global positioning of all frames is first determined using multiple registration of input frames: a robust and maximally consistent motion

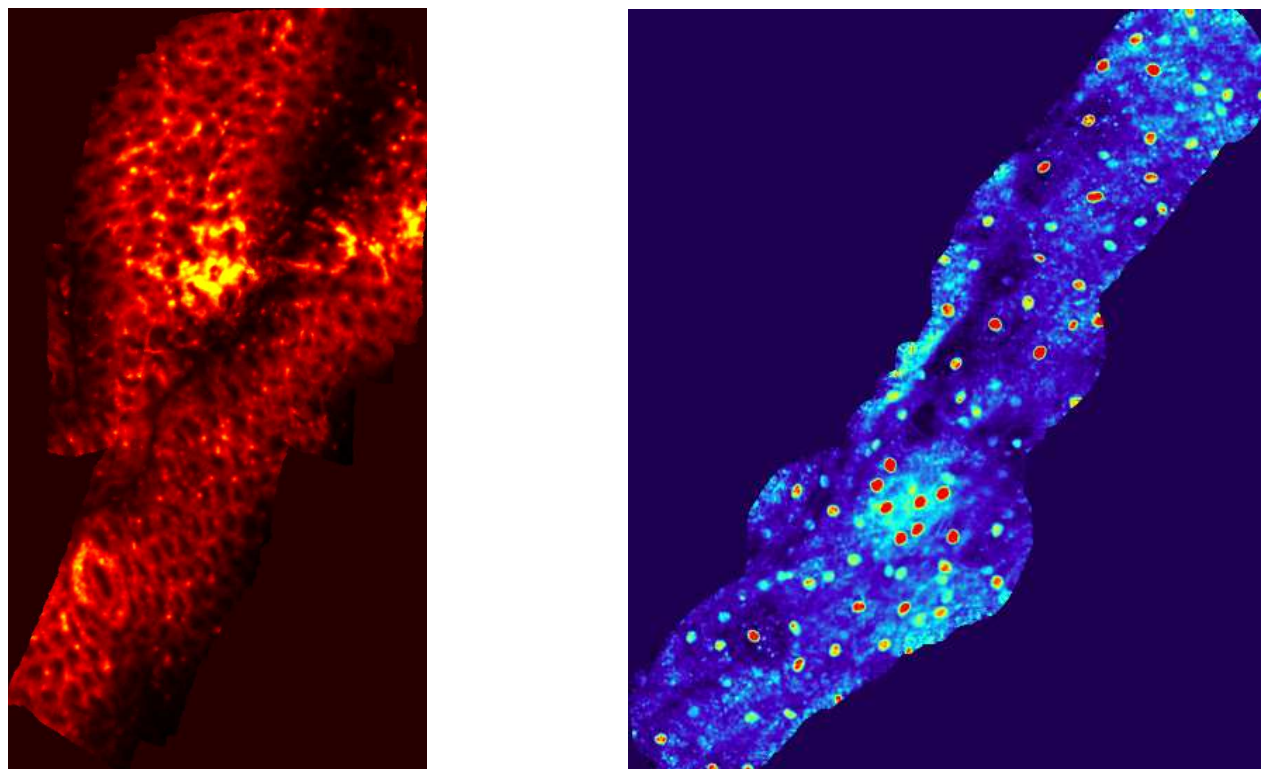


Figure 4.4: **Left:** Mosaic of 50 live mouse colon images (Fluorescence FCM). The mouse colon, stained by acriflavine, show both normal and aberrant crypts. The image sequence is courtesy of Danijela Vignjevic, Sylvie Robine, Daniel Louvard, Institut Curie, Paris, France. **Right:** Mosaic of 243 live human mouth images (Reflectance FCM).

sequence is extracted using optimization techniques on Lie groups (the method is more formally described in Section 4.2.3 as the Bronze Standard for a different application). The laser-scanning induced motion artifacts are easily modeled and corrected from the estimated motion sequence. The whole sequence (registration of pairs of corrected frames, globally consistent alignment estimation, and correction of distortions) is iterated to improve the motion parameters. Then, we proposed an original and efficient scattered data fitting method to reconstruct the global 2D scene from irregularly sampled images (the registered and motion-corrected frames). The residual small non-rigid tissue deformations are finally taken into account by iteratively registering an input frame to the mosaic, thanks to a demon's like non-rigid registration algorithm, and updating the mosaic.

Controlled experiments on a phantom (a silicon wafer) with a computer numerical control milling machine provided a gold standard motion. Results indicate that the accuracy of the mosaicing framework (without deformation) was of the order of the fiber inter-core distance ($1.3 \mu\text{m}$). Moreover, the mosaic clearly displays a super-resolution effect compared to the acquired image frames. Multiple experiments with in-vivo acquisitions in the mouse and human colon, mouth mucosa, kidney, etc. (see e.g. Fig. 4.4 or [Vercauteren et al., 2006] for more images) demonstrated the interest of mosaicing for in vivo soft tissue microscopy: not only the field of view is enlarged, but we also observe in most cases an important improvement of the signal to noise ratio.

Future work will concentrate on robustifying the method and make it real-time (the rigid part took 3 minutes and the non-rigid deformation compensation 15min on a 2GHz PC for the mouse colon mosaic displayed in Fig. 4.4). Indeed, even a simplified version would allow the operator to interact with the mosaicing during the acquisition, for instance to ensure the covering of an important final field of view and to reconnect the mosaic parts when there is a jump in the motion sequence.

4.2 Evaluation of the registration performances

A transversal axis of my research was to develop performance evaluation methods for rigid registration algorithms in terms of robustness, precision and accuracy. For the sake of analysis, one may consider registration algorithms as black boxes that take images as input and output a transformation. Considering the input data and the output transformation as random variables naturally leads to quantify the variability of the transformation with its standard deviation, or more interestingly with the covariance matrix as the transformation uncertainty is usually non isotropic (this also solve the problem of radians and millimeters for rotations and translation parts). Then, the variability of the transformation can be propagated to some target points to obtain the covariance on the transformed test points, or its trace, the variance. Depending on the distance to the "true" transformation, one usually distinguish gross errors (convergence to wrong local minima) and small errors around the exact transformation. The *robustness* quantifies the size of the basin of attraction of the right solution or the probability of false positives. The *accuracy* measures the error with respect to the truth (which may be unknown) for small errors. The *repeatability* or precision only measures the deviation from the average value, i.e. it does not take into account *systematic biases*, which are often hidden.

One should be careful that registration algorithms perform differently for different types of input data. For instance, one algorithm may perform very well for the registration of MR images of the

head, but poorly for the same type of images of the abdomen. This means that the evaluation data set has to be representative of the typical clinical application problem we are targeting: all sources of perturbation in the data should be represented, such as acquisition noise and artifacts, pathologies, etc. We cannot just conclude from one experiment that one algorithm is better than the others for all applications.

One of the simplest evaluation schemes is to simulate noisy data and to measure how far is the registration result from the true one (the ground truth is obviously known). The main drawback of synthetic data is that it is very difficult to identify and model faithfully all the sources of variability, and especially unexpected events (pathologies, artifacts, etc). Forgetting one single source of error (e.g. camera calibration errors in 2D-3D registration) automatically leads to underestimate the final transformation variability. Moreover, the faithful simulation of images (e.g. SPECT [Grova et al., 2001] and MRI [Benoit-Cattin et al., 2005]) are computationally extremely demanding due to the complexity of image acquisition physics.

The second evaluation level is to use real data in a controlled environment, for instance imaging a physical phantom. In our research, we used such a phantom in [Nicolau et al., 2003b, Nicolau et al., 2003a] to evaluate the 2D/3D registration of video and CT images described in Section 4.1.3. To obtain a gold standard, one need to measure precisely the motion or deformation of the phantom with an external apparatus. However, it is difficult to test all the clinical conditions (e.g. different types or localizations of pathologies). Moreover, it is often argued that these phantoms are not representative of real in vivo biological system. One level closer to the reality, experiments on cadavers correctly take into account the anatomy, but fail to exhibit all the errors due to the physiology. Moreover, images may be very different from the in-vivo ones, for instance in MR.

The last level of evaluation methods, relies on a database of in-vivo real images representative of the clinical application. Such a database should be large enough to span all sources of variability. However, establishing a gold standard registration for realistic clinical images is very difficult. This was done for instance in [Maurer et al., 1997] for the evaluation of the ACUSTAR Advanced Neurosurgical Navigation System. As a side bonus, it allows the retrospective comparison of many multimodal registration algorithm [West et al., 1997, West et al., 1996], but such a study is hardly reproducible for all types of data. Thus, my research focused more on the more general setup: the absence of gold-standard.

4.2.1 Error prediction

In generalized least-squares feature-based rigid registration algorithms, we can formulate the optimal registration as an implicit function of the features by equating the criterion derivative to zero. The error is then propagated from the features to the resulting transformation using first order linearizations of the criterion derivatives [Pennec and Thirion, 1995, Pennec and Thirion, 1997, Nicolau et al., 2003b]. We proposed this type of error prediction method for the registration of monomodal images based on extremal points [Pennec et al., 2000], and for the marker based 2D/3D registration criteria of [Nicolau et al., 2004a]. A similar but highly simplified noise propagation analysis was performed in [Fitzpatrick et al., 1998] for the case of point features. However, the noise assumptions in these error prediction methods are often too simplistic for more generic registration methods. Firstly, they assume independent errors on the features, which forbids the use of such

methods for surfaces and intensity-based criteria. Secondly, and probably more importantly, one often forgets to include some sources of error in the model. For instance, we put into evidence a bias of 0.2mm due to chemical shift between MR images acquired at the same time while the uncertainty of the registration was of the order of 0.1mm only [Pennec, 1997, Pennec et al., 1998]. In another experiment, camera calibration errors consistently biased all the images of the sequence by about 1mm [Nicolau et al., 2004a]. All these bias lead to a drastic underestimation of the final error on the transformation. Thus, even if we can predict the registration error, one needs a performance evaluation setup to verify that all the sources of error are correctly taken into account.

4.2.2 Consistency loops

For general registration algorithms, it has been proposed to perform a cross comparison of the criteria optimized by different algorithms [Hellier et al., 2003]. However, this does not give any insights about the transformation itself. We believe that a more interesting method is the use of consistency loops [Pennec and Thirion, 1997, Holden et al., 2000, Roche et al., 2001]. The principle is to compose transformations that form a closed circuit and to measure the difference of the composition from the identity. This criterion does not require any ground truth, but it only measures the repeatability as any bias will get once again unnoticed.

Originally, we have proposed this type of loops to validate the error prediction on the generalized Least-squares feature-based registration criteria that we proposed in [Pennec and Thirion, 1997]: when the covariance matrix of the transformation loop is known, the Mahalanobis distance of the loop to the identity should be χ_6^2 distributed under a Gaussian assumption. We called this value the validation index. By repeating experiments with many different configurations one can test if the covariance is statistically correctly predicted by verifying the mean and the variance of the validation index (resp. 6 and 12), or even by performing a Kolmogorov-Smirnov test to verify that the empirical distribution matches the theoretical one. Results on the rigid registration of time series of dual echo MR T2 images of the brain using crest lines showed that our accuracy prediction was perfectly validated within the times series of each echo, but put into light a statistically significant bias of 0.2mm in translation due to the chemical shift (voxel size was 1x1x3mm) [Pennec et al., 1998, Pennec et al., 2000]. The same technique was also used to validate the accuracy prediction of the 3D/2D point-based registration criteria of section 4.1.3 [Nicolau et al., 2004a]. This time, we found that the prediction was correct when it was above 1mm. The limited factor was in this case the noise on the camera calibration that was not taken into account.

In [Roche et al., 2000, Roche et al., 2001], we adapted the registration loop technique to estimate the accuracy performances of the MR/US registration detailed in Section 4.1.1. Similar registration loop techniques were also proposed at the same time for other registration problems [Holden et al., 2000, Penney et al., 2001]. Typical loops are sketched in Fig. 4.5 for a series of MR and US images acquired on a deformable phantom. If we were given perfectly registered images within MR and US modalities, applying the transformations of the loop in turn to a test point would lead to a displacement that is only due to the errors of the two MR/US registrations. Since variance are additives, the observed target registration error (TRE) should be $\sigma_{loop}^2 = 2\sigma_{MR/US}^2$. In most cases, the intramodality transformations are not perfectly known and need to be estimated. Thus, we have to take into account their variability and the *expected accuracy* or consistency is quantified by: $2\sigma_{MR/US}^2 = \sigma_{loop}^2 - \sigma_{MR/MR}^2 - \sigma_{US/US}^2$. Using that framework, we were able to show

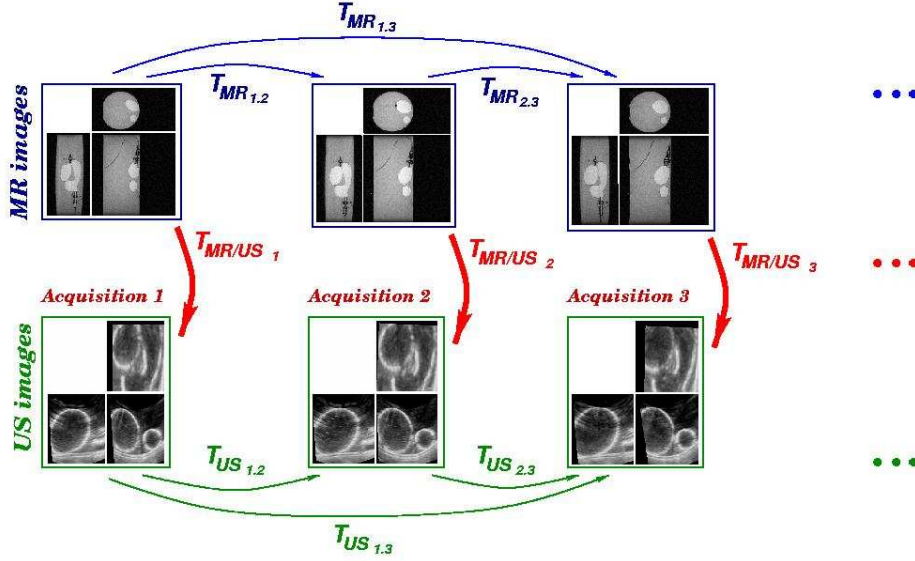


Figure 4.5: Registration loops used to estimate the registration consistency.

that the accuracy of the MR/US registration was of the order of the MR voxel size (US images were more finely sampled), i.e. below 2mm even in the case of per-operative images of the brain for tumor resection.

In practice, the variability analysis is performed on the transformations rather than on test points with a simplified model of noise to minimize the number of unknowns (e.g. diagonal or two variances only for rotation and translations). In both cases (test points and transformations), we need to estimate the variance of the intra-modality registrations. This led us to develop the following bronze standard estimation procedure.

4.2.3 The bronze standard method

The principle of the bronze standard method is similar the STAPLE algorithm proposed for the validation of segmentation [Warfield et al., 2004]: we consider the gold standard registration as a hidden variable, as well as the distance of our results to this reference (EM like algorithms). From a set of pairwise registrations between images, the goal is thus to estimate the exact transformations and the variability of the registration results with respect to these references. The bronze standard technique was first presented in [Roche et al., 2000, Roche et al., 2001] for the previous MR/US registration problem, and then adapted and refined in [Granger, 2003] and [Nicolau et al., 2003b] for other registration problems.

Let us assume that we have n images of the same organ of the patient and m methods to register them, i.e. $m.n^2$ transformations $T_{i,j}^k$ (we denote here by k the index of the method and by i and j the indexes of the reference and target images). Our goal here is to estimate the $n - 1$ free transformations $\bar{T}_{i,i+1}$ that relate successive images and that best explain the measurements $T_{i,j}^k$.

The bronze standard transformation between images i and j is obtained by composition: $\bar{T}_{i,j} = \bar{T}_{i,i+1} \circ \bar{T}_{i+1,i+2} \circ \dots \circ \bar{T}_{j-1,j}$ if $i < j$ (or the inverse of both terms if $j > i$). The free transformation parameters are computed by minimizing the prediction error on the observed registrations:

$$C(\bar{T}_{1,2}, \bar{T}_{2,3}, \dots, \bar{T}_{n-1,n}) = \sum_{i,j \in [1,n], k \in [1,m]} d\left(T_{i,j}^k, \bar{T}_{i,j}\right)^2 \quad (4.1)$$

where d is a robust variant of the left-invariant Riemannian distance on rigid transformation presented in Chapter 2:

$$d(T_1, T_2) = \min\left(\mu^2(T_1^{(-1)} \circ T_2), \chi^2\right) \quad \text{with} \quad \mu^2(R(\theta, n), t) = \frac{\theta^2}{\sigma_r^2} + \frac{\|t\|^2}{\sigma_t^2}$$

In this process, we do not only estimate the optimal transformations, but also the rotational and translational variance of the “transformation measurements”, which are propagated through the criterion to give an estimation of the variance of the optimal transformations. Of course, these variances should be considered as a fixed effect (i.e. these parameters are common to all patients for a given image registration problem, contrarily to the transformations) so that they can be computed more faithfully by multiplying the number of patients.

Considering a given registration method, the variability due to the noise in the data decreases as the number of images n increases, and the registration computed converges toward the perfect registration up to the intrinsic bias introduced by the method. Now, using different registration procedures based on different methods, the intrinsic bias of each method also becomes a random variable, which is hopefully centered around zero and averaged out in the minimization procedure. The different bias of the methods are now integrated into the transformation variability, hence the name bronze standard. To fully reach this goal, it is important to use as many independent registration methods as possible.

The optimized criterion is in fact the log-likelihood of the observations $T_{i,j}^k$ assuming Gaussian errors around the bronze standard registrations. An interesting variant is to relax the assumption of the same variances for all algorithms, and to unbiased the estimation of these variances. This can be realized by using only $m - 1$ out of the m methods to determine the bronze standard registration, and use the obtained reference to determine the accuracy of the last method (a kind of leave-one-method-out test).

In the case of registration of the surface of the jaw extracted from CT images, we found for instance that the multi-scale EM-ICP algorithm of [Granger and Pennec, 2002a] was twice times more accurate than intensity-based registration algorithms such as **Baladin** [Ourselin et al., 2000] (a block matching strategy optimizing the coefficient of correlation and a robust least-trimmed-squares transformation estimation) and **Yasmina** (Powell optimization of the SSD or of a robust variant of the correlation ratio (CR)) [Roche et al., 2001], or the registration using crest-line and extremal points [Pennec et al., 2000]. This result contradicts the general assumption that intensity-based are more accurate than feature-based registration methods and illustrate the fact that the accuracy of a registration algorithm is application dependent.

For the CT images of the abdominal phantom [Nicolau et al., 2003b] used in Section 4.1.3, one could observe that the registration based on fiducials (the markers stuck on the phantom skin) was 2 to 3 times less accurate than image-based registration algorithms (the same as above), even with

20 markers. This could be explained by the soft nature of the skin, which undergone (realistic) motions of the order of 1.5mm between the different CT acquisitions).

4.2.4 Grid-based registration evaluation

Even though registration computations are usually tractable on simple PCs, the large number of input data and registration algorithms required to compute the bronze standard makes this method computationally intensive. A grid infrastructure can handle the load of the computations involved and help in managing the medical image database to process. Grid platforms offer computing power, data storage capacities, algorithm and data sharing functionalities through standardized interfaces and protocols. They are an opportunity to enlarge the impact of image processing tools and to transfer this experimental research to clinical practice. The availability of algorithms and datasets will ease the development, prototyping, and the validation of algorithms. Advanced users will be able to experiment and compare existing techniques on common data sets. In fine, one could expect that grid-enabled algorithms will be accessible for clinical use [Blanquer et al., 2004].

The evaluation of a new registration method with respect to existing reference algorithms is an interesting first level scenario. Doing that on a local host or cluster requires to be able to get the code, compile, parameterize and execute all the reference algorithms that may be developed by different people, coming from various institutes. Such a procedure is very time-consuming and hardly long-term manageable if new versions of the algorithms are released. But if the algorithms are available as grid services, it becomes easy because the implementation and maintenance details are delegated to the authors of the algorithms.

Another possible evaluation scenario is the assessment of a couple of algorithms on particular registration problem. In this case, building a suitable evaluation image database is difficult because it involves specific images that may not be widely available. The data sharing potential of the grid may facilitate such a collection by enabling queries on suitable meta-data to shared image databases. A secure interface between DICOM servers and the grid, allowing such a scenario is for example presented in [Montagnat et al., 2006].

The goal of the PhD of Tristan Glatard is to investigate in more depth the potential of the GRID for medical imaging applications by implementing some of these scenarios. This PhD is a central element of the AGIR project (Grid Analysis of Radiological Images Data <http://www.aci-agir.org/> - in French: Analyse Globalisées des données d'Imagerie Radiologique), funded by the French Research Ministry through the ACI (Action Concertée Incitative) Masses de Données. This project gathers researchers in Computer Science, physics and medicine from CNRS, INRIA, University, INSERM, and hospitals. It aims at defining and validating on the one hand new grid services that address some of the requirements of complex medical image processing and data manipulation application ; and on the other hand new medical image processing algorithms that take advantage of the underlying grid infrastructure for compute and data intensive needs [Germain et al., 2005a, Germain et al., 2005b].

In this context, the bronze standard is an interesting evaluation algorithm for medical image analysis, and a good benchmark for the medical grid. Comparing and sharing registration algorithms implies that each registration service is semantically described. A complete system would include an ontology of registration problems (modalities, anatomical region, rigid or non-rigid registration, etc), of registration algorithms (input/output data types, method used, etc)

and of image and transformation formats. Following a first experiment on the interoperability of 3 rigid and non-rigid registration algorithms in [Hill et al., 2004], we simply wrapped in [Glatard et al., 2006d, Glatard et al., 2005b, Glatard et al., 2005a] each registration algorithm into a standard Web service. Those Web services are responsible for the grid execution of their algorithm on the data sets specified at invocation. Algorithms are thus standard black boxes, ready to be assembled into an application.

Then, the workflow of the bronze standard was described as a data pipeline. Control links may also be specified in order to describe precedence constraints between algorithms. We chose the Scuff language [Oinn et al., 2004] which is a good trade off between high expressiveness and simplicity. To efficiently execute such a workflow on a grid, we developed a workflow manager called MOTEUR [Glatard et al., 2006e, Glatard et al., 2006c]. We focused in particular on optimizing the time-performances, which are critical in the case of data-intensive applications. MOTEUR enables three different kinds of parallelism (workflow, data and service parallelism), in order to exploit the massively parallel resources available on the grid infrastructure. Moreover, it groups sequential jobs to lower the number of services invocations and minimize the grid overhead resulting from jobs submission, scheduling and data transfers. Finally, MOTEUR can execute workflows on grid systems with very different scales: We made experiments on the EGEE production grid¹ (including 18,000 CPUs all over the world and 5 PB storage capacity), as well as on the Grid5000 experimental infrastructure² (1,400 CPUs and hundreds of GB storage capacity) [Glatard et al., 2006b].

The Bronze standard workflow was experimented on a database of longitudinal MRIs in the context of the clinical follow-up of brain tumors during radiotherapy [Glatard et al., 2006f]. In the evaluation database build by Dr. P.-Y. Bondiau (Centre Antoine Lacassagne, Nice, France), 29 patients had more than 2 time points and were suitable to inclusion in our rigid registration evaluation study. Up to now, we only used gadolinium-injected T1 images. We are currently extending the description of the workflow and the statistical averaging program to handle the other T1 and T2 modalities of images. The main novelty is that each pair of modality requires different algorithm parameters and should have a different accuracy. The same registration algorithm as above were used (Baladin, Yasmina, Crest-Match), except the EM-ICP because extracting a meaningful surface on these images is challenging. A first run of the bronze standard workflow (720 registrations) rejected many transformations as outliers. A careful inspection revealed that there was two groups of images tilted by either +1.19 or -1.22 degree. The rigidity assumption was violated while registering images from one group to the other, and these transformations were detected as having an unacceptably bad accuracy with respect to intra-group transformations. It is interesting to notice the bronze standard procedure is powerful enough to enlighten this feature which remained unnoticed during two years of usage of this database!

A second run with the group of images with a positive tilt only (25 patients, 504 registrations) led to 20 outlier transformations only, among which 15 were concerning two patients with a very high deformation in the tumor area, leading to some global deformations of the brain. In that situation the rigidity assumption does not hold and several "optimal" rigid registration may be valid depending on the area of the brain. The last 5 rejected transformations involve two acquisitions with phase-encoded motion artifacts which impacted differently feature-based and intensity-based

¹Enabling Grids for E-sciencE, <http://www.eu-egee.org>

²Grid5000 national grid, <http://www.grid5000.org>

registration algorithms, leading to two non-compatible sets of transformations. Excluding these 20 transformations, we obtained mean errors of 0.130 degree on the rotations and 0.345 mm on the translations. The propagation of this error on the estimated bronze standard leads to an accuracy of 0.05 degree and 0.148 mm. The unbiased accuracy of each of the algorithms, obtained by comparing its results to the bronze standard computed from the 3 others methods show slightly higher but equivalent values for all algorithms.

The execution times of the whole workflow was compared on the EGEE and Grid5000 platforms, for different numbers of image pairs to register. Even though the EGEE production infrastructure gathers many more processors than Grid5000, the workflow was always faster on Grid5000 (2h10 versus 5h for 126 image pairs). It can be explained by the high overhead introduced by the EGEE grid, coming from the large scale of this platform and its multi-users nature. However, the speed-up obtained on Grid5000 is decreasing with the number of input images (5.6 for 66 image pairs, 2.3 only for 126). The Grid5000 platform progressively enters a saturation phase, where all the available processors are used by the application, while the EGEE grid is more scalable and less impacted by the growth of the input data set size. These results highlight the difference between an experimental grid, GRID5000, which has low overheads but a limited amount of resources, and an ever-loaded production platform like EGEE, which exhibit larger overheads but a very high scalability.

4.3 Non-linear registration

One usually classify non-linear registration algorithms by the dimension of the sought parameters. A first class relies on a parametric model of transformation that have (much) less parameters than voxels in the images. These algorithms are naturally called parametric. A second class of algorithms recovers the displacement of each voxel of one of the image, i.e. a dense deformation field. My research focused primarily on dense registration algorithms, first with the analysis and extension of Demon's like algorithms (Sections 4.3.1 and 4.3.3), then with the development of non stationary regularization criteria that can take into account some a priori about the anatomy and the pathologies (Section 4.3.5). To even better control the transformation while decreasing the number of degrees of freedom, we design with V. Arsigny in Section 4.3.6 the Polyrigid and Polyaffine transformation that locally behave as rigid or affine within specific regions.

4.3.1 Demon's like algorithms

In the nineties, several non-rigid registration algorithms were proposed. The original contribution might be traced to [Bajcsy and Kovačič, 1989], who differentiated the linear correlation criterion and used a fixed fraction of its gradient as an external force to interact with a linear elasticity model. [Christensen et al., 1997] argued that the linear elasticity was only valid for small displacements and could not guarantee the conservation of the topology of the objects as the displacements become larger. Thus, they proposed a viscous fluid model of transformations that effectively handles larger displacement. However, the computational price was very high and this type of algorithm had to be run on massively parallel machines. [Bro-Nielsen, 1996, Bro-Nielsen and Gramkow, 1996] used the linearity of partial differential equations to establish a regularization filter corresponding to this fluid model, several order of magnitude faster than the previous finite element method. In that context,

[Thirion, 1998] proposed to consider non rigid registration as a diffusion process. He introduced in the images entities (demons) that push according to local characteristics of the images in a similar way Maxwell did for solving the Gibbs paradox in thermodynamics. The forces he proposed were inspired from the optical flow equations:

$$f = \frac{(I - J \circ T) \cdot \nabla_I}{\|\nabla_I\|^2 + \alpha \cdot (I - J \circ T)^2}$$

and the method alternates the computation of the forces and their regularization by a simple Gaussian smoothing to obtain the displacement field. This resulted into a computationally very efficient algorithm which was much faster than the previous ones. This algorithm was used in several teams as reported by [Dawant et al., 1999, Bricault et al., 1998, Webb et al., 1999, Prima et al., 1998].

Our goal in [Pennec et al., 1999, Cachier et al., 1999] was to provide a theoretical derivation of the Demon's in order to understand the underlying assumptions and potentially modify them. The key idea was to consider non-rigid registration as a gradient descent technique. Let I be the reference, J the image to register, T the current transformation and $\nabla_J \circ T$ (resp. $\mathcal{H}_J \circ T$) be the transformed gradient (resp. Hessian) of image J . The gradient and Hessian³ of the Sum of Square Differences (SSD) criterion $SSD(T) = \int (I - J \circ T)^2$ are:

$$\begin{aligned} \nabla_{SSD}(T) &= 2(J \circ T - I) \cdot (\nabla_J \circ T) \\ \mathcal{H}_{SSD}(T) &= 2(\nabla_J \circ T) \cdot (\nabla_J \circ T)^T + 2(J \circ T - I) \cdot (\mathcal{H}_J \circ T) \end{aligned}$$

Approximating the criterion at the second order for a small perturbation by a displacement field $u(x)$, we have: $\nabla_{SSD}(T + u) \simeq \nabla_{SSD}(T) + \mathcal{H}_{SSD}(T) \cdot u$. If the Hessian matrix of the criterion is positive definite, the minimum is obtained for a null gradient, i.e. for $u = -\mathcal{H}_{SSD}^{-1}(T) \cdot \nabla_{SSD}(T)$. This formula require to invert the Hessian matrix $\mathcal{H}_{SSD}(T)$ at each point x of the image. To speed up the process, we approximate this matrix by the closest scalar matrix (in the Froebenius sense). In practice, we have modified this Newton optimization scheme into a Levenberg-Marquardt method where the adjustment vector field is given at each step by $u = -(\lambda + tr(\mathcal{H}_{SSD}))^{-1} \cdot \nabla_{SSD}$. Dropping the (possibly negative) second order terms in the Hessian, we are left with:

$$u = \frac{-3 \cdot (J \circ T - I) \cdot (\nabla_J \circ T)}{\|\nabla_J \circ T\|^2 + \lambda} \quad (4.2)$$

The parameter λ performs a tradeoff between a first order gradient descent and a second order gradient descent. Taking $\lambda = \alpha \|J \circ T - I\|^2$ lead to a formula which is close to the demon's forces but involves the gradient of the moving image J . We showed in [Pennec et al., 1999] that minimizing the reverse SSD criterion $\int (I \circ T^{(-1)} - J)^2$ with the Eulerian (compositive) adjustment rule: $\hat{T}_{i+1} = \hat{T}_i \circ (\text{Id} + f)$ was actually leading to the "force" proposed by Thirion.

In [Cachier and Pennec, 2000], we developed a more complex similarity measure that can handle local intensity changes: the sum of Gaussian-windowed local correlation coefficients (LCC). One of the main contributions was to provide an efficient computation scheme using convolutions. Let $G \star f$

³Notice that the Hessian of the criterion is generally a convolution kernel $(\mathcal{H}_{SSD}(T) \cdot u)(y) = \int K(x, y)(T) \cdot u(x) \cdot dx$. However, as the regularization is not taken into account, there is no correlation between two different point so that this kernel is purely diagonal and can be represented by a matrix.

be the convolution of f by the Gaussian, $\bar{I} = (G \star I)$ the *local mean*, $\text{Var}(I) = G \star (I - \bar{I})^2$ the *local variance*, $\text{COV}(I, J \circ T) = G \star [(I - \bar{I})(J \circ T - \overline{J \circ T})]$ the *local covariance* between image I and image $J \circ T$. The *local correlation coefficient* is $\rho(I, J \circ T) = \text{COV}(I, J \circ T) / \sqrt{\text{Var}(I) \cdot \text{Var}(J \circ T)}$ and integrating it at each image point lead to the the LCC:

$$LCC(T) = \int \rho(I, J \circ T)(x) \cdot dx = \int \frac{\text{COV}(I, J \circ T)}{\sqrt{\text{Var}(I) \cdot \text{Var}(J \circ T)}}$$

As this criterion is not a least-square, we investigated in [Cachier and Pennec, 2000] several methods to compute efficiently its gradient using convolutions. Our conclusion was that the following approximation of the gradient was performing an ideal tradeoff:

$$\nabla_{LCC} \simeq \left((I - \bar{I}) - (J \circ T - \overline{J \circ T}) \cdot \frac{(\overline{I \cdot J \circ T} - \bar{I} \cdot \overline{J \circ T})}{\sqrt{\text{Var}(J \circ T)}} \right) \frac{\nabla_{J \circ T}}{\sqrt{\text{Var}(I) \cdot \sqrt{\text{Var}(J \circ T)}}$$

The LCC similarity measure tends to be one of the more powerful in terms of applications. Indeed, highly multimodal problems require a highly constrained transformation, otherwise the effective number of degrees of freedom becomes larger than the number of measure equations and the algorithm get stuck in numerous local minima. Thus, the main application of non-rigid registration are for slightly multimodal problems for which the relationship between intensities can be considered as locally affine.

4.3.2 The Pasha algorithm

At that point, only half of our initial goal was fulfilled: we justified the Demon's forces as a second order gradient descent, but not the regularization scheme. In [Pennec et al., 1999], we derived a Gaussian smoothing step by modifying the harmonic energy $Reg(T) = \int \|\nabla T\|^2$. However, we were not able to show that this modified regularization energy was well posed. It is interesting to see that [Modersitzki, 2004] justifies the Demon's by keeping the harmonic energy but modifying the SSD criterion. In that case, it became difficult to analyze the underlying noise assumptions on the image intensities.

In order to end-up with the global minimization of a well posed criterion, Pascal Cachier proposed to introduce a hidden variable in the registration process: correspondences [Cachier et al., 2003]. The idea is to consider the regularization criterion as a prior on the smoothness of the transformation T , but instead of requiring that point correspondences between image voxels (a vector field C) be exact realizations of the transformation, one allows some error independently at each image point. Considering a Gaussian noise on displacements, we end-up in the simple monomodal case with the global energy:

$$E(T, C) = \frac{1}{\sigma_I^2} \int (I - J \circ C)^2 + \frac{1}{\sigma_x^2} \int \|C - T\|^2 + \frac{1}{\sigma_T^2} \int \|\nabla T\|^2$$

This amounts to consider that there is a spatial uncertainty of σ_x on the voxel positions. This new variable is easy to set: it should be of the order or less of the voxel size.

The interest of this auxiliary variable is that an alternated optimization over C and T now perfectly decouples the complex global minimization into two simple and very efficient estimation

steps. Starting from an initial transformation $T_0 = \text{Id}$ at iteration zero (after possibly a rigid or affine transformation), we iteratively:

- Find the best matches at fixed transformation by minimizing $\int (I - J \circ C)^2 + \sigma_I^2 / \sigma_x^2 \|C - T\|^2$ using a gradient descent as we previously described. In fact, the gradient *computed at* $C = T$ is the same as before, and an additional term $\sigma_I^2 / \sigma_x^2 \text{Id}$ appears in the Hessian (taken once again at $C = T$). Thus, the scalar second order Gauss-Newton gradient descent gives the optimal correction $\delta C = (J \circ T - I) \cdot (\nabla_J \circ T) / (\|\nabla_J \circ T\|^2 + n \cdot \sigma_I^2 / \sigma_x^2)$ (n is the dimension of the space).
- Find the transformation that best approximate the correspondences by minimizing $\int \|C - T\|^2 / \sigma_x^2 + \|\nabla T\|^2 / \sigma_T^2$. This minimization has a closed-form solution using a single convolution when the regularization is quadratic and uniform. For instance, the optimal transformation is the convolution of the correspondence field by a Gaussian with the above harmonic criteria, but more complex vectorial filters can be designed [Cachier and Ayache, 2004].

The regularization can also be modified to handle elastic and fluid-like models. The basic idea was to use a transformation regularization criterion of the form:

$$\text{Reg}(T, dT) = \omega R(T) + (1 - \omega) R(dT)$$

When the regularization kernel is quadratic and uniform, e.g. for $R(T) = \int \|\nabla T\|^2$, we still end-up with a closed-form formula for the update of the transformation:

$$T_{i+1} = \omega(T_i + K \star (C_i - T_i)) + (1 - \omega)K \star C_i$$

where K is a convolution kernel that depend on R and on the variances [Cachier et al., 2003].

It is interesting to remark that σ_I^2 can be replaced by the purely local estimation $(J \circ T - I)^2$ (or a smoothed version) in the Gauss-Newton matches estimation step, which gives another justification of the demons' forces. Moreover, the penalization term allows to implement very efficiently any other optimization scheme: the search for the correspondence is constrained to be local: the correspondence field is the closest local minimum to the current transformation.

We were able to draw in [Cachier et al., 2003] interesting limit behavior corresponding to other registration algorithms. For instance, when the uncertainty on the voxel position σ_x tends towards zero, then the regular transformation T is gradually enforced to be closer and closer to the correspondences (and vice-versa). In fine, the optimal solution is obtained for $C = T$, which corresponds to the optimization of the usual sum of a similarity and a regularization criterion, as investigated for instance in [Hermosillo et al., 2002]. Thus, σ_x can be seen as a kind of scale variable and used as such in the optimization strategy.

When both σ_x and σ_T jointly tend towards zero in a fixed ratio, then the regularization step remains unchanged, but the penalizing term for the distance to the current transformation becomes weaker and weaker in the matches estimation step. In that case, the algorithm converges towards our previous explanation of the demons (without having to tweak the regularization term as we did in [Pennec et al., 1999]).

Last but not least, one can interpret the PASHA algorithm as a generalized ICP in the sense of [Feldmar and Ayache, 1996]. The idea is to consider images as intensity isosurfaces represented

by two sets of points (x_i, I_i) in a $(n + 1)$ dimensional space. A locally affine spatial transformation can then be retrieved using an ICP algorithm: in a first step, the closest point in the second image is matched to each point in the first one after deformation with the current transformation; in a second step, a new locally affine transformation is computed from the matches. The distance used in the first step is the standard (re-weighted) Euclidean distance in the augmented space: $dist^2((x, I(x)), (y, J(y))) = (I(x) - J(y))^2/\sigma_I^2 + \|x - y\|^2/\sigma_x^2$. Optimizing the sum over all voxel positions for $y = C(x)$ lead to a formula close to the first two terms of the Pasha criterion. Using the regularization kernel corresponding to the locally affine transformation, one can see that the criterion optimized by Feldmar's ICP algorithm is a particular case of the PASHA one.

Thus, the PASHA algorithm generalizes the usual similarity plus regularization formulation, the Demons, and the image ICP algorithms. However, it provides much more flexibility than all these algorithms because it allows to change the similarity measure and the regularization criterion to better fit the image and transformation assumptions. It also allows very efficient optimization techniques: the typical registration time for 256x256x128 MR images ranges from 5 to 40 minutes depending on the complexity of the transformation.

We have demonstrated in [Cachier et al., 2003] the performance of this approach for the study of the preoperative pneumocephalus during deep brain stimulation of Parkinsonian patients. In [Pennec et al., 2003, Pennec et al., 2001a, Pennec et al., 2001b], we have also used this algorithm for the per-operative tracking of brain deformations in sequences of 3D ultrasound images (see also Section 4.1.1). We showed that it could recover an important part of the deformations and issue smooth deformations despite the noisy nature of the US images. Experiments on animal and phantom data indicate that an accuracy of 1-2 mm is achievable in the areas where there is an elastic deformation. This is encouraging since the accuracy of the clinicians without per-operative imaging is estimated to be around 3-5 mm. In our experiments, we observed that the SSD criterion was well adapted to the registration of successive US images of the time sequence. However, the appearance of some tissues in US images is known to change along time, and the LCC criterion might be more adapted to long times sequences in a clinical setup.

4.3.3 Hybrid iconic and geometric registration

While intra-subject registration is usually a well-posed problem because there is an underlying physical deformation, inter-subject registration from images intensities only is basically an ill-posed problem because the topology of the brain, and especially the cortex, varies strongly from one individual to another. However, it is believed that these geometrical ambiguities could be partially resolved when using higher level anatomical knowledge like information about sulci.

Following [Le Goualher et al., 1999, Hellier and Barillot, 2003, Thompson and Toga, 1996, Vaillant and Davatzikos, 1999] and others, we proposed in [Cachier et al., 2001] to extend the PASHA framework to this type of geometric correspondences. The sulci were extracted from the MR images and automatically labeled using the tools developed by J.F. Mangin and his team at CEA-SHFJ [Mangin et al., 1995, Rivière et al., 2002]. As the labeling error rate is 24% (this is also the inter-rater variability), we chose to enforce label matching only for the most well known sulci. From the surface of each sulci, we extracted the top and bottom sulcal lines, which were used as geometrical features for the registration. From a computational point of view, using one dimensional features drastically reduces the number of points to be processed and thus does not hamper the

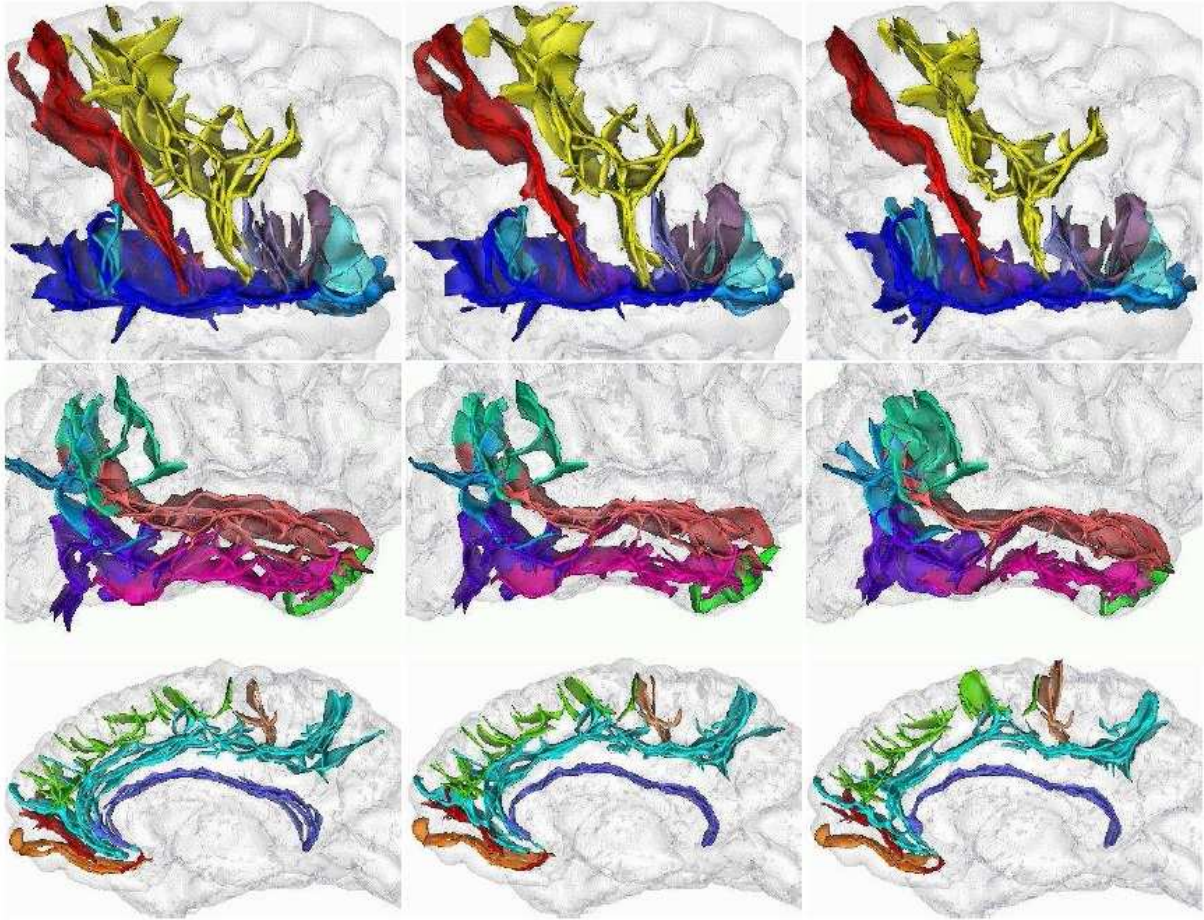


Figure 4.6: Result of the hybrid feature and iconic PASHA registration on 5 images on the brain. Superimposition of a few sulci after affine registration (left column), after the PASHA non-linear registration without (middle column) and with (right column) sulcal matching. The sulcus matching helps to pair homologous sulci when they are initially far apart, and also improve the accuracy of the matching especially when the topology of the sulci is complex.

speed of the algorithm. From an anatomical point of view, the sulcal top line corresponds to the junction of the sulcal surface with the hull of the brain (similarly to the sulcal lines we will use in Section 5.2), and the sulcal bottom line should be close to the shallow creases that appear on the fetal brain at the beginning of the cortical folding process. According to this theory, these sulcal roots should be very stable topologically and geometrically across individuals because they delimit the main structural and functional areas of the human brain [Régis et al., 1995, Welker, 1989]. Hence, we enforced a looser geometric matching constraint on the sulcal top lines than on the bottom ones.

To integrate the matching of sulcal line in the PASHA algorithm, the idea is to introduce a new auxiliary variable: the set of correspondences C_s between the points of the sulcal lines S_I from

image I and the points of sulcal lines S_J of image J . This amounts to add two terms in the global criterion: a normalized distance $E_S(S_I, S_J, C_s) = d^2(S_I, S_J \circ C_s)/\sigma_s^2$ quantifying the closeness of sulcal lines after matching (we used in fact a robust distance to account for topological changes and different variances for bottom and top lines), and a distance from these new correspondences to the transformation. We end-up with the global hybrid iconic and feature based energy:

$$E(T, C_i, C_s) = \int \frac{(I - J \circ C_i)^2}{\sigma_I^2} + \int \frac{\|C_i - T\|^2}{\sigma_{x_i}^2} + \frac{d^2(S_I, S_J \circ C_s)}{\sigma_s^2} + \int \frac{\|C_s - T\|^2}{\sigma_{x_s}^2} + \int \frac{\|\nabla T\|^2}{\sigma_T^2}$$

The optimization is done alternatively on the intensity correspondences C_i (there is no change with respect to the normal PASHA algorithm), on the sulcal correspondences C_s using a nearest neighbor search (this is an ICP algorithm), and on the transformation T . There is still a closed-form for this last step: the resulting transformation is a linear combination of the Gaussian smoothing of the dense correspondences C_i and of a splines interpolation of the sparse point correspondences C_s . Thus, the efficiency of all the optimization steps is conserved.

We have experimented this algorithm on 5 labeled brain from the CEA-SHFJ. The visual result is presented in Fig. 4.6. The original PASHA method relying only on intensities was able to match the sulci when their topology was simple (i.e. mostly linear) and where the affine initial registration was good enough. For instance, the central sulci (in red) are generally well matched. However, it was relatively backward for one brain and has been partly matched to the precentral sulcus of the reference brain because it was the closest sulcus at that location after the initial affine alignment. Adding the sulcal constraint allows to match it correctly all along. Sulcus matching also helps to register more efficiently sulci with a more complex topology such as the precentral sulcus, and generally improves the accuracy of the matching of all sulci. Interestingly the optimal transformation was still very smooth and one-to-one. In fact, seen from the intensity point of view, it seems that the geometric constraints simply help to bridge some unwanted local minima and to reach more proper ones. This strongly indicate that more prior information than just intensities is needed for inter-subject registration.

4.3.4 High performance computing for "human-time" registration

With the PhD of Radu Stefanescu, we focused on bringing non-rigid registration algorithms closer to a clinical use. A careful analysis of the needs of a clinical environment led us to conclude that usability and speed were major constraints: either the algorithm is robust and completely automatic, in which case it can be run offline for applications such as atlas-based segmentation in pre-operative planning, or there is a need for interaction (for instance tuning the parameters), and the computation time has to be reduced from about one hour to just a few minutes. We summarized in this section our investigation on the parallelization of registration algorithms to obtain "human time" computations, while Section 4.3.5 will focus on the improvements brought to the registration method to better adapt it to the problem at hand and to improve its robustness.

In contrast with dedicated expensive high-performance computing solutions, cluster computing now offers a large processing power at a low cost with a great flexibility. One can use a dedicated cluster with very high-speed connections or even the available PCs of the lab connected by Ethernet. Such a hardware configuration is already available in many hospitals. Thus the distributed mem-

ory architectures appear to provide a higher degree of scalability and reusability for the software components that need to be parallelized than shared memory ones.

We first showed in [Ourselin et al., 2002] that a generic rigid/affine multi-modal registration algorithm (namely Aladin) could be easily parallelized on a cheap and standard cluster to become real-time, without loss of generality or performance. Then, we tackled in [Stefanescu et al., 2004b] the parallelization of demons' like algorithms (e.g. PASHA). Such an algorithm has a regular structure with three main algorithmic components: the subsampling of the images and the oversampling of the displacement field for the multi-resolution approach; the computation of the correspondence field; its "regularization" to obtain the displacement field. Since each point of the image is processed in a similar manner, the algorithm is a good candidate for a parallelization using a data decomposition, rather than a task decomposition. We chose to decompose the correspondence and displacement fields into parallel slices perpendicular to one axis only, each slice being assigned to one node of the cluster (i.e. one processor). The reason for this specific decomposition is that each algorithmic bloc (especially filtering) can be parallelized very efficiently without time-costly data redistributions.

In fact, the oversampling of the displacement field is done by tri-linear interpolation, which only requires that each processor sends the boundary values of its block to the neighboring processor. Gradients are pre-computed and distributed along with the images to all processors at the beginning, so that the computation of the forces is done purely locally. The only difficult part is the parallelization of the regularization step. As the isotropic Gaussian filter is separable, convolving a 3D image is equivalent to successively convolving the image with a 1D Gaussian along each axis. By adopting a block decomposition *along one axis only*, the filtering along two directions can be done within each block without any communication.

For filtering along the decomposition axis, we proposed two implementations. The *send-borders algorithm* is a parallel Gaussian filter for small variances based on the exponential decay of the Gaussian. The idea is to consider it as negligible outside 3 standard deviations. If each processor sends a border of this width to the neighboring processor, then all processors can compute the filtered value on their original domain. The drawback of this algorithm is that the results are not rigorously correct and using larger borders makes the parallel algorithm less efficient. Secondly, each process has to apply the filter to a larger domain than its own, and the amount of data sent through the network is proportional to the filter's standard deviation.

The second solution we proposed was to parallelize the recursive implementation of the Gaussian [Deriche, 1992]. This filter basically consists in a forward step followed by a reverse step. At each step, the result of the filtering on the 4 preceding values is needed to process a new point (this is a 4th order filter). Thus, processing one single line cannot be done in parallel. However, different processors can deal with their part of *different lines* simultaneously. Thus, the idea is to mimic an industrial pipeline process, where the first processor deals with the beginning of line 1, then sends the 4 last values to the second processor, which can process the second part of line 1. Meanwhile, processor 1 processes the beginning of line 2. They both send the last values to their neighboring processors and so on. The pipeline process takes a number of steps equal to the number of processors before working at its full capacity. The full acceleration is achieved if the number of lines is much larger than the number of processes, which is usually true in a cluster of workstations. To decrease the network usage, each processor can process several lines before sending a grouped message, at

the cost of a longer pipeline filling time.

An analysis of the theoretical performances in terms of computation time, maximum acceleration and network usage (amount of data and number of messages sent) showed that the send-borders algorithm can take advantage of very high latency networks. The pipeline recursive implementation has a greater accuracy and can efficiently tackle the case of very wide Gaussians, sparing processor time and network bandwidth. It can also be adapted to high latency networks by tuning the message grouping parameter. The practical performances were measured for the registration of 256x256x120 MR T1 images of the brain. We obtained an acceleration of 11 by using 15 2GHz PC's connected through a 1GB/s Ethernet network and reduced the computation time from 40min to 3min30 [Stefanescu et al., 2004b]. For the parallel filtering section of the algorithm, the pipeline recursive filtering algorithm was almost twice faster than the send-border algorithm when a large number of processors was used. Interestingly, the measured time was almost always above the theoretical one for both algorithms. For instance, an acceleration of 20 has been measured with 15 processors, whereas our model predicted 13.4. This is most probably due to the better performances in accessing the memory for smaller domains (cache misses effect): relatively more data fit in the memory caches whose access is much faster than standard memory. This enlighten the fact that memory access times can be more important than the computation time!

In order to further optimize the ease of use of the parallel registration tool, we investigate in [Stefanescu et al., 2005] the transparent use of a cluster through a distant graphic client. The graphical user interface runs on a workstation within the clinical environment and locally loads and visualize the images to register. A user interface button enables the user to connects to a registration service running on a cluster within our laboratory by using an SSL-based secure connection. Only the image data that are necessary (image size and raw data) are sent, so that the patient anonymity is preserved. During the registration, the user receives real-time information about the status of the algorithm (small size messages), as well as some intermediate resampled image (several megabytes of data) that are displayed on the GUI. The user is thus able to control the registration and, if needed, stop and restart it with modified parameters. Upon termination, the registration result (transformation and resampled image) is sent back to the GUI. Since the user and the computation cluster are at distant locations and linked through a low-performance network, the data is compressed before being sent through the network, and decompressed upon receipt.

Our tests show that the software has reasonable response times even if we use a network as slow as a 16kB/s ADSL modem. The GUI was running on a standard 600MHz Pentium III laptop with a wireless network interface. The registration service was running on a cluster of 15 2GHz Pentium IV PC's running linux linked through a 1GB/s Ethernet network. The image upload (3.3MB after compression) took 40 seconds on a high speed network to 3min30 on a home Asymmetric DSL connection. The update time for intermediate results was 18 seconds (resp. 1min30), and the registration was completed in 7 to 10 minutes in the worst case (home ADSL), including image transfer time. This proves that our non-rigid registration service can be used from almost everywhere with a very modest equipment.

4.3.5 Non stationary regularization with anatomical a priori

The type of transformation regularization is a very sensitive choice. In the previous works, we made the assumption of a "uniform elastic" like material. This might seem adapted for the deformations

of the brain tissues (white and gray matter) for an intra-subject registration, but some improvements are needed to cope with the fluid deformations that occur within the CSF (particularly in the ventricles), especially for inter-subject registrations: there is a need for a space-varying regularization, depending on the underlying brain tissue type. Also, the information present in the images at different places is not equally important: we would like to register precisely homologous points in the regions where the image information is reliable (e.g. edges), while interpolating the deformation field where it is not (e.g. uniform areas). Last but not least, enforcing the invertibility of the transformation is important to avoid space folds and in practice to resample the segmentation from the atlas to the patient geometry in atlas-based segmentation.

Following [Trouvé, 1998, Hermosillo et al., 2002] we first restated in [Stefanescu et al., 2004c] the implementation of Demons and Pasha algorithms in a Eulerian framework, i.e. with the “compositional” update equation: $T_{i+1} = T_i \circ v_i$ instead of the Lagrangian additive one $T_{i+1} = T_i + u_i$. The two incremental displacements are related by $u = \nabla T^T v + O(\|v\|^2)$. When propagated into the derivatives, the major difference with the additive scheme lies that we now take the gradient of the resampled image $\nabla(J \circ U)$ instead of the resampled gradient of the original image $(\nabla J) \circ U$. From a computational point of view, filtering to compute gradient is as efficient as resampling (we basically have to sweep the memory for the image values), so that the computation time is only 25% larger (1 scalar resampling and 3 scalar filterings versus 3 scalar resamplings). It is worth noticing that limiting the maximal displacement in v to less than half the voxel size actually ensures that the displacement field is diffeomorphic using tri-linear interpolation. By composing only diffeomorphic updates, we enforce in practice the same property on the final transformation. We observed that the accuracy was similar to the regriding method of [Christensen et al., 1996] with a computation time of one third only.

The second contribution was to propose a non-stationary “elastic” regularization tailored to the anatomy. Real deformations are often highly inhomogeneous and contain highly localized fine details close to large smooth areas. When regularizing with a stationary Gaussian filtering, the standard deviation of the filter is either too large, preventing the retrieval of fine details, or too small, which yields a noisy deformation field in smooth areas. Our solution is to use a priori information about the variability of the different structures in the images (e.g. a variance or a covariance matrix field) to locally adapt the level of regularity. However, non-stationary Gaussian smoothing is computational expensive as we cannot rely on recursive filters. Instead, as the stationary Gaussian smoothing corresponds to the heat flow in a homogeneous material, we chose the use the following anisotropic smoothing of the displacement components : $\partial U_\alpha / \partial t = \text{div}(D \cdot \nabla U_\alpha)$, where D is the “diffusion” (or stiffness) tensor.

In uniform areas, the gradient of the image similarity metric is close to zero, whereas it may be high at edges where we have an information. The usual regularization of the speed vector field consider that all the points carry the same information so that the speed is weakened at edges and slightly diffused around it. This means that uniform areas in the image tend to stick at their positions while edges are constrained to move slowly, even in the case of a pure translation. Our idea was to interpolate the speed in unreliable regions from neighboring information rather than lowering it. This was realized in [Stefanescu et al., 2004c] using the anisotropic diffusion equation $\partial v / \partial t = (1 - k)(\Delta v)$, where the field k measures the *local confidence* that we have in the similarity criterion. If $k(x) = 1$, the local speed is locally unaffected. For smaller values, the gradient of the

speed is locally smoothed, so that we end-up with a pure interpolation for $k(x) = 0$. Points that are reliable landmarks in the source image are those where the neighborhood has a characteristic pattern that cannot be produced by noise. We used an expression derived from [Weickert, 2000] for the non stationary diffusion of images: $k = \exp(-c/(\|\nabla J\|/\lambda)^4)$.

From a numerical point of view, both the confidence-based filtering and the non-stationary regularization can be described as non-stationary diffusion PDEs on scalar fields. The differential operator can be written as a big (time-dependent) matrix A_t acting the vector of all values v_t at time t , so that the discrete equation to solve is: $\dot{v}_t = A_t.v_t$. The explicit scheme approximates \dot{v}_t by $(v_{t+dt} - v_t)/dt$, so that the resolution is simply $v_{t+dt} = v_t - dt.A_t.v_t$. However, the time step has to be very small in order to avoid divergence [Weickert et al., 1998], which makes the approach very slow. This drawback can be avoided by solving the *implicit scheme*, obtained by taking the value right hand side of the equation at $t + dt$, which gives: $v_{t+dt} = (\text{Id} - dt.A_{t+dt})^{(-1)}.v_t$. This scheme is guaranteed to be stable for all values of dt . However, it is complicated to solve (since we do not know A_{t+dt}), and therefore the *semi-implicit scheme* $v_{t+dt} = (\text{Id} - dt.A_t)^{(-1)}.v_t$ is often preferred.

In one dimension, the matrix A_t is tridiagonal. The inversion of such a matrix can be achieved efficiently using Thomas algorithm, which basically consist in a LR decomposition followed by forward and backward substitution steps. This first order recursive algorithm operates in linear time. In the 3D case, the matrix is not longer tri-diagonal. To address this problem, [Weickert et al., 1998] introduced the *Additive Operator Scheme* (AOS). For separable operators, the differential operator can be decomposed as a sum of tri-diagonal operators along each space axes $A_t = \sum_{\alpha} A_t^{\alpha}$. A Taylor expansion of the semi-implicit scheme then provides:

$$v_{t+dt} = (\text{Id} - dt. \sum_{\alpha} A_t^{\alpha})^{(-1)}.v_t = \frac{1}{3} \sum_{\alpha} (\text{Id} - dt.A_t^{\alpha})^{(-1)}.v_t + O(dt^2)$$

This amounts to replacing the inversion of a non-tridiagonal matrix with three inversions of tridiagonal ones. In practice, we obtained an equivalent computational load for one AOS regularization step and for the computation of the gradient of the similarity criterion. The second interest of the AOS is that matrix inversions are solved using first order recursive filters. Thus, they can be easily parallelized using our previous pipelining algorithm. To our knowledge, this was the first efficient parallel implementation of the AOS scheme on distributed memory computers.

We first tested our algorithm by registering several 3D T1-weighted MRI images of Parkinsonian subjects. These images were acquired pre-operatively under stereotactic conditions, in order to select optimal targets for deep brain stimulation. After a global affine registration, all images have the same sizes $256 \times 256 \times 124$. The stiffness field was taken to be the probability of not being in the white matter, gray matter or fat thanks to a simple fuzzy k-means classification of the image. The algorithm was run on a cluster of 15 2GHz Pentium IV PCs, linked through a 1GB/s Ethernet network. The computation time was 5 minutes instead of 1 hour on a single sequential computer. These experiments confirmed that our confidence-based filtering of the speed was leading to a faster (10% less iterations) and more accurate convergence of the algorithm, that the non-stationary smoothing of the deformation was providing much larger deformation than the purely ‘‘Gaussian-elastic’’ method, and much more regular ones than the purely ‘‘fluid’’ approach while matching the images as well. In other experiments [Stefanescu, 2005], we used the structure tensor of a binary image as an anisotropic stiffness tensor fields, and we were able to simulate quite accurately the

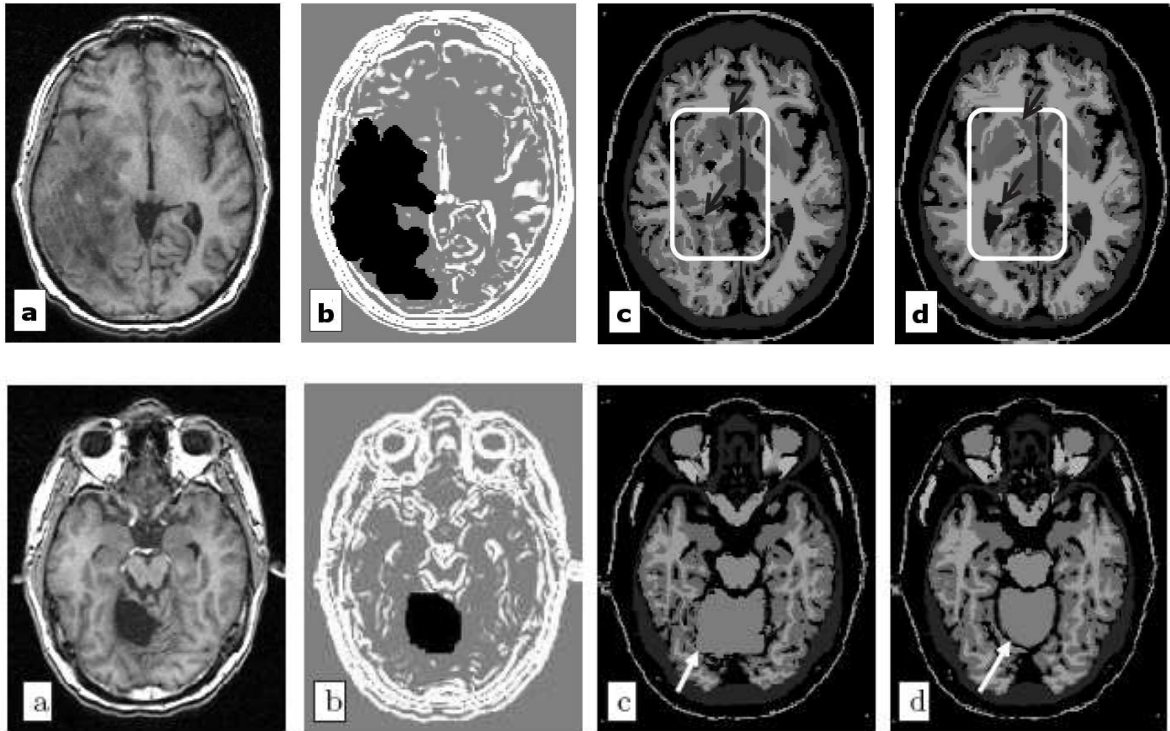


Figure 4.7: Atlas-based segmentation of a patient image containing a tumor (top line) or a resection (bottom line). (a) Patient image. (b) Tumor and resection segmentations. (c) Result produced by a registration un-aware of the pathology. (d) Result produced by our algorithm, exhibiting a better segmentation (see white and black arrows).

deformation behavior of a 2D thin membrane in 3D (a balloon).

We also experimented in [Stefanescu et al., 2004a] this algorithm for atlas to patient registration in the context of radiotherapy planning. In that case, a very important issue is the presence of pathologies such as tumors or surgical resections in the patient image. These structures have no equivalent in the atlas, which usually lead the non-rigid registration to important errors, especially around the pathology which is exactly the area of interest for radiotherapy. We tested the atlas registration on 22 T1-weighted MR images of different patients. After a preliminary rigid registration, the images sizes are $256 \times 256 \times 60$. The surgical resections and tumors were automatically segmented in the images using a dedicated image analysis workflow, and the confidence in the image similarity measure at these points was set to zero. The pathology segmentation takes between 1 and 3 minutes, and the non-rigid registration takes about 4 minutes on a cluster of 15 personal computers (2GHz Pentium IV processors, 1GB/s network), which amounts to a total computation time of 5 to 10 minutes. Results have been visually inspected by a radiotherapist, and appear satisfactory. Fig. 4.7 present examples where the patient brains have a large tumor and a surgical resection. A simple non-rigid registration is not able to follow the contour of the cerebellum in the last case (see white

arrow on the bottom line of Fig. 4.7c). With the use of the confidence-based filtering algorithm, the segmentation is largely improved.

4.3.6 Polyrigid and Polyaffine Transformations

In between rigid/affine transformations and deformation fields or diffeomorphisms, a few parametric transformations such as B-Splines [Rueckert et al., 1999], Thin-Plate-Splines [Bookstein, 1999], or finite elements mechanical models [Ferrant et al., 1999] are used in medical image registration because they provide an intermediate number of degrees of freedom. However, in the case of anatomical structures incorporating rigid elements (such as bone articulations), or structures which are subject to simple local deformations, like histological slices, we believe that none of them is fully appropriate, especially when rotations are substantial. In [Arsigny et al., 2003, Arsigny et al., 2005c], we introduced a novel kind of geometrical transformations, named Polyrigid and Polyaffine, that efficiently encode locally rigid or affine deformations with a very small number of intuitive parameters. The key advantage of this approach with respect to other parameterizations of deformations is the guarantee of invertibility of the global transformation and the simple form taken by its inverse.

Our idea is to use simple fuzzy regions defined by a membership function w_i and the associated rigid or affine transformation T_i . In [Arsigny et al., 2003, Arsigny et al., 2005c], we use renormalized Gaussians $w_i(x) = p_i \cdot G_i(x) / (\sum_j p_j \cdot G_j(x))$ with $G_i(x) = G_{(a_i, \sigma_i)}(x)$, where the standard deviations σ_i control the rate of decay and the p_i 's rank the global influence of the each component. The usual way of interpolation the transformation is to do a simple Euclidean averaging of the displacements induced by each region $T(x) = \sum_i w_i(x) \cdot T_i(x)$. However, this approach leads to space folds and invertibility problems. The solution we proposed was to average the infinitesimal displacements (instantaneous speed) instead of the displacements, and to recover the global transformation by integrating the resulting flow. The resulting transformation is parameterized by very few parameters (the center, the variance, the influence and the rigid transformation of each component) and is guaranteed to be diffeomorphic. Moreover, we were able to provide several numerical schemes to compute the differential of the transformation at each point so that any image similarity metric could be easily optimized using gradient descent in ITK. The method was demonstrated on histological slices [Arsigny et al., 2003].

The general framework was reformulated in [Arsigny et al., 2006b] as follows: first, determine an admissible vector field $v_i(x, t)$ for each region such that the integration of the ODE $\dot{x}(t) = v_i(x, t)$ between time 0 and 1 gives back $T_i(x)$. This corresponds in essence to taking a ‘‘logarithm’’ of the transformation. Then average the vector fields between regions: $v(x, t) = \sum_i w_i(x) v_i(x, t)$. Finally integrate the flow of the resulting vector field $v(x, t)$ to obtain the transformation $T(x)$. This last part can be seen as a ‘‘geodesic’’ walking step. For rigid and affine transformations, several admissible logarithms are possible. We previously used one simple formula involving the logarithm of rotations to define Polyrigid transformations but its extension to affine and larger transformation groups was not really clear. By taking the principal matrix logarithm of the affine transformations in homogeneous coordinates:

$$\log \left(\begin{bmatrix} A_i & t_i \\ 0 & 1 \end{bmatrix} \right) = \begin{bmatrix} L_i & v_i \\ 0 & 0 \end{bmatrix}$$

V. Arsigny ended up in [Arsigny et al., 2006b] with stationary vector fields $v_i(x, t) = v_i + L_i \cdot x$. This

means that we are left after averaging with the integration of the stationary or autonomous ODE: $\dot{x} = \sum_i w_i(x)(v_i + L_i.x)$. What is remarkable is that the family of transformations $T^s(x)$ obtained by integrating such stationary vector fields from time 0 to time s do constitute a one-parameter subgroup of diffeomorphisms. In the case of a single affine component, these are the one parameter subgroups of the affine transformations. Conversely, all one parameter subgroups of affine transformations are of this form. With several components, the transformations are more general one-parameter subgroups of diffeomorphisms that were called Log-Euclidean Polyaffine Transformations (LEPTs). The remarkable properties of these transformations is that they are invariant by an affine changes of coordinate system and stable by inversion. Moreover, V. Arsigny generalized the scaling and squaring method, originally used to compute matrix exponential, to compute very efficiently the “exponential” of a vector field, i.e. to integrate stationary ODEs. This led to a very efficient algorithm to compute LEPTs [Arsigny et al., 2006b].

This framework can also handle more general transformations than local rigid and affine one: one can also compute general diffeomorphisms arising from the integration of general stationary vector fields [Arsigny et al., 2006a]. Conversely, a practical iterative square-root and scaling method was developed to compute the logarithm of a diffeomorphisms. Computing the exponential of vector fields and the logarithm of diffeomorphisms can be viewed as a generalization of the the Log-Euclidean framework developed on tensors in [Arsigny et al., 2006c] to general diffeomorphic transformations. Such a framework could prove very useful to make statistics on the deformations since it allows usual statistics to be performed on diffeomorphisms in a simple *vectorial* way on the logarithms of transformations. Moreover, it has interesting properties such as inverse-invariance. From a theoretical point of view, there are still some problems due to the infinite-dimensional nature of diffeomorphisms that are yet to be completely solved. In particular, it would be desirable to have a simple characterization of the conditions under which the principal logarithm of diffeomorphism exists. However, the algorithms presented to compute the exponential of vector fields and logarithm of diffeomorphisms are very efficient and seem to be quite reliable, as has been shown in [Arsigny et al., 2006a] with statistics on the deformation from an atlas to 9 subjects. In fact, exploring physically or statistically constrained transformations in registration is one of the computational method used to model the anatomical and biological variability of the anatomy, which will be the subject of next chapter.

Chapter 5

Computational models of the anatomy

Computational anatomy is an emerging discipline that aim at analyzing and modeling the biological variability of the human anatomy through computational tools [Grenander and Miller, 1998, Thompson et al., 2004]. The goal is not only to model the mean (or a representative) anatomy and its normal variations among a population, but also to discover morphological differences between normal and pathological populations. These steps are necessary to detect, model and classify the pathologies from structural abnormalities, but also to faithfully guide the adaptation of generic models (atlases) towards patient-specific models. To reach this goal, the method is to identify anatomically representative geometric features (points, tensors, curves, surfaces, volume transformations), and to describe their statistical distribution. This can be done for instance via a mean shape and covariance structure after a group-wise matching. Then, in order to compare populations, there is a need to compare feature distributions and to test for statistical differences. There is a whole hierarchy of anatomical features ranging from point-wise features (landmarks), to curves (e.g. crest or sulcal lines on the cortex), surfaces, images (3D functions) and finite- or even infinite-dimensional transformations (rigid, locally affine, diffeomorphisms). These geometric features most often belong to manifolds rather than to Euclidean spaces, which raises the need for geometrical methods.

There are nowadays a growing number of geometrical and physically-based biomechanical methods that can deal with intra-patient deformations. However, it is more difficult to model the relationship between the anatomy of different subjects: one need to introduce statistics and to learn this relationship from observations, most often images. Therefore, computational anatomy is at the interface of geometry, statistics and image analysis. This is currently a very active research field, as exemplified by the quality of the submissions and the number of attendees (more than 50 people) to the first workshop on the Mathematical Foundations of Computational Anatomy (MFCA'06) organized in conjunction with MICCAI'06 [Pennec and Joshi, 2006].

In the context of computational anatomy, the statistical computing framework on manifolds that we developed in Chapters 2 and 3 has an immediate application as it allows to decouple the anatomical modeling problem (representing the observations with the minimal amount of maximally informative parameters) from the technical difficulties of computing with the model due to manifold nature of the space of parameters. This is illustrated in this chapter with the construction of statistical models of the anatomy of the spine and the brain.

In Section 5.1, we develop a statistical articulated model of the spine in view of an augmented reality system. The goal of such systems is to guide therapeutic gestures with an optimal accuracy while minimizing the amount of per-operative information needed, hence allowing a minimal invasiveness. However, recovering complex anatomical deformations from very few information requires the availability of a very strong prior knowledge.

In Section 5.2, we propose to model the variability of the brain from a dataset of precisely delineated anatomical structures (sulcal lines) on the cerebral cortex. We obtain a dense 3D variability map which proves to be in accordance with previously published results on smaller samples subjects. We also propose statistical tests which demonstrate that our model is globally able to recover the missing information and innovative methods to analyze the asymmetry of brain variability.

Registration as described in Chapter 4 is also closely linked to computational anatomy: firstly, it is needed to find the correspondences between the anatomical manifolds. Conversely, the anatomical statistics should better constrain the personalization of the representative anatomy to specific subject images. Following this idea, we tackle in Section 5.3 the variability problem from the deformation point of view. We propose a consistent mathematical framework to learn the deformation metric from a population of deformations and to use it as a regularization penalization in non-rigid registration. Preliminary results indicate that the method is sound and effective.

The next step will be to analyze the results on a database of brains with different registration algorithms and to compare and combine them to the ones we obtained using sulcal lines. Indeed, using only one kind of features provides a partial and very limited view of the anatomical variability. We believe that acquiring and combining information coming from different types of features (intensity-based, segmented structures likes points, curves and surfaces, etc.) is needed to correctly characterize the probability of the anatomy. Using different types of methods will also be necessary to remove the potential biases introduced by each method. Then, the next challenge will be to compare our variability models with some structural anatomical information like the one obtained through diffusion tensor imaging.

5.1 A statistical model of the scoliotic spine

There are nowadays quite a few augmented reality systems (see e.g. [Nicolau et al., 2005, Nicolau et al., 2004b] and Section 4.1). However, most of them were developed for orthopedic or neurosurgery because bones bones constitute reliable landmarks that do not deform: we only have to find the rigid-body transformation that brings the pre-operative plan into the reference of the patient on the operative room. We believe that the next generation augmented reality systems will need to tackle deformations. One could think for instance to soft-tissues in the abdomen, but such a system should take into account the very complex deformations due to digestion, breathing and the heart beating. In between rigid motions and soft-tissues, there is an intermediate step that can probably be tackle more easily: articulated motions.

5.1.1 Towards an augmented reality system for laparoscopic spine surgery

Laparoscopic spine surgery is a relatively new surgical intervention that allows small incisions, less blood loss, reduced post-operative pain, earlier discharge from the hospital and a faster post-

operative rehabilitation. However, the limited visualization offered to the surgeon is a source of difficulties. One of the solutions to this problem is to develop an augmented reality system which will overlay 3D models of anatomical structures (such as vertebrae or the spinal cord) on the laparoscopic images. To be useful, such a system should rely on the pre-operative data that are currently used in clinic, in this case bi-planar radiographies. The goal is thus to recover the deformation of the spine between the pre-operative X-Ray images and the per-operative laparoscopic images [Boisvert, 2005].

In partnership with Farida Cheriet at Montreal's Sainte-Justine hospital and at the Polytechnic School of Montreal, we investigated with Jonathan Boisvert a 3D articulated model of the spine based on the the relative configurations of the vertebrae along the spinal chord: the parameters are the rigid transforms that superpose neighboring vertebrae rather than the position and orientation of each vertebra in some kind of general reference frame [Boisvert et al., 2006d, Boisvert et al., 2006c]. The local representation is indeed much better capturing some small local motions that may have a large global repercussion. To properly constrain the fit of this articulated model to 2D X-Ray images, it is necessary to capture its statistical behavior. We can differentiate two very different types of variability: the first one is the inter-subject variability of the spinal chord in the reference posture of the pre-operative images (standing up), while the second is the variability of the physical articulated motion of the spine between this pre-operative posture and the per-operative position (patient lying prone or supine, depending on the surgical approach).

5.1.2 Mean spine shape and local variability

We focused in [Boisvert et al., 2006d, Boisvert et al., 2006c] on the inter-subject 3D anatomical variability of the spine shape. We relied for that on a database of bi-planar radiographies of 307 untreated scoliotic patients. The position and orientation of each vertebra was computed from anatomical landmarks reconstructed in 3D using two radiographies. Then, the rigid transformations between successive vertebrae were computed. To capture the statistics on the population, our statistical computing framework on manifolds was used to compute the Fréchet mean and the generalized covariance. The selection of subjects did not take into account individual factors such as the age, sex or type of scoliotic curve. Therefore, our variability statistics capture the anatomical variability inherent to the pathology but also growth stage, posture, landmarks reconstruction error, etc. However, posture during data acquisition was normalized to limit its influence on the results, and additional experiments suggested that landmarks reconstruction error could only account for a very small proportion of the observed inter-subject variability (about 0.8 mm of the 2 to 5mm in translation and 2.5 of 7 to 12 degrees in rotation)

The mean spine shape and the variability are illustrated in figure 5.1. One can observe a curvatures of the mean shape in the lateral plane, that correspond to healthy kyphosis and lordosis. However, the light curve in the frontal plane is not part of the normal anatomy of the spine and is caused by scoliosis. It is also interesting to note that the curve is on the right side because of the prevalence of right thoracic curves among scoliotic patients. The variability is also inhomogeneous (lumbar vertebrae were more variable than for the thoracic ones) and anisotropic: the strongest translational variability is found along the axial direction and the maximal rotational variability in the coronal plane around the antero-posterior axis, as can be seen by the extension of the covariance ellipsoid of the rotation vector along that axis. These findings are clinically relevant, and could lead to the optimization of treatment strategies or diagnostic methods (by taking advantage of the strong

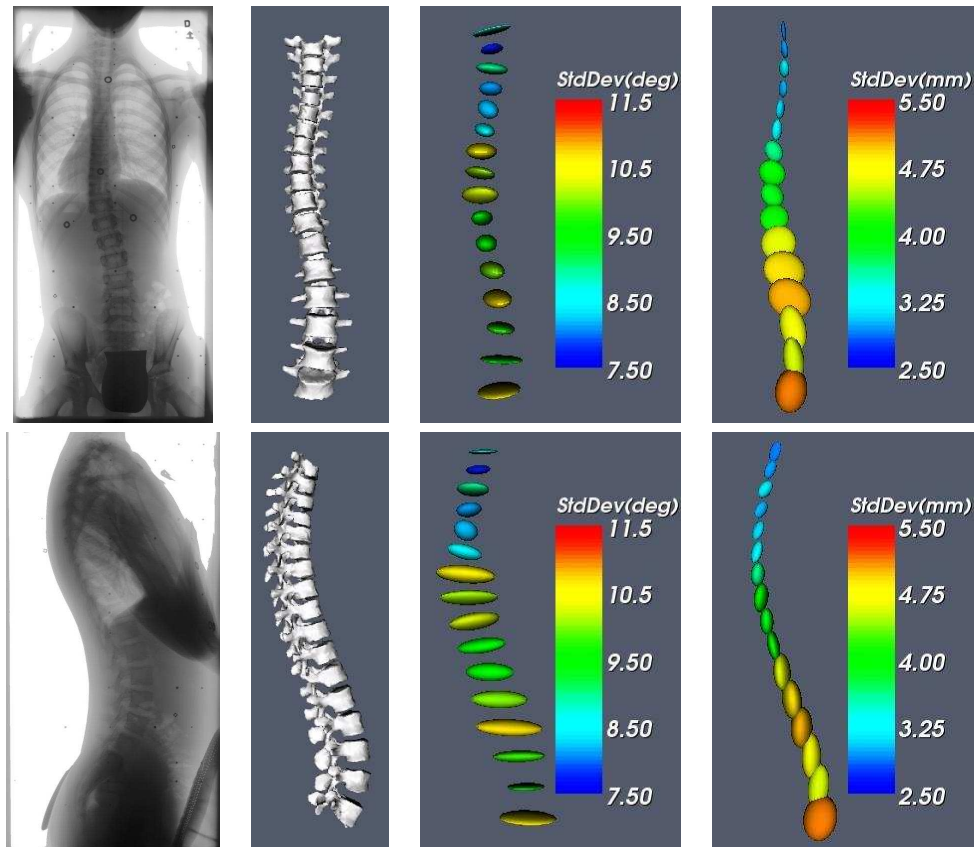


Figure 5.1: Statistical spine model. From left to right: Example of a Bi-planar radiographies of the human trunk, mean spine model, rotation and translation covariance. Top: Postero-anterior view. Bottom: lateral view.

variability in the coronal plane, for example).

5.1.3 Principal modes of variation

The analysis of the variability of each inter-vertebral joint individually is rather limited as one expect to have some correlation between the different joints. Moreover, as there are 102 degrees of freedom (5 lumbar and 12 thoracic vertebrae, excluding cervical vertebrae), the analysis of such a large covariance matrix can hardly be performed by a clinician (nor by a computer scientist). It is therefore necessary to extract only the most meaningful modes of variability. For that purpose, we relied in [Boisvert et al., 2006e, Boisvert et al., 2006b] on the Principal Geodesic Analysis (PGA). This extension of PCA to Riemannian manifolds was originally proposed by [Fletcher et al., 2003] for the statistical analysis of shapes based on medial axis representations (M-reps). Here, by using a proper articulated model of the spine including positions and orientations of each vertebra, we expect to find a better separation of different physiological phenomena such as pathological deformations

and normal growth than with classical PCA on 3D coordinates.

The basic idea of PGA is to find a low dimensional submanifold generated by some geodesic subspaces that best explain the measurements (i.e. such that the squared Riemannian distance from the measurements to that submanifold is minimized). However, geodesic subspaces are not orthogonal in general manifolds, so that they do not generate Riemannian submanifolds. To get out of this intractable problem, the solution retained by [Fletcher et al., 2003] was finally to rely on an approximation using a standard PCA of the Riemannian covariance matrix in the tangent space at the mean. In our case, we believe that this approach is much better suited anyway as we want to find a few Gaussian modes that best explain the variance, and not a submanifold of unconstrained deformations from which the observations can deviate with a residual error.

The first four principal deformation modes are illustrated in Fig. 5.2. A visual inspection reveals that these modes have clinical meanings and explain curve patterns that are routinely used in different clinical classifications of scoliosis (see [Boisvert et al., 2006e, Boisvert et al., 2006b] for details). For instance, the first mode appears to be associated with the patient growth with a mild thoracic curve (King’s type II or III depending on the amplitude of the mode), the second could be described as a double thoraco-lumbar curve (King’s type I), the third one as a simple thoracic curve (King’s type IV) and the fourth one is a lumbar lordosis. A more quantitative analysis showed that there is a statistically significant link between our 4 principal modes and King’s classes, although each class is generally linked to a combination of modes rather than only one mode [Boisvert et al., 2006b].

Those classification patterns were previously derived from surgeons’ intuition using 2D measures on radiographies and clinical indices. It is now possible to automatically compute them, and to compare to compare principal deformation modes of different subgroups of scoliotic patients. A variability model like one also offers many ways to improve image analysis algorithms because *a priori* insights could be easily introduced in the form of a variability model. Future directions might include the development of temporal variability models to assess the evolution of the pathology or the effect of orthopedic treatments (such as braces and surgeries) [Boisvert et al., 2006c, Boisvert et al., 2006a] and of course the integration of this model into a registration algorithms to be used in the augmented reality system for laparoscopic spine surgery.

5.2 Modeling the anatomical variability of the brain

Brain structures differ greatly in shape and size even among normal subjects, and these variations make it difficult to identify abnormal differences due to disease. Understanding the degree and quality of brain variation is vital for distinguishing signs of disease from normal variations. Neuroscientists are also interested in identifying the causes of brain variability at a genetic or environmental level. An efficient, parsimonious model of the complex patterns of brain variation would help in identifying factors that contribute to it.

A major class of anatomical variations can be thought of as arising from the smooth deformation of a reference anatomy, where the deformation is represented as a 3D displacement field, after affine differences are factored out. Ideally, one would model the joint variability of all pairs of points to see how the displacement of one any point in a specific subject with respect to the reference anatomy co-varies with the displacement of neighboring or distant points in the brain (e.g. symmetric ones

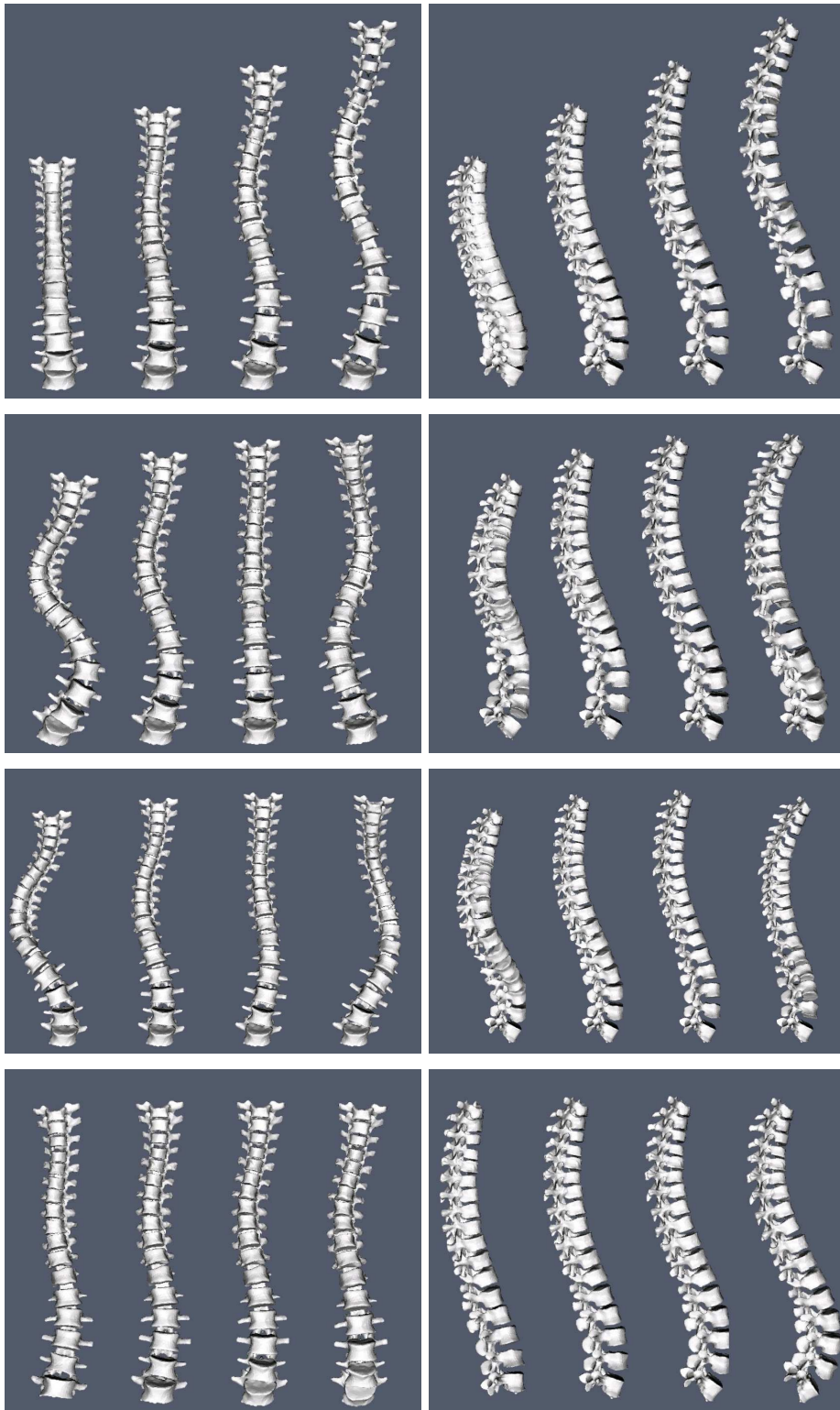


Figure 5.2: Statistical spine model. From top to bottom: the 4 first principal modes of variation. Frontal (postero-anterior) view on the left, and lateral view on the right. Each mode is depicted by the variation at -3 , -1 , 1 and 3 times its standard deviation.

in the opposite hemisphere). In such a program, the first step is to model the variability of each anatomical point independently. Assuming that the mean deformation of the reference anatomy is null (this can be somehow ensured by applying the mean deformation to the reference anatomy), the first interesting moment of the 3D displacement distribution of a point is its covariance matrix, which will be called a *variability tensor*. Thus, the goal is to compute the field of variability tensors within the brain from information that may be sparsely distributed. The reason that tensor representations are used, rather than simple scalar fields, is that variation may not be the same in all directions: there is some evidence that structural variation is greatest along certain preferred directions [Thompson et al., 2001b]. Once this first simplified variability model will be established, the second step will be to investigate the correlation between the motion at neighboring points, i.e. the local regularization kernel that has to be used for nonlinear registration. Then, the third step will be detect potential long distance correlations, for instance at symmetric points in the brain.

To measure inter-subject brain variability, we need to gather statistics on 3D displacements computed between a reference anatomy and many individuals. A first idea would be to use inter-subject registration algorithm between an atlas (the reference) and many subject images, which would provide dense displacement fields. This is in essence the approach that we will explore in Sec. 5.3. However, it is necessary to estimate the influence of the chosen registration method. For instance, it is likely that the displacement along the isosurfaces of the images is mainly driven by the regularization criterion since the image provides only a matching constraints in the direction of the gradient (the aperture problem).

For that purpose, we need to provide information that is completely independent of volumetric image registration algorithms. We chose in [Fillard et al., 2005c, Fillard et al., 2006c] to rely on lower dimensional structures, such as cortical landmarks identified by expert Neuroscientists following a formalized protocol, with known inter- and intra-rater reliability. Since extracting and matching surfaces (e.g. the hippocampus, corpus callosum, or even the whole cortex as in [Thompson et al., 2000]) is still a very active research area, we chose to focus on anatomically well defined 3D curves that could be considered as ground truth data. This choice naturally led us to the primary anatomical landmarks on the cortex: the sulci. A large number of sulcal landmarks consistently appear in all normal individuals and allow a consistent subdivision of the cortex into major lobes and gyri [Mangin et al., 2004b].

5.2.1 Measuring the variability of sulcal lines

In the framework of the associated team program between Epidaure/Asclepios at INRIA and LONI at UCLA¹, we use a dataset of sulcal lines manually delineated in 98 subjects by expert Neuroanatomists according to a precise protocol with formal rules governing the handling of branching patterns, breaks in sulci, and doubling of specific sulci². The inter- and intra-rater error (reliability) is better than 2mm (in r.m.s.) everywhere, and in most regions less than 1mm, far less than the inter-subject anatomical variance. Delineations were made in 3D on cortical surfaces extracted from MR images linearly aligned to the ICBM stereotactic space [Collins et al., 1995], thus providing a common coordinate system for all traced curves (examples are provided on Fig

¹<http://www-sop.inria.fr/epidaure/Collaborations/UCLA/atlas.html>

²http://www.loni.ucla.edu/~khayashi/Public/medial_surface/

5.3. We used the 72 sulcal curves that consistently appear in all normal subjects. In the following, we abusively call these sulcal lines *sulci* to simplify the description. An interesting future development will be to compare the variability results obtained from other sulcal data such as [Le Goualher et al., 1999, Mangin et al., 2004b, Kao et al., 2006].

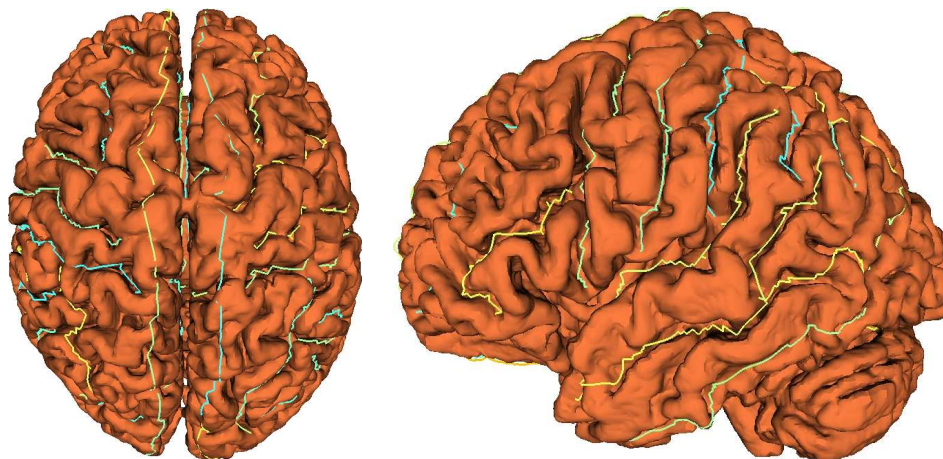


Figure 5.3: Example of sulcal lines drawn on the cortical surface.

Many criteria have been proposed in the literature to evaluate the mean of a set of curves and to assess the appropriateness of one-to-one correspondences between geometric objects. They usually invoke local differential characteristics such as the tangent space, curvature, the local Frénet frame for a curve on a surface [Guéziec and Ayache, 1994], regional shape information [Pitiot et al., 2003], etc. In our case, the variability is so large that using such refined measures is difficult. In general, sulcal curves do not have consistent geometric features from subject to subject. Therefore, we simply use the variance of observed curves w.r.t. the mean as a global criterion to optimize. Minimizing this variance greatly reduces the variability due to inadequate correspondences.

Practically, we alternately improve the correspondences between the mean curve and each sample by dynamic programming and optimize the average curve position by a first-order gradient descent with an adaptive step. This optimization strategy converges toward the mean curve in a few iterations. We then compute the variability tensor at each point of the mean sulcal line as the empirical covariance of the correspondences. Initially, images were affinely registered onto a common reference image (in our case the ICBM305 space). In [Fillard et al., 2006c], we added the global affine transformation of each subject to the mean as a new set of hidden variables in our alternated optimization scheme. This is simply realized by re-estimating the affine transformation from the correspondences of all sulci in a third step.

Results of covariance tensors estimated along the 72 sulci are shown in Fig. 5.4. The optimization of mean curves and correspondences reduces the amount of variability to 70% of the initial value. Reestimating the affine transform further reduces the amount of variability to 60% of its initial value with very few changes to the global variability pattern. Variability is greater at the extremities of the curves, which are landmarks identified by neuroanatomists. At these points, we do not have the ambiguity of line matching: the uncertainty along the tangent is the same as orthogonally, whereas

it is much larger everywhere else on the curve. However, we suspect a bias in the estimation of the end points of our mean curve that could explain a large part of their variability. To remain consistent, we chose to remove these points from further analysis in a first step.

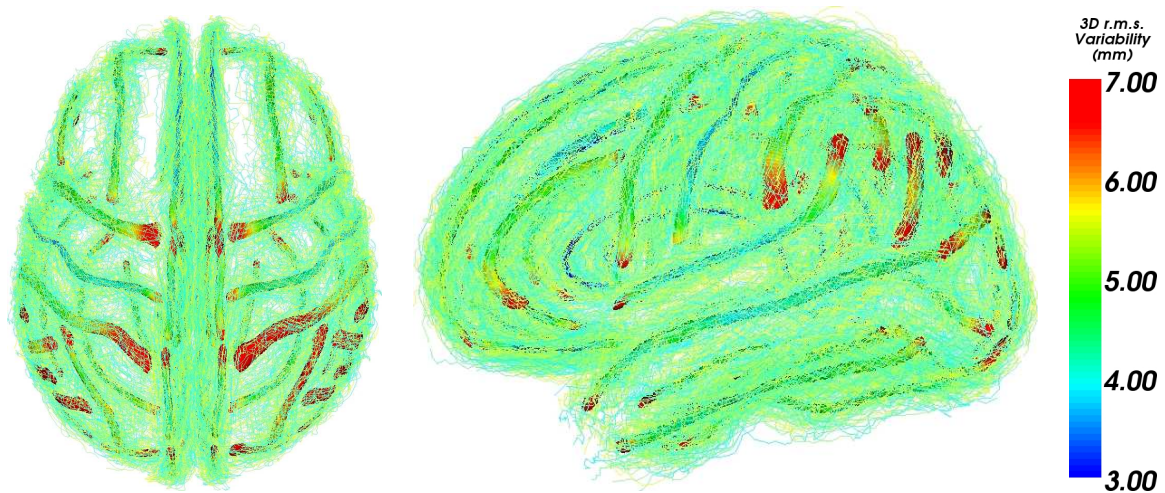


Figure 5.4: **Sulcal variability.** Covariance matrices (ellipsoids at one σ) are overlapped at regularly sampled spatial positions along the mean sulci. The color codes for the trace: Note that tensors close to the sulci extremities are larger.

5.2.2 A model of the full brain variability by extrapolation

The measure variability is highly regular in size and shape along each sulcal curve. Therefore, some of this information is therefore redundant and could be simplified by selecting only a few tensors at specific points along the mean sulcus, and interpolating (using the geodesic tensor interpolation) in between them. For each sulci, we picked the minimal number of tensors to reconstruct the variability tensors with a given mean error. Results of this operation are presented in Fig. 5.5 (middle panel): by choosing tensors at adequate positions, one can qualitatively reconstruct the full variability of each sulcus using 4 to 10 covariance matrices, depending on its length and shape. The variability of all the major sulci can be adequately represented by 366 variability tensors out of 2000 initially.

The next step consists of extrapolating these selected tensors to the full brain, using the framework developed in Sec. 3.2.5. Fig. 5.5 presents the extrapolation results on a discrete grid (voxel size of 2^3 mm^3) in the ICBM 305 space. Of course, this only account for the variability of the sulci we chose. We believe that a fairly comprehensive set of sulci was selected on the cortex (at least for the scale at which we are modeling the variability at this point). Obviously, using the information given by the sulci is not enough to infer the variability of the full brain, particularly within the brain (e.g. in the white matter and deep gray matter nuclei). Including a number of subcortical structures such as the ventricles would be necessary to faithfully measure the variability in the full brain volume. Thus, even if the extrapolation is performed on the full volume of the brain, we restrict the interpretation and evaluation of our model to the cortex.

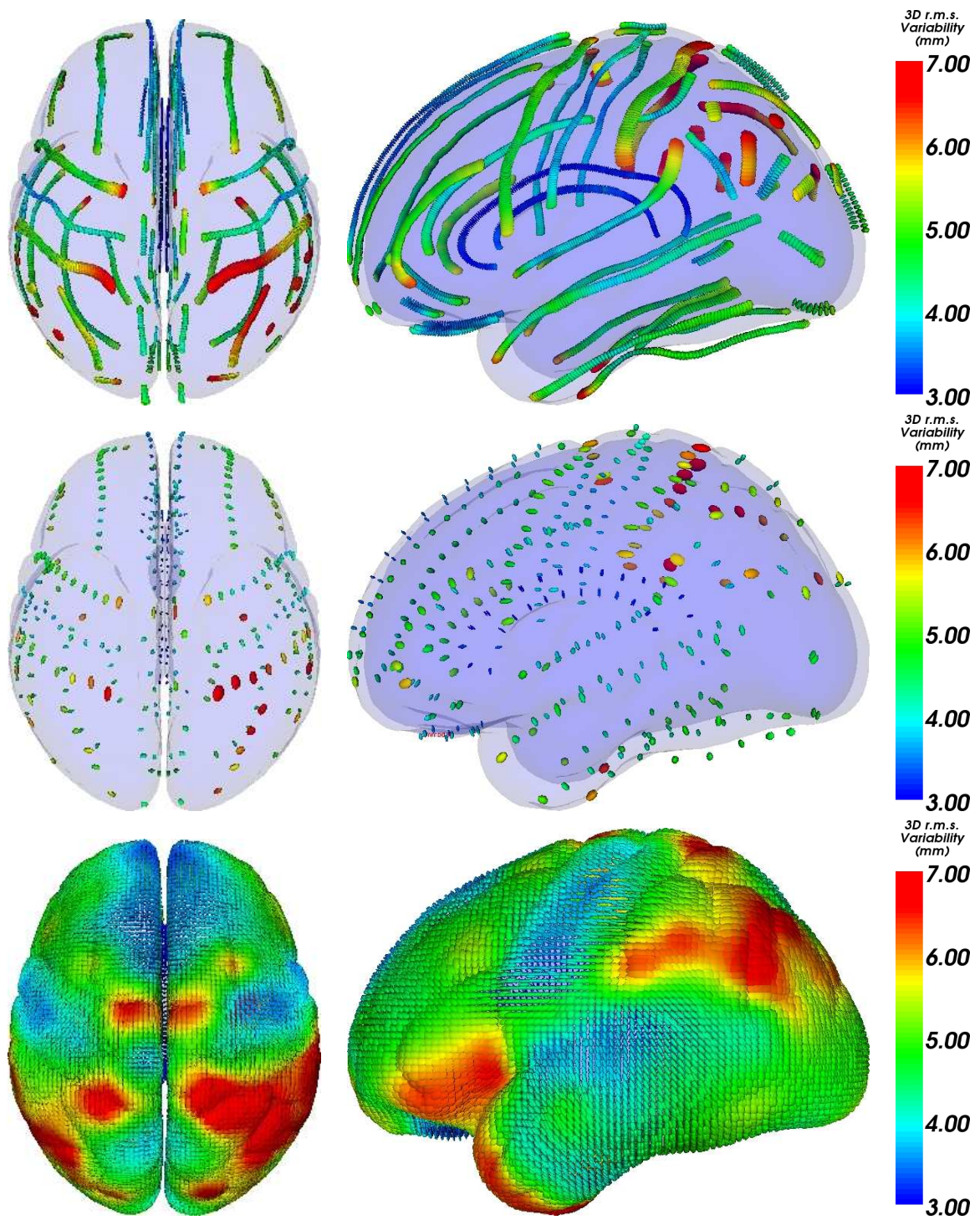


Figure 5.5: The cortical variability step by step. **Top:** Covariance matrices calculated along mean sulci. **Middle:** Matrices selected by the tensor picking operation. **Bottom:** Result of the extrapolation.

5.2.3 Model evaluation

To verify the predictive power of our extrapolation method and the influence of the number of tensor picked before the extrapolation, we compared the results of the extrapolation using 2000, 1000, 366 and 144 tensors, respectively. The first value corresponds to retaining all tensors. The second value is obtained by taking one tensor every two. The third value is the number of tensors retained by the tensor picking operation. The last value is the minimum number of tensors that

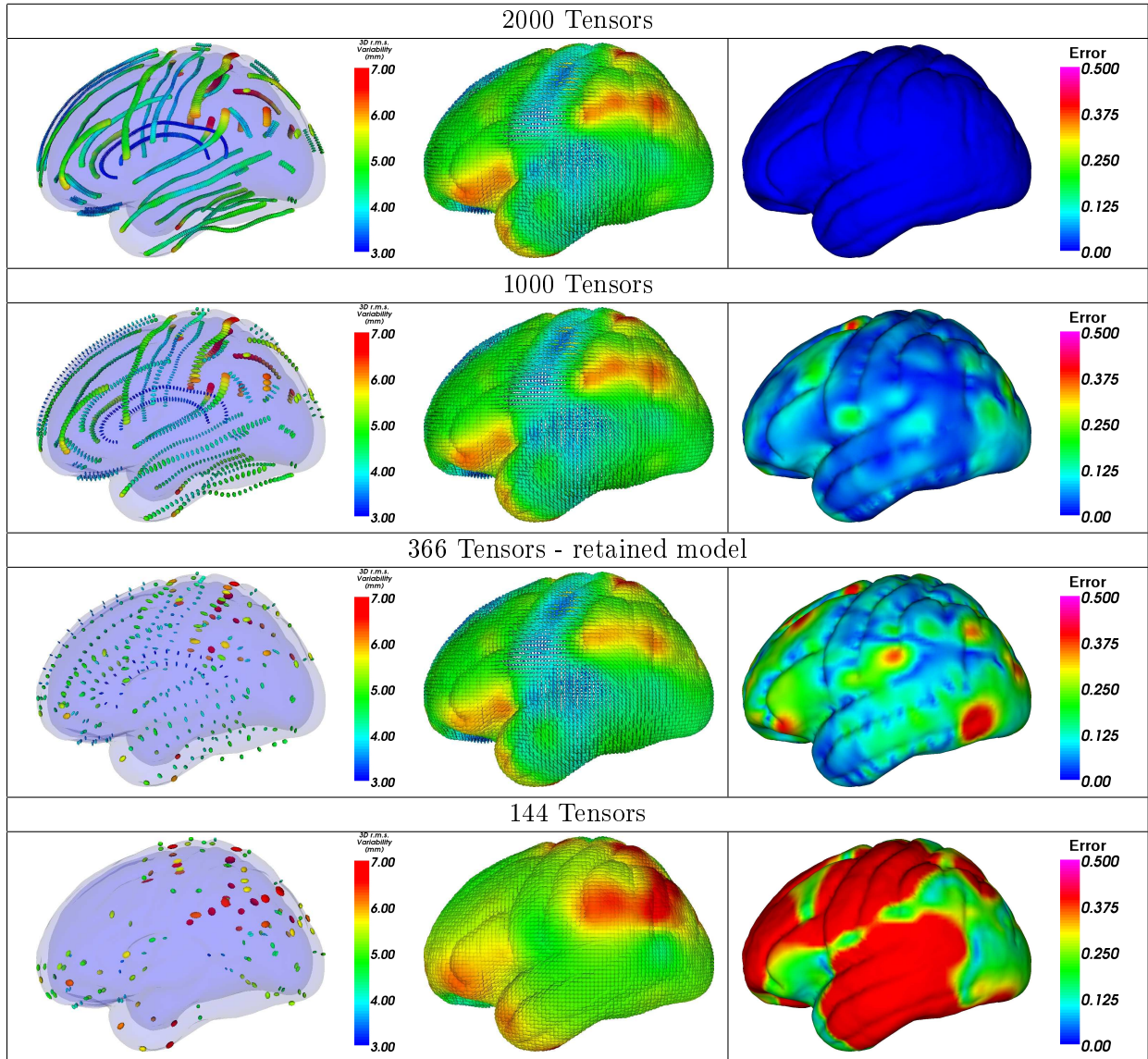


Figure 5.6: Sparsity of the model parameters versus the reconstruction error. **Left:** The tensors (parameters) picked for the model. **Middle:** Results of the extrapolation. **Right:** Error (Riemannian distance) between the extrapolated and the measured covariance matrices field.

can be used (2 measures for each of the 72 sulci). The means reconstruction error (measured with the affine-invariant metric on the variability tensors) very slowly grows from 0.0? for 2000 tensors to 0.2 for 366 tensors. Then, the error increases quite rapidly (0.3 for 248 tensors, 0.5 for 191) to overpass 1 for 144 tensors. Figure 5.6 summarizes the results with maps of the errors: local errors arise when the correlation of variability between neighboring sulci is too low (see regions with hot colors in Fig. 5.6, right column).

We also run a series of *leave one sulcus out* tests where the principle is to remove from our model parameters all the information coming from one sulcus, and to compare the result of the extrapolation with the original measured variability. This test was performed on 3 sulci: the Sylvian Fissure, the Superior Temporal Sulcus and the Inferior Temporal Sulcus. The prediction error with missing sulci is globally 2 to 3 times larger than the one incurred by interpolating or extrapolating the full model, but the difference is globally not significant. However, one can see some locally significant errors (primarily in the tangential direction to the mean sulcus) at points where two sulci meet orthogonally (e.g. the Sylvian fissure). These are not really errors but rather model limitations as our model does not explicitly take into account the minimization of the tangential variability (the aperture problem for curves). We have proposed in [Fillard et al., 2005c, Fillard et al., 2006c] a partial error which basically projects the reconstruction error onto the normal component of the variability. This modified “distance” correctly accounts for the aperture problem in the reconstruction errors.

The leave one sulcus out test is obviously not applicable everywhere: the variability of some sulci is not correlated with that of their neighbors (e.g. the Central Sulcus which is much less variable than the pre- and post-central ones). These sulci carry some independent variability information, and should definitely be part of any brain variability model. Our experiment shows that the model is able to recover a correct estimation of the variability in almost all areas with only 1/6 of the original tensor data. Reducing more the number of tensors leads to miss some important local variability information. By the sparsity principle, it seems that 366 tensors is close to the optimal number of parameters necessary to model the sulcal variability, and that our Riemannian computing and extrapolation framework is perfectly capturing the non-linear relationship between these parameters and the variability observations.

5.2.4 Neuroanatomical interpretations

To better visualize and interpret the results, we present in Fig. 5.7 two scalar measures from the extrapolated variability tensor field. We are deeply indebted to Paul Thompson (LONI, UCLA) for all the following neuroanatomical interpretations of these maps, as well as for the interpretation of the asymmetry measurements of the next section. The left column is the usual RMS variability map given by the square root of the trace of each covariance matrix. One can see highly variable regions (such as the parietal cortex and Broca’s area) with hot colors, and more stable areas (such as the primary sensorimotor cortex) with cold colors. The second map on the right column of Fig. 5.7 shows the principal direction of each tensor (i.e., the eigenvector associated to the largest eigenvalue), whose coordinates are mapped on the RGB sphere (right column). This map confirms the anatomical intuition that there are sets of sulci in certain cortical sectors that tend to vary in a consistent way. For instance in the top view, the principal direction of variation is lateral-to-medial for the superior frontal and parietal sulci, but the central and precentral sulci tend to vary more

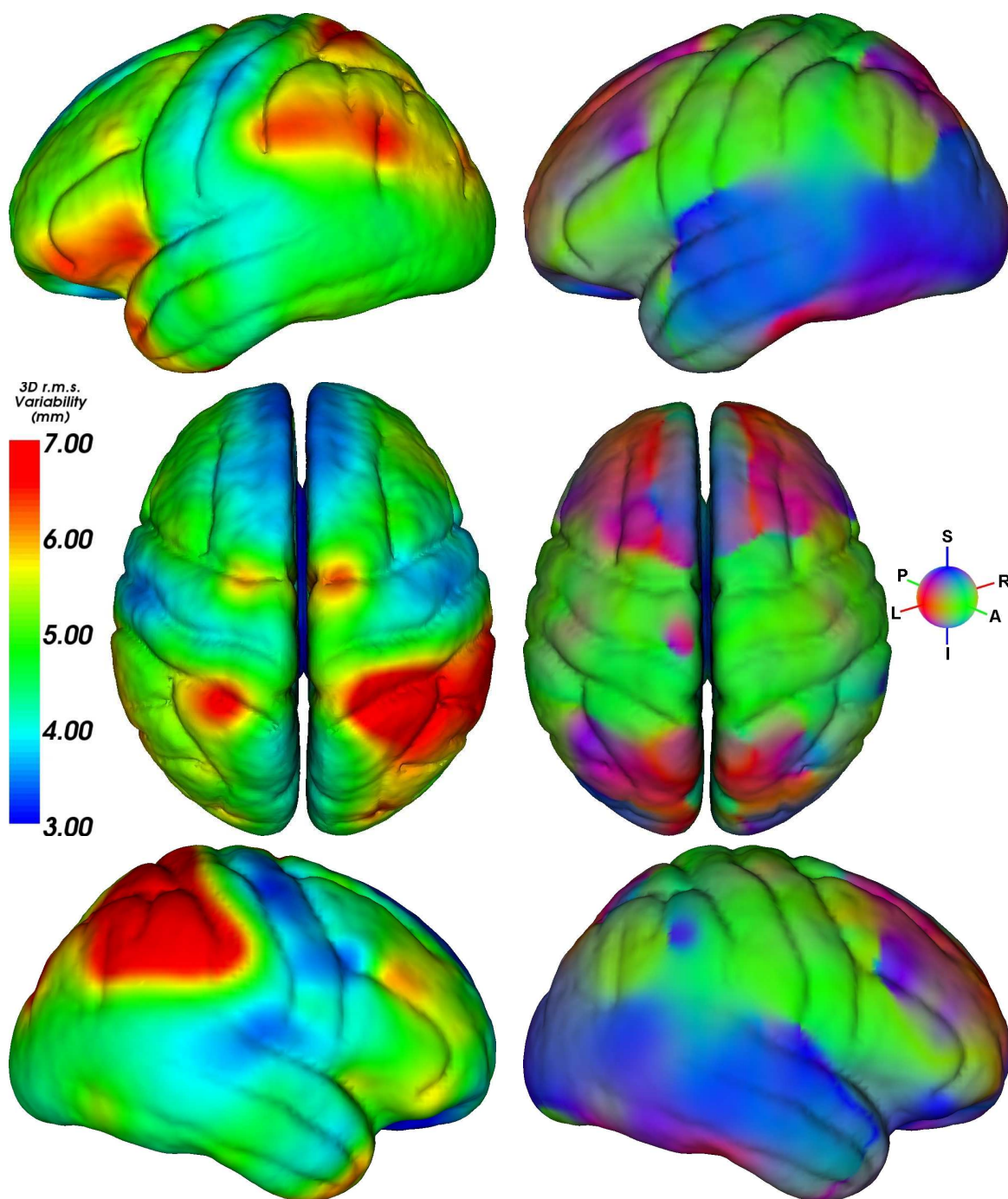


Figure 5.7: Scalar maps of the sulcal variability predicted by the extrapolation model on the cortex. **Left column:** The color codes for the 3D rms variability (mm). Hot colors mean high variations among subjects. **Right column:** Maps showing the main direction of variability. The color codes for the main direction of the variability tensor at each point. Red: left-right oriented tensor, Green: posterior-anterior oriented, Blue: inferior-superior oriented.

along an anterior-posterior direction. The temporal lobe sulci also tend to be consistent in varying with the same principal direction.

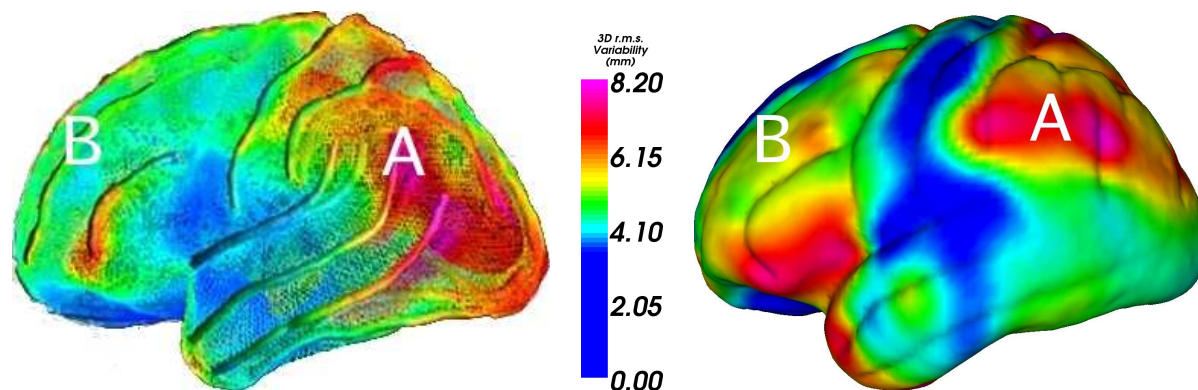


Figure 5.8: Comparison of two independent models of brain variability. The scalar value mapped on the mean cortex is the trace of the tensors (the variance). **Left:** Cortical variability map from [Thompson et al., 2000]. **Right:** Extrapolation of our simplified sulci variability model to the full brain. Note the similarity in the temporo-parietal cortex [shown in red colors (A)] and the superior frontal gyrus (B).

The spatial pattern of variability agrees with established neuroanatomical data. For instance, [Thompson et al., 2000] computed the variability of the cortex surface in an independent normal sample (15 controls) using a non-linear surface registration algorithm. Fig. 5.8 compares his variability map with ours: one can observe the same high values in the temporo-parietal cortex (red and purple area, marked “A” in Fig. 5.8) and low values in the superior frontal gyrus (marked “B” in Fig. 5.8), Broca’s area, and the lower limits of the primary sensorimotor cortices in the central and precentral gyri. Phylogenetically older areas (e.g. orbitofrontal cortex), and primary cortices that myelinate earliest during development (e.g., primary somatosensory and auditory cortex) exhibit least variability. The planum parietale (marked “A” in Fig. 5.8) consistently shows the highest variance of any cortical area, consistent with the complex pattern of secondary fissures surrounding the supramarginal and angular gyri (the perisylvian language cortex). It is also reasonable that the temporo-parietal areas around the Sylvian fissures are the most variable: they specialize and develop in different ways in each hemisphere, and are also the most asymmetric in terms of gyral patterning and volumes [Toga and Thompson, 2003].

5.2.5 Measuring the asymmetry

Measuring brain asymmetry (i.e. differences between hemispheres) is of special interest as it sheds light on how the functions of the two hemispheres become specialized [Toga and Thompson, 2003]. Structural and functional lateralization are of interest in mapping brain development and in disorders such as dyslexia, epilepsy, and schizophrenia. The two brain hemispheres develop according to slightly different genetic programs: the right hemisphere is torqued forward relative to the left, with greatest volume asymmetries in the planum temporale and language cortex surrounding the Sylvian fissures (typically larger in the left hemisphere). If the types of variation in the two hemispheres

could be differentiated, it would be easier to isolate specific effects of genetic polymorphisms on these normal variations and asymmetries [Thompson et al., 2001a], and their genetic basis would be easier to investigate. For example, many neurodevelopmental disorders are associated with subtle variations in the patterning of the cortex, and new computational anatomy techniques are making these features easier to identify (e.g., increased cortical complexity in Williams syndrome [Thompson et al., 2005]).

We measured the symmetry/asymmetry of brain variability by computing the distance between the variability tensor at one point and the (symmetrized) tensor at the symmetric point in the brain. Several definitions of the symmetric point in the brain can be imagined. A first geometric method is to use the symmetry with respect to the mid-sagittal plane in the stereotactic space (mid-sagittal symmetry). With our brain variability model, we can directly compute a dense asymmetry map from the extrapolated tensor values at each 3D point of a hemisphere (Fig. 5.9, left). Another possibility is to measure the brain asymmetry on sulcal lines, and extrapolate those measures to the whole brain (sulcal symmetry). We end up with another dense asymmetry map, whose color is proportional to the distance between left-right tensors (Fig. 5.9 right). One important remark is that the measure of asymmetry in our framework is a relative measure as we used the affine-invariant distance between (symmetrized) variability tensors.

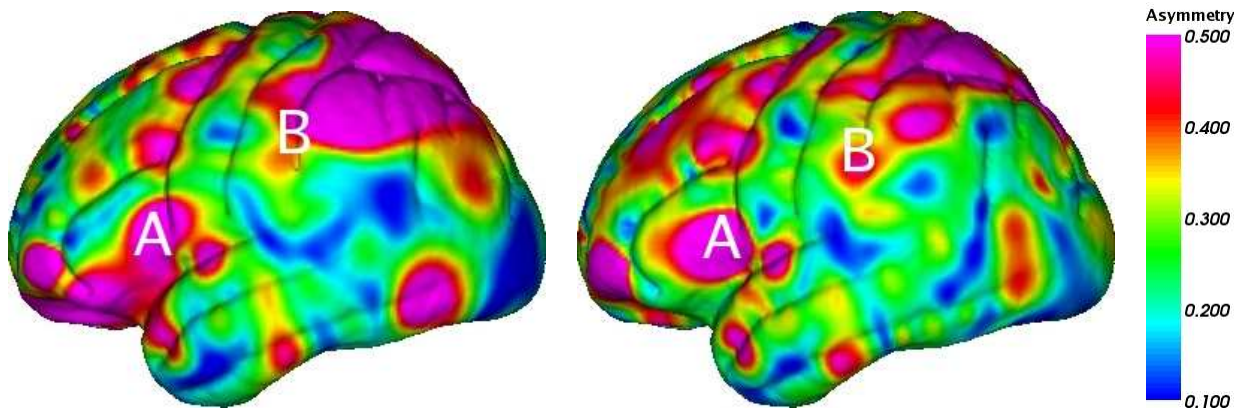


Figure 5.9: Maps of brain variability asymmetry. **Left:** The mid-sagittal asymmetry. **Right:** The sulcal asymmetry.

A very interesting result is that the regions with greatest asymmetries in variability include (with both definitions) the main language areas, Broca's speech area (labeled A in Fig. 5.9) as well as the parietal cortex, which exhibits the greatest gross anatomical variation of any cortical area (labeled B in Fig. 5.9). As expected, these areas are more structurally variable in the left hemisphere which is typically dominant for language in normal right-handers. The greater left hemisphere variation may be attributable to the greater volumes of structures such as the planum temporale in the left hemisphere. One surprise is that the tips of the Sylvian fissures do not show the greatest difference in variability between the hemispheres, as these are regions with highly variably branching patterns that have been studied extensively in the language and dyslexia literature. Also as expected, the primary sensorimotor areas (central and pre-central gyri) are relatively symmetric in their variance,

as the absolute variability is lower, as is their degree of hemispheric specialization (i.e. they perform analogous functions in each hemisphere, but innervate opposite sides of the body).

The amplitude and asymmetry of variability are greatest in the most phylogenetically recent developments in the cortex (e.g. frontal lobe, dorsolateral prefrontal cortex, and in the more dorsal areas of the parietal association cortices). The language areas, in particular, have fundamentally different developmental programs in each brain hemisphere, leading to volumetric and functional asymmetries (e.g. left hemisphere language dominance). This variance asymmetry is seen in Broca's area, which is specialized in the left hemisphere for producing speech, but is less commonly associated with structural asymmetries. Lower variance was seen in cortical regions subserving primary brain functions (e.g., touch, motor function, hearing) and these areas are the earliest to mature in utero. It would be interesting to hypothesize that the areas of the brain that emerged most recently in human evolution are the same ones that have greatest differences in variation patterns between the hemispheres, reflecting the drive towards hemispheric specialization of function in higher primates and man. It could also help understand whether there is an asymmetry in the power to detect consistent task-related or group-specific activation patterns in functional brain imaging studies, due to structural variance asymmetries.

5.2.6 Conclusion

Based on the Riemannian computing and extrapolation framework of Chapters 2 and 3, we proposed in this section a first order brain variability model that is able to recover the estimation of the sulcal variability with only 366 tensor parameters. Results are globally consistent with previously known results in neuroanatomy and show that the proposed geometrical framework perfectly captures the non-linear relationship between these parameters and the variability observations. The main weakness is the unknown variability along the direction tangent to the mean sulci (aperture problem). We are currently tackling this problem by relaxing the data attachment term to the original variability measurements in this direction. Other approaches could include the use of data from functional imaging modalities such as fMRI and MEG.

The next step will be to investigate the local and distant correlations between displacements: preliminary results indicate that the displacement of the symmetric point is correlated, which was more or less expected. However, other long distance correlations also appear. Their statistical significance still needs to be established before presenting any result.

The ultimate goal of our variability model will be to include many other sources of information, like sulcal ribbons [Mangin et al., 1996], variability obtained from the matching of surfaces, (e.g., ventricles or basal ganglia), fiber pathways mapped from DTI, or of full 3D images. As these sources of information are also subject to an aperture problem (we mainly retrieve the deformation in the direction of the gradient of the image), we expect to observe a good agreement in some areas, and complementary measures in other areas.

5.3 Learning the metric of anatomical deformations

From an image analysis point of view, the geometric variability of the anatomy makes the automated segmentation and labeling of brain structures difficult. Statistical information on brain variability

would make this task easier and could be used as a very informative prior for nonlinear registration in order to adjust for anatomical variations across subjects prior to group analysis of brain function or metabolism. Conversely, a way to gather statistics on inter-subject brain variability is to perform multiple deformable registration between a reference image and subject images. The main difficulty is to formulate these two problems in a common consistent framework.

Most non-linear image registration algorithms optimize a criterion comprised of an image intensity similarity and a regularization term (see e.g. Section 4.3). Many image similarity criteria are now available, ranging from the simple sum of squared intensity differences to robust information theory based measures. In inter-subject registration, the main problem is not really the intensity similarity measure but rather the regularization criterion. Some authors used physical models like elasticity or fluid models [Bajcsy and Kovačič, 1989, Christensen et al., 1997]. For efficiency reasons, other authors proposed to use non-physical but efficient regularization methods like Gaussian filtering [Thirion, 1998, Pennec et al., 1999, Modersitzki, 2004]. This type of regularization was then extended to more general (e.g. non separated) but still isotropic vectorial filters [Cachier and Ayache, 2004], and to non-stationary diffusion in order to take into account some anatomical information about the tissue types [Lester et al., 1999, Stefanescu et al., 2004c]. Very few extensions deal with anisotropic and non-stationary and regularization criteria.

However, since we do not have in general a model of the deformation of organs across subjects, no regularization criterion is obviously more justified than the others. We could think of relating the anatomy of two different subjects by building a model of the developing organ: inverting the model from the first subject to a sufficiently early stage and growing toward the second subject image would allow to relate the two anatomies. However, such a computational model is out of reach now, and most of the existing work in the literature rather try to capture the organ variability from a statistical point of view on a representative population of subjects (see e.g. [Thompson et al., 2000, Rueckert et al., 2003, Fillard et al., 2005c]). Although the image databases are now large enough to be representative of the organ variability, the problem remains of how to use this information to better guide inter-subject registration.

5.3.1 Deformation statistics to improve inter-subject registration

In [Commowick et al., 2005], we adapted the registration algorithm of [Stefanescu, 2005] (see Section 4.3.5) to better suit the needs of brain atlas registration in the context of conformal radiotherapy. The planning requires the accurate localization of the tumor and of the critical structures. To segment them in a patient image, the idea is to register a previously labeled atlas to the patient image. The atlas segmentation can then be used directly, or as an initialization for a more complex segmentation algorithm. The main difficulty is to obtain an inter-subject registration algorithm which is accurate enough and, more importantly, robust to the pathologies (tumors may be quite important) and to the anatomical variability.

The algorithm RUNA developed during the PhD of R. Stefanescu [Stefanescu et al., 2004c, Stefanescu, 2005] was a first attempt to obtain a computationally efficient but highly steerable nonlinear registration algorithm. It uses a non-stationary transformation regularization which is strong where the local deformability is expected to be low, and conversely. Moreover, the regularization can be locally tuned along spatial directions through the use of a tensor field. In [Commowick et al., 2005], we introduced a method to compute scalar and tensor based deformabil-

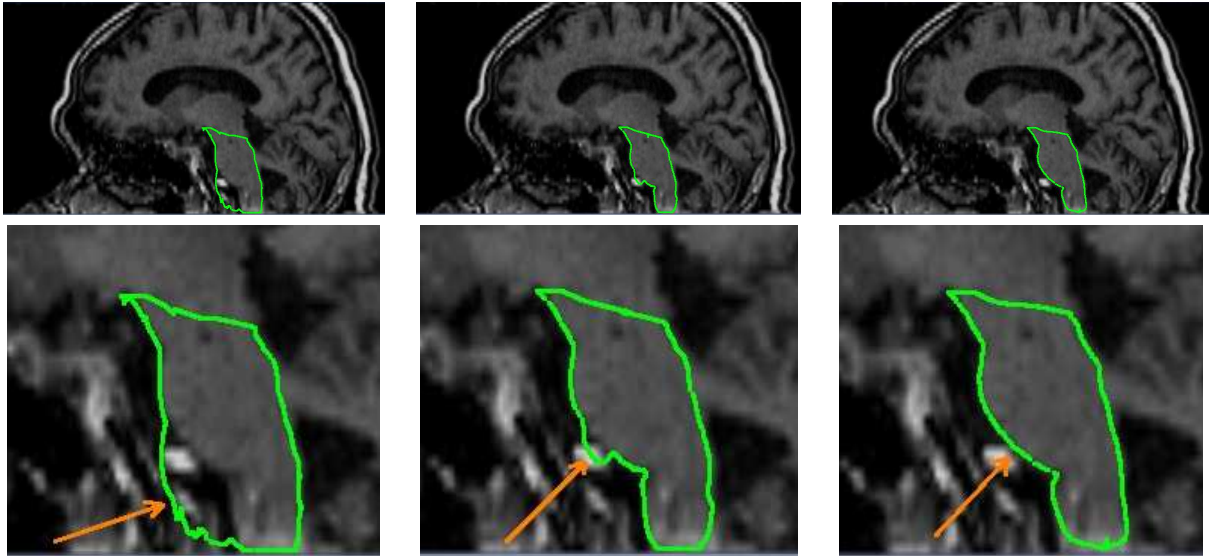


Figure 5.10: Comparative results of the atlas-based segmentation using RUNA guided by the heuristic scalar stiffness map (left), the scalar statistical stiffness map (middle) and the statistical tensor stiffness map (right). Top: Top: Sagittal slice of the 3D patient image with the segmentation superimposed. Bottom: close-up on the brain-stem area. The inclusion of the statistical information clearly allows to better deform the brain stem area in an anatomically more meaningful way, resulting in a better and smoother segmentation. Brain images are courtesy of Dr. P.-Y. Bondiau, CAL, Nice.

ity statistics over a database of patient MRI. However, we had to modify these statistics through a complex nonlinear transfer function in order to obtain the range of tensor values that were expected by the algorithm. Despite this lack of physical consistency between the statistics and the regularization parameters, we obtain qualitatively and quantitatively better results with this method (figure 5.10).

5.3.2 Riemannian elasticity: an integrated framework

In parallel to the previous work, we proposed in [Pennec et al., 2005b] an integrated framework to compute the statistics on deformations and reintroduce them in the registration procedure. The basic idea is to interpret the elastic energy as a distance in the space of positive definite symmetric matrices (tensors). By changing the classical Euclidean metric for a more suitable one, we define a natural framework for computing statistics on the strain tensor. Taking them into account in a statistical distance lead to the Riemannian elasticity energy.

Let $\Phi(x)$ be a diffeomorphic space transformation. The general registration method is to optimize an energy of the type: $C(\Phi) = Sim(Images, \Phi) + Reg(\Phi)$. Starting from an initial transformation, a first order gradient descent methods computes the gradient of the energy $\nabla C(\Phi)$, and update the transformation using: $\Phi_{t+1} = \Phi_t - \eta \nabla C(\Phi_t)$. From a computational points of view,

this Lagrangian framework can be advantageously changed into a Eulerian framework to better conserve the diffeomorphic nature of the mappings [Stefanescu et al., 2004c]. The regularization can also be applied to the temporal derivative of the deformation field to obtain fluid-like methods [Thirion, 1998, Cachier et al., 2003, Modersitzki, 2004].

In continuum mechanics [Ciarlet, 1988], one characterizes the deformation of an infinitesimal volume element in the Lagrangian framework using the right Cauchy-Green deformation tensor $\Sigma = \nabla\Phi^T \nabla\Phi$. This positive definite symmetric matrix measures the local amount of non-rigidity. In the standard St Venant-Kirchoff Elastic energy, the deviation of the positive definite symmetric matrix Σ (the strain tensor) from the identity (the rigidity) is measured using the Euclidean matrix distance $\text{dist}_{Eucl}^2(\Sigma, \text{Id}) = \frac{\mu}{4}\text{Tr}((\Sigma - \text{Id})^2) + \frac{\lambda}{8}\text{Tr}(\Sigma - \text{Id})^2$ (λ, μ are the Lamé coefficients).

However, we have seen in Chapter 3 that the Euclidean metric is not a good metric for positive definite symmetric matrices because null or negative eigenvalues are at a finite distance. For instance, an isotropic expansion of a factor $\sqrt{2}$ ($\Sigma = 2 \text{Id}$) is at the same Euclidean distance from the identity than the “black hole” transformation $\Phi(x) = 0$ ($\Sigma = 0$). In non-linear registration, this asymmetry of the regularization leads to different results if we look for the forward or the backward transformation: this is the inverse-consistency problem [Christensen and Johnson, 2001].

The idea we propose is to use affine-invariant or the log-Euclidean metrics, for which null eigenvalues are at an infinite distance from any tensor. With such metrics, we automatically have the local inverse-consistency since the means are geometric. In [Pennec et al., 2005b], we used the log-Euclidean metric for its simplicity: the local deviation of Φ from the rigidity is measured by the vector $\log(\Sigma)$. Interestingly, this tensor is known in continuum mechanics as the logarithmic or Hencky strain tensor [Hencky, 1928], and is used for modeling very large deformations [Rougée, 1997]. It is considered as the natural strain tensor for many materials, but its use was hampered for a long time because of its computational complexity [Freed, 1995].

For registration, we thus replace the elastic energy with a regularization that measures the amount of logarithmic strain by taking the Riemannian distance between Σ and Id . In the isotropic case, we obtain:

$$\text{Reg}_{IRE}(\Phi) = \int \frac{\mu}{4}\text{Tr}((\log(\Sigma))^2) + \frac{\lambda}{8}\text{Tr}(\log(\Sigma))^2$$

To incorporate statistics in this framework, we consider the strain tensor as a random variable in the Riemannian space of tensors. In the context of inter-subject or atlas-to-image registration, this statistical point of view is particularly well adapted since we do not know a priori the deformability of the material. Starting from a population of transformations $\Phi_i(x)$, we define the *a priori* deformability $\bar{\Sigma}(x)$ as the Riemannian mean of deformation tensors $\Sigma_i(x)$. A related idea was suggested directly on the Jacobian matrix of the transformation $\nabla\Phi$ in [Woods, 2003], but using a general matrix instead of a symmetric one raises important computational and theoretical problems. With the Log-Euclidean metric on strain tensors, the statistics are quite simple since we have explicitly the mean value $\bar{\Sigma}(x) = \exp(\bar{W}(x))$ with $\bar{W}(x) = 1/N \sum_i \log(\Sigma_i(x))$. Going one step further, we can compute the covariance matrix of the random process: $\text{Cov} = \frac{1}{N} \sum \text{Vect}(W_i - \bar{W}) \text{Vect}(W_i - \bar{W})^T$, where Vect is a projection of the elements of the symmetric tensor $W = \log(\Sigma)$ onto an orthonormal basis.

Finally, we take into account these first and second order moments of the random deformation

process using the Mahalanobis distance to define the *statistical Riemannian elasticity (SRE)* energy:

$$Reg_{SRE}(\Phi) = \frac{1}{4} \int \mu_{(\bar{W}, Cov)}^2(\log(\Sigma(x))) = \frac{1}{4} \int \text{Vect}(W - \bar{W}) \text{Cov}^{(-1)} \text{Vect}(W - \bar{W})^T$$

This least-squares criterion may be interpreted as the log-likelihood of a Gaussian process on strain tensor fields³: we are implicitly modeling the a-priori probability of the deformation but the link with a "Gaussian distribution" on deformations through Brownian warps [Nielsen et al., 2002, Markussen, 2004] remains to be established. In a registration framework, this point of view is particularly interesting as it would open the way to use Bayesian estimation methods for non-linear registration.

5.3.3 Optimizing the Riemannian elasticity

To use the Riemannian energy as a regularization criterion in our registration framework, we need to compute its gradient. Using homogeneous Neumann boundary conditions, we showed that $(\partial_\alpha$ is the directional derivative along the space axis α):

$$\nabla Reg(\Phi) = - \sum_\alpha \partial_\alpha (Z \partial_\alpha \Phi) \quad \text{where} \quad \begin{cases} Z_{Elast} = \mu(\Sigma - \text{Id}) + \frac{\lambda}{2} \text{Tr}(\Sigma - \text{Id}) \text{Id} \\ Z_{IRE} = \mu \partial_W \log(\Sigma) + \frac{\lambda}{2} \text{Tr}(W) \Sigma^{(-1)} \\ Z_{SRE} = \partial_X \log(\Sigma) \quad \text{with} \quad \text{Vect}(X) = \text{Cov}^{(-1)} \text{Vect}(W - \bar{W}) \end{cases}$$

Here, Z is the derivative of the density of energy at each point with respect to the strain tensor Σ and is known as the 2nd Piola-Kirchoff tensor. The 3rd order tensor $Z \partial_\alpha \Phi$ is the first Piola-Kirchoff tensor and corresponds to the derivative of the density of energy with respect to the Jacobian of the transformation. Notice the similarity with the gradient of the standard elasticity.

In practice, a simple and easily parallelizable implementation is the following. First, one computes the image of the gradient of the transformation, for instance using finite differences. This operation is not computationally expensive, but requires to access the value of the transformation field at neighboring points, which can be time consuming due to systematic memory page faults in large images. Then, we process these 3 vectors completely locally to compute 3 new vectors $v_\alpha = Z(\partial_\alpha \Phi)$. This operation is computationally more expensive but is memory efficient as the resulting vectors can replace the old directional derivatives. Finally, the gradient of the criterion $\nabla E = \sum_\alpha \partial_\alpha v_\alpha$ may be computed using finite differences on the resulting image. Once again, this is not computationally expensive, but it requires intensive memory accesses.

This implementation of the standard and isotropic Riemannian elasticity was tested in conjunction with the local correlation ratio in an experimental version of the RUNA algorithm. Riemannian Elasticity was only 3 times slower than the standard Euclidean elasticity, which was itself about 4 times longer than the standard RUNA algorithm (partially because of more inefficiency due to the weaker parallelism)⁴. In terms of deformation, the results were globally similar for both methods (in the absence of any a priori statistical information, we took the same values $\mu = \lambda = 0.2$ for both elasticity). One could however notice a slightly larger and better deformation of the brain ventricles with the Riemannian elasticity.

³Defining properly likelihoods on deformations is actually much more difficult due to the infinite number of dimensions.

⁴The assumptions used in RUNA for the parallelization are not completely satisfied by the standard and Riemannian elasticity. A correct parallel implementation would require a new version of the overall registration algorithm.

5.3.4 Left-Invariant Riemannian Elasticity

In [Pennec, 2006b], we investigated the invariance properties in view of relating the Riemannian Elasticity to metrics on diffeomorphisms. We previously noticed that the isotropic logarithmic distance of a strain tensor to the identity was locally inverse-consistent. However, this property does not hold globally due to the change of the volume element during the change of variable $y = \Phi(x)$. Following an idea suggested in [Nielsen et al., 2002], we can integrate with a volume element which is the geometric mean between the one in the original space and the one in the arrival space, i.e.: $\sqrt{|\nabla\Phi(x)|}.dx = |\Sigma(x)|^{1/4}.dx$.

Using the resampled tensor fields $\hat{\Sigma}_\phi = \Sigma_\Phi \circ \Phi^{(-1)}$, we obtained the following formula for the globally Inverse Consistent (isotropic) Riemannian Elasticity:

$$Reg_{ICRE}(\Phi) = \int \left\| \log(\hat{\Sigma}) \right\|^2 \cdot |\hat{\Sigma}|^{-1/4}$$

where the norm $\|\cdot\|$ refers to an isotropic norm on symmetric matrices. This inverse invariant energy on diffeomorphisms allows us to optimize directly their regularity in registration processes without having to integrate numerically along the transformation trajectory for computing the length of geodesics, as is needed for the invariant metrics on diffeomorphisms proposed in [Joshi and Miller, 2000, Beg et al., 2005].

This energy can be turned into a left-invariant “distance” by left-translation: $\text{dist}_L^2(\Phi, \Psi) = Reg_{ICRE}(\Phi^{(-1)} \circ \Psi)$. The corresponding right-invariant distance is automatically given by $\text{dist}_R(\Phi, \Psi) = \text{dist}_L(\Phi^{(-1)}, \Psi^{(-1)})$. The expression of the left-invariant distance can be simplified, and it turns out that it make use of the affine-invariant distance on symmetric matrices $\text{dist}_{Aff}^2(\Phi, \Psi) = \|\log(\Psi^{-1/2} \cdot \Phi \cdot \Psi^{-1/2})\|^2$ instead of the log-Euclidean one as we originally proposed for the statistical Riemannian elasticity.

$$\text{dist}_L^2(\Phi, \Psi) = \int \text{dist}_{Aff}^2(\hat{\Sigma}_\Phi, \hat{\Sigma}_\Psi) \cdot \det(\hat{\Sigma}_\Psi)^{-1/4} \cdot \det(\hat{\Sigma}_\Phi)^{-1/4}$$

This “distance” is positive, symmetric (thanks to the inverse-consistence), and is null if and only if the two diffeomorphisms differ by a local rotation everywhere. However, to show that this is really a left-invariant distance on diffeomorphisms of rigid shapes, the triangular inequality remains to be established. Moreover, we suspect that we obtain an extrinsic distance and not a Riemannian one.

Following the statistical framework of Chapter 2, computing the derivatives will allow determining the barycentric equation of the Fréchet “mean diffeomorphisms” according to these “metrics”, and a gradient descent algorithm to obtain them. Then, we hope to be able to compute second order moment and to define a kind of Mahalanobis distance (including local anisotropy and non-stationarity) on shape diffeomorphisms.

5.3.5 Conclusion

Riemannian elasticity is an integrated framework to compute the statistics on deformations and re-introduce them as constraints in non-linear registration algorithms. This framework is based on the interpretation of the elastic energy as a Euclidean distance between the Cauchy-Green strain tensor and the identity (i.e. the local rigidity). By providing the space of tensors with a more

suitable Riemannian metric, for instance a Log-Euclidean one, we can define proper statistics on deformations, like the mean and the covariance matrix. Taking these measurements into account in a statistical (i.e. a Mahalanobis) distance, we end-up with the statistical Riemannian elasticity regularization criterion. This criterion can also be viewed as the log-likelihood of the deformation probability, which opens the way to Bayesian deformable image registration.

We showed that it was possible to obtain an inverse-consistent criterion by modifying the spatial integration measure. It is remarkable that this allows to define a left or right invariant energy between two diffeomorphisms without having to optimize for the geodesic path between them. However, many questions are left open. For instance, it remains to be established that our energy is a distance, i.e. that the triangular inequality is valid. Moreover, we conjecture that this is not a Riemannian distance on diffeomorphisms, but an extrinsic distance. Determining the geodesics (if they exist) would also be very interesting to better understand the properties of these energies. This would probably help also in generalizing the statistical Riemannian elasticity in a consistent way, in order to measure and take into account anisotropic and non-stationary behavior of the deformations. On a more theoretical point of view, it would be interesting to make the link between our approach and the Brownian warps of [Nielsen et al., 2002, Markussen, 2004].

On a practical point of view, we demonstrated with the isotropic version that it is also an effective regularization criterion for non-linear registration algorithms. However, a much smarter implementation that can cope efficiently with very large deformations is needed to fully exploit the deformation statistics. First experiments were already performed to analyze statistically the deformation tensor issued from a fluid registration algorithm in normal versus AIDS patients [Lepore et al., 2006]. Results tend to show that the deformation tensor has a better discriminative power than its Jacobian usually used in the so called tensor based morphometric analyzes. However, we believe that it will be necessary to recompute these statistics with several different algorithms to reduce the biases induced by the particular regularization of each algorithm. The next step will be develop methods to compare the variability results obtained by this deformation analysis and by the sulcal variability model presented in Section 5.2. More generally, a central research topic for computational anatomy will be to build models from different sources of anatomical manifolds like curves, surfaces (cortex, sulcal ribbons), volumes and images (voxel-based and tensor-based morphometry), but also from other important anatomical modalities like diffusion tensor images as well as functional modalities like fMRI. We will need to design methods to compare the statistics on this hierarchy of anatomical manifolds at locations where they are comparable (validation by consensus), and to combine them at locations where they are complementary.

Chapter 6

Perspectives

We have shown in this work that statistical computing on manifolds, image registration and computational anatomy were three inter-related problems. Many advances in each domain over the last years have allowed the other fields to progress a lot. However, there are still a lot of question marks and open research avenues. A fundamental problem of computational anatomy is that the number of degrees of freedom is so large than the mathematical construction of an optimal atlas is an ill-posed problem, raising the need for a precise program in order to reach any goal (Section 6.1). Most of the geometrical models of the anatomy rely on sets of landmark features, curves, surfaces or deformations, which belong to infinite dimensional manifolds. Investigating their statistical properties over a population requires new methods for statistical computing on manifolds (Section 6.2). The statistical estimation of computational models of the variability implies the set-up of rigorous generative models of the observations (most often images). Conversely, the estimated statistical model may be used as a very efficient prior to adapt generic models of the anatomy (atlases) to patient-specific data, opening the way to more robust and more powerful image analysis applications (Section 6.3).

6.1 Computational anatomy

The study of biological shapes is an old problem [D’Arcy Thompson, 1917]. Several theoretical advances have been made, for instance with Kendall who considered the shape space as the invariants of a number of landmarks under the action of a transformation group [Dryden and Mardia, 1998, Small, 1996] (quotient space). However, we need to use much more complex features like curves (e.g. sulcal lines), surfaces or even volumetric deformations to represent the full variability of anatomical shapes, and it would be necessary to consider all these anatomical manifolds in a unified framework. Grenander [Grenander, 1996] proposed for instance to encode the mean anatomy as a template, which could be comprised of curves, surfaces, images, and its variability as a probability of deformation in the transformation space. It is not clear that one template is sufficient to describe the full variability, especially for the brain where there are some topological differences across a population. Moreover, the number of degrees of freedom is so large than the mathematical construction of an optimal atlas is ill-posed. Thus, we believe that we should focus in a first step on capturing statistics on the anatomically most meaningful features rather than on the general

integrative framework. In a second step, it will be necessary to compare the statistics obtained with several different methods on the same data in order to identify the biases induced by the assumption of each method. One step further, we will have to compare the statistics on the different anatomical manifolds at locations where they are comparable (validation by consensus), and to combine them at locations where they are complementary. Last but not least, extending the modeling to growth (or more generally evolving processes) and using other anatomical or functional modalities like DTI or fMRI are central research topics for the future.

Statistics on anatomical manifolds

The strategy will be to identify the main representative anatomical manifolds and to analyze their variability across subjects. The brain is particularly appealing because of its complexity and of the numerous applications in medicine and in neuroscience. Moreover, many anatomical manifolds were already identified as having interesting shape: cortical landmarks like sulcal ribbons and gyri, or the surface of internal structures like the ventricles, the hippocampus or the corpus callosum. We have already started in to study the variability of the trace of sulci at the surface of the cortex [Fillard et al., 2006c]. This type of analysis should be extended in a first step to similar but independent features, such as the sulcal ribbons [Mangin et al., 2004a, Le Goualher et al., 1999].

We focused so far on a second order description of the process individually at each point. With such a simple variability model, we could already investigate the asymmetry of the variability, which is an important variable in neuroscience. However, an immediate objective is to extend our statistical analysis to several points of the brain together, in order to test for the correlation of the deformation (Green's function). It is obvious that there is a correlation between neighboring spatial displacements. It will be necessary to distinguish the part of this correlation which is imposed by the matching method (or by other assumptions of the extraction method) from the intrinsic local regularity kernel. Once this local kernel is modeled, one expects to be able to put into evidence some long-range correlation, for instance with the symmetric points.

Fusion of information from different anatomical models

The classical approach to compute statistics on anatomical manifolds is to extract curves or surfaces from images, build a mean model while matching the points of the model to each observation, and then extract some kind of summary statistics from the point correspondences. With this extrinsic analysis, we have to deal with the aperture problem on curves, surfaces and volumes. Indeed, each type of feature provides geometrically meaningful information in some specific directions only: along the normal for a surface, orthogonally to the tangent for a curve, or to the gradient for a dense image registration. The goal will be to verify that variability measures coming from different methods are consistent in the directions where they are compatible, and to fuse the information in the directions where they are complementary. Another theoretical research track to get rid of the aperture problem will be to investigate new methods for *intrinsic* statistical analysis.

In both extrinsic and intrinsic cases, the metric used and the underlying assumptions of the matching method will inevitably bias the results. For instance, the prior on the regularization drastically changes the transformation result in a multi-subject registration even if this is hardly visible on the resampled images. Thus, we believe that we should not focus on one single method,

but on multiple ones. For instance, we are currently trying to compare the space variability on the sulcal line determined as in Section 5.2 with the variability of the space diffeomorphic line matching of [Vaillant and Glaunes, 2005]. It will also be interesting to compare these methods to other approaches like [Christensen et al., 1997, Miller and Younes, 2001, Avants and Gee, 2004, Faugeras and et al., 2004].

Each anatomical manifold carry only a limited part of the global anatomical information of the organ. Moreover, it is inevitably biased by the underlying assumptions of the image extraction method. Thus, exactly like for the matching methods, we believe that we should not rely one single source of data. This implies comparing and fusing the variability results coming from different anatomical manifolds. For the brain, we already saw several methods to extract sulcal lines and ribbons. Comparing surface and line variability at the same location is the first step and will allow to understand the reliable part of each method. The second step will be to compare variability at points farther away on the “same” anatomical manifold, such as on top and bottom sulcal lines (sulcal roots). One more step to understand the cortical variability could be to compare the results with the gyral variability as studied by [Lohmann et al., 2006]. By increasing gradually the hierarchy of anatomical structures taken into account, one could end-up with anatomical atlas that have a more reliable estimation of the structural variability.

Anatomical data being generally sparse and localized at different places in space, they are not easy to compare. The extrapolation method we proposed in Section 5.2 is one solution. However, it is obviously biased by the regularization kernel used. It will be necessary to investigate other methods to validate this kernel, and to generalize the extrapolation PDE to the joint variability of several points. An alternative method is to use statistics on deformations as an integrative model. For instance, we are currently investigating with LONI the use of the the Riemannian elasticity framework (Section 5.3.2) to compute the variability on the deformations of the brain from images. Other solution include statistics on diffeomorphisms as proposed in [Vaillant et al., 2004] or in [Arsigny et al., 2006a] (see also Section 4.3.6). Preliminary results indicate that this type of statistics do carry some interesting information [Lepore et al., 2006] but a more in-depth analysis remains to be done. For instance, we need to compare the statistics obtained using different image registration algorithms. The advantage of encoding the variability with statistics on the transformation is that we can extend the registration algorithm to take into account other anatomical manifolds in addition to the image intensities in the spirit of the hybrid PASHA method ([Cachier et al., 2001] and Section 4.3.3).

Towards multimodal and evolving models

Other sources of data could provide some deep insight about the anatomical and the functional variability. For instance, white fiber tracts connecting the different cortical areas may act as the main source of structural rigidity during the brain growth. The main tracts would constrain the folding of the cortex surface during its expansion, giving birth to be sulci and gyri. Building atlases of fiber tracts and of their variability such as in [Corouge et al., 2005] would be an important step to confirm this hypothesis. Moreover, this would provide a dense variability information within the brain while previous gyral and sulcal informations were only located around the surface of the cortex. A similar problem is currently under investigation for another organ: the heart. The electrophysiological simulation of [Sermesant et al., 2006] depends on the orientation of the heart muscle

fibers. Because this information cannot be measured *in vivo* for each subject, one need to use a geometric model: its variability should be assessed. Preliminary statistics on the diffusion tensor of canine hearts tend to show that the measurements are highly reproducible, but there might be two different means fiber shape patterns [Peyrat et al., 2006].

The next big challenge will be to investigate joint models of growth (or more generally evolution) and normal population variability. Currently, several cross sectional atlases are build at different ages. However, this only provides a mean view of the population at given age, and does not provide any information about the evolution of a single subject (nor even on the mean!). We believe that new mathematical methods taking explicitly into account the longitudinal axis need to be designed. From a statistical point of view, this type of problem can only be addressed using large pediatric image databases, such as the MRI Normal Brain Development Study funded by NIH¹. Joint growth and variability models would allow to predict the evolution of personalized models. An insight about the variability of the evolution would also allow to detect pathological evolutions. Moreover, the evolution of pathologies and the growth process occurred concurrently in children and interact together. This is one of the subject that we intend to tackle in the framework of the European project Health-e-Child².

In some cases, it will be interesting to correlate the inter and intra subject variability (during motion or time evolution for instance) to see if an ergodic assumption is valid. One could imagine for instance that the shape of the scoliotic spine is the exaggeration of a particular motion of a normal spine. The ergodic assumption would allow to greatly increase the power of many statistical tests as acquiring longitudinal studies is more difficult that cross-sectional ones.

GRID Computing Strategy

The large amount of data and methods needed to study the variability requires a collaboration with many different groups and databases, which are not centralized. Moreover, the amount of computations needed to compare and fuse all the methods on all the available data requires to design statistical algorithms and workflows that can be distributed. We believe that the grid may prove to be an integrative tool for that: wrapping algorithms in standardized web services accessible from the grid would ease the sharing of methods; providing restricted but on the fly accesses to the image database for the members of the virtual computational anatomy community could allow to keep the control of the data while promoting their use; last but not least, efficient grid workflow managers (e.g. MOTEUR [Glatard et al., 2006a]) would allow to share the computing resources very efficiently for the whole community.

6.2 Statistical computing on manifolds

In Chapter 2, we were able to show that the Riemannian metric was a sufficient structure to provide the bases for a consistent theory of statistics on manifolds (mean, covariance matrix, Mahalanobis distance, Gaussian...). This was extended in Chapter 3 to a complete computing framework on

¹http://www.bic.mni.mcgill.ca/nihpd_info/

²<http://www.Health-e-Child.org>

manifolds to perform interpolation, filtering, anisotropic regularization through weighted means and PDEs.

Extensions of the Riemannian approach

In this framework, the choice of the metric is crucial as it determines the fundamental properties of the manifold. For instance, the Log-Euclidean and affine-invariant metrics on positive definite symmetric matrices put matrices with null eigenvalues at an infinite distance from any regular tensor. They are well suited to diffusion tensors or to covariance matrices (Section 3.1.3), where this type of matrix is unphysical and poses some computational problems, but not for structure tensors where a perfect edge is represented exactly by that type of matrix [Fillard et al., 2005a]. Likewise, one can interpret the regularization prior in non-rigid registration as the metric on the transformation space (Section 5.3.2, [Trouvé, 1998]), and it is well known that changing the regularization drastically changes the transformation result. Thus, the question is how to determine the “optimal” metric for each problem, optimal meaning here that all the “structure” is included in the metric and that we are left with a small Gaussian noise.

To partially answer this question, one track is to study families of metrics with some invariance property on simple manifolds like we partially did for tensors. This provide a kind of maximally non-informative metric. However, the closed form examples are probably very limited. Another interesting solution is to determine the metric from a statistical model of the measurements, for instance the Fisher information metric [Lenglet et al., 2006] or the entropy differential metric [Burbea and Rao, 1982]. A last interesting track is to learn the global metric from local distance measurements [Brun, 2006, Brun et al., 2005]. This method could be particularly well suited for surfaces represented by point sets or graphs for which there is a known (or guessed) local Euclidean embedding.

From a theoretical point of view, the Gaussian we define by minimizing the intrinsic entropy does not correspond to the Brownian motion on manifolds. The alternative would be to rely on the heat kernel, smallest positive fundamental solution of the heat equation $\Delta f = \dot{f}$. This kernel is compatible with the intrinsic operations on a probabilistic manifold [Grigor’yan, 2006]. However, it is intrinsically isotropic with respect to the Riemannian metric used, so it cannot represent anisotropic Gaussians. A solution is to encode the anisotropy (i.e. the shape of the covariance matrix) in the Riemannian metric itself. Similar problems appear when one wants to do a PCA on a distribution strongly elongated along a direction where the manifold folds onto itself (e.g. a uniform distribution along a great circle on the sphere). The link between the Riemannian metric, the covariance matrix and the heat kernel should thus be clarified.

From a practical point of view, it would be necessary to develop distributions with several modes (e.g. mixture models) for shape distributions arising from discrete or even continuous hidden variables, and to generalize the related inference algorithms (e.g. EM). Such mixture models would be particularly well suited for manually segmented surfaces where some experts may decide that a small substructure is include in the segmentation while other experts will exclude it. Likewise, depending on the intensity level that they chose to follow, the boundary of the object is consistently biased toward the interior or the exterior of the object. Taking properly into account these kind of hidden variables in intrinsic surface statistics would allow to generalize algorithms like STAPLE [Warfield et al., 2004] from voxel-based to surface-based segmentations and to design better priors

for deformable models. This could also allow to take into account topological changes and not only geometrical changes in sulcal ribbons for instance.

Statistics on deformations and surfaces

The Riemannian approach that we presented here is not perfectly consistent with the structure of Lie groups as soon as they are not compact nor Abelian (Section 2.4.3), which is already the case for rigid body transformations. In that case, there is no left and right invariant metric, and most of the operations that we defined (e.g. the mean) with either the left or the right invariant metric are not consistent with inversion.

To find an alternative to the Riemannian structure for Lie groups, we investigate with V. Arsigny the idea on relying on one-parameter subgroups instead of geodesics. Preliminary results indicate that this may provide an interesting structure (see [Arsigny et al., 2006b, Arsigny et al., 2006a] and Section 4.3.6). For instance, one can design bi-invariant means that are fully compatible with the group structure [Arsigny et al., 2006e]. They are defined through fixed point equations which are very similar to the Riemannian ones. However, these equations do not derive from a well posed metric. It would be interesting to see what part of the statistical computing framework still holds if we replace the distance by a simple positive or negative energy. This probably amounts to considering the connection as the basic structure of the manifold instead of the Riemannian metric.

A key problem is to extend our statistical computing framework to infinite dimensional manifolds such as surfaces and diffeomorphism groups. From a theoretical point of view, we know how to provide the diffeomorphism group with left or right invariant Riemannian metrics that are sufficiently smooth to compute the geodesics by optimization [Beg et al., 2005, Miller et al., 2003, Miller and Younes, 2001, Joshi and Miller, 2000]. Through the so called EPDiff equation (Euler-Poincaré equation for diffeomorphisms), this optimization framework has been recently rephrased in an exponential/logarithm framework similar to the one developed here [Miller et al., 2006]. Thus, the basic algorithmic tools are the same, except that optimizing each time to compute the exponential and the logarithm has a deep impact on the computational times. However, one difficulty is that the infinite number of dimensions forbids the use of many tools like the probability density functions! Thus, even if simple statistics like the mean and the principal component analysis of a finite set of samples may still be computed [Vaillant et al., 2004], one should be very careful about ML-like statistical estimation in these spaces: there is always a finite number of data for an infinite number of parameters. In particular, there are infinitely many left- or right-invariant metrics on diffeomorphisms, and learning the optimal metric is an ill-posed problem. Estimations need to be regularized with priori models or performed within finite dimensional families of metrics whose assumptions are suited for the problem at hand. An interesting track for that is to establish specific models of the Green's function based on the mixture of smoothly varying local and long-distance interaction convolution kernels. If we only consider the local kernel, the Riemannian elasticity (Section 5.3.2) could be an interesting family of metrics allowing to measure statistically the properties of the virtual underlying material.

Last but not least, surfaces are an important source of anatomical manifolds in computational anatomy, and one needs to design efficient methods and metrics to capture their statistical properties. It would also be useful to fuse the information coming from image deformations and from surfaces in a single framework. We know from a few years that courants (generaliza-

tion of distributions) provide consistent mathematical tools for discrete and continuous surfaces [Cohen-Steiner and Morvan, 2003]. More recently, [Vaillant and Glaunes, 2005] proposed a diffeomorphic registration algorithm of surfaces based on that notion. Investigating this tool in more depth would probably allow to find in which cases approximations leading to efficient algorithms could be justified. In particular, I believe that the links between courants and the numerous efficient point-sets methods developed so far need to be established. A few insights on the convergence of the two kind of methods were presented as the first Mathematical Foundations of Computational Anatomy workshop [Pennec and Joshi, 2006].

6.3 Applications in medical image analysis

Computational models of the anatomy have many applications. In neuroscience, for instance, the anatomical variability need to be removed in population studies to understand the localization of functions and its variability. In more classical medical image analysis, statistics on shapes is needed to provide informative priors in deformable models. Likewise, informative priors on the deformability are needed in many registration problems. Relying on highly constrained deformations is critical in augmented reality system in order to ensure the robustness of the therapeutic gesture guidance. This is why most of the systems are currently limited to rigid motions. With precise variability models, one could relax this constrain. For instance one could take into account breathing in the liver puncture guidance system of Section 4.1.3. The statistical articulated model of the spine of Section 5.1 could also be used to guide endoscopic surgical operations with very few per-operative information. Inter-subject brain variability models will also be very important for obtaining more robust personalized atlases, for instance in radiotherapy planning. However, even with good anatomical priors, a generic registration algorithm will most probably not be perfectly robust and accurate in several clinical contexts without many improvements. One idea is to add some interaction so that the user can correct the result, for instance to get out of a local minimum. The interesting thing would be to integrate these corrections in the priors in order to iteratively learn how to solve each problem. Many other clinical applications of computational anatomy are foreseeable. We hope to demonstrate a few of them in the coming years.

Bibliography

- [Allasonnière et al., 2005] Allasonnière, S., Trouvé, A., and Younes, L. (2005). Geodesic shooting and diffeomorphic matching via textured models. In et al., A. R., editor, *Proc. of EMMCVPR 2005*, LNCS 3757, page 365–381.
- [Amari, 1990] Amari, S.-i. (1990). *Differential-geometric methods in Statistics*, volume 28 of *Lecture Notes in Statistics*. Springer, 2nd corr. print edition.
- [Arnaudon, 1995] Arnaudon, M. (1995). Barycentres convexes et approximations des martingales continues dans les variétés. In J. Azema, P.A. Meyer, M. Y., editor, *Séminaire de probabilités XXIX*, volume 1613 of *Lect. Notes in Math.*, pages 70–85. Springer-Verlag.
- [Arsigny et al., 2006a] Arsigny, V., Commowick, O., Pennec, X., and Ayache, N. (2006a). A Log-Euclidean framework for statistics on diffeomorphisms. In *Proc. of the 9th International Conference on Medical Image Computing and Computer Assisted Intervention (MICCAI'06), Part I*, number 4190 in LNCS, pages 924–931.
- [Arsigny et al., 2006b] Arsigny, V., Commowick, O., Pennec, X., and Ayache, N. (2006b). A Log-Euclidean polyaffine framework for locally rigid or affine registration. In Plum, J., Likar, B., and Gerritsen, F., editors, *Proceedings of the Third International Workshop on Biomedical Image Registration (WBIR'06)*, volume 4057 of LNCS, pages 120–127, Utrecht, The Netherlands. Springer Verlag.
- [Arsigny et al., 2005a] Arsigny, V., Fillard, P., Pennec, X., and Ayache, N. (2005a). Fast and simple calculus on tensors in the log-Euclidean framework. In Duncan, J. and Gerig, G., editors, *Proceedings of the 8th Int. Conf. on Medical Image Computing and Computer-Assisted Intervention - MICCAI 2005, Part I*, volume 3749 of LNCS, pages 115–122, Palm Springs, CA, USA, October 26-29. Springer Verlag.
- [Arsigny et al., 2005b] Arsigny, V., Fillard, P., Pennec, X., and Ayache, N. (2005b). Fast and simple computations on tensors with log-Euclidean metrics. Research Report RR-5584, INRIA, Sophia-Antipolis, France.
- [Arsigny et al., 2006c] Arsigny, V., Fillard, P., Pennec, X., and Ayache, N. (2006c). Geometric means in a novel vector space structure on symmetric positive-definite matrices. *SIAM Journal on Matrix Analysis and Applications*. In press.

- [Arsigny et al., 2006d] Arsigny, V., Fillard, P., Pennec, X., and Ayache, N. (2006d). Log-Euclidean metrics for fast and simple calculus on diffusion tensors. *Magnetic Resonance in Medicine*, 56(2):411–421.
- [Arsigny et al., 2003] Arsigny, V., Pennec, X., and Ayache, N. (2003). Polyrigid and polyaffine transformations: A new class of diffeomorphisms for locally rigid or affine registration. In Ellis, R. E. and Peters, T. M., editors, *Proc. of MICCAI'03, Part II*, volume 2879 of *LNCS*, pages 829–837, Montreal. Springer Verlag. MICCAI 2003 Best Student Award in Image Processing and Visualization.
- [Arsigny et al., 2005c] Arsigny, V., Pennec, X., and Ayache, N. (2005c). Polyrigid and polyaffine transformations: a novel geometrical tool to deal with non-rigid deformations - application to the registration of histological slices. *Medical Image Analysis*, 9(6):507–523.
- [Arsigny et al., 2006e] Arsigny, V., Pennec, X., and Ayache, N. (2006e). Bi-invariant means in Lie groups. application to left-invariant polyaffine transformations. Research report RR-5885, INRIA Sophia-Antipolis.
- [Arsigny et al., 2005d] Arsigny, V., Pennec, X., Fillard, P., and Ayache, N. (2005d). Dispositif perfectionné de traitement ou de production d'images de tenseurs. French patent filing number 0503483.
- [Aubert and Kornprobst, 2001] Aubert, G. and Kornprobst, P. (2001). *Mathematical problems in image processing*, volume 147 of *Applied Mathematical Sciences*. Springer.
- [Avants and Gee, 2004] Avants, B. and Gee, J. (2004). Geodesic estimation for large deformation anatomical shape averaging and interpolation. *Neuroimage*, 23(Suppl 1):S139–150.
- [Bajcsy and Kovačič, 1989] Bajcsy, R. and Kovačič, S. (1989). Multiresolution elastic matching. *Computer Vision, Graphics and Image Processing*, 46:1–21.
- [Basser et al., 1994] Basser, P., Mattiello, J., and Bihan, D. L. (1994). MR diffusion tensor spectroscopy and imaging. *Biophysical Journal*, 66:259–267.
- [Batchelor et al., 2005] Batchelor, P., Moakher, M., Atkinson, D., Calamante, F., and Connelly, A. (2005). A rigorous framework for diffusion tensor calculus. *Mag. Res. in Med.*, 53:221–225.
- [Beg et al., 2005] Beg, M., Miller, M., Trouvé, A., and Younes, L. (2005). Computing large deformation metric mappings via geodesic flows of diffeomorphisms. *Int. Journal of Computer Vision*, 61(2):139–157.
- [Benoit-Cattin et al., 2005] Benoit-Cattin, H., Collewet, G., Belaroussi, B., Saint-Jalmes, H., and Odet, C. (2005). The SIMRI project: A versatile and interactive MRI simulator. *Journal of Magnetic Resonance*, 173:97–115.
- [Bhatia, 2003] Bhatia, R. (2003). On the exponential metric increasing property. *Linear Algebra and its Applications*, 375:211–220.

- [Bhattacharya and Patrangenaru, 2002] Bhattacharya, R. and Patrangenaru, V. (2002). Nonparametric estimation of location and dispersion on Riemannian manifolds. *Journal of Statistical Planning and Inference*, 108:23–36.
- [Bhattacharya and Patrangenaru, 2003] Bhattacharya, R. and Patrangenaru, V. (2003). Large sample theory of intrinsic and extrinsic sample means on manifolds, I. *Annals of Statistics*, 31(1):1–29.
- [Bierkens, 2004] Bierkens, G. (2004). Geometric methods in diffusion tensor regularization. Master’s thesis, Technische Universiteit Eindhoven, Dept. of Math and Comp. Sci.
- [Bingham, 1974] Bingham, C. (1974). An antipodally symmetric distribution on the sphere. *Annals of Statistics*, 2(6):1201–1225.
- [Blanquer et al., 2004] Blanquer, I., Hernandez, V., Lonsdale, G., Dean, K., Lloyd, S., McClatchey, R., Montagnat, J., Brady, M., Pennec, X., Bolofsky, H., Jones, C., Hofmann, M., Solmonides, T., Oliveira, I. C., Sanchez, J. P., Lopez, V., Moor, G. D., Claerhout, B., and Harveg, J. A. (2004). Healthgrid white paper: <http://whitepaper.healthgrid.org/>. Edited by Cisco System.
- [Boisvert, 2005] Boisvert, J. (2005). Système de navigation 3D pour les chirurgies minimalement invasives du rachis. Research report (candidacy examination report), École Polytechnique de Montréal.
- [Boisvert et al., 2006a] Boisvert, J., Cheriet, F., Pennec, X., Ayache, N., and Labelle, H. (2006a). Assessment of brace local action on vertebrae relative poses. In *Research into Spinal Deformities*, volume 123 of *Studies in Health Technology and Informatics*, pages 372–378.
- [Boisvert et al., 2006b] Boisvert, J., Cheriet, F., Pennec, X., Ayache, N., and Labelle, H. (2006b). A novel framework for the 3D analysis of spine deformation modes. In *Research into Spinal Deformities*, volume 123 of *Studies in Health Technology and Informatics*, pages 176–182.
- [Boisvert et al., 2006c] Boisvert, J., Cheriet, F., Pennec, X., Labelle, H., and Ayache, N. (2006c). Geometric variability of the scoliotic spine using statistics on articulated shape models. *Submitted to IEEE Trans. Medical Imaging*.
- [Boisvert et al., 2006d] Boisvert, J., Pennec, X., Ayache, N., Labelle, H., and Cheriet, F. (2006d). 3D anatomic variability assesment of the scoliotic spine using statistics on Lie groups. In *Proceedings of the Third IEEE International Symposium on Biomedical Imaging (ISBI 2006)*, pages 750–753, Crystal Gateway Marriott, Arlington, Virginia, USA. IEEE.
- [Boisvert et al., 2006e] Boisvert, J., Pennec, X., Labelle, H., Cheriet, F., and Ayache, N. (2006e). Principal spine shape deformation modes using Riemannian geometry and articulated models. In *Proc of the IV Conference on Articulated Motion and Deformable Objects, Andratx, Mallorca, Spain, 11-14 July*, LNCS. Springer. AMDO best paper award 2006.
- [Bookstein, 1999] Bookstein, F. L. (1999). Linear methods for nonlinear maps: Procrustes fits, thin-plate splines, and the biometric analysis of shape variability. In Toga, A., editor, *Brain Warping*, pages 157–181. Academic Press.

- [Bricault et al., 1998] Bricault, I., Ferretti, G., and Cinquin, P. (1998). Registration of Real and CT-Derived Virtual Bronchoscopic Images to Assist Transbronchial Biopsy. *Transactions in Medical Imaging*, 17(5):703–714.
- [Bro-Nielsen, 1996] Bro-Nielsen, M. (1996). *Medical Image Registration and Surgery Simulation*. PhD thesis, Institut for Matematisk Modellering, Danmarks Tekniske Universitet, Lyngby, Denmark.
- [Bro-Nielsen and Gramkow, 1996] Bro-Nielsen, M. and Gramkow, C. (1996). Fast fluid registration of medical images. In *Proceedings VBC'96*, pages 267–276.
- [Brox et al., 2004] Brox, T., Weickert, J., Burgeth, B., and Mrázek, P. (2004). Nonlinear structure tensors. Technical report, Saarland University.
- [Brun, 2006] Brun, A. (2006). Manifold learning and representations for image analysis and visualization. Master's thesis, Dept. of Biomedical Engineering, Linköping Univ., Sweden.
- [Brun et al., 2005] Brun, A., Westin, C.-F., Herberthson, M., and Knutsson, H. (2005). Fast manifold learning based on riemannian normal coordinates. In *Proc. of SCIA 2005*, volume 3540 of *LNCS*, pages 920–929. Springer.
- [Burbea and Rao, 1982] Burbea, J. and Rao, C. (1982). Entropy differential metric, distance and divergence measures in probability spaces: a unified approach. *Journal of Multivariate Analysis*, 12:575–596.
- [Cachier and Ayache, 2004] Cachier, P. and Ayache, N. (2004). Isotropic energies, filters and splines for vectorial regularization. *J. of Math. Imaging and Vision*, 20(3):251–265.
- [Cachier et al., 2003] Cachier, P., Bardinet, E., Dormont, D., Pennec, X., and Ayache, N. (2003). Iconic feature based nonrigid registration: The pasha algorithm. *Comp. Vision and Image Understanding*, 89(2-3):272–298. Special Issue on Nonrigid Registration.
- [Cachier et al., 2001] Cachier, P., Mangin, J.-F., Pennec, X., Rivière, D., Papadopoulos-Orfanos, D., Régis, J., and Ayache, N. (2001). Multisubject non-rigid registration of brain MRI using intensity and geometric features. In Niessen, W. and Viergever, M., editors, *4th Int. Conf. on Medical Image Computing and Computer-Assisted Intervention (MICCAI'01)*, volume 2208 of *LNCS*, pages 734–742, Utrecht, The Netherlands.
- [Cachier and Pennec, 2000] Cachier, P. and Pennec, X. (2000). 3D non-rigid registration by gradient descent on a Gaussian-windowed similarity measure using convolutions. In *Proc. of IEEE Workshop on Mathematical Methods in Biomedical Image Analysis (MMBIA'00)*, pages 182–189, Hilton Head Island, South Carolina, USA. IEEE Computer society.
- [Cachier et al., 1999] Cachier, P., Pennec, X., and Ayache, N. (1999). Fast non-rigid matching by gradient descent: Study and improvements of the demons algorithm. Research Report 3706, INRIA.

- [Calvo and Oller, 1991] Calvo, M. and Oller, J. (1991). An explicit solution of information geodesic equations for the multivariate normal model. *Statistics and Decisions*, 9:119–138.
- [Castano-Moraga et al., 2006] Castano-Moraga, C., Lenglet, C., Deriche, R., and Ruiz-Alzola, J. (2006). A fast and rigorous anisotropic smoothing method for dt-mri. In *Proc. of ISBI 2006*.
- [Chefd’hotel et al., 2002] Chefd’hotel, C., Tschumperlé, D., Deriche, R., and Faugeras, O. (2002). Constrained flows of matrix-valued functions: Application to diffusion tensor regularization. In Heyden, A., Sparr, G., Nielsen, M., and Johansen, P., editors, *Proc. of ECCV 2002*, volume 2350 of *LNCS*, pages 251–265. Springer Verlag.
- [Chefd’hotel et al., 2004] Chefd’hotel, C., Tschumperlé, D., Deriche, R., and Faugeras, O. (2004). Regularizing flows for constrained matrix-valued images. *J. Math. Imaging and Vision*, 20(1-2):147–162.
- [Christensen and Johnson, 2001] Christensen, G. and Johnson, H. (2001). Consistent image registration. *IEEE Trans Med Imaging*, 20(7):568–82.
- [Christensen et al., 1997] Christensen, G. E., Joshi, S. C., and Miller, M. I. (1997). Volumetric transformation of brain anatomy. *IEEE Trans. Med. Imaging*, 16(6):864–877.
- [Christensen et al., 1996] Christensen, G. E., Rabitt, R. D., and Miller, M. I. (1996). Deformable templates using large deformation kinematics. *IEEE Transactions on Image Processing*, 5(10):1435–1447.
- [Ciarlet, 1988] Ciarlet, P. (1988). *Mathematical elasticity Vol. 1: Three-dimensionnal elasticity*. Elsevier Science B.V.
- [Cohen-Steiner and Morvan, 2003] Cohen-Steiner, D. and Morvan, J. (2003). Restricted delaunay triangulations and normal cycle. In *Proceedings of the nineteenth annual symposium on Computational geometry*, pages 312–321.
- [Collins et al., 1995] Collins, D., Holmes, C., Peters, T., and Evans, A. (1995). Automatic 3D model-based neuroanatomical segmentation. *Human Brain Mapping*, 3(3):190–208.
- [Commowick et al., 2005] Commowick, O., Stefanescu, R., Fillard, P., Arsigny, V., Ayache, N., Pennec, X., and Malandain, G. (2005). Incorporating statistical measures of anatomical variability in atlas-to-subject registration for conformal brain radiotherapy. In Duncan, J. and Gerig, G., editors, *Proceedings of the 8th Int. Conf. on Medical Image Computing and Computer-Assisted Intervention - MICCAI 2005, Part II*, volume 3750 of *LNCS*, pages 927–934, Palm Springs, CA, USA, October 26-29. Springer Verlag.
- [Corouge et al., 2005] Corouge, I., Fletcher, P. T., Joshi, S. C., Gilmore, J. H., and Gerig, G. (2005). Fiber tract-oriented statistics for quantitative diffusion tensor mri analysis. In *Proc. of MICCAI, part I*, number 3749 in *LNCS*, pages 131–139.
- [Coulon et al., 2004] Coulon, O., Alexander, D., and Arridge, S. (2004). Diffusion tensor magnetic resonance image regularization. *Medical Image Analysis*, 8(1):47–67.

- [D'Arcy Thompson, 1917] D'Arcy Thompson, W. (1917). *On Growth and Form*. Cambridge University Press, England.
- [Darling, 1996] Darling, R. (1996). Martingales on non-compact manifolds: maximal inequalities and prescribed limits. *Annales de l'institut Poincaré - Probabilités et Statistiques*, 32(4):431–454.
- [Dawant et al., 1999] Dawant, B., Hartmann, S., and S., G. (1999). Brain atlas deformation in the presence of large space-occupying tumors. In *Proc. of MICCAI'99*, LNCS 1679, pages 589–596, Cambridge, UK.
- [Delingette et al., 2006] Delingette, H., Pennec, X., Soler, L., Marescaux, J., and Ayache, N. (2006). Computational models for image guided, robot-assisted and simulated medical interventions. *Proceedings of the IEEE*. In press.
- [Deriche, 1992] Deriche, R. (1992). Recursively implementing the gaussian and its derivatives. In *Proc. Second International Conference On Image Processing (ICIP'92)*, pages 263–267.
- [do Carmo, 1992] do Carmo, M. (1992). *Riemannian Geometry*. Mathematics. Birkhäuser, Boston, Basel, Berlin.
- [Dryden and Mardia, 1991] Dryden, I. and Mardia, K. (1991). Theoretical and distributional aspects of shape analysis. In *Probability Measures on Groups, X (Oberwolfach, 1990)*, pages 95–116, New York. Plenum.
- [Dryden and Mardia, 1998] Dryden, I. and Mardia, K. (1998). *Statistical Shape Analysis*. John Wiley, Chichester.
- [D.W. Eggert, 1997] D.W. Eggert, A. Lorusso, R. F. (1997). Estimating 3d rigid body transformations: A comparison of four major algorithms. *Machine Vision Applications, Special Issue on Performance Characteristics of Vision Algorithms*, 9(5/6):272–290.
- [Edelman et al., 1998] Edelman, A., Arias, T., and Smith, S. (1998). The geometry of algorithms with orthogonality constraints. *SIAM Journal of Matrix Analysis and Applications*, 20(2):303–353.
- [Emery, 1989] Emery, M. (1989). *Stochastic Calculus in Manifolds*. Springer, Berlin.
- [Emery and Mokobodzki, 1991] Emery, M. and Mokobodzki, G. (1991). Sur le barycentre d'une probabilité dans une variété. In J. Azema, P.A. Meyer, M. Y., editor, *Séminaire de probabilités XXV*, volume 1485 of *Lect. Notes in Math.*, pages 220–233. Springer-Verlag.
- [Etienne et al., 2000a] Etienne, D., Stankoff, A., Pennec, X., Granger, S., Lacan, A., and Derycke, R. (2000a). A new approach for dental implant aided surgery. 4th Congresso Panamericano de Periodontologia, 17-19 august 2000, Santiago, Chili.
- [Etienne et al., 2000b] Etienne, D., Stankoff, A., Pennec, X., Granger, S., Lacan, A., and Derycke, R. (2000b). A new approach for dental implant aided surgery. A pilot evaluation. In Lemke, H., Vannier, M., Inamura, K., Farman, A., and Doi, K., editors, *Proc. of CARS'2000*, pages 927–931. Elsevier.

- [Facon et al., 2005] Facon, D., Ozanne, A., Fillard, P., Lepeintre, J.-F., Tournoux-Facon, C., and Ducreux, D. (2005). Mr diffusion tensor imaging and fiber tracking in spinal cord compression. *American Journal of Neuroradiology (AJNR)*, 26:1587–1594.
- [Faugeras and et al., 2004] Faugeras, O. and et al. (2004). Variational, geometric and statistical methods for modeling brain anatomy and function. *Neuroimage*, 23(Suppl 1):S46–55.
- [Feldmar and Ayache, 1996] Feldmar, J. and Ayache, N. (1996). Rigid, affine and locally affine registration of free-form surfaces. *The International Journal of Computer Vision*, 18(2):99–120.
- [Ferrant et al., 1999] Ferrant, M., Warfield, S., Guttman, C., Mulkern, R., Jolesz, F., and Kikinis, R. (1999). 3D image matching using a finite element based elastic deformation model. In *Proc. of MICCAI'99*, LNCS 1679, pages 202–209.
- [Fillard et al., 2005a] Fillard, P., Arsigny, V., Ayache, N., and Pennec, X. (2005a). A Riemannian framework for the processing of tensor-valued images. In Olsen, O. F., Florak, L., and Kuijper, A., editors, *Deep Structure, Singularities, and Computer Vision (DSSCV)*, number 3753 in LNCS, pages 112–123. Springer Verlag.
- [Fillard et al., 2005b] Fillard, P., Arsigny, V., Pennec, X., and Ayache, N. (2005b). Joint estimation and smoothing of clinical DT-MRI with a log-Euclidean metric. Research Report RR-5607, INRIA, Sophia-Antipolis, France.
- [Fillard et al., 2006a] Fillard, P., Arsigny, V., Pennec, X., and Ayache, N. (2006a). Clinical DT-MRI estimation, smoothing and fiber tracking with log-Euclidean metrics. In *Proceedings of the Third IEEE International Symposium on Biomedical Imaging (ISBI 2006)*, pages 786–789, Crystal Gateway Marriott, Arlington, Virginia, USA.
- [Fillard et al., 2006b] Fillard, P., Arsigny, V., Pennec, X., and Ayache, N. (2006b). Clinical DT-MRI estimation, smoothing and fiber tracking with log-Euclidean metrics. *Submitted to IEEE Trans. Medical Imaging*.
- [Fillard et al., 2006c] Fillard, P., Arsigny, V., Pennec, X., Hayashi, K. M., Thompson, P. M., and Ayache, N. (2006c). Measuring brain variability by extrapolating sparse tensor fields measured on sulcal lines. *Neuroimage*. In press.
- [Fillard et al., 2005c] Fillard, P., Arsigny, V., Pennec, X., Thompson, P. M., and Ayache, N. (2005c). Extrapolation of sparse tensor fields: Application to the modeling of brain variability. In Christensen, G. and Sonka, M., editors, *Proc. of Information Processing in Medical Imaging 2005 (IPMI'05)*, volume 3565 of LNCS, pages 27–38, Glenwood springs, Colorado, USA. Springer.
- [Fillard et al., 2003a] Fillard, P., Gilmore, J., Lin, W., Piven, J., and Gerig, G. (2003a). Quantitative analysis of white matter fiber properties along geodesic paths. In *Proc of MICCAI'03, Part I*, volume 2879 of LNCS, pages 16–23. Springer. MICCAI'03 Award: Best Student Paper in Image Analysis.

- [Fillard et al., 2003b] Fillard, P., Gilmore, J., Piven, J., Lin, W., and Gerig, G. (2003b). Quantitative analysis of white matter fiber properties along geodesic paths. In Ellis, R. E. and Peters, T. M., editors, *Proc. of MICCAI'03, Part II*, volume 2879 of *LNCS*, pages 16–23, Montreal. Springer Verlag.
- [Fitzpatrick et al., 1998] Fitzpatrick, J., West, J., and Maurer, C. J. (1998). Predicting error in rigid-body point-based registration. *IEEE Trans. on Medical Imaging*, 17(5).
- [Flandin, 2004] Flandin, G. (2004). *Utilisation d'informations géométriques pour l'analyse statistique des données d'IRM fonctionnelle*. PhD thesis, Université de Nice-Sophia Antipolis.
- [Flandin et al., 2002] Flandin, G., Kherif, F., Pennec, X., Malandain, G., Ayache, N., and Poline, J.-B. (2002). Improved detection sensitivity in functional MRI data using a brain parcelling technique. In Dohi, T. and Kikinis, R., editors, *Medical Image Computing and Computer-Assisted Intervention (MICCAI'02)*, volume 2488 of *LNCS*, pages 467–474, Tokyo. Springer.
- [Fletcher et al., 2003] Fletcher, P., Joshi, S., Lu, C., and Pizer, S. (2003). Gaussian distributions on Lie groups and their application to statistical shape analysis. In Taylor, C. and Noble, A., editors, *Proc. of Information Processing in Medical Imaging (IPMI'2003)*, volume 2732 of *LNCS*, pages 450–462. Springer.
- [Fletcher and Joshi, 2004] Fletcher, P. T. and Joshi, S. C. (2004). Principal geodesic analysis on symmetric spaces: Statistics of diffusion tensors. In *Computer Vision and Mathematical Methods in Medical and Biomedical Image Analysis, ECCV 2004 Workshops CVAMIA and MMBIA, Prague, Czech Republic, May 15, 2004*, volume 3117 of *LNCS*, pages 87–98. Springer.
- [Förstner and Moonen, 1999] Förstner, W. and Moonen, B. (1999). A metric for covariance matrices. In Krumm, F. and Schwarze, V. S., editors, *Qua vadis geodesia...? Festschrift for Erik W. Grafarend on the occasion of his 60th birthday*, number 1999.6 in Tech. Report of the Dpt of Geodesy and Geoinformatics, pages 113–128. Stuttgart University.
- [Fréchet, 1944] Fréchet, M. (1944). L'intégrale abstraite d'une fonction abstraite d'une variable abstraite et son application à la moyenne d'un élément aléatoire de nature quelconque. *Revue Scientifique*, pages 483–512.
- [Fréchet, 1948] Fréchet, M. (1948). Les éléments aléatoires de nature quelconque dans un espace distancié. *Annales de l'Institut Henri Poincaré*, 10:215–310.
- [Freed, 1995] Freed, A. (1995). Natural strain. *J. of Eng. Materials & Technology*, 117:379–385.
- [Gallier and Xu, 2002] Gallier, J. and Xu, D. (2002). Computing exponentials of skew-symmetric matrices and logarithms of orthogonal matrices. *International Journal of Robotics and Automation*, 17(4).
- [Gallot et al., 1993] Gallot, S., Hulin, D., and Lafontaine, J. (1993). *Riemannian Geometry*. Springer Verlag, 2nd edition edition.

- [Gamkrelidze, 1991] Gamkrelidze, R., editor (1991). *Geometry I*, volume 28 of *Encyclopaedia of Mathematical Sciences*. Springer Verlag.
- [Gerig et al., 1992] Gerig, G., Kikinis, R., Kübler, O., and Jolesz, F. (1992). Nonlinear anisotropic filtering of MRI data. *IEEE Transactions on Medical Imaging*, 11(2):221–232.
- [Germain et al., 2005a] Germain, C., Breton, V., Clarysse, P., Gaudeau, Y., Glatard, T., Jeannot, E., Legré, Y., Loomis, C., Magnin, I., Montagnat, J., Moureau, J.-M., Osorio, A., Pennec, X., and Texier, R. (2005a). Grid-enabling medical image analysis. *Journal of Clinical Monitoring and Computing*, 19(4-5):339–349.
- [Germain et al., 2005b] Germain, C., Breton, V., Clarysse, P., Gaudeau, Y., Glatard, T., Jeannot, E., Legré, Y., Loomis, C., Montagnat, J., Moureaux, J.-M., Osorio, A., Pennec, X., and Texier, R. (2005b). Grid-enabling medical image analysis. In *proceedings of the IEEE/ACM International Symposium on Cluster Computing and the Grid (Biogrid'05)*, pages 487–495, Cardiff, UK. IEEE.
- [Glatard et al., 2006a] Glatard, T., Montagnat, J., Lingrand, D., and Pennec, X. (2006a). Flexible and efficient workflow deployment of data-intensive applications on grids with MOTEUR. *International Journal of High Performance Computing Applications*. To appear in the special issue on Workflow Systems in Grid Environments.
- [Glatard et al., 2005a] Glatard, T., Montagnat, J., and Pennec, X. (2005a). Grid-enabled workflows for data intensive applications. In *Proc. 18th IEEE Symp. on Computer Based Medical Systems (CBMS'05), Dublin, Ireland, June 23-24*, pages 537–542. IEEE.
- [Glatard et al., 2005b] Glatard, T., Montagnat, J., and Pennec, X. (2005b). An optimized workflow enactor for data-intensive grid applications. Technical Report I3S/RR-2005-32, Nice-Sophia-Antipolis University, I3S Lab, RAINBOW project.
- [Glatard et al., 2006b] Glatard, T., Montagnat, J., and Pennec, X. (2006b). An experimental comparison of Grid5000 clusters and the EGEE grid. In *Proc of the Workshop on Experimental Grid testbeds for the assessment of large-scale distributed applications and tools (EXPGRID'06), Paris, France, 19-23 june*.
- [Glatard et al., 2006c] Glatard, T., Montagnat, J., and Pennec, X. (2006c). Medical image registration algorithms assessment: Bronze standard application enactment on grids using the MOTEUR workflow engine. In *Proc. of the HealthGrid conference (HealthGrid'06), Valencia, Spain, June 7-9*.
- [Glatard et al., 2006d] Glatard, T., Montagnat, J., and Pennec, X. (2006d). Probabilistic and dynamic optimization of job partitioning on a grid infrastructure. In *14th euromicro conference on Parallel, Distributed and network-based Processing (PDP06)*, pages 231–238, Montbéliard-Sochaux. IEEE.
- [Glatard et al., 2006e] Glatard, T., Montagnat, J., Pennec, X., Emsellem, D., and Lingrand, D. (2006e). MOTEUR: a data-intensive service-based workflow manager. Technical Report I3S/RR-2006-07-FR, I3S RAINBOW team, Univ. Nice-Sophia-Antipolis.

- [Glatard et al., 2006f] Glatard, T., Pennec, X., and Montagnat, J. (2006f). Performance evaluation of grid-enabled registration algorithms using bronze-standards. In *Proc. of the 9th International Conference on Medical Image Computing and Computer Assisted Intervention (MICCAI'06), Part II*, number 4191 in LNCS, pages 152–160. Springer.
- [González Ballester et al., 2004] González Ballester, M. A., Pennec, X., Linguraru, M. G., and Ayache, N. (2004). Generalized image models and their application as statistical models of images. *Medical Image Analysis*, 8(3):361–369.
- [Gramkow, 2001] Gramkow, C. (2001). On averaging rotations. *International Journal of Computer Vision*, 42(1-2):7–16.
- [Granger, 2003] Granger, S. (2003). *Une approche statistique multi-échelle au recalage rigide de surfaces : Application à l'implantologie dentaire*. Thèse de sciences, Ecole des Mines de Paris.
- [Granger and Pennec, 2002a] Granger, S. and Pennec, X. (2002a). Multi-scale EM-ICP: A fast and robust approach for surface registration. In Heyden, A., Sparr, G., Nielsen, M., and Johansen, P., editors, *European Conference on Computer Vision (ECCV 2002)*, volume 2353 of LNCS, pages 418–432, Copenhagen, Denmark. Springer.
- [Granger and Pennec, 2002b] Granger, S. and Pennec, X. (2002b). Statistiques exactes et approchées sur les normales aléatoires. Research report RR-4533, INRIA.
- [Granger et al., 2001] Granger, S., Pennec, X., and Roche, A. (2001). Rigid point-surface registration using an EM variant of ICP for computer guided oral implantology. In Niessen, W. and Viergever, M., editors, *4th Int. Conf. on Medical Image Computing and Computer-Assisted Intervention (MICCAI'01)*, volume 2208 of LNCS, pages 752–761, Utrecht, The Netherlands.
- [Grenander, 1963] Grenander, U. (1963). *Probabilities on Algebraic Structures*. Wiley.
- [Grenander, 1996] Grenander, U. (1996). *Elements of Pattern Theory*. The Johns Hopkins University Press, Baltimore, MD.
- [Grenander et al., 1998] Grenander, U., Miller, M., and Srivastava, A. (1998). Hilbert-schmidt lower bounds for estimators on matrix Lie groups for ATR. *IEEE Transactions on Pattern Analysis and Machine Intelligence (PAMI)*, 20(8):790–802.
- [Grenander and Miller, 1998] Grenander, U. and Miller, M. I. (1998). Computational anatomy: an emerging discipline. *Q. Appl. Math.*, LVI(4):617–694.
- [Grigor'yan, 2006] Grigor'yan, A. (2006). Heat kernels on weighted manifolds and applications. In Jorgenson, J. and Walling, L., editors, *The Ubiquitous Heat Kernel*, volume 398 of *Contemporary Mathematics*, pages 91–190. AMS.
- [Grova et al., 2001] Grova, C., Biraben, A., Scarabin, J.-M., Jannin, P., Buvat, I., Benali, H., and Gibaud, B. (2001). A methodology to validate MRI/SPECT registration methods using realistic simulated SPECT data. In Niessen, W. and Viergever, M., editors, *Proc of MICCAI 2001*, volume 2208 of LNCS, pages 275–282, Utrecht, The Netherlands.

- [Guéziec and Ayache, 1994] Guéziec, A. and Ayache, N. (1994). Smoothing and matching of 3-D space curves. *The International Journal of Computer Vision*, 12(1):79–104.
- [Guéziec et al., 1997] Guéziec, A., Pennec, X., and Ayache, N. (1997). Medical image registration using geometric hashing. *IEEE Computational Science & Engineering, special issue on Geometric Hashing*, 4(4):29–41. Oct-Dec.
- [Hairer et al., 2002] Hairer, E., Lubich, C., and Wanner, G. (2002). *Geometric numerical integration : structure preserving algorithm for ordinary differential equations*, volume 31 of *Springer series in computational mathematics*. Springer.
- [Helgason, 1978] Helgason, S. (1978). *Differential Geometry, Lie groups, and Symmetric Spaces*. Academic Press.
- [Hellier and Barillot, 2003] Hellier, P. and Barillot, C. (2003). Coupling dense and landmark-based approaches for nonrigid registration. *IEEE Trans. Medical Imaging*, 22(2):217–227.
- [Hellier et al., 2003] Hellier, P., Barillot, C., Corouge, I., Gibaud, B., Le Goualher, G., Collins, D. L., Evans, A., Malandain, G., Ayache, N., Christensen, G. E., and Johnson, H. J. (2003). Retrospective evaluation of intersubject brain registration. *IEEE Trans Med Imaging*, 22(9):1120–30.
- [Helmke and Moore, 1994] Helmke, U. and Moore, J. B. (1994). *Optimization and Dynamical Systems*. Communication and Control Engineering Series. Springer.
- [Hencky, 1928] Hencky, H. (1928). Über die form des elastizitätsgesetzes bei ideal elastischen stoffen. *Zeit. Techn. Phys.*, 9:241–247.
- [Hendricks, 1991] Hendricks, H. (1991). A Cramer-Rao type lower bound for estimators with values in a manifold. *Journal of Multivariate Analysis*, 38:245–261.
- [Hermosillo et al., 2002] Hermosillo, G., Chetd’Hotel, C., and Faugeras, O. (2002). Variational methods for multimodal image matching. *International Journal of Computer Vision*, 50(3):329–343.
- [Hill et al., 2004] Hill, D., Pennec, X., Burns, M., Parkin, M., Hajnal, J., Stefanescu, R., Rueckert, D., and Montagnat, J. (2004). Intraoperable medical image registration grid service. In *Proc. of HealthGrid 2004*, Clermont-Ferrand. European Commission, DG Information Society.
- [Holden et al., 2000] Holden, M., Hill, D., Denton, E., Jarosz, J., Cox, T., Rohlfing, T., Goodey, J., and Hawkes, D. (2000). Voxel Similarity Measures for 3D Serial MR Brain Image Registration. *IEEE Trans. Med. Imaging*, 19(2).
- [Joshi and Miller, 2000] Joshi, S. C. and Miller, M. I. (2000). Landmark matching via large deformation diffeomorphisms. *IEEE Trans. Image Processing*, 9(8):1357–1370.
- [Jupp and Mardia, 1989] Jupp, P. and Mardia, K. (1989). A unified view of the theory of directional statistics, 1975-1988. *International Statistical Review*, 57(3):261–294.

- [Kao et al., 2006] Kao, C.-Y., Hofer, M., Sapiro, G., Stern, J., Rehm, K., and Rottenberg, D. A. (2006). A geometric method for automatic extraction of sulcal fundi. In *Proc. ISBI'06*, pages 1168–1171. IEEE.
- [Karcher, 1977] Karcher, H. (1977). Riemannian center of mass and mollifier smoothing. *Communications in Pure and Applied Mathematics*, 30:509–541.
- [Kaya and Noakes, 1997] Kaya, C. Y. and Noakes, J. L. (1997). Geodesics and an optimal control algorithm. In *Proceedings of the 36th IEEE Conference on Decision and Control, San Diego, CA, U.S.A.*, pages 4918–4919.
- [Kendall, 1989] Kendall, D. (1989). A survey of the statistical theory of shape (with discussion). *Statistical Science*, 4:87–120.
- [Kendall and Moran, 1963] Kendall, M. and Moran, P. (1963). *Geometrical probability*. Number 10 in Griffin’s statistical monographs and courses. Charles Griffin & Co. Ltd.
- [Kendall, 1990] Kendall, W. (1990). Probability, convexity, and harmonic maps with small image I: uniqueness and fine existence. *Proc. London Math. Soc.*, 61(2):371–406.
- [Kendall, 1991] Kendall, W. (1991). Convexity and the hemisphere. *Journal of the London Mathematical Society*, 43(2):567–576.
- [Kent, 1992] Kent, J. (1992). *The art of Statistical Science*, chapter 10 : New Directions in Shape Analysis, pages 115–127. John Wiley & Sons. K.V. Mardia, ed.
- [Klassen et al., 2004] Klassen, E., Srivastava, A., Mio, W., and Joshi, S. (2004). Analysis of planar shapes using geodesic path on shape spaces. *IEEE Trans. on PAMI*, 26(3):372–383.
- [Klingenberg, 1982] Klingenberg, W. (1982). *Riemannian Geometry*. Walter de Gruyter, Berlin, New York.
- [Kobayashi and Nomizu, 1969] Kobayashi, S. and Nomizu, K. (1969). *Foundations of differential geometry, vol. II*. Number 15 in Interscience tracts in pure and applied mathematics. John Wiley & Sons.
- [Le and Kendall, 1993] Le, H. and Kendall, D. (1993). The Riemannian structure of Euclidean shape space: a novel environment for statistics. *Annals of Statistics*, 21:1225–1271.
- [Le Bihan et al., 2001] Le Bihan, D., Mangin, J.-F., Poupon, C., Clark, C., Pappata, S., Molko, N., and Chabriat, H. (2001). Diffusion tensor imaging: Concepts and applications. *Journal Magnetic Resonance Imaging*, 13(4):534–546.
- [Le Goualher et al., 2004] Le Goualher, G., Perchant, A., Genet, M. abd Cavé, C., Viellerobe, B., Berier, F., Abrat, B., and Ayache, N. (2004). Towards optical biopsies with an integrated fibered confocal fluorescent microscope. In Barillot, C., Haynor, D., and Hellier, P., editors, *Proc. of MICCAI'04*, volume 3217 of *LNCS*, pages 761–768, Saint-Malo, France. Springer Verlag.

- [Le Goualher et al., 1999] Le Goualher, G., Procyk, E., Collins, D., Venugopal, R., Barillot, C., and Evans, A. (1999). Automated extraction and variability analysis of sulcal neuroanatomy. *IEEE Trans. Medical Imaging*, 18(3):206–217.
- [Lenglet et al., 2004] Lenglet, C., Rousson, M., Deriche, R., and Faugeras, O. (2004). Toward segmentation of 3D probability density fields by surface evolution: Application to diffusion MRI. Research Report 5243, INRIA.
- [Lenglet et al., 2006] Lenglet, C., Rousson, M., Deriche, R., and Faugeras, O. (2006). Statistics on the manifold of multivariate normal distributions: Theory and application to diffusion tensor MRI processing. *Journal of Mathematical Imaging and Vision*. To appear. A preliminary version is available as INRIA Research Report RR-5242, 2004.
- [Lepore et al., 2006] Lepore, N., Brun, C. A., Chiang, M.-C., Chou, Y.-Y., Lopez, O. L., Aizenstein, H. J., Toga, A. W., Becker, J. T., and Thompson, P. M. (2006). Multivariate statistics of the jacobian matrices in tensor based morphometry and their application to HIV/AIDS. In Larsen, R., Nielsen, M., and Sporring, M., editors, *Medical Image Computing and Computer-Assisted Intervention - MICCAI'06*, volume 4190 of *LNCS*. Springer.
- [Lester et al., 1999] Lester, H., Arridge, S., Jansons, K., Lemieux, L., Hajnal, J., and Oatridge, A. (1999). Non-linear registration with the variable viscosity fluid algorithm. In *Proc of IPMI'99*, pages 238–251.
- [Lohmann et al., 2006] Lohmann, G., von Cramon, D., and Colchester, A. (2006). Investigating cortical variability using a generic gyral model. In *Proc. of the 9th International Conference on Medical Image Computing and Computer Assisted Intervention (MICCAI'06), Part II*, number 4191 in *LNCS*, pages 109–116.
- [Lovrić and Min-Oo, 2000] Lovrić, M. and Min-Oo, M. (2000). Multivariate normal distributions parametrized as a Riemannian symmetric space. *Journal of Multivariate Analysis*, 74(1):36–48.
- [Maillot, 1997] Maillot, H. (1997). Différentielle de la variance et centrage de la plaque de coupure sur une variété riemannienne compacte. Communication personnelle.
- [Mangin et al., 1995] Mangin, J., Frouin, V., Bloch, I., Régis, J., and López-Kahe, J. (1995). From 3D MR images to structural representations of the cortex topography using topological preserving deformations. *Journal of Mathematical Imaging and Vision*, 5(4):297–318.
- [Mangin et al., 1996] Mangin, J.-F., Frouin, V., Régis, J., Bloch, I., Belin, P., and Samson, Y. (1996). Towards better management of cortical anatomy in multi-modal multi-individual brain studies. *Physica Medica*, 12(Supplement 1):103–107.
- [Mangin et al., 2004a] Mangin, J.-F., Riviere, D., Cachia, A., Duchesnay, E., Cointepas, Y., Papadopoulos-Orfanos, D., Collins, D. L., Evans, A. C., and Régis, J. (2004a). Object-based morphometry of the cerebral cortex. *IEEE Trans. Med. Imaging*, 23(8):968–982.

- [Mangin et al., 2004b] Mangin, J.-F., Rivière, D., Cachia, A., Duchesnay, E., Cointepas, Y., Papadopoulos-Orfanos, D., Scifo, P., Ochiai, T., Brunelle, F., and Régis, J. (2004b). A framework to study the cortical folding patterns. *NeuroImage*, 23(Supplement 1):S129–S138.
- [Mardia, 1999] Mardia, K. (1999). Directional statistics and shape analysis. *Journal of applied Statistics*, 26(949-957).
- [Mardia and Jupp, 2000] Mardia, K. and Jupp, P. (2000). *Directional statistics*. Wiley, Chichester.
- [Markussen, 2004] Markussen, B. (2004). A statistical approach to large deformation diffeomorphisms. *2004 Conference on Computer Vision and Pattern Recognition Workshop (CVPRW'04)*, 12:181.
- [Matheron, 1975] Matheron, G. (1975). *Random Sets and Integral Geometry*. Wiley series in probability and mathematical statistics. John Wiley & Sons.
- [Maurer et al., 1997] Maurer, C. R. J., Fitzpatrick, J. M., Wang, M. Y., Galloway, R. L., Maciunas, R. J., and Allen, G. S. (1997). Registration of head volume images using implantable fiducial markers. *IEEE Trans. on Medical Imaging*, 16(4):447–462.
- [Medioni et al., 2000] Medioni, G., Lee, M.-S., and Tang, C.-K. (2000). *A Computational Framework for Segmentation and Grouping*. Elsevier.
- [Meijering, 2002] Meijering, E. (2002). A chronology of interpolation: From ancient astronomy to modern signal and image processing. *Proceedings of the IEEE*, 90(3):319–342.
- [Michor and Mumford, 2006] Michor, P. W. and Mumford, D. (2006). Riemannian geometries on spaces of plane curves. *J. Eur. Math. Soc. (JEMS)*, 8:1–48. ESI Preprint 1425, arXiv:math.DG/0312384.
- [Miller et al., 2003] Miller, M., Trouvé, A., and Younes, L. (2003). On the metrics and Euler-Lagrange equations of computational anatomy. *Annual Re-view of Biomedical Engineering*, pages 375–405.
- [Miller and Younes, 2001] Miller, M. and Younes, L. (2001). Group actions, homeomorphisms, and matching: A general framework. *International Journal of Computer Vision*, 41(1/2):61–84.
- [Miller et al., 2006] Miller, M. I., Trouvé, A., and Younes, L. (2006). Geodesic shooting for computational anatomy. *Journal of Mathematical Imaging and Vision*.
- [Moakher, 2002] Moakher, M. (2002). Means and averaging in the group of rotations. *SIAM Journal of Matrix Analysis and Applications*, 24(1):1–16.
- [Moakher, 2005] Moakher, M. (2005). A differential geometric approach to the geometric mean of symmetric positive-definite matrices. *SIAM Journal of Matrix Analysis and Applications*, 26(3):735–747.
- [Modersitzki, 2004] Modersitzki, J. (2004). *Numerical Methods for Image Registration*. Numerical Mathematics and Scientific Computations. Oxford University Press.

- [Mohammadi et al., 1997] Mohammadi, B., Borouchaki, H., and George, P. (1997). Delaunay mesh generation governed by metric specifications. Part II: applications. *Finite Elements in Analysis and Design*, pages 85–109.
- [Montagnat et al., 2006] Montagnat, J., Jouvenot, D., Pera, C., Frohner, A., Kunszt, P., Koblitz, B., Santos, N., and Loomis, C. (2006). Bridging clinical information systems and grid middleware: a medical data manager. In *Proceedings of the HealthGrid conference (HealthGrid'06)*, pages 14–24, Valencia, Spain. IOS Press.
- [Moran et al., 2005] Moran, B., Suvorova, S., and Howard, S. (2005). Sensor management for radar: a tutorial. In *Advances in Sensing with Security Applications 17–30 July 2005, Il Ciocco, Italy*. NATO Advanced Study Institute.
- [Nicolau et al., 2003a] Nicolau, S., Garcia, A., Pennec, X., Soler, L., and Ayache, N. (2003a). Augmented reality guided radio-frequency tumor ablation. In *Proceedings of Augmented and Virtual Reality Workshop (AVIR03)*, pages 34–35, Genève.
- [Nicolau et al., 2005] Nicolau, S., Garcia, A., Pennec, X., Soler, L., and Ayache, N. (2005). An augmented reality system to guide radio-frequency tumor ablation. *Computer Animation and Virtual World (previously the Journal of Visualization & Computer Animation)*, 16(1):1–10.
- [Nicolau et al., 2003b] Nicolau, S., Pennec, X., Soler, L., and Ayache, N. (2003b). Evaluation of a new 3D/2D registration criterion for liver radio-frequencies guided by augmented reality. In Ayache, N. and Delingette, H., editors, *International Symposium on Surgery Simulation and Soft Tissue Modeling (IS4TM'03)*, volume 2673 of *Lecture Notes in Computer Science*, pages 270–283, Juan-les-Pins, France. INRIA Sophia Antipolis, Springer-Verlag.
- [Nicolau et al., 2004a] Nicolau, S., Pennec, X., Soler, L., and Ayache, N. (2004a). An accuracy certified augmented reality system for therapy guidance. In *Proc. of the 8th European Conference on Computer Vision (ECCV 04), Part III*, volume LNCS 3023, pages 79–91, Prague.
- [Nicolau et al., 2004b] Nicolau, S., Pennec, X., Soler, L., and Ayache, N. (2004b). An augmented reality system to guide liver punctures. In *Workshop AMI-ARCS 2004 held in conjunction with MICCAI'04*, pages 77–86. IRISA Rennes.
- [Nicolau et al., 2006] Nicolau, S., Pennec, X., Soler, L., and Ayache, N. (2006). An augmented reality system for liver punctures: Design and evaluation on clinical cases. *Submitted to Medical Image Analysis*.
- [Nicolau et al., 2004c] Nicolau, S., Schmid, J., Pennec, X., Soler, L., and Ayache, N. (2004c). An augmented reality & virtuality interface for a puncture guidance system: Design and validation on an abdominal phantom. In Yang, G.-Z. and Jiang, T., editors, *Proc of the Second Int. Workshop on Medical Imaging and Augmented Reality MIAR 2004*, volume 3150 of *LNCS*, pages 302–310, Beijing, China. Springer Verlag.
- [Nielsen et al., 2002] Nielsen, M., Johansen, P., Jackson, A., and Laurrup, B. (2002). Brownian warps: A least committed prior for non-rigid registration. In *Proc of MICCAI'02, Part II*, volume 2489 of *LNCS*, pages 557 – 564.

- [Nomizu, 1954] Nomizu, K. (1954). Invariant affine connections on homogeneous spaces. *American J. of Math.*, 76:33–65.
- [Oinn et al., 2004] Oinn, T., Addis, M., Ferris, J., Marvin, D., Greenwood, M., Carver, T., Wipat, A., and Li, P. (2004). Taverna : A tool for the composition and enactment of bioinformatics workflows. *Bioinformatics journal*. <http://taverna.sourceforge.net/>.
- [Oller and Corcuera, 1995] Oller, J. and Corcuera, J. (1995). Intrinsic analysis of statistical estimation. *Annals of Statistics*, 23(5):1562–1581.
- [Ourselin et al., 2000] Ourselin, S., Roche, A., Prima, S., and Ayache, N. (2000). Block matching: A general framework to improve robustness of rigid registration of medical images. In DiGioia, A. and Delp, S., editors, *Third International Conference on Medical Robotics, Imaging And Computer Assisted Surgery (MICCAI 2000)*, volume 1935 of *Lectures Notes in Computer Science*, pages 557–566, Pittsburgh, Penn, USA. Springer.
- [Ourselin et al., 2002] Ourselin, S., Stefanescu, R., and Pennec, X. (2002). Robust registration of multi-modal images: towards real-time clinical applications. In Dohi, T. and Kikinis, R., editors, *Medical Image Computing and Computer-Assisted Intervention (MICCAI'02)*, volume 2489 of *LNCS*, pages 140–147, Tokyo. Springer. A preliminary version appeared as INRIA RR-4333.
- [Pennec, 1996] Pennec, X. (1996). *L'incertitude dans les problèmes de reconnaissance et de recalage - Applications en imagerie médicale et biologie moléculaire*. Thèse de sciences (phd thesis), Ecole Polytechnique, Palaiseau (France).
- [Pennec, 1997] Pennec, X. (1997). Registration of uncertain geometric features: Estimating the pose and its accuracy. In Moigne, J. L., editor, *Proc of the First Image Registration Workshop, November 20-21 1997, Greenbelt, Maryland, USA*, pages 263–272. CEDDIS.
- [Pennec, 1998a] Pennec, X. (1998a). Computing the mean of geometric features - application to the mean rotation. Research Report RR-3371, INRIA.
- [Pennec, 1998b] Pennec, X. (1998b). Toward a generic framework for recognition based on uncertain geometric features. *Videre: Journal of Computer Vision Research*, 1(2):58–87.
- [Pennec, 1999] Pennec, X. (1999). Probabilities and statistics on Riemannian manifolds: Basic tools for geometric measurements. In Cetin, A., Akarun, L., Ertuzun, A., Gurcan, M., and Yardimci, Y., editors, *Proc. of Nonlinear Signal and Image Processing (NSIP'99)*, volume 1, pages 194–198, June 20-23, Antalya, Turkey. IEEE-EURASIP.
- [Pennec, 2002] Pennec, X. (2002). Action de développement IRMf - rapport d'activité 2001. <http://www.inria.fr/valorisation/actions-developpement/IRMf2001.fr.html>.
- [Pennec, 2004] Pennec, X. (2004). Probabilities and statistics on Riemannian manifolds: A geometric approach. Research Report 5093, INRIA. An extended version will appear in the *Int. Journal of Mathematical Imaging and Vision*.
- [Pennec, 2005] Pennec, X. (2005). Recaler pour mieux soigner. *Pour la science*, (338):126–131.

- [Penneec, 2006a] Penneec, X. (2006a). Intrinsic statistics on Riemannian manifolds: Basic tools for geometric measurements. *Journal of Mathematical Imaging and Vision*, 25(1):127–154. A preliminary appeared as INRIA RR-5093, January 2004.
- [Penneec, 2006b] Penneec, X. (2006b). Left-invariant Riemannian elasticity: a distance on shape diffeomorphisms? In Penneec, X. and Joshi, S., editors, *Proc. of the International Workshop on the Mathematical Foundations of Computational Anatomy (MFCA-2006)*, pages 1–13.
- [Penneec and Ayache, 1996] Penneec, X. and Ayache, N. (1996). Randomness and geometric features in computer vision. In *IEEE Conf. on Computer Vision and Pattern Recognition (CVPR'96)*, pages 484–491, San Francisco, Cal, USA. Published in *J. of Math. Imag. and Vision* 9(1), July 1998, p. 49-67.
- [Penneec and Ayache, 1998] Penneec, X. and Ayache, N. (1998). Uniform distribution, distance and expectation problems for geometric features processing. *Journal of Mathematical Imaging and Vision*, 9(1):49–67. A preliminary version appeared as INRIA Research Report 2820, March 1996.
- [Penneec et al., 2001a] Penneec, X., Ayache, N., Roche, A., and Cachier, P. (2001a). Non-rigid MR/US registration for tracking brain deformations. In Press, I. C. S., editor, *Proc of Int. Workshop on Medical Imaging and Augmented Reality (MIAR 2001), 10-12 June 2001, Shatin, Hong Kong*, pages 79–86.
- [Penneec et al., 2000] Penneec, X., Ayache, N., and Thirion, J.-P. (2000). Landmark-based registration using features identified through differential geometry. In Bankman, I., editor, *Handbook of Medical Imaging*, chapter 31, pages 499–513. Academic Press.
- [Penneec et al., 1999] Penneec, X., Cachier, P., and Ayache, N. (1999). Understanding the “demon’s algorithm”: 3D non-rigid registration by gradient descent. In Taylor, C. and Colchester, A., editors, *Proc. of 2nd Int. Conf. on Medical Image Computing and Computer-Assisted Intervention (MICCAI'99)*, volume 1679 of *LNCS*, pages 597–605, Cambridge, UK. Springer Verlag.
- [Penneec et al., 2001b] Penneec, X., Cachier, P., and Ayache, N. (2001b). Tracking brain deformations in time sequences of 3D US images. In Insana, M. and Leahy, R., editors, *Proc. of IPMI'01*, number 2082 in *LNCS*, pages 169–175, Davis, CA, USA. Springer Verlag.
- [Penneec et al., 2003] Penneec, X., Cachier, P., and Ayache, N. (2003). Tracking brain deformations in time-sequences of 3D US images. *Pattern Recognition Letters*, 24(4-5):801–813. Special Issue on Ultrasonic Image Processing and Analysis.
- [Penneec et al., 2006] Penneec, X., Fillard, P., and Ayache, N. (2006). A Riemannian framework for tensor computing. *International Journal of Computer Vision*, 66(1):41–66. A preliminary version appeared as INRIA Research Report 5255, July 2004.
- [Penneec et al., 1998] Penneec, X., Guttman, C. R., and Thirion, J.-P. (1998). Feature-based registration of medical images: Estimation and validation of the pose accuracy. In *Proc. of First Int. Conf. on Medical Image Computing and Computer-Assisted Intervention (MICCAI'98)*, volume 1496 of *LNCS*, pages 1107–1114, Cambridge, USA. Springer Verlag.

- [Pennec and Joshi, 2006] Pennec, X. and Joshi, S., editors (2006). *Proceedings of the First International Workshop on Mathematical Foundations of Computational Anatomy - Geometrical and Statistical Methods for Modelling Biological Shape Variability, October 1st, 2006 Copenhagen, Denmark*.
- [Pennec et al., 2005a] Pennec, X., Roche, A., Cathier, P., and Ayache, N. (2005a). Non-rigid MR/US registration for tracking brain deformations. In Blum, R. and Liu, Z., editors, *Multi-Sensor Image Fusion and Its Applications*, volume 26 of *Signal Processing and Communications*, chapter 4, pages 107–143. CRC Press - Taylor and Francis.
- [Pennec et al., 2005b] Pennec, X., Stefanescu, R., Arsigny, V., Fillard, P., and Ayache, N. (2005b). Riemannian elasticity: A statistical regularization framework for non-linear registration. In Duncan, J. and Gerig, G., editors, *Proceedings of the 8th Int. Conf. on Medical Image Computing and Computer-Assisted Intervention - MICCAI 2005, Part II*, volume 3750 of *LNCS*, pages 943–950, Palm Springs, CA, USA, October 26-29. Springer Verlag.
- [Pennec and Thirion, 1995] Pennec, X. and Thirion, J.-P. (1995). Validation of 3D registration methods based on points and frames. In *Proc. of the 5th Int. Conf on Comp. Vision (ICCV'95)*, pages 557–562, Cambridge, Ma. Published in *Int. J. of Comp. Vision* 25(3), 1997, p. 203-229.
- [Pennec and Thirion, 1997] Pennec, X. and Thirion, J.-P. (1997). A framework for uncertainty and validation of 3D registration methods based on points and frames. *Int. Journal of Computer Vision*, 25(3):203–229.
- [Penney et al., 2001] Penney, G., Blackall, J., Hayashi, D., Sabharwal, T., Adam, A., and Hawkes, D. (2001). Overview of an Ultrasound to CT or MR Registration System for use in Thermal Ablation of Liver Metastases. In *Proc of Medical Image Understanding and Analysis (MIUA'01)*.
- [Perona and Malik, 1990] Perona, P. and Malik, J. (1990). Scale-space and edge detection using anisotropic diffusion. *IEEE Trans. Pattern Analysis and Machine Intelligence (PAMI)*, 12(7):629–639.
- [Peyrat et al., 2006] Peyrat, J.-M., Sermesant, M., Delingette, H., Pennec, X., Xu, C., McVeigh, E., and Ayache, N. (2006). Towards a statistical atlas of cardiac fiber structure. In *Proc. of the 9th International Conference on Medical Image Computing and Computer Assisted Intervention (MICCAI'06), Part I*, number 4190 in *LNCS*, pages 297–304.
- [Picard, 1994] Picard, J. (1994). Barycentres et martingales sur une variété. *Annales de l'institut Poincaré - Probabilités et Statistiques*, 30(4):647–702.
- [Pitiot et al., 2003] Pitiot, A., Delingette, H., Toga, A., and Thompson, P. M. (2003). Learning object correspondences with the observed transport shape measure. In Taylor, C. and Noble, J. A., editors, *Information Processing in Medical Imaging IPMI'03*, volume 2732 of *LNCS*, pages 25–37. Springer Verlag.
- [Poincaré, 1912] Poincaré, H. (1912). *Calcul des probabilités*. 2nd edition, Paris.

- [Prima et al., 1998] Prima, S., Thirion, J.-P., Subsol, G., and Roberts, N. (1998). Automatic Analysis of Normal Brain Dissymmetry of Males and Females in MR Images. In *Proc. of MICCAI'98*, volume 1496 of *Lecture Notes in Computer Science*, pages 770–779.
- [Provenzale et al., 2006] Provenzale, J. M., Mukundan, S., and Barboriak, D. P. (2006). Diffusion-weighted and perfusion MR imaging for brain tumor characterization and assessment of treatment response. *Radiology*, 239(3):632 – 649.
- [Rasouli, 2002] Rasouli, V. (2002). *Application of Riemannian multivariate statistics to the analysis of rock fracture surface roughness*. PhD thesis, University of London.
- [Régis et al., 1995] Régis, J., Mangin, J.-F., Frouin, V., Sastre, F., Peragut, J., and Samson, Y. (1995). Generic model for the localization of the cerebral cortex and preoperative multimodal integration in epilepsy surgery. *Stereotactic Functional Neurosurgery*, 65:72–80.
- [Rey et al., 2002] Rey, D., Subsol, G., Delingette, H., and Ayache, N. (2002). Automatic detection and segmentation of evolving processes in 3D medical images: Application to multiple sclerosis. *Medical Image Analysis*, 6(2):163–179.
- [Rivière et al., 2002] Rivière, D., Mangin, J.-F., Papadopoulos, D., Martinez, J.-M., Frouin, V., and Régis, J. (2002). Automatic recognition of cortical sulci using a congregation of neural networks. *Medical Image Analysis*, 6:77–92.
- [Roche et al., 1998a] Roche, A., Malandain, G., Pennec, X., and Ayache, N. (1998a). The correlation ratio as a new similarity measure for multimodal image registration. In *Proc. of First Int. Conf. on Medical Image Computing and Computer-Assisted Intervention (MICCAI'98)*, volume 1496 of *LNCS*, pages 1115–1124, Cambridge, USA. Springer Verlag.
- [Roche et al., 1998b] Roche, A., Malandain, G., Pennec, X., and Ayache, N. (1998b). Multimodal image registration by maximization of the correlation ratio. Research Report RR-3378, INRIA. Published in MICCAI'98, Cambridge, USA, LNCS 1496, p. 1115-1124.
- [Roche et al., 2001] Roche, A., Pennec, X., Malandain, G., and Ayache, N. (2001). Rigid registration of 3D ultrasound with MR images: a new approach combining intensity and gradient information. *IEEE Transactions on Medical Imaging*, 20(10):1038–1049.
- [Roche et al., 2000] Roche, A., Pennec, X., Rudolph, M., Auer, D. P., Malandain, G., Ourselin, S., Auer, L. M., and Ayache, N. (2000). Generalized correlation ratio for rigid registration of 3D ultrasound with MR images. In DiGioia, A. and Delp, S., editors, *Proc. of the 3rd Int. Conf. on Medical Image Computing and Computer-Assisted Intervention (MICCAI'00)*, volume 1935 of *LNCS*, pages 567–577, Pittsburgh, Pennsylvania, USA. Published in IEEE TMI 20(10), oct. 2001, p. 25-31.
- [Rougée, 1997] Rougée, P. (1997). *Mécanique des grandes transformations*. Number 25 in *Mathématiques & Applications*. Springer.
- [Rousseeuw and Leroy, 1987] Rousseeuw, P. and Leroy, A. (1987). *Robust Regression and Outliers Detection*. Wiley series in prob. and math. stat. J. Wiley and Sons.

- [Rovaris et al., 2005] Rovaris, M., Gass, A., Bammer, R., Hickman, S., Ciccarelli, O., Miller, D., and Filippi, M. (2005). Diffusion mri in multiple sclerosis. *Neurology*, 65:1526–1532.
- [Rueckert et al., 2003] Rueckert, D., Frangi, A., and Schnabel, J. (2003). Automatic construction of 3D statistical deformation models of the brain using non-rigid registration. *IEEE TMI*, 22:1014–1025.
- [Rueckert et al., 1999] Rueckert, D., Sonoda, L. I., Hayes, C., Hill, D. L. G., Leach, M. O., and Hawkes, D. J. (1999). Non-rigid registration using free-form deformations: Application to breast MR images. *IEEE Trans. Medical Imaging*, 18(8):712–721.
- [Santalo, 1976] Santalo, L. (1976). *Integral Geometry and Geometric Probability*, volume 1 of *Encyclopedia of Mathematics and its Applications*. Addison-Wesley Publishing Company.
- [Sermesant et al., 2006] Sermesant, M., Delingette, H., and Ayache, N. (2006). An electromechanical model of the heart for image analysis and simulation. *IEEE Transactions in Medical Imaging*, 25(5):612–625.
- [Sijbers et al., 1998] Sijbers, J., den Dekker, A., Scheunders, P., and Dyck, D. V. (1998). Maximum likelihood estimation of Rician distribution parameters. *TMI*, 17(3).
- [Skovgaard, 1984] Skovgaard, L. (1984). A Riemannian geometry of the multivariate normal model. *Scand. J. Statistics*, 11:211–223.
- [Small, 1996] Small, C. (1996). *The Statistical Theory of Shapes*. Springer series in statistics. Springer.
- [Soler et al., 2004a] Soler, L., Ayache, N., Nicolau, S., Pennec, X., Forest, C., Delingette, H., and Marescaux, J. (2004a). Traitement d’images médicales pour la planification, la simulation et l’aide intra-opératoire des actes chirurgicaux. *La Revue de l’Electricité et de l’Electronique*, pages 64–71.
- [Soler et al., 2004b] Soler, L., Ayache, N., Nicolau, S., Pennec, X., Forest, C., Delingette, H., Mutter, D., and Marescaux, J. (2004b). Traitements d’images médicales pour la planification, la simulation et l’aide intra-opératoire des actes chirurgicaux. In Faupel, M., Smigielski, P., and Grzymala, R., editors, *Imagerie et Photonique pour les sciences du vivant et la médecine*, pages 19–31. Edition Fontis Media. ISBN 2-88476-005-9.
- [Soler et al., 2004c] Soler, L., Ayache, N., Nicolau, S., Pennec, X., Forest, C., Delingette, H., Mutter, D., and Marescaux, J. (2004c). Virtual reality, augmented reality and robotics in surgical procedures of the liver. In Buzug, T. M. and Lueth, T. C., editors, *Perspectives in Image-guided Surgery. Proceedings of the Scientific Workshop on Medical Robotics, Navigation and Visualization (MRNV) 2004*, pages 476–484, RheinAhrCampus Remagen, Germany. World Scientific.
- [Soler et al., 2004d] Soler, L., Nicolau, S., Schmid, J., Koehl, C., Marescaux, J., Pennec, X., and Ayache, N. (2004d). Virtual reality and augmented reality in digestive surgery. In *Proc. of IEEE International Symposium on Mixed and Augmented Reality (ISMAR’04)*, pages 278–279.

- [Spivak, 1979] Spivak, M. (1979). *Differential Geometry*, volume 1. Publish or Perish, Inc., 2nd edition.
- [Stefanescu, 2005] Stefanescu, R. (2005). *Parallel nonlinear registration of medical images with a priori information on anatomy and pathology*. Thèse de sciences, Université de Nice – Sophia-Antipolis.
- [Stefanescu et al., 2004a] Stefanescu, R., Commowick, O., Malandain, G., Bondiau, P.-Y., Ayache, N., and Pennec, X. (2004a). Non-rigid atlas to subject registration with pathologies for conformal brain radiotherapy. In Barillot, C., Haynor, D., and Hellier, P., editors, *Proc. of the 7th Int. Conf on Medical Image Computing and Computer-Assisted Intervention - MICCAI 2004*, volume 3216 of *LNCS*, pages 704–711, Saint-Malo, France. Springer Verlag.
- [Stefanescu et al., 2004b] Stefanescu, R., Pennec, X., and Ayache, N. (2004b). Grid-enabled non-rigid registration of medical images. *Parallel Processing Letters*, 14(2):197–216.
- [Stefanescu et al., 2004c] Stefanescu, R., Pennec, X., and Ayache, N. (2004c). Grid powered nonlinear image registration with locally adaptive regularization. *Medical Image Analysis*, 8(3):325–342. MICCAI 2003 Special Issue.
- [Stefanescu et al., 2005] Stefanescu, R., Pennec, X., and Ayache, N. (2005). A grid service for the interactive use of a parallel non-rigid registration algorithm of medical images. *Methods of Information in Medicine*, 44(2).
- [Swann and Olsen, 2003] Swann, A. and Olsen, N. H. (2003). Linear transformation groups and shape space. *Journal of Mathematical Imaging and Vision*, 19(1):49 – 62.
- [Thévenaz et al., 2000] Thévenaz, P., Blu, T., and Unser, M. (2000). Interpolation revisited. *IEEE Transactions on Medical Imaging*, 19(7):739–758.
- [Thirion, 1998] Thirion, J.-P. (1998). Image matching as a diffusion process: an analogy with maxwell’s demons. *Medical Image Analysis*, 2(3):243–260.
- [Thompson et al., 2001a] Thompson, P., Cannon, T., Narr, K., van Erp, T., Poutanen, V., Huttenen, M., Lönngqvist, J., Standertskjöld-Nordenstam, C., Kaprio, J., Khaledy, M., Dail, R., Zoumalan, C., and Toga, A. (2001a). Genetic influences on brain structure. *Nature Neuroscience*, 4(12):1253–1258.
- [Thompson et al., 2005] Thompson, P., Lee, A., Dutton, R., Geaga, J., Hayashi, K., Eckert, M., Bellugi, U., Galaburda, A., Korenberg, J., Mills, D., Toga, A., and Reiss, A. (2005). Abnormal cortical complexity and thickness profiles mapped in Williams syndrome. *Journal of Neuroscience*, 25(16):4146–4158.
- [Thompson et al., 2000] Thompson, P., Mega, M., Narr, K., Sowell, E., Blanton, R., and Toga, A. (2000). Brain image analysis and atlas construction. In Fitzpatrick, M. and Sonka, M., editors, *Handbook of Medical Image Proc. and Analysis*, chapter 17. SPIE.

- [Thompson et al., 2001b] Thompson, P., Mega, M., Woods, R., Zoumalan, C., Lindshield, C., Blanton, R., Moussai, J., Holmes, C., Cummings, J., and Toga, A. (2001b). Cortical change in Alzheimer’s disease detected with a disease-specific population-based brain atlas. *Cerebral Cortex*, 11(1):1–16.
- [Thompson et al., 2004] Thompson, P., Miller, M., Ratnanather, J., Poldrack, R., and Nichols, T. (2004). Editorial of the special issue on mathematics in brain imaging. *NeuroImage*, 23(1).
- [Thompson and Toga, 1996] Thompson, P. and Toga, A. (1996). A surface-based technique for warping 3-dimensional images of the brain. *IEEE Trans. Medical Imaging*, 15(4):402–417.
- [Toga and Thompson, 2003] Toga, A. and Thompson, P. (2003). Mapping brain asymmetry. *Nature Reviews Neuroscience*, 4(1):37–48.
- [Trouvé, 1998] Trouvé, A. (1998). Diffeomorphisms groups and pattern matching in image analysis. *International Journal of Computer Vision*, 28(3):213–221.
- [Tschumperlé, 2002] Tschumperlé, D. (2002). *PDE-Based Regularization of Multivalued Images and Applications*. PhD thesis, University of Nice-Sophia Antipolis.
- [Vaillant and davatzikos, 1999] Vaillant, M. and davatzikos, C. (1999). Hierarchical matching of cortical features for deformable brain image registration. In *Proc. of IPMI’99, Visegrad, Hungary*, volume 1613 of *LNCS*, pages 182–195. Springer.
- [Vaillant and Glaunes, 2005] Vaillant, M. and Glaunes, J. (2005). Surface matching via currents. In *Proc. of IPMI’05*, pages 381–392.
- [Vaillant et al., 2004] Vaillant, M., Miller, M., Younes, L., and Trouvé, A. (2004). Statistics on diffeomorphisms via tangent space representations. *NeuroImage*, 23(Supp. 1):S161–S169.
- [Vercauteren et al., 2006] Vercauteren, T., Perchant, A., Malandain, G., Pennec, X., and Ayache, N. (2006). Robust mosaicing with correction of motion distortions and tissue deformation for in vivo fibered microscopy. *Medical Image Analysis*, 10(5):673–692. Annual Medical Image Analysis (MedIA) Best Paper Award 2006.
- [Vercauteren et al., 2005] Vercauteren, T., Perchant, A., Pennec, X., and Ayache, N. (2005). Mosaicing of confocal microscopic in vivo soft tissue video sequences. In Duncan, J. and Gerig, G., editors, *Proceedings of the 8th Int. Conf. on Medical Image Computing and Computer-Assisted Intervention - MICCAI 2005, Part I*, volume 3749 of *LNCS*, pages 753–760, Palm Springs, CA, USA, October 26-29. Springer Verlag.
- [Wang et al., 2004] Wang, Z., Vemuri, B., Chen, Y., and Mareci, T. (2004). A constrained variational principle for direct estimation and smoothing of the diffusion tensor field from complex DWI. *IEEE Trans. on Medical Imaging*.
- [Warfield et al., 2004] Warfield, S., Zou, K., and Wells, W. (2004). Simultaneous truth and performance level estimation (STAPLE): An algorithm for the validation of image segmentation. *IEEE Transactions on Medical Imaging*, 23(7):903–921.

- [Webb et al., 1999] Webb, J., Guimond, A., Roberts, N., and D. Chadwick, P. E., Meunier, J., and Thirion, J.-P. (1999). Automatic Detection of Hippocampal Atrophy on Magnetic Resonance Images. *Magnetic Resonance Imaging*, 17(8):1149–1161.
- [Weickert, 2000] Weickert, J. (2000). Applications of nonlinear diffusion in image processing and computer vision. *Acta Mathematica Universitatis Comenianae*, 70(1):33–50.
- [Weickert and Brox, 2002] Weickert, J. and Brox, T. (2002). Diffusion and regularization of vector- and matrix-valued images. In Nashed, M. and Scherzer, O., editors, *Inverse Problems, Image Analysis, and Medical Imaging*, volume 313 of *Contemporary Mathematics*, pages 251–268, Providence. AMS.
- [Weickert et al., 1998] Weickert, J., Haar, B., and Viergever, R. (1998). Efficient and reliable schemes for nonlinear diffusion filtering. *IEEE Transactions on Image Processing*, 7:398–410.
- [Weickert and Hagen, 2006] Weickert, J. and Hagen, H., editors (2006). *Visualization and Processing of Tensor Fields*. Mathematics and Visualization. Springer.
- [Welker, 1989] Welker, W. (1989). Why does the cerebral cortex fissure and fold. *Cerebral Cortex*, 8(B):3–135.
- [West et al., 1996] West, J., Fitzpatrick, J., Wang, M., Dawant, B., Maurer, Jr., C., Kessler, R., Maciunas, R., Barillot, C., Lemoine, D., Collignon, A., Maes, F., Suetens, P., Vandermeulen, D., van den Elsen, P., Hemler, P., Napel, S., Sumanaweera, T., Harkness, B., Hill, D., Studholme, C., Malandain, G., Pennec, X., Noz, M., Maguire, Jr., G., Pollack, M., Pelizzari, C., Robb, R., Hanson, D., and Woods, R. (1996). Comparison and evaluation of retrospective intermodality image registration techniques. In *Medical Imaging 1996: Image Processing*, volume 2710 of *SPIE proceedings series*, Newport Beach, California, USA.
- [West et al., 1997] West, J., Fitzpatrick, J. M., Wang, M. Y., Dawant, B. M., Maurer, Jr., C. R., Kessler, R. M., Maciunas, R. J., Barillot, C., Lemoine, D., Collignon, A., Maes, F., Suetens, P., Vandermeulen, D., van den Elsen, P. A., Napel, S., Sumanaweera, T. S., Harkness, B., Hemler, P. F., Hill, D. L. G., Hawkes, D. J., Studholme, C., Maintz, J. B. A., Viergever, M. A., Malandain, G., Pennec, X., Noz, M. E., Maguire, Jr., G. Q., Pollack, M., Pelizzari, C. A., Robb, R. A., Hanson, D., and Woods, R. P. (1997). Comparison and evaluation of retrospective intermodality brain image registration techniques. *Journal of Computer Assisted Tomography*, 21(4):554–566.
- [Westin et al., 2002] Westin, C., Maier, S., Mamata, H., Nabavi, A., Jolesz, F., and Kikinis, R. (2002). Processing and visualization for diffusion tensor MRI. *Medical Image Analysis*, 6(2):93–108.
- [Woods, 2003] Woods, R. (2003). Characterizing volume and surface deformations in an atlas framework: theory, applications, and implementation. *NeuroImage*, 18(3):769–788.
- [Younes, 1998] Younes, L. (1998). Computable elastic distances between shapes. *SIAM Journal on Applied Mathematics*, 58(2):565–586.

- [Zefran et al., 1999] Zefran, M., Kumar, V., and Croke, C. (1999). Metrics and connections for rigid-body kinematics. *Int. Journal of Robotics Research*, 18(2):243–258.

Part II

Synthesis of Activities

Curriculum Vitae

PENNEC Xavier

<http://www.inria.fr/epidaure/personnel/Xavier.Pennec/>

Nationality: French

Date of birth: Mai the 2nd, 1970

INRIA Sophia - Asclepios team,
2004 Route des Lucioles BP 93,
06902 Sophia Antipolis Cedex, France

Tel: +33 4 92 38 76 64

Fax: +33 4 92 38 76 69

Email: Xavier.Pennec@sophia.inria.fr

Education

- 1996** **Ph.D., École Polytechnique, Paris, France**, in Computer Science, with highest honors.
- 1993** **Master degree (DEA), École Polytechnique - École Normale Supérieure, Paris, France**, in Mathematical Computer Science and Applications, specialization in Geometric Computing, with highest honors.
- 1992** **Graduate of the École Polytechnique, Paris, France**. Specialization in Computer Science and Physics.
- 1987** **Baccalauréat** in Mathematics and Techniques, with highest honors.

Positions

- Since 2000** Senior Research Scientist (CR1) at INRIA, Epidaure / Asclepios team.
- 1998-2000** Junior Research Scientist (CR2) at INRIA, Epidaure team.
- 1998** Postdoctoral/Expert Engineer in charge of the European project ROBOSCOPE. INRIA, Epidaure team.
- 1997** Postdoctoral Associate at MIT, Artificial Intelligence Lab, Vision Group. Advisor: Pr. W.E.L. Grimson. *Theory of Uncertainty on Geometric Features: Extensions and Applications*.
- 1993-1996** Ph.D. student at INRIA, Epidaure team. Supervisor: Pr. N. Ayache. *Uncertainty in Recognition and Registration Problems - Application in Medical Imaging and Molecular Biology*.
- 1993** Master degree research training period (6 months) at INRIA, Epidaure team. Supervisor: Pr. N. Ayache. *Error Handling in Geometric Hashing and Alignment Methods: a Theoretical Study*.
- 1992** Graduate degree research training period (4 months) at ONERA Châtillon, DMIGIA (FRANCE). Supervisor: J.-J. Bourrelly. *Improvement of Some Neuro-Mimetic Techniques with Application in Hand-Written Capital Letter Recognition*.
- 1990** Military service: company commanding officer in the French Air Force.

Grants and Contracts

European projects

- **HEALTH-e-CHILD (2006-2009):** *An Integrated healthcare platform for European paediatrics. A Grid-enabled European network of leading clinical centers. Individualized disease prevention, screening, early diagnosis, therapy and follow-up of pediatric heart diseases, inflammatory diseases, and brain tumors.* (IST 027749, INRIA amount: 900 000 euros). Industrial partners: Siemens, Maat G-knowledge, CERN. Universities: West-England (Bristol, UK), Athens (GR), Genoa (IT); Hospitals: Gaslini (Genoa, IT), Necker (Paris, FR), GOSH/UCL (London, UK). <http://www.health-e-child.org/>. Proposal writing and project inception from 2003 to 2005. Leader of WP11 (*integrated disease modeling*), member of the *Executive board* and of the *Project management team*, deputy of N. Ayache to the *Governing board*.
- **ROBOSCOPE (1998-2000):** *Ultrasound-image-guided manipulator-assisted system for minimally invasive endo-neuro-surgery*, HC-4018 (INRIA amount: 506 800 ECU). IBMT-Fraunhofer, ISM, Fokker Control, Imperial College. Scientific responsible of the project for INRIA; Leader of the *Multi Modal Image Fusion Tools* workpackage (including KU Leuven as sub-contractor); WP and INRIA deputy at the annual EC evaluation.

Industrial contracts

- **Siemens Corporate Research (2004-2008) :** *Learning for error correction and validation of non-rigid registration algorithms.* Joint elaboration and follow-up of the contract (DEA of A. Azar, PhD of J.-M. Peyrat).
- **Medtronics (2004-2005) :** *Localization and segmentation of deep gray nuclei for electrode stimulation implantation in Alzheimer's disease.* Technical follow-up of the post-doctoral fellow (R. Stefanescu).
- **AREALL (1998-2002):** *A surgical navigation system for dental implantology.* Consultant from 1998 to 2002. Preparation and follow-up of the the research contract and Cifre fellowship for the PhD of S. Granger (2000-2002).
- **CNES (2002):** *Comparison of the performances of non-linear registration algorithms on aerial and satellite images.*
- **QuantifiCare (2001-):** *Medical image analysis for pharmaceutical applications.* Software and patents transfer. Founder and Scientific Council member

Research grants

- **ACI Masses de données AGIR (2004-2007):** *Grid Analysis of Radiological Images Data.* CRAN, LORIA, INRIA, LIMSI, LRI, LPC. French multi-disciplinary project aiming at leveraging medical imaging algorithms trough grid systems. <http://www.aci-agir.org/>. Proposal writing, principal investigator at INRIA-Sophia, joint advisor of the PhD of T. Glatard.

- **Associated team Brain Atlas with LONI at UCLA (2001-2006):** *Development of new methods to build atlases and to quantify the variability of the brain.* <http://www-sop.inria.fr/epidaure/Collaborations/UCLA/> and <http://www.loni.ucla.edu/Research/INRIA.html>. General coordination of the collaboration with P. Thompson.
- **Development Action IRMf (2000-2002):** *Non-linear registration of anatomical and functional MR images.* Robotvis, Vista (INRIA), INSERM (U494), CEA-SHFJ (DRM). <http://www-sop.inria.fr/epidaure/Collaborations/IRMf/>. Joint writing of the proposal, general coordinator of the action.
- **ARC MC2 (2000-2001):** *New methods to fuse MRI and MEEG.* Robotvis, Vista (INRIA), CNRS UPR 640, CEA-SHFJ.
- **GRID 5000 (2003-):** *A highly reconfigurable, controllable and monitorable experimental Grid platform.* <http://www-sop.inria.fr/grid5000/>.
- **Specific Action on Non-Rigid Registration (2003-2004):** CNRS, ENS, GET/TNT, LSIIT. <http://www-artemis.int-evry.fr/~rougon/AS-RNR/>

Scientific responsibilities

Participation to PhD committees

- Niels Holm Olsen, IT University of Copenhagen, Denmark, March 2003. Opponent.
- R-C. Stefanescu, 2005, S. Nicolau, 2004, G. Flandin, 2004, S. Granger, 2003, P. Cachier, 2002. Co-supervisor.

Conference Organization:

- General Chair of the First International Workshop on *Mathematical foundations of Computational Anatomy*, associated to MICCAI'06, Copenhagen, October 1st, 2006. http://www-sop.inria.fr/epidaure/Workshops/Workshop_MFCA_MICCAI06.html.
- Session chair at MICCAI'04 and MICCAI'06.

Reviewing work

- **Conference Program Committees:** Distrib. Databases and processing in Medical Image Comp. (DIDAMIC) 2004, Int. W. on Augmented environments for Med. Imag. and Comp.-aided Surgery (AMI-ARCS) 2004, IEEE W. on Math. Methods in Biomed. Image Analysis (MMBIA) 2006, W. on Biomed. Image Registration (WBIR) 2003, 2006, From Statistical Atlases to Personalized Models (SA2PM'06), W. on Image Registration in Deformable Environments (DEFORM'06).
- **Conferences Review Committees:** IJCAI'99, MICCAI (2002 to 2005), ISBI 2002, 2004 and 2006, HealthGrid'03, FIMH 2003, GRETSI'03, EUROGRAPHICS'05, CVPR 2006.

- **Journal Review Committees:** Int. Journal of Computer Vision (IJCV), IEEE Trans. in Medical Imaging (TMI), Medical Image Analysis (MedIA), Journal of Mathematical Imaging and Vision (JMIV), IEEE Trans. on Robotics and Automation, NeuroImage, IEEE Trans. on Image Processing (TIP), Traitement du Signal (TS), Image and Vision Computing (IVC), IEE Proceedings - Vision, Image and Signal Processing, IEEE Trans. Pattern Analysis and Machine Intelligence (PAMI), Computer Vision and Image Understanding (CVIU), Computer Aided Surgery (CAS), Methods of Information in Medicine (MIM).

Expertise

Member of the Jury of the SPECIF PhD award (2006-2009).

Evaluator the French ANR-CIS program (Intensive Computations and Simulations) in 2005, the INRIA post-doctoral fellowships in mai 2003, for the “new interfaces in mathematics ACI” in April 2003, for the Council of Physical Science of the Netherlands Organization for Scientific Research (NWO), 2002.

Participation as expert to the *Imaging, Medical Analysis and Grid Environments* workshop, (National e-Science Center, Edinburgh, sept. 2003), and to the American working group *Issues in Multimodal Medical Image Registration* (Rochester, MI, June 1997 and Greenbelt, MA, Nov. 1997).

Software

- **Pasha:** (25 %) Non-rigid registration of 3D images (C++, 21 000 lines). Transferred to 4 universities and about to be distributed on the web.
- **Baladin:** (5 %) Multimodal registration of images using block-matching (C, 15 000 lines). Transferred to 2 universities and one industrial partner; exploitation licenses.
- **MIPS:** (5 %) Effort to gather and capitalize all the software developments of the Epidaure/Asclepios team on visualization and analysis of medical images. The library comprises le visualization tool Yav++ (C++, OpenGL and Tcl/Tk) and the other softwares of this section.
- **Yasmina:** (5%) Multimodal registration of medical images (C, 15000 lines). Transferred to 3 universities and 3 industrial partners; exploitation licenses; patent.
- **Roboscope MMIT package:** integration and distribution in the consortium of 115000 line of C, 122000 of C++ code and 5000 of Tcl code.
- **PFRegister, PFMatchICP, PFMatchIT, PFMatchGH:** (100 %) softwares for the registration and matching of geometric features (C, 27000 lines); registered at the APP in June 1997; Transferred to 3 universities and one industrial partner; Exploitation license.
- **Prospect:** (100 %) software for detecting common substructures in protein structures (C, 5000 lines); Registered at the APP in December 1997; Transferred to 3 universities.

Patents

1. Vincent Arsigny, Xavier Pennec, Pierre Fillard, and Nicholas Ayache. Dispositif perfectionné de traitement ou de production d'images de tenseurs. French patent filing number 0503483, April 2005.
2. Alexis Roche, Grégoire Malandain, Nicholas Ayache, and Xavier Pennec. Electronic device for automatic registration of images. US patent No US 6,539,127 B1, Mars 25, 2003, March 2003.
3. Alexis Roche, Grégoire Malandain, Nicholas Ayache, and Xavier Pennec. Dispositif électronique de recalage automatique d'images. French patent No FR 98 09649, Bulletin officiel de la propriété intellectuelle no 00/39 du Sept. 09 2000. European extension No 99401881, September 2000.

Prizes and Awards

- Annual Medical Image Analysis best paper award 2006 for *Mosaicing of Confocal Microscopic In Vivo Soft Tissue Video Sequences*, coauthored by T. Vercauteren, A. Perchant, X. Pennec G. Malandain and N. Ayache.
- AMDO best paper award 2006 for *Principal Spine Shape Deformation Modes Using Riemannian Geometry and Articulated Models* by J. Boisvert, X. Pennec, H. Labelle, F. Chériet and N. Ayache.
- Co-author of a paper awarded the Best Student Presentation in Image Processing and Visualization of MICCAI'03 (Polyrigid transformations, MICCAI 2003, LNCS 2879).
- Giovanni DiChiro Award for Outstanding Scientific Research (*Journal of Computer Assisted Tomography*, 21(4):554-566, 1997).
- INRIA Post-doctoral Fellowship, 1998.
- Highest honors (mention très honorable avec les félicitations du jury) for the PhD, Ecole Polytechnique (Palaiseau), 1996.
- DRET/CNRS PhD Fellowship, 1993-1996.
- DEA fellowship from the Ecole Polytechnique, 1992-1993.
- Highest honors (mention très bien) at the Baccalauréat, Limoges, 1987.

Invited plenary talks in conferences

1. 15th ERNSI (European Network on System Identification) Workshop on System Identification. Linköping, Sweden. September 20-21, 2006.
2. Mathematics and Image Analysis (MIA'06), Paris, 18-21 September, 2006.
3. Shape Spaces. IMA, Minneapolis, April 3-7, 2006. <http://www.ima.umn.edu/imaging/spring/W4.3-7.06.html>.
4. Conference-winter school on singularities and applications, CIRM, Luminy, February 7-11, 2005.
5. Workshop on Computational Topology (ECG'02), Sophia-Antipolis, October 21-25, 2002.
6. CARS 2002, "Validation of medical image processing in image-guided therapy session", Paris, June 2002.
7. Journées "Mathématiques et sciences du vivant", Nice-Sophia Antipolis University, March 2002.
8. First Astronomical and Medical Imaging Meeting (AMI'01), Royal Statistical Society, London, UK, April 2001.
9. Journées Statistiques, INRIA Rennes IRISA, November 15-16, 2001.
10. Image Analysis and High Level Vision, IMA workshop, Minneapolis, MN, USA, December 13-17, 2000.

Invited talks at seminars

- John Hopkins University, Baltimore, April 2006. *Statistical Computing on Manifolds: From Riemannian Geometry to Computational Anatomy.*
- Univ. Utah, Salt Lake City, July 2005. *Statistical Computing on Riemannian Manifolds: From Riemannian Geometry to Computational Anatomy.*
- Univ. North-Carolina (UNC) at Chapel Hill, July 2005. *Statistical Computing on Riemannian Manifolds: From Riemannian Geometry to Computational Anatomy.*
- Univ. Southern California (USC) Los-Angeles, July 2004. *From statistical models of curves and surfaces to intrinsic tensor computing.*
- DTU, Copenhagen, Denmark, mars 2003. *Statistics on Riemannian manifolds with application to the evaluation of the rigid registration accuracy.*
- Univ. of Granada, Spain, December 1999. *Probabilities and Statistics on Riemannian Manifolds: Basic Tools for Geometric Measurements.*

- Université Claude Bernard Lyon 1, March 1998. *Un cadre statistique pour le traitement de données géométriques.*
- Artificial Intelligence Lab. Seminar Series, MIT, March 1997. *Uncertainty in registration and recognition problems.*
- Université Claude Bernard Lyon 1, April 1996. *Probabilités et statistiques sur les primitives géométriques.*
- Lab. Biologie Moléculaire des Relations Plantes-Microorganismes (LBMRPM), Toulouse, April 1995. *Reconnaissance et recalage efficace d'objets 3D en biologie moléculaire et en imagerie médicale.*

Tutorials

- *Statistical Computing on Riemannian Manifolds: From Riemannian Geometry to Computational Anatomy.* MICCAI'05, Palm Spring, (CA, USA), October 2005.
- *Grids services for medical image analysis and registration.* MICCAI'04, Saint-Malo, September 2004.
- *Performance evaluation of registration algorithms in the absence of gold standard.* MICCAI'03, Montreal, November 2003.

Teaching

- IT Univ. Copenhagen. *Non-linear shape modeling.* PhD Course, December 5-10, 2005. 30 h. module, with S. Joshi.
- Univ. Nice-Sophia Antipolis (UNSA). *Introduction to medical imaging.* DUT informatique, numerical images option, March 2003 (4h).
- ENSTA. *Introduction to medical image analysis.* 3rd year of engineer school, 1999 (3h).
- IMAC. *Recognition and registration techniques.* 3rd year of engineer school, 1998 (3h).

Supervision of research activities

Former PhD Students

1. **Radu-Constantin Stefanescu:** *Parallel nonlinear registration of medical images with a priori information on anatomy and pathology.* University of Nice-Sophia-Antipolis, March 2005. Co-supervision (90%) with N. Ayache (supervisor).

Email: Radu.Stefanescu@wanadoo.fr

- [R. Stefanescu](#), [X. Pennec](#), and N. Ayache. A grid service for the interactive use of a parallel non-rigid registration algorithm of medical images. *Methods of Information in Medicine*, 44(2), 2005.
- [R. Stefanescu](#), [X. Pennec](#), and N. Ayache. Grid powered nonlinear image registration with locally adaptive regularization. *Medical Image Analysis*, 8(3):325–342, 2004.
- [R. Stefanescu](#), [X. Pennec](#), and N. Ayache. Grid-enabled non-rigid registration of medical images. *Parallel Processing Letters*, 14(2):197–216, 2004.
- [R. Stefanescu](#), O. Commowick, G. Malandain, P.-Y. Bondiau, N. Ayache, and [X. Pennec](#). Non-rigid atlas to subject registration with pathologies for conformal brain radiotherapy. In *Proc. of MICCAI 2004*, volume 3216 of *LNCS*, pages 704–711, Saint-Malo, France, September 2004.
- [R. Stefanescu](#), [X. Pennec](#), and N. Ayache. A grid service for the interactive use of a parallel non-rigid registration algorithm. In *Proc. of HealthGrid 2004*, Clermont-Ferrand, January 2004. European Commission, DG Information Society.
- [R. Stefanescu](#), [X. Pennec](#), and N. Ayache. Parallel non-rigid registration on a cluster of workstations. In Sofie Norager, editor, *Proc. of HealthGrid'03*, Lyon, January 2003. European Commission, DG Information Society.
- [R. Stefanescu](#), [X. Pennec](#), and N. Ayache. Grid enabled non-rigid registration with a dense transformation and a priori information. In *Proc. of MICCAI'03, Part II*, volume 2879 of *LNCS*, pages 804–811, Montreal, November 2003.

2. **Stéphane Nicolau:** *An augmented reality system for hepatic surgery.* University of Nice-Sophia-Antipolis, November 2004. Co-supervision (50%) with L. Soler (IRCAD, Strasbourg) and N. Ayache (supervisor).

Email: stephane.nicolau@ircad.u-strasbg.fr

- S. Nicolau, A. Garcia, X. Pennec, L. Soler, and N. Ayache. An augmented reality system to guide radio-frequency tumor ablation. *Computer Animation and Virtual World (previously the Journal of Visualization & Computer Animation)*, 16(1):1–10, 2005.
 - S. Nicolau, X. Pennec, L. Soler, and N. Ayache. An augmented reality system for liver punctures: Design and evaluation on clinical cases. *Submitted to Medical Image Analysis*, 2006.
 - S. Nicolau, X. Pennec, L. Soler, and N. Ayache. A complete augmented reality guidance system for liver punctures: First clinical evaluation. In *Proc. of MICCAI 2005, Part I*, volume 3749 of *LNCS*, pages 539–547, Palm Springs, CA, USA, October 26-29, 2005. Springer Verlag.
 - S. Nicolau, X. Pennec, L. Soler, and N. Ayache. An augmented reality system to guide liver punctures. In *Proc. of AMI-ARCS 2004 workshop*, pages 77–86. IRISA Rennes, September 2004.
 - S. Nicolau, J. Schmid, X. Pennec, L. Soler, and N. Ayache. An augmented reality & virtuality interface for a puncture guidance system: Design and validation on an abdominal phantom. In *Proc of MIAR 2004*, volume 3150 of *LNCS*, pages 302–310, Beijing, China, August 2004. Springer Verlag.
 - S. Nicolau, X. Pennec, L. Soler, and N. Ayache. An accuracy certified augmented reality system for therapy guidance. In *Proc. of ECCV'04, Part III*, volume 3023 of *LNCS*, pages 79–91, Prague, May 2004.
 - S. Nicolau, X. Pennec, L. Soler, and N. Ayache. Evaluation of a new 3D/2D registration criterion for liver radio-frequencies guided by augmented reality. In *Proc. of IS4TM'03*, volume 2673 of *LNCS*, pages 270–283, Juan-les-Pins, France, 2003.
 - S. Nicolau, A. Garcia, X. Pennec, L. Soler, and N. Ayache. Augmented reality guided radio-frequency tumor ablation. In *Proceedings of Augmented and Virtual Reality Workshop (AVIR03)*, pages 34–35, Genève, 2003.
 - S. Nicolau, X. Pennec, L. Soler, and N. Ayache. Vision augmentée de structures anatomiques abdominales recalées par stéréoscopie. In *Actes du quatrième colloque francophone. Méthodes et Techniques Optiques pour l'Industrie*, volume 1, pages 413–418, Belfort, 2003.
 - S. Nicolau, A. Garcia, X. Pennec, L. Soler, and N. Ayache. Guidage de ponctions percutanées à l'aide d'un système de vision basé sur une méthode de recalage 3D/2D. In *Actes du colloque Imagerie pour les sciences du vivant et de l'ingénieur (IMVIE03)*, Strasbourg, 2003.
3. **Guillaume Flandin:** *Using geometric information for the statistical analysis of fMRI data.* University of Nice-Sophia-Antipolis, March 2004. Co-supervision (50%) with J.-B. Poline (CEA-SHFJ, Orsay) and N. Ayache (supervisor).
Email: guillaume@artefact.tk
- G. Flandin, X. Pennec, A. Roche, W. Penny, N. Ayache, and J.-B. Poline. Multi-subject anatomo-functional classification for activation studies. In *NeuroImage (HBM'04)*, Budapest, Hungary, 2004.

- G. Flandin, W. Penny, X. Pennec, N. Ayache, and J.-B. Poline. A multisubject anatomofunctional parcellation of the brain. In *NeuroImage (HBM'03)*, New York, USA, 2003.
 - G. Flandin, F. Kherif, X. Pennec, G. Malandain, N. Ayache, and J.-B. Poline. Improved detection sensitivity in functional MRI data using a brain parceling technique. In *Proc of MICCAI'02*, volume 2488 of *LNCS*, pages 467–474, Tokyo, Sept. 2002.
 - G. Flandin, F. Kherif, X. Pennec, D. Rivière, N. Ayache, and J.-B. Poline. Parcellation of brain images with anatomical and functional constraints for fMRI data analysis. In *Proc of ISBI'02*, pages 907–910, Washington, USA, 2002.
 - G. Flandin, F. Kherif, X. Pennec, D. Rivière, N. Ayache, and J.-B. Poline. A new representation of fMRI data using anatomofunctional constraints. In *NeuroImage (HBM'02)*, Sendai, Japan, 2002.
4. Sébastien Granger: *Registration and reconstruction of surfaces: a multi-scale statistical approach. Application to computer-assisted dental implantology*. École des Mines de Paris, April 2003, with highest honors. Co-supervision (95%) with N. Ayache (supervisor).
Email: seb.granger@free.fr
- S. Granger and X. Pennec. Multi-scale EM-ICP: A fast and robust approach for surface registration. In *Proc. of ECCV 2002*, volume 2353 of *LNCS*, pages 418–432, Copenhagen, Denmark, 2002.
 - S. Granger, X. Pennec, and A. Roche. Rigid point-surface registration using an EM variant of ICP for computer guided oral implantology. In *Proc of MICCAI'01*, volume 2208 of *LNCS*, pages 752–761, Utrecht, The Netherlands, October 2001.
 - S. Granger and X. Pennec. Statistiques exactes et approchées sur les normales aléatoires. Research report RR-4533, INRIA, 2002.
5. Pascal Cathier (previously Cachier): *Non-rigid registration of tri-dimensional medical images. Contributions to iconic and geometric approaches*. Ecole Centrale Paris, January 2002, with highest honors. Co-supervision (40%) with N. Ayache (supervisor).
Email: cathier@shfj.cea.fr
- X. Pennec, A. Roche, P. Cathier, and N. Ayache. Non-rigid MR/US registration for tracking brain deformations. In R.S. Blum and Zh. Liu, editors, *Multi-Sensor Image Fusion and Its Applications*, volume 26 of *Signal Processing and Communications*, chapter 4, pages 107–143. CRC Press - Taylor and Francis, July 2005.
 - P. Cachier, E. Bardinet, D. Dormont, X. Pennec, and N. Ayache. Iconic feature based nonrigid registration: The pasha algorithm. *Computer Vision and Image Understanding*, 89(2-3):272–298, Feb.-march 2003.
 - X. Pennec, P. Cachier, and N. Ayache. Tracking brain deformations in time-sequences of 3D US images. *Pattern Recognition Letters*, 24(4-5):801–813, February 2003.
 - P. Cachier, J.-F. Mangin, X. Pennec, D. Rivière, D. Papadopoulos-Orfanos, J. Régis, and N. Ayache. Multisubject non-rigid registration of brain MRI using intensity and

- geometric features. In *Proc of MICCAI'01*, volume 2208 of *LNCS*, pages 734–742, Utrecht, The Netherlands, October 2001.
- X. Pennec, N. Ayache, A. Roche, and P. Cachier. Non-rigid MR/US registration for tracking brain deformations. In *Proc of MIAR 2001, 10-12 June 2001, Shatin, Hong Kong*, pages 79–86, June 2001.
 - X. Pennec, P. Cachier, and N. Ayache. Tracking brain deformations in time sequences of 3D US images. In M.I. Insana and R.M. Leahy, editors, *Proc. of IPMI'01*, number 2082 in *LNCS*, pages 169–175, Davis, CA, USA, June 2001.
 - P. Cachier and X. Pennec. 3D non-rigid registration by gradient descent on a Gaussian-windowed similarity measure using convolutions. In *Proc. of MMBIA'00*, pages 182–189, Hilton Head Island, South Carolina, USA, June 2000. IEEE Computer society.
 - X. Pennec, P. Cachier, and N. Ayache. Understanding the “demon’s algorithm”: 3D non-rigid registration by gradient descent. In C. Taylor and A. Colchester, editors, *Proc. of MICCAI'99*, volume 1679 of *LNCS*, pages 597–605, Cambridge, UK, September 1999.

Current PhD Students

1. Vincent Arsigny: *Statistical analysis of shapes, application to anatomical atlases*. École Polytechnique. Co-supervision (60%) with N. Ayache (supervisor).

Email: Vincent.Arsigny@sophia.inria.fr

- V. Arsigny, X. Pennec, P. Fillard, and N. Ayache. Dispositif perfectionné de traitement ou de production d’images de tenseurs. French patent filing number 0503483, April 2005.
- V. Arsigny, P. Fillard, X. Pennec, and N. Ayache. Log-Euclidean metrics for fast and simple calculus on diffusion tensors. *Magnetic Resonance in Medicine*, 56(2):411-421, August 2006.
- V. Arsigny, P. Fillard, X. Pennec, and N. Ayache. Geometric means in a novel vector space structure on symmetric positive-definite matrices. *SIAM Journal on Matrix Analysis and Applications*, 2006. In Press.
- V. Arsigny, X. Pennec, and N. Ayache. Polyrigid and polyaffine transformations: a novel geometrical tool to deal with non-rigid deformations - application to the registration of histological slices. *Medical Image Analysis*, 9(6):507–523, December 2005.
- V. Arsigny, O. Commowick, X. Pennec, and N. Ayache. A log-Euclidean framework for statistics on diffeomorphisms. In *Proc. of MICCAI'06*, *LNCS*, 2-4 October 2006. To appear.
- V. Arsigny, O. Commowick, X. Pennec, and N. Ayache. A log-Euclidean polyaffine framework for locally rigid or affine registration. In *Proc. of WBIR'06*, *LNCS*, Utrecht, The Netherlands, 9 - 11 July 2006. Springer. To appear.
- V. Arsigny, P. Fillard, X. Pennec, and N. Ayache. Fast and simple calculus on tensors in the log-Euclidean framework. In *Proc. of MICCAI 2005, Part I*, volume 3749 of *LNCS*, pages 115–122, Palm Springs, CA, USA, October 26-29, 2005.

- V. Arsigny, X. Pennec, and N. Ayache. Polyrigid and polyaffine transformations: A new class of diffeomorphisms for locally rigid or affine registration. In *Proc. of MICCAI'03, Part II*, volume 2879 of *LNCS*, pages 829–837, Montreal, November 2003. Springer Verlag. MICCAI 2003 Best Student Award in Image Processing and Visualization.
- V. Arsigny, X. Pennec, and N. Ayache. Bi-invariant means in Lie groups. application to left-invariant polyaffine transformations. Research report, INRIA Sophia-Antipolis, April 2006.

- Jonathan Boisvert: *Articulated models for augmented reality - Application to minimally invasive spine surgery*. University of Nice-Sophia-Antipolis and Polytechnique School of Montreal, Canada. Co-supervision (30%) with N. Ayache (supervisor in France) and Farida Cheriet (supervisor in Canada, Montreal's Sainte-Justine Hospital and the Polytechnique School of Montreal).

Email: Jonathan.Boisvert@sophia.inria.fr

- J. Boisvert, F. Cheriet, X. Pennec, H. Labelle and N. Ayache. Geometric Variability of the Scoliotic Spine using Statistics on Articulated Shape Models. *Submitted to IEEE Trans. on Medical Imaging*.
- J. Boisvert, X. Pennec, H. Labelle, F. Cheriet, and N. Ayache. Principal spine shape deformation modes using Riemannian geometry and articulated models. In *Proc of the IV Conference on Articulated Motion and Deformable Objects, Andratx, Mallorca, Spain, 11-14 July*. AMDO best paper award 2006
- J. Boisvert, X. Pennec, N. Ayache, H. Labelle, and F. Cheriet. 3D anatomic variability assessment of the scoliotic spine using statistics on lie groups. In *Proc. of ISBI 2006*, Crystal Gateway Marriott, Arlington, Virginia, USA, 2006.
- J. Boisvert, F. Cheriet, X. Pennec, N. Ayache, and H. Labelle. A novel framework for the 3D analysis of spine deformation modes. In *Research into Spinal Deformities*, volume 123 of *Studies in Health Technology and Informatics*, pages 176–182, 2006.
- J. Boisvert, F. Cheriet, X. Pennec, N. Ayache, and H. Labelle. Assessment of brace local action on vertebrae relative poses". In *Research into Spinal Deformities*, volume 123 of *Studies in Health Technology and Informatics*, pages 372–378, 2006.'

- Pierre Fillard: *Statistical modeling of the anatomical variability of the cortex*. University of Nice-Sophia Antipolis. Co-supervision (60%) with N. Ayache.

Email: Pierre.Fillard@sophia.inria.fr

- X. Pennec, P. Fillard, and N. Ayache. A Riemannian framework for tensor computing. *International Journal of Computer Vision*, 66(1):41–66, January 2006. A preliminary version appeared as INRIA Research Report 5255, July 2004.
- P. Fillard, V. Arsigny, X. Pennec, and N. Ayache. Clinical DT-MRI estimation, smoothing and fiber tracking with log-Euclidean metrics. *Submitted to IEEE Trans. Medical Imaging*, 2006.

- P. Fillard, V. Arsigny, X. Pennec, P. M. Thompson, and N. Ayache. Measuring brain variability by extrapolating sparse tensor fields measured on sulcal lines. *NeuroImage*, 2006. In press.
 - P. Fillard, V. Arsigny, X. Pennec, and N. Ayache. Clinical DT-MRI estimation, smoothing and fiber tracking with log-Euclidean metrics. In *Proc. of ISBI 2006*, pages 786–789, Crystal Gateway Marriott, Arlington, Virginia, USA, April 2006.
 - P. Fillard, V. Arsigny, N. Ayache, and X. Pennec. A Riemannian framework for the processing of tensor-valued images. In *Deep Structure, Singularities, and Computer Vision (DSSCV)*, volume 3753 of LNCS, pages 112–123. Springer Verlag, June 2005.
 - P. Fillard, V. Arsigny, X. Pennec, P. Thompson, and N. Ayache. Extrapolation of sparse tensor fields: Application to the modeling of brain variability. In *Proc. of IPMI'05*, volume 3565 of LNCS, pages 27–38, Glenwood springs, Colorado, USA, July 2005. Springer.
4. Tristan Glatard: *Computing with Massive Medical Image Databases on the GRID for the evaluation of clinical image analysis protocols*. University of Nice-Sophia Antipolis. Co-supervision (40%) with J. Montagnat (50%, Rainbow team, I3S, UNSA), N. Ayache and M. Riveill (Rainbow team, I3S, UNSA).
Email: Tristan.Glatard@sophia.inria.fr
- T. Glatard, J. Montagnat, and X. Pennec. Performance analysis of workflow-based applications on production grids. *Submitted to Journal of Grid Computing*, 2006.
 - T. Glatard, J. Montagnat, D. Lingrand, and X. Pennec. Flexible and efficient workflow deployment of data-intensive applications on grids with MOTEUR. *International Journal of High Performance Computing Applications*, 2006. To appear in the special issue on Workflow Systems in Grid Environments.
 - T. Glatard, X. Pennec, and J. Montagnat. Performance evaluation of grid-enabled registration algorithms using bronze-standards. In *Proc. of MICCAI'06*, LNCS, 2-4 October 2006.
 - T. Glatard, J. Montagnat, and X. Pennec. Efficient services composition for grid-enabled data-intensive applications. In *Proc. of HPDC'06, Paris, France, June 19, 2006*.
 - T. Glatard, J. Montagnat, and X. Pennec. Probabilistic and dynamic optimization of job partitioning on a grid infrastructure. In *Proc. of PDP06*, Montbéliard-Sochaux, February 2006.
 - T. Glatard, J. Montagnat, and X. Pennec. An experimental comparison of grid5000 clusters and the EGEE grid. In *Proc of the EXPGRID'06 workshop, Paris, France, June 19-23, 2006*.
 - T. Glatard, J. Montagnat, and X. Pennec. Medical image registration algorithms assessment: Bronze standard application enactment on grids using the MOTEUR workflow engine. In *Proc. of HealthGrid'06, Valencia, Spain, June 7-9, 2006*.
 - T. Glatard, J. Montagnat, and X. Pennec. Grid-enabled workflows for data intensive applications. In *Proc. of CBMS'05, Dublin, Ireland, June 23-24. IEEE*, 2005.

5. Heike Hufnagel: *Statistical shape analysis of normal and pathological organs within the abdomen*. University of Hamburg. Co-supervision (50%) with Pr.-Dr. H. Handels (univ. Hamburg) and N. Ayache.
Email: Heike.Hufnagel@sophia.inria.fr
 - [H. Hufnagel](#), [X. Pennec](#), G. Malandain, H. Handels, and N. Ayache. Non-linear 2D and 3D registration using block-matching and B-splines. In *Bildverarbeitung fuer die Medizin 2005*, Heidelberg, Germany, March 2005. Deutsches Krebsforschungszentrum.
6. Tom Vercauteren: *Mosaicing and analysis of temporal sequences of in vivo confocal microscopic images*. École des Mines de Paris. Cifre with Mauna-Kea-Technologies. Co-supervision (30%) with N. Ayache.
Email: Tom.Vercauteren@sophia.inria.fr
 - [T. Vercauteren](#), A. Perchant, G. Malandain, [X. Pennec](#), and N. Ayache. Robust mosaicing with correction of motion distortions and tissue deformation for in vivo fibered microscopy. *Medical Image Analysis*, 10(5):673-692, October 2006. Annual Medical Image Analysis (MedIA) Best Paper Award 2006
 - [T. Vercauteren](#), A. Perchant, [X. Pennec](#), and N. Ayache. Mosaicing of confocal microscopic in vivo soft tissue video sequences. In *Proc. of MICCAI 2005, Part I*, volume 3749 of *LNCS*, pages 753–760, Palm Springs, CA, USA, October 26-29, 2005.

DEA and Master Students

1. Antoine Azar: *An Interactive Intensity- and Feature-Based Non-Rigid Registration Framework for 3D Medical Images*. Master IGMMV, University of Nice-Sophia Antipolis, 2005.
2. Pierre Fillard: *A Riemannian Framework for Tensor Imaging*. Master Optique-Image-Vision, Jean Monnet University, Saint-Etienne, 2004.
3. Heike Hufnagel: *Robust deformable registration of medical images using block matching*. Diploma Thesis, University of Luebeck, Germany, 2004.
4. Radu-Constantin Stefanescu: *Parallelization of registration algorithms*. DEA, Ecole Polytechnique, 2001.
5. Niels Raynaud: *A statistical approach for liver segmentation from tri-dimensional images*. DEA Mathématiques, Vision, Apprentissage, ENS Cachan, 2000.
6. Alejandro Ribes: *2D-3D registration for augmented reality*. DEA ARAVIS, University of Nice-Sophia-Antipolis, 1999.
7. Pascal Cachier: *Registration of tri-dimensional ultrasonic images*. DEA Math. and Artificial Intelligence, ENS Cachan, 1998.
8. Frédéric Nahon: *Image registration by maximization of mutual information*. Graduate degree, École Polytechnique, 1996.

Publications

This bibliography is available online at (<http://www-sop.inria.fr/epidaure/BIBLIO/Author/PENNEC-X.html>) with links on most of the publications. The main publications on which this habilitation is based are highlighted and an URL is provided to retrieve the documents.

Books and Proceedings

1. Xavier Pennec and Sarang Joshi, editors. *Proceedings of the First International Workshop on Mathematical Foundations of Computational Anatomy - Geometrical and Statistical Methods for Modeling Biological Shape Variability, October 1st, 2006 Copenhagen, Denmark*, 2006.

Ph.D. Thesis

1. Xavier Pennec. *L'incertitude dans les problèmes de reconnaissance et de recalage – Applications en imagerie médicale et biologie moléculaire*. Thèse de sciences (phd thesis), Ecole Polytechnique, Palaiseau (France), December 1996.

Articles in international peer-reviewed journals

1. Pierre Fillard, Vincent Arsigny, Xavier Pennec, Kiralee M. Hayashi, Paul M. Thompson, and Nicholas Ayache. Measuring brain variability by extrapolating sparse tensor fields measured on sulcal lines. *NeuroImage*, 2006. In press. <ftp://ftp-sop.inria.fr/asclepios/Publications/Pierre.Fillard/Fillard.Neuroimage.2006.pdf>
2. Tristan Glatard, Johan Montagnat, Diane Lingrand, and Xavier Pennec. Flexible and efficient workflow deployment of data-intensive applications on grids with MOTEUR. *International Journal of High Performance Computing Applications*, 2006. To appear in the special issue on Workflow Systems in Grid Environments.
3. Tom Vercauteren, Aymeric Perchant, Grégoire Malandain, Xavier Pennec, and Nicholas Ayache. Robust mosaicing with correction of motion distortions and tissue deformation for in vivo fibered microscopy. *Medical Image Analysis*, 10(5):673–692, October 2006. Medical Image Analysis Best MICCAI Paper Award 2006. <ftp://ftp-sop.inria.fr/epidaure/Publications/Vercauteren/RobustMosaicingMotionDistoTissueDefInVivoFCM-MedIA06-Vercauteren.pdf>

4. Vincent Arsigny, Pierre Fillard, Xavier Pennec, and Nicholas Ayache. **Log-Euclidean metrics for fast and simple calculus on diffusion tensors.** *Magnetic Resonance in Medicine*, 56(2):411–421, August 2006.
ftp://ftp-sop.inria.fr/epidaure/Publications/Arsigny/arsigny_mrm_2006.pdf
5. Vincent Arsigny, Pierre Fillard, Xavier Pennec, and Nicholas Ayache. Geometric means in a novel vector space structure on symmetric positive-definite matrices. *SIAM Journal on Matrix Analysis and Applications*, 2006. In press.
6. Hervé Delingette, Xavier Pennec, Luc Soler, Jacques Marescaux, and Nicholas Ayache. Computational models for image guided, robot-assisted and simulated medical interventions. *Proceedings of the IEEE*, 2006. In press.
7. Xavier Pennec. **Intrinsic statistics on Riemannian manifolds: Basic tools for geometric measurements.** *Journal of Mathematical Imaging and Vision*, 25(1):127–154, July 2006. Preliminary version: INRIA RR-5093, January 2004.
<ftp://ftp-sop.inria.fr/epidaure/Publications/Pennec/Pennec.JMIV06.pdf>
8. Xavier Pennec, Pierre Fillard, and Nicholas Ayache. **A Riemannian framework for tensor computing.** *International Journal of Computer Vision*, 66(1):41–66, January 2006. Preliminary version: INRIA Research Report 5255, July 2004.
<ftp://ftp-sop.inria.fr/epidaure/Publications/Pennec/Pennec.JMIV06.pdf>
9. Vincent Arsigny, Xavier Pennec, and Nicholas Ayache. Polyrigid and polyaffine transformations: a novel geometrical tool to deal with non-rigid deformations - application to the registration of histological slices. *Medical Image Analysis*, 9(6):507–523, December 2005.
10. C. Germain, V. Breton, P. Clarysse, Y. Gaudeau, T. Glatard, E. Jeannot, Y. Legré, C. Loomis, I. Magnin, J. Montagnat, J.-M. Moureau, A. Osorio, X. Pennec, and R. Texier. Grid-enabling medical image analysis. *Journal of Clinical Monitoring and Computing*, 19(4-5):339–349, October 2005.
11. Stéphane Nicolau, Alain Garcia, Xavier Pennec, Luc Soler, and Nicholas Ayache. An augmented reality system to guide radio-frequency tumour ablation. *Computer Animation and Virtual World (previously the Journal of Visualization & Computer Animation)*, 16(1):1–10, 2005.
12. Radu Stefanescu, Xavier Pennec, and Nicholas Ayache. **A grid service for the interactive use of a parallel non-rigid registration algorithm of medical images.** *Methods of Information in Medicine*, 44(2), 2005.
<ftp://ftp-sop.inria.fr/epidaure/Publications/Pennec/Pennec.HMIP.pdf>
13. Miguel Angel González Ballester, Xavier Pennec, Marius George Linguraru, and Nicholas Ayache. Generalized image models and their application as statistical models of images. *Medical Image Analysis*, 8(3):361–369, September 2004.

14. Radu Stefanescu, Xavier Pennec, and Nicholas Ayache. Grid powered nonlinear image registration with locally adaptive regularization. *Medical Image Analysis*, 8(3):325–342, September 2004. MICCAI 2003 Special Issue.
15. Radu Stefanescu, Xavier Pennec, and Nicholas Ayache. Grid-enabled non-rigid registration of medical images. *Parallel Processing Letters*, 14(2):197–216, 2004.
16. Pascal Cachier, Eric Bardinet, Didier Dormont, Xavier Pennec, and Nicholas Ayache. Iconic feature based nonrigid registration: The pasha algorithm. *Comp. Vision and Image Understanding*, 89(2-3):272–298, Feb.-march 2003. Special Issue on Nonrigid Registration.
17. Xavier Pennec, Pascal Cachier, and Nicholas Ayache. Tracking brain deformations in time-sequences of 3D US images. *Pattern Recognition Letters*, 24(4-5):801–813, February 2003. Special Issue on Ultrasonic Image Processing and Analysis.
18. Maxime Sermesant, Clément Forest, Xavier Pennec, Hervé Delingette, and Nicholas Ayache. Deformable biomechanical models: Application to 4D cardiac image analysis. *Medical Image Analysis*, 7(4):475–488, December 2003.
19. Sébastien Ourselin, Alexis Roche, Gérard Subsol, Xavier Pennec, and Nicholas Ayache. Reconstructing a 3D structure from serial histological sections. *Image and Vision Computing*, 19(1-2):25–31, January 2001.
20. Alexis Roche, Xavier Pennec, Grégoire Malandain, and Nicholas Ayache. Rigid registration of 3D ultrasound with MR images: a new approach combining intensity and gradient information. *IEEE Transactions on Medical Imaging*, 20(10):1038–1049, October 2001.
21. Xavier Pennec. Toward a generic framework for recognition based on uncertain geometric features. *Videre: Journal of Computer Vision Research*, 1(2):58–87, 1998.
22. Xavier Pennec and Nicholas Ayache. Uniform distribution, distance and expectation problems for geometric features processing. *Journal of Mathematical Imaging and Vision*, 9(1):49–67, July 1998. A preliminary version appeared as INRIA Research Report 2820, March 1996.
23. Xavier Pennec and Nicholas Ayache. A geometric algorithm to find small but highly similar 3D substructures in proteins. *Bioinformatics*, 14(6):516–522, 1998.
24. André Guézic, Xavier Pennec, and Nicholas Ayache. Medical image registration using geometric hashing. *IEEE Computational Science & Engineering, special issue on Geometric Hashing*, 4(4):29–41, 1997. Oct-Dec.
25. Xavier Pennec and Jean-Philippe Thirion. A framework for uncertainty and validation of 3D registration methods based on points and frames. *Int. Journal of Computer Vision*, 25(3):203–229, December 1997.
26. J. West, J. M. Fitzpatrick, M. Y. Wang, B. M. Dawant, C. R. Maurer, Jr., R. M. Kessler, R. J. Maciunas, C. Barillot, D. Lemoine, A. Collignon, F. Maes, P. Suetens, D. Vandermeulen, P. A. van den Elsen, S. Napel, T. S. Sumanaweera, B. Harkness, P. F. Hemler, D. L. G. Hill,

D. J. Hawkes, C. Studholme, J. B. A. Maintz, M. A. Viergever, G. Malandain, X. Pennec, M. E. Noz, G. Q. Maguire, Jr., M. Pollack, C. A. Pelizzari, R. A. Robb, D. Hanson, and R. P. Woods. Comparison and evaluation of retrospective intermodality brain image registration techniques. *Journal of Computer Assisted Tomography*, 21(4):554–566, 1997.

Submitted Journal Papers

1. Jonathan Boisvert, Farida Cheriet, Xavier Pennec, Hubert Labelle, and Nicholas Ayache. Geometric variability of the scoliotic spine using statistics on articulated shape models. *Submitted to IEEE Trans. Medical Imaging*, 2006.
2. Pierre Fillard, Vincent Arsigny, Xavier Pennec, and Nicholas Ayache. Clinical DT-MRI estimation, smoothing and fiber tracking with log-Euclidean metrics. *Submitted to IEEE Trans. Medical Imaging*, 2006.
3. Tristan Glatard, Johan Montagnat, and Xavier Pennec. Performance analysis of workflow-based applications on production grids. *Submitted to Journal of Grid Computing*, 2006.
4. Soler Nicolau, Xavier Pennec, Luc Soler, and Nicholas Ayache. An augmented reality system for liver punctures: Design and evaluation on clinical cases. *Submitted to Medical Image Analysis*, 2006.

Book chapters, editorials and general purpose magazine articles

1. Xavier Pennec. Recaler pour mieux soigner. *Pour la science*, (338):126–131, December 2005.
2. **Xavier Pennec, Alexis Roche, Pascal Cathier, and Nicholas Ayache. Non-rigid MR/US registration for tracking brain deformations. In R.S. Blum and Zh. Liu, editors, *Multi-Sensor Image Fusion and Its Applications*, volume 26 of *Signal Processing and Communications*, chapter 4, pages 107–143. CRC Press - Taylor and Francis, July 2005.**
ftp://ftp-sop.inria.fr/epidaure/Publications/Pennec/Pennec.MRUS_Fusion.pdf
3. Ignacio Blanquer, Vincent Hernandez, Guy Lonsdale, Kevin Dean, Sharon Lloyd, Richard McClatchey, Johan Montagnat, Mike Brady, Xavier Pennec, Howard Bolofsky, Chris Jones, Martin Hofmann, Tony Solmonides, Ilidio C. Oliveira, Juan Pedro Sanchez, Victoria Lopez, George De Moor, Brecht Claerhout, and Jean A.M. Harveg. Healthgrid white paper: <http://whitepaper.healthgrid.org/>. Edited by Cisco System, September 2004.
4. Luc Soler, Nicholas Ayache, Stéphane Nicolau, Xavier Pennec, Clément Forest, Hervé Delingette, Didier Mutter, and Jacques Marescaux. Traitements d'images médicales pour la planification, la simulation et l'aide intra-opératoire des actes chirurgicaux. In M. Faupel, P. Smigielski, and R. Grzymala, editors, *Imagerie et Photonique pour les sciences du vivant et la médecine*, pages 19–31. Edition Fontis Media, 2004. ISBN 2-88476-005-9.

5. Luc Soler, Nicholas Ayache, Stéphane Nicolau, Xavier Pennec, Clément Forest, Hervé Delingette, and Jacques Marescaux. Traitement d'images médicales pour la planification, la simulation et l'aide intra-opératoire des actes chirurgicaux. *La Revue de l'Electricité et de l'Electronique*, pages 64–71, janvier 2004.
6. P. Jannin, J.M. Fitzpatrick, D.J. Hawkes, X. Pennec, R. Shahidi, and M.W. Vannier. Validation of medical image processing in image-guided therapy. *IEEE Trans. on Medical Imaging*, 21(12):1445–1449, December 2002.
7. **Xavier Pennec, Nicholas Ayache, and Jean-Philippe Thirion. Landmark-based registration using features identified through differential geometry. In I. Bankman, editor, *Handbook of Medical Imaging*, chapter 31, pages 499–513. Academic Press, September 2000.**
<ftp://ftp-sop.inria.fr/epidaure/Publications/Pennec/Pennec.HMIP.pdf>

Full-length articles in selective international peer-reviewed conferences

1. Vincent Arsigny, Olivier Commowick, Xavier Pennec, and Nicholas Ayache. A Log-Euclidean framework for statistics on diffeomorphisms. In *Proc. of the 9th International Conference on Medical Image Computing and Computer Assisted Intervention (MICCAI'06), Part I*, number 4190 in LNCS, pages 924–931, 2-4 October 2006.
ftp://ftp-sop.inria.fr/epidaure/Publications/Arsigny/arsigny_miccai06.pdf
2. Vincent Arsigny, Olivier Commowick, Xavier Pennec, and Nicholas Ayache. A Log-Euclidean polyaffine framework for locally rigid or affine registration. In J.P.W. Pluim, B. Likar, and F.A. Gerritsen, editors, *Proceedings of the Third International Workshop on Biomedical Image Registration (WBIR'06)*, volume 4057 of LNCS, pages 120–127, Utrecht, The Netherlands, 9 - 11 July 2006. Springer Verlag.
3. Antoine Azar, Chenyang Xu, Xavier Pennec, and Nicholas Ayache. An interactive intensity- and feature-based non-rigid registration framework for 3D medical images. In *Proceedings of the Third IEEE International Symposium on Biomedical Imaging (ISBI 2006)*, pages 824–827, Crystal Gateway Marriott, Arlington, Virginia, USA, April 2006.
4. Jonathan Boisvert, Xavier Pennec, Hubert Labelle, Farida Cheriet, and Nicholas Ayache. Principal spine shape deformation modes using Riemannian geometry and articulated models. In *Proc of the IV Conference on Articulated Motion and Deformable Objects, Andratx, Mallorca, Spain, 11-14 July*, LNCS. Springer, 2006. AMDO best paper award 2006. ftp://ftp-sop.inria.fr/epidaure/Publications/Pennec/Boisvert.AMDO06_SpinePCA.pdf

5. Jonathan Boisvert, Xavier Pennec, Nicholas Ayache, Hubert Labelle, and Farida Cheriet. 3D anatomic variability assessment of the scoliotic spine using statistics on Lie groups. In *Proceedings of the Third IEEE International Symposium on Biomedical Imaging (ISBI 2006)*, pages 750–753, Crystal Gateway Marriott, Arlington, Virginia, USA, April 2006. IEEE.
6. Pierre Fillard, Vincent Arsigny, Xavier Pennec, and Nicholas Ayache. **Clinical DT-MRI estimation, smoothing and fiber tracking with log-Euclidean metrics.** In *Proceedings of the Third IEEE International Symposium on Biomedical Imaging (ISBI 2006)*, pages 786–789, Crystal Gateway Marriott, Arlington, Virginia, USA, April 2006.
<ftp://ftp-sop.inria.fr/epidaure/Publications/Fillard/Fillard.ISBI.06.pdf>
7. Tristan Glatard, Xavier Pennec, and Johan Montagnat. **Performance evaluation of grid-enabled registration algorithms using bronze-standards.** In *Proc. of the 9th International Conference on Medical Image Computing and Computer Assisted Intervention (MICCAI'06), Part II*, number 4191 in LNCS, pages 152–160. Springer, 2-4 October 2006.
<ftp://ftp-sop.inria.fr/epidaure/Publications/Pennec/Glatard.MICCAI06.pdf>
8. Tristan Glatard, Johan Montagnat, and Xavier Pennec. Efficient services composition for grid-enabled data-intensive applications. In *Proceedings of the IEEE International Symposium on High Performance Distributed Computing (HPDC'06), Paris, France, June 19, 2006*.
9. Tristan Glatard, Johan Montagnat, and Xavier Pennec. Probabilistic and dynamic optimization of job partitioning on a grid infrastructure. In *14th Euromicro conference on Parallel, Distributed and network-based Processing (PDP06)*, pages 231–238, Montbéliard-Sochaux, February 2006. IEEE.
10. Jean-Marc Peyrat, Maxime Sermesant, Hervé Delingette, Xavier Pennec, Chenyang Xu, Elliot McVeigh, and Nicholas Ayache. Towards a statistical atlas of cardiac fiber structure. In *Proc. of the 9th International Conference on Medical Image Computing and Computer Assisted Intervention (MICCAI'06), Part I*, number 4190 in LNCS, pages 297–304, 2-4 October 2006.
11. Vincent Arsigny, Pierre Fillard, Xavier Pennec, and Nicholas Ayache. Fast and simple calculus on tensors in the log-Euclidean framework. In J. Duncan and G. Gerig, editors, *Proceedings of the 8th Int. Conf. on Medical Image Computing and Computer-Assisted Intervention - MICCAI 2005, Part I*, volume 3749 of LNCS, pages 115–122, Palm Springs, CA, USA, October 26-29, 2005. Springer Verlag.
12. Olivier Commowick, Radu Stefanescu, Pierre Fillard, Vincent Arsigny, Nicholas Ayache, Xavier Pennec, and Grégoire Malandain. Incorporating statistical measures of anatomical variability in atlas-to-subject registration for conformal brain radiotherapy. In J. Duncan and G. Gerig, editors, *Proceedings of the 8th Int. Conf. on Medical Image Computing and Computer-Assisted Intervention - MICCAI 2005, Part II*, volume 3750 of LNCS, pages 927–934, Palm Springs, CA, USA, October 26-29, 2005. Springer Verlag.

13. Pierre Fillard, Vincent Arsigny, Nicholas Ayache, and Xavier Pennec. A Riemannian framework for the processing of tensor-valued images. In Ole Fogh Olsen, Luc Florak, and Arjan Kuijper, editors, *Deep Structure, Singularities, and Computer Vision (DSSCV)*, number 3753 in LNCS, pages 112–123. Springer Verlag, June 2005.
14. Pierre Fillard, Vincent Arsigny, Xavier Pennec, Paul M. Thompson, and Nicholas Ayache. Extrapolation of sparse tensor fields: Application to the modeling of brain variability. In Gary Christensen and Milan Sonka, editors, *Proc. of Information Processing in Medical Imaging 2005 (IPMI'05)*, volume 3565 of LNCS, pages 27–38, Glenwood springs, Colorado, USA, July 2005. Springer.
15. Cécile Germain, Vincent Breton, Patrick Clarysse, Y. Gaudeau, Tristan Glatard, Emmanuel Jeannot, Yannick Legré, Charles Loomis, Johan Montagnat, Jean-Marie Moureaux, Angel Osorio, Xavier Pennec, and Romain Texier. Grid-enabling medical image analysis. In *proceedings of the IEEE/ACM International Symposium on Cluster Computing and the Grid (Biogrid'05)*, pages 487–495, Cardiff, UK, May 2005. IEEE.
16. Tristan Glatard, Johan Montagnat, and Xavier Pennec. Grid-enabled workflows for data intensive applications. In *Proc. 18th IEEE Symp. on Computer Based Medical Systems (CBMS'05), Dublin, Ireland, June 23-24*, pages 537–542. IEEE, 2005.
17. **Stéphane Nicolau, Xavier Pennec, Luc Soler, and Nicholas Ayache. A complete augmented reality guidance system for liver punctures: First clinical evaluation.** In J. Duncan and G. Gerig, editors, *Proceedings of the 8th Int. Conf. on Medical Image Computing and Computer-Assisted Intervention - MICCAI 2005, Part I*, volume 3749 of LNCS, pages 539–547, Palm Springs, CA, USA, October 26-29, 2005. Springer Verlag.
`ftp://ftp-sop.inria.fr/epidaure/Publications/Pennec/Nicolau.MICCAI05.pdf`
18. Xavier Pennec, Radu Stefanescu, Vincent Arsigny, Pierre Fillard, and Nicholas Ayache. Riemannian elasticity: A statistical regularization framework for non-linear registration. In J. Duncan and G. Gerig, editors, *Proceedings of the 8th Int. Conf. on Medical Image Computing and Computer-Assisted Intervention - MICCAI 2005, Part II*, volume 3750 of LNCS, pages 943–950, Palm Springs, CA, USA, October 26-29, 2005. Springer Verlag.
19. Tom Vercauteren, Aymeric Perchant, Xavier Pennec, and Nicholas Ayache. Mosaicing of confocal microscopic in vivo soft tissue video sequences. In J. Duncan and G. Gerig, editors, *Proceedings of the 8th Int. Conf. on Medical Image Computing and Computer-Assisted Intervention - MICCAI 2005, Part I*, volume 3749 of LNCS, pages 753–760, Palm Springs, CA, USA, October 26-29, 2005. Springer Verlag.
20. Stéphane Nicolau, Xavier Pennec, Luc Soler, and Nicholas Ayache. An accuracy certified augmented reality system for therapy guidance. In *Proc. of the 8th European Conference on Computer Vision (ECCV 04), Part III*, volume LNCS 3023, pages 79–91, Prague, May 2004.
21. Stéphane Nicolau, Jérôme Schmid, Xavier Pennec, Luc Soler, and Nicholas Ayache. An augmented reality & virtuality interface for a puncture guidance system: Design and validation

- on an abdominal phantom. In Guang-Zhong Yang and Tianzi Jiang, editors, *Proc of the Second Int. Workshop on Medical Imaging and Augmented Reality MIAR 2004*, volume 3150 of *LNCS*, pages 302–310, Beijing, China, August 2004. Springer Verlag.
22. Luc Soler, Nicholas Ayache, Stéphane Nicolau, Xavier Pennec, Clément Forest, Hervé Delingette, Didier Mutter, and Jacques Marescaux. Virtual reality, augmented reality and robotics in surgical procedures of the liver. In Th. M. Buzug and T. C. Lueth, editors, *Perspectives in Image-guided Surgery. Proceedings of the Scientific Workshop on Medical Robotics, Navigation and Visualization (MRNV) 2004*, pages 476–484, RheinAhrCampus Remagen, Germany, March 11-12 2004. World Scientific.
 23. Luc Soler, Stéphane Nicolau, Jérôme Schmid, Christophe Koehl, Jacques Marescaux, Xavier Pennec, and Nicholas Ayache. Virtual reality and augmented reality in digestive surgery. In *Proc. of IEEE International Symposium on Mixed and Augmented Reality (ISMAR'04)*, pages 278–279, November 2004.
 24. Radu Stefanescu, Olivier Commowick, Grégoire Malandain, Pierre-Yves Bondiau, Nicholas Ayache, and Xavier Pennec. Non-rigid atlas to subject registration with pathologies for conformal brain radiotherapy. In C. Barillot, D.R. Haynor, and P. Hellier, editors, *Proc. of the 7th Int. Conf on Medical Image Computing and Computer-Assisted Intervention - MICCAI 2004*, volume 3216 of *LNCS*, pages 704–711, Saint-Malo, France, September 2004. Springer Verlag.
 25. Vincent Arsigny, Xavier Pennec, and Nicholas Ayache. Polyrigid and polyaffine transformations: A new class of diffeomorphisms for locally rigid or affine registration. In Randy E. Ellis and Terry M. Peters, editors, *Proc. of MICCAI'03, Part II*, volume 2879 of *LNCS*, pages 829–837, Montreal, November 2003. Springer Verlag. MICCAI 2003 Best Student Award in Image Processing and Visualization.
 26. Miguel Angel González Ballester, Xavier Pennec, and Nicholas Ayache. Generalized image models and their application as statistical models of images. In Randy E. Ellis and Terry M. Peters, editors, *Proc. of MICCAI'03*, volume 2879 of *Lecture Notes in Computer Science*, pages 150–157, Montreal, Canada, November 2003. Springer.
 27. Stéphane Nicolau, Xavier Pennec, Luc Soler, and Nicholas Ayache. Evaluation of a new 3D/2D registration criterion for liver radio-frequencies guided by augmented reality. In N. Ayache and H. Delingette, editors, *International Symposium on Surgery Simulation and Soft Tissue Modeling (IS4TM'03)*, volume 2673 of *Lecture Notes in Computer Science*, pages 270–283, Juan-les-Pins, France, 2003. INRIA Sophia Antipolis, Springer-Verlag.
 28. Radu Stefanescu, Xavier Pennec, and Nicholas Ayache. Grid enabled non-rigid registration with a dense transformation and a priori information. In Randy E. Ellis and Terry M. Peters, editors, *Proc. of MICCAI'03, Part II*, volume 2879 of *LNCS*, pages 804–811, Montreal, November 2003. Springer Verlag.
 29. Guillaume Flandin, Ferath Kherif, Xavier Pennec, Grégoire Malandain, Nicholas Ayache, and Jean-Baptiste Poline. Improved detection sensitivity in functional MRI data using a brain

- parcelling technique. In Takeyoshi Dohi and Ron Kikinis, editors, *Medical Image Computing and Computer-Assisted Intervention (MICCAI'02)*, volume 2488 of *LNCS*, pages 467–474, Tokyo, September 2002. Springer.
30. Guillaume Flandin, Ferath Kherif, Xavier Pennec, Denis Rivière, Nicholas Ayache, and Jean-Baptiste Poline. Parcellation of brain images with anatomical and functional constraints for fMRI data analysis. In *IEEE International Symposium on Biomedical Imaging*, pages 907–910, Washington, USA, 2002.
 31. **Sébastien Granger and Xavier Pennec. Multi-scale EM-ICP: A fast and robust approach for surface registration. In A. Heyden, G. Sparr, M. Nielsen, and P. Johansen, editors, *European Conference on Computer Vision (ECCV 2002)*, volume 2353 of *LNCS*, pages 418–432, Copenhagen, Denmark, 2002. Springer. <ftp://ftp-sop.inria.fr/epidaure/Publications/Granger/eccv-2002.pdf>**
 32. Sébastien Ourselin, Radu Stefanescu, and Xavier Pennec. Robust registration of multi-modal images: towards real-time clinical applications. In Takeyoshi Dohi and Ron Kikinis, editors, *Medical Image Computing and Computer-Assisted Intervention (MICCAI'02)*, volume 2489 of *LNCS*, pages 140–147, Tokyo, September 2002. Springer. A preliminary version appeared as INRIA RR-4333.
 33. Maxime Sermesant, Clément Forest, Xavier Pennec, Hervé Delingette, and Nicholas Ayache. Biomechanical model construction from different modalities: Application to cardiac images. In Takeyoshi Dohi and Ron Kikinis, editors, *Medical Image Computing and Computer-Assisted Intervention (MICCAI'02)*, volume 2488 of *LNCS*, pages 714–721, Tokyo, September 2002. Springer.
 34. Pascal Cachier, Jean-François Mangin, Xavier Pennec, Denis Rivière, Dimitri Papadopoulos-Orfanos, Jean Régis, and Nicholas Ayache. Multisubject non-rigid registration of brain MRI using intensity and geometric features. In W.J. Niessen and M.A. Viergever, editors, *4th Int. Conf. on Medical Image Computing and Computer-Assisted Intervention (MICCAI'01)*, volume 2208 of *LNCS*, pages 734–742, Utrecht, The Netherlands, October 2001.
 35. Sébastien Granger, Xavier Pennec, and Alexis Roche. Rigid point-surface registration using an EM variant of ICP for computer guided oral implantology. In W.J. Niessen and M.A. Viergever, editors, *4th Int. Conf. on Medical Image Computing and Computer-Assisted Intervention (MICCAI'01)*, volume 2208 of *LNCS*, pages 752–761, Utrecht, The Netherlands, October 2001.
 36. Xavier Pennec, Nicholas Ayache, Alexis Roche, and Pascal Cachier. Non-rigid MR/US registration for tracking brain deformations. In IEEE Computer Society Press, editor, *Proc of Int. Workshop on Medical Imaging and Augmented Reality (MIAR 2001), 10-12 June 2001, Shatin, Hong Kong*, pages 79–86, June 2001.
 37. Xavier Pennec, Pascal Cachier, and Nicholas Ayache. Tracking brain deformations in time sequences of 3D US images. In M.I. Insana and R.M. Leahy, editors, *Proc. of IPMI'01*, number 2082 in *LNCS*, pages 169–175, Davis, CA, USA, June 2001. Springer Verlag.

38. A. Roche, X. Pennec, M. Rudolph, D. P. Auer, G. Malandain, S. Ourselin, L. M. Auer, and N. Ayache. Generalized correlation ratio for rigid registration of 3D ultrasound with MR images. In A.M. DiGioia and S. Delp, editors, *Proc. of the 3rd Int. Conf. on Medical Image Computing and Computer-Assisted Intervention (MICCAI'00)*, volume 1935 of *LNCS*, pages 567–577, Pittsburgh, Pennsylvania, USA, October 11-14 2000. Published in *IEEE TMI* 20(10), oct. 2001, p. 25-31.
39. Pascal Cachier and Xavier Pennec. 3D non-rigid registration by gradient descent on a Gaussian-windowed similarity measure using convolutions. In *Proc. of IEEE Workshop on Mathematical Methods in Biomedical Image Analysis (MMBIA'00)*, pages 182–189, Hilton Head Island, South Carolina, USA, June 2000. IEEE Computer society.
40. Xavier Pennec, Pascal Cachier, and Nicholas Ayache. Understanding the “demon’s algorithm”: 3D non-rigid registration by gradient descent. In C. Taylor and A. Colchester, editors, *Proc. of 2nd Int. Conf. on Medical Image Computing and Computer-Assisted Intervention (MICCAI'99)*, volume 1679 of *LNCS*, pages 597–605, Cambridge, UK, September 1999. Springer Verlag.
41. Xavier Pennec. Probabilities and statistics on Riemannian manifolds: Basic tools for geometric measurements. In A.E. Cetin, L. Akarun, A. Ertuzun, M.N. Gurcan, and Y. Yardimci, editors, *Proc. of Nonlinear Signal and Image Processing (NSIP'99)*, volume 1, pages 194–198, June 20-23, Antalya, Turkey, 1999. IEEE-EURASIP.
42. Xavier Pennec, Charles R.G. Guttmann, and Jean-Philippe Thirion. Feature-based registration of medical images: Estimation and validation of the pose accuracy. In *Proc. of First Int. Conf. on Medical Image Computing and Computer-Assisted Intervention (MICCAI'98)*, volume 1496 of *LNCS*, pages 1107–1114, Cambridge, USA, October 1998. Springer Verlag.
43. Alexis Roche, Grégoire Malandain, Xavier Pennec, and Nicholas Ayache. The correlation ratio as a new similarity measure for multimodal image registration. In *Proc. of First Int. Conf. on Medical Image Computing and Computer-Assisted Intervention (MICCAI'98)*, volume 1496 of *LNCS*, pages 1115–1124, Cambridge, USA, October 1998. Springer Verlag.
44. Xavier Pennec and Nicholas Ayache. Randomness and geometric features in computer vision. In *IEEE Conf. on Computer Vision and Pattern Recognition (CVPR'96)*, pages 484–491, San Francisco, Cal, USA, June 1996. Published in *J. of Math. Imag. and Vision* 9(1), July 1998, p. 49-67.
45. Xavier Pennec and Jean-Philippe Thirion. Validation of 3D registration methods based on points and frames. In *Proc. of the 5th Int. Conf on Comp. Vision (ICCV'95)*, pages 557–562, Cambridge, Ma, June 1995. Published in *Int. J. of Comp. Vision* 25(3), 1997, p. 203-229.

Articles in international conferences and workshops

1. Jonathan Boisvert, Farida Cheriet, Xavier Pennec, Nicholas Ayache, and Hubert Labelle. A novel framework for the 3D analysis of spine deformation modes. In *Research into Spinal*

- Deformities*, volume 123 of *Studies in Health Technology and Informatics*, pages 176–182, 2006.
2. Jonathan Boisvert, Farida Cheriet, Xavier Pennec, Nicholas Ayache, and Hubert Labelle. Assessment of brace local action on vertebrae relative poses. In *Research into Spinal Deformities*, volume 123 of *Studies in Health Technology and Informatics*, pages 372–378, 2006.
 3. J. Freund, D. Comaniciu, Y. Ioannis, P. Liu, R. McClatchey, E. Moley-Fletcher, X. Pennec, G. Pongiglione, and X.S. Zhou. Health-e-child: An integrated biomedical platform for grid-based pediatrics. In *Proc of Health-Grid 2006*, Valancia, Spain, 2006.
 4. Tristan Glatard, Johan Montagnat, and Xavier Pennec. An experimental comparison of Grid5000 clusters and the EGEE grid. In *Proc of the Workshop on Experimental Grid testbeds for the assessment of large-scale distributed applications and tools (EXPGRID'06)*, Paris, France, 19-23 June, 2006.
 5. Tristan Glatard, Johan Montagnat, and Xavier Pennec. Medical image registration algorithms assessment: Bronze standard application enactment on grids using the MOTEUR workflow engine. In *Proc. of the HealthGrid conference (HealthGrid'06)*, Valencia, Spain, 7-9 June, 2006.
 6. **Xavier Pennec. Left-invariant Riemannian elasticity: a distance on shape diffeomorphisms?** In X. Pennec and S. Joshi, editors, *Proc. of the International Workshop on the Mathematical Foundations of Computational Anatomy (MFCA-2006)*, pages 1–13, 2006.
<ftp://ftp-sop.inria.fr/epidaure/Publications/Pennec/Pennec.MFCA06.pdf>
 7. Guillaume Flandin, Xavier Pennec, Alexis Roche, Will Penny, Nicholas Ayache, and Jean-Baptiste Poline. Multi-subject anatomo-functional classification for activation studies. In *NeuroImage (HBM'04)*, Budapest, Hungary, 2004.
 8. Derek Hill, Xavier Pennec, Michael Burns, Michael Parkin, Jo Hajnal, Radu Stefanescu, Daniel Rueckert, and Johan Montagnat. Intraoperable medical image registration grid service. In *Proc. of HealthGrid 2004*, Clermont-Ferrand, January 2004. European Commission, DG Information Society.
 9. Stéphane Nicolau, Xavier Pennec, Luc Soler, and Nicholas Ayache. An augmented reality system to guide liver punctures. In *Workshop AMI-ARCS 2004 held in conjunction with MICCAI'04*, pages 77–86. IRISA Rennes, September 2004.
 10. Radu Stefanescu, Xavier Pennec, and Nicholas Ayache. A grid service for the interactive use of a parallel non-rigid registration algorithm. In *Proc. of HealthGrid 2004*, Clermont-Ferrand, January 2004. European Commission, DG Information Society.
 11. Radu Stefanescu, Xavier Pennec, and Nicholas Ayache. Parallel non-rigid registration on a cluster of workstations. In Sofie Norager, editor, *Proc. of HealthGrid'03*, Lyon, January 2003. European Commission, DG Information Society.

12. Guillaume Flandin, Will Penny, Xavier Pennec, Nicholas Ayache, and Jean-Baptiste Poline. A multisubject anatomo-functional parcellation of the brain. In Tomas Paus, Ed Bullmore, and Jonathan D. Cohen, editors, *NeuroImage (HBM'03)*, New York, USA, 2003. Academic Press.
13. Stéphane Nicolau, Alain Garcia, Xavier Pennec, Luc Soler, and Nicholas Ayache. Augmented reality guided radio-frequency tumor ablation. In *Proceedings of Augmented and Virtual Reality Workshop (AVIRO3)*, pages 34–35, Genève, 2003.
14. Guillaume Flandin, Ferath Kherif, Xavier Pennec, Denis Rivière, Nicholas Ayache, and Jean-Baptiste Poline. A new representation of fMRI data using anatomo-functional constraints. In *NeuroImage (HBM'02)*, Sendai, Japan, 2002.
15. P. Jannin, J.M. Fitzpatrick, D.J. Hawkes, X. Pennec, R. Sahidi, and M.W. Vannier. White paper: validation of medical image processing in image-guided therapy. In H.U. Lemke, M.W. Vannier, K. Inamura, A.G. Farman, K. Doi, and J.H.C. Reiber, editors, *Proc. of Int. Conf. on Computer Assisted Radiology (CARS 2002)*, pages 299–305. Springer, 2002.
16. Nicholas Ayache, Xavier Pennec, and Pascal Cachier. Fusing 3-D ultrasound and MRI for real-time image-guided neurosurgery. In *Medical Physics and Clinical Engineering Conference*, 2001. Invited talk, *Physica Medica (European journal of Medical Physics)* 17(3).
17. Xavier Pennec. Evaluation of the uncertainty in various registration problems. In K.W. Bowyer, M.H. Loew, H. S. Stiehl, and M. Viergever, editors, *Methodology of Evaluation in Computational Medical Imaging*, pages 15–16, Dagstuhl, March 2001. Schloss Dagstuhl, Int. Conf. and Research Center for Computer Science. Dagstuhl Seminar 01111.
18. D. Etienne, A. Stankoff, X. Pennec, S. Granger, A. Lacan, and R. Derycke. A new approach for dental implant aided surgery. A pilot evaluation. In H.U. Lemke, M.W. Vannier, K. Inamura, A.G. Farman, and K. Doi, editors, *Proc. of CARS'2000*, pages 927–931. Elsevier, 2000.
19. D. Etienne, A. Stankoff, X. Pennec, S. Granger, A. Lacan, and R. Derycke. A new approach for dental implant aided surgery. 4th Congresso Panamericano de Periodontologia, 17-19 august 2000, Santiago, Chili, 2000.
20. Sébastien Ourselin, Alexis Roche, Gérard Subsol, and Xavier Pennec. Automatic alignment of histological sections. In F. Pernus, S. Kovacic, H.S. Stiehl, and M.A. Viergever, editors, *International Workshop on Biomedical Image Registration, WBIR'99*, pages 1–13, Bled (Slovénie), August 1999.
21. J. West, J.M. Fitzpatrick, M.Y. Wang, B.M. Dawant, C.R. Maurer, Jr., R.M. Kessler, R.J. Maciunas, C. Barillot, D. Lemoine, A. Collignon, F. Maes, P. Suetens, D. Vandermeulen, P.A. van den Elsen, P.F. Hemler, S. Napel, T.S. Sumanaweera, B. Harkness, D.L.G. Hill, C. Studholme, G. Malandain, X. Pennec, M.E. Noz, G.Q. Maguire, Jr., M. Pollack, C.A. Pelizzari, R.A. Robb, D. Hanson, and R.P. Woods. Comparison and evaluation of retrospective intermodality image registration techniques. In *Medical Imaging 1996: Image Processing*,

volume 2710 of *SPIE proceedings series*, Newport Beach, California, USA, February 10-15 1996.

22. Xavier Pennec and Nicholas Ayache. An $\mathcal{O}(n^2)$ algorithm for 3D substructure matching of proteins. In A. Califano, I. Rigoutsos, and H.J. Wolson, editors, *Shape and Pattern Matching in Computational Biology – Proc. First Int. Workshop, Seattle, Wash, June 20, 1994*, pages 25–40. Plenum Publishing, 1994. Published in *Bioinformatics* 14(6), 1998, p. 516-522.

National reviewed workshops

1. Heike Hufnagel, Xavier Pennec, Grégoire Malandain, Hans Handels, and Nicholas Ayache. Non-linear 2D and 3D registration using block-matching and B-splines. In *Bildverarbeitung fuer die Medizin 2005*, Heidelberg, Germany, March 2005. Deutsches Krebsforschungszentrum.
2. Stéphane Nicolau, Xavier Pennec, Luc Soler, and Nicholas Ayache. Vision augmentée de structures anatomiques abdominales recalées par stéréoscopie. In *Actes du quatrième colloque francophone. Méthodes et Techniques Optiques pour l'Industrie*, volume 1, pages 413–418, Belfort, 2003.
3. Stéphane Nicolau, Alain Garcia, Xavier Pennec, Luc Soler, and Nicholas Ayache. Guidage de ponctions percutanées à l'aide d'un système de vision basé sur une méthode de recalage 3D/2D. In *Actes du colloque Imagerie pour les sciences du vivant et de l'ingénieur (IMVIE03)*, Strasbourg, 2003.
4. Xavier Pennec. Registration of uncertain geometric features: Estimating the pose and its accuracy. In J. Le Moigne, editor, *Proc of the First Image Registration Workshop, November 20-21 1997, Greenbelt, Maryland, USA*, pages 263–272. CESDIS, November 1997.
5. Xavier Pennec and Nicholas Ayache. Quelques problèmes posés par la gestion des primitives géométriques en vision par ordinateur. In *Journées ORASIS*, pages 111–116, May 1996.
6. Xavier Pennec. Multiple registration and mean rigid shape - application to the 3D case. In K.V. Mardia, C.A. Gill, and Dryden I.L., editors, *Image Fusion and Shape Variability Techniques (16th Leeds Annual Statistical Workshop)*, pages 178–185. University of Leeds, UK, July 1996.

Research Reports

1. Jean-Marc Peyrat, Maxime Sermesant, Hervé Delingette, Xavier Pennec, Chenyang Xu, Elliot McVeigh, and Nicholas Ayache. Towards a statistical atlas of cardiac fiber architecture. Research Report 5906, INRIA, May 2006.

2. Tristan Glatard, Johan Montagnat, Xavier Pennec, David Emsellem, and Diane Lingrand. MOTEUR: a data-intensive service-based workflow manager. Technical Report I3S/RR-2006-07-FR, I3S RAINBOW team, Univ. Nice-Sophia-Antipolis, March 2006.
3. Vincent Arsigny, Xavier Pennec, and Nicholas Ayache. Bi-invariant means in lie groups. application to left-invariant polyaffine transformations. Research report RR-5885, INRIA Sophia-Antipolis, April 2006.
4. Vincent Arsigny, Olivier Commowick, Xavier Pennec, and Nicholas Ayache. A fast and Log-Euclidean polyaffine framework for locally affine registration. Research report RR-5865, INRIA Sophia-Antipolis, March 2006.
5. Pierre Fillard, Vincent Arsigny, Xavier Pennec, Kiralee M. Hayashi, Paul M. Thompson, and Nicholas Ayache. Measuring brain variability by extrapolating sparse tensor fields measured on sulcal lines. Research Report 5887, INRIA, April 2006.
6. Vincent Arsigny, Pierre Fillard, Xavier Pennec, and Nicholas Ayache. Fast and simple computations on tensors with log-Euclidean metrics. Research Report RR-5584, INRIA, Sophia-Antipolis, France, May 2005.
7. Pierre Fillard, Vincent Arsigny, Xavier Pennec, and Nicholas Ayache. Joint estimation and smoothing of clinical DT-MRI with a log-Euclidean metric. Research Report RR-5607, INRIA, Sophia-Antipolis, France, June 2005.
8. Tristan Glatard, Johan Montagnat, and Xavier Pennec. An optimized workflow enactor for data-intensive grid applications. Technical Report I3S/RR-2005-32, Nice-Sophia-Antipolis University, I3S Lab, RAINBOW project, 2005.
9. Xavier Pennec, Pierre Fillard, and Nicholas Ayache. A Riemannian framework for tensor computing. Research Report 5255, INRIA, July 2004. Published in *Int. Journal of Computer Vision* 65(1), October 2005.
10. Xavier Pennec. Probabilities and statistics on Riemannian manifolds: A geometric approach. Research Report 5093, INRIA, January 2004. An extended version will appear in the *Int. Journal of Mathematical Imaging and Vision*.
11. Vincent Arsigny, Xavier Pennec, and Nicholas Ayache. A novel family of geometrical transformations: Polyrigid transformations. Application to the registration of histological slices. Research report 4837, INRIA, 2003.
12. Stéphane Nicolau, Xavier Pennec, Luc Soler, and Nicholas Ayache. Validation of a new 3D/2D registration criterion including error prediction. Application to image guided radio-frequency ablation of the liver tumors. Research report 4993, INRIA, 2003.
13. Sébastien Granger and Xavier Pennec. Statistiques exactes et approchées sur les normales aléatoires. Research report RR-4533, INRIA, 2002.

14. Sébastien Granger, Xavier Pennec, and Alexis Roche. Rigid point-surface registration using oriented points and an EM variant of ICP for computer guided oral implantology. Research report RR-4169, INRIA, 2001. Published in MICCAI'01, Utrecht, Netherlands, LNCS 2208, p.752-761.
15. Sébastien Ourselin, Xavier Pennec, Radu Stefanescu, Grégoire Malandain, and Nicholas Ayache. Robust registration of multi-modal medical images: Towards real-time clinical applications. Research report 4333, INRIA, 2001.
16. Xavier Pennec, Pascal Cachier, and Nicholas Ayache. Tracking brain deformations in time-sequences of 3D US images. Research report RR-4091, INRIA, December 2000.
17. Alexis Roche, Xavier Pennec, Grégoire Malandain, Nicholas Ayache, and Sébastien Ourselin. Generalized correlation ratio for rigid registration of 3D ultrasound with MR images. Research Report RR-3980, INRIA, July 2000. Published in IEEE TMI 20(10), oct. 2001, p. 25-31.
18. Pascal Cachier, Xavier Pennec, and Nicholas Ayache. Fast non-rigid matching by gradient descent: Study and improvements of the demons algorithm. Research Report 3706, INRIA, June 1999.
19. Sébastien Ourselin, Alexis Roche, Gérard Subsol, Xavier Pennec, and Christophe Sattouet. Automatic alignment of histological sections for 3D reconstruction and analysis. Research Report RR-3595, INRIA, December 1998.
20. Alexis Roche, Grégoire Malandain, Xavier Pennec, and Nicholas Ayache. Multimodal image registration by maximization of the correlation ratio. Research Report RR-3378, INRIA, August 1998. Published in MICCAI'98, Cambridge, USA, LNCS 1496, p. 1115-1124.
21. Xavier Pennec. Registration of uncertain geometric features: Estimating the pose and its accuracy. Technical Report AIM-1623, MIT Artificial Intelligence Lab, January 1998.
22. Xavier Pennec. Toward a generic framework for recognition based on uncertain geometric features. Memo AIM-1622, MIT Artificial Intelligence Lab, January 1998. Published in Videre 1(2), 1998, p.58-87.
23. Xavier Pennec. Computing the mean of geometric features - application to the mean rotation. Research Report RR-3371, INRIA, March 1998.
24. Xavier Pennec and Nicholas Ayache. Randomness and geometric features in computer vision. Research Report RR-2820, INRIA, March 1996. Published in J. of Math. Imag. and Vision 9(1), July 1998, p. 49-67.
25. Xavier Pennec and Jean-Philippe Thirion. Validation of 3D registration methods based on points and frames. Research Report RR-2470, INRIA, January 1995. Published in Int. J. of Comp. Vision 25(3), 1997, p. 203-229.
26. Xavier Pennec and Nicholas Ayache. An $\mathcal{O}(n^2)$ algorithm for 3D substructure matching of proteins. Research report RR-2274, INRIA, May 1994. Published in Bioinformatics 14(6), 1998, p. 516-522.

27. Xavier Pennec. Correctness and robustness of 3D rigid matching with bounded sensor error. Research report RR-2111, INRIA, November 1993.
28. Xavier Pennec. Traitement de l'erreur dans les méthodes de hachage géométrique et d'alignement, une étude théorique. Rapport de dea, DEA Informatique, Mathématique et Applications, École Polytechnique, ENS Ulm, July 1993.
29. Xavier Pennec. Etude d'améliorations possibles de techniques neuro-mimétiques appliquées à la reconnaissance de caractères manuscrits. Rapport interne, ONERA - DMI/GIA, 1992. Also in Rapport de stage d'option, Ecole Polytechnique.

Technical Reports and Deliverables

1. Xavier Pennec, Radu Stefanescu, and Eric Bardinet. Rapport d'étude de l'action CNES "r&t mise en correspondance". Technical report, INRIA, October 2002.
2. Xavier Pennec and Alexis Roche. NM2: Non-rigid matching MR/US second generation (Roboscope MMIT deliverable 25). Technical report, European project Roboscope, April 2000.
3. Xavier Pennec and Pascal Cachier. NT2: Non-rigid tracking US/US, second generation (Roboscope MMIT deliverable 26). Technical report, European project Roboscope, May 2000.
4. Xavier Pennec and Pascal Cachier. NT1: Non-rigid tracking US/US, first generation (Roboscope MMIT deliverable 19). Technical report, European project Roboscope, December 1999.
5. Alexis Roche and Xavier Pennec. NM1: Non-rigid matching MR/US first generation (Roboscope MMIT deliverable 18). Technical report, European project Roboscope, September 1999.
6. Xavier Pennec. AdV: Adapted viewing tools for the user interface (Roboscope MMIT deliverable 13). Technical report, European project Roboscope, September 1999.
7. Xavier Pennec. CoR1: Co-registration tools for MR/robot (Roboscope MMIT deliverable 12). Technical report, European project Roboscope, April 1999.
8. Xavier Pennec. RM1: Rigid matching tools for MR images (Roboscope MMIT deliverable 11). Technical report, European project Roboscope, April 1999.